RENEWABLE ENERGY LANSCAPES: MAPPING THE FOOTPRINT AND IMPACT OF SOLAR AND WIND ENERGY DEVELOPMENT ACROSS UNITED STATES

By

Jacob T. Stid

A DISSERTATION

Submitted to
Michigan State University
in partial fulfillment of the requirements
for the degree of

Earth and Environmental Sciences—Doctor of Philosophy

2025

ABSTRACT

The transition to renewable energy is essential for mitigating climate change, reducing air pollution, and enhancing energy security. Solar and wind energy with battery storage are now the most inexpensive and broadly available forms of new electricity generation and are thus projected to play a dominant role in a net-zero emissions future. However, solar and wind energy both require the semi-permanent transformation of land, a finite and valuable resource with opportunity costs. The tradeoffs of renewable energy landscapes depend on the siting, construction (and design), and management of the energy development, with key concerns including food security—when transforming agricultural land, habitat loss or fragmentation, reduction in property value, and land degradation. As land-use tradeoffs remain one of the most contentious aspects of renewable energy deployment for supporters and opponents alike, numerous approaches have emerged to mitigate the negative effects of land transformation and enhance the economic and ecosystem services provided. However, the rate of expansion has outpaced the availability of comprehensive spatial and temporal data, leaving knowledge gaps about the footprint of existing landscapes, what practices are being realized and where, and under what policies and incentives can influence the future of renewable energy landscapes. This dissertation addresses these gaps by leveraging remote sensing, geospatial analysis, and publicly available data to quantify the spatial footprint, land use patterns, and tradeoffs of renewable energy infrastructure in the United States (US).

Chapter 1 provides a high-level overview of the motivation for this research, and a literature review on ways that ground-mounted solar photovoltaic (PV) installations alter the water cycle at local and regional scales. I compile available knowledge on the approach, scale, climate, limitations, and hydrological outcomes to identify gaps in study design and the data needed to upscale approaches. Together, the literature indicates that solar PV installations unequivocally alter local and regional hydrological processes, and the implications depend on the needs of a region. Importantly, the information needed to replicate many modeling approaches does not exist beyond these few well-studied installations, making it difficult to determine the effects of converting larger portions of watersheds to solar.

Chapter 2 addresses this gap, introducing the Ground-Mounted Solar Energy in the United States (GM-SEUS) dataset, the most comprehensive publicly available repository of solar energy infrastructure in the US. Using a combination of high-spatial resolution machine learning and

object-based approaches and high-temporal resolution time series segmentation approaches, this dataset cultivates over 15,000 arrays covering 3,000 km^2 and nearly 3 million panel-row boundaries covering 470 km^2, with standardized and new metadata attributes. Building on existing data sources, GM-SEUS standardizes the definition of an array footprint, improves the spatial accuracy of datasets with uncertainty, and includes under-represented commercial-scale installations, setting the foundation for landscape-scale assessment of the US solar energy landscape. **Chapter 3** uses this new dataset to analyze land use and land management conditions of the existing US solar energy landscape through 2024. I find that most solar energy in the US occupies agricultural land and likely lacks a productive vegetation ground cover, presenting opportunities for dual-use practices to have broader adoption. Roughly one quarter of both commercial- and utility-scale solar installations were found to reside on economically marginal land, and commercial-scale installations were preferentially sited on land of significantly low-productivity. Together, these results emphasize the need for stronger policy incentives and improved land management practices to motivate broader development of vegetated and dual-use practices.

Shifting to wind energy, **Chapter 4** evaluates the agricultural footprint and impact of wind turbines on agricultural production in the US Corn Belt. Wind turbines reduce local crop yields and production, yet the overall effect on food security is small, and decreasing through time. Land leases more than compensate for lost production, increasing incomes for commodity crop farm landowners. These findings demonstrate that wind power can simultaneously support environmental goals and economic security for farmers, without jeopardizing food security. **Chapter 5** pulls together the findings of these chapters and reiterates a need for comprehensive and publicly available data on a rapidly expanding renewable energy landscape. With such data, researchers, policymakers, and interest-holders have the opportunity to study the multi-scale tradeoffs and synergies of existing renewable energy land transformation and focus future efforts by investigating what incentives and policies will result in real changes across the landscape.

This dissertation is dedicated to those who have been harmed by anti-science disinformation, rhetoric, and aggression, and to those who have, are, or will be persecuted by merchants of doubt in the pursuit of science, wisdom, and truth.

ACKNOWLEDGMENTS

This dissertation holds within the culmination of nearly six years of scientific exploration, collaboration, personal growth within the Michigan State University Hydrogeology Lab and beyond. As with anything worth achieving, it would not have been possible without the vast network of people surrounding me with extraordinary support, guidance, and encouragement. First and foremost, I would like to thank my advisor, Dr. Anthony Kendall. Anthony, I cannot explain thoroughly enough the positive impact you have had on my professional and personal life. You are above and beyond what I assumed an advisor and mentor could be, a friend. Your brilliant guidance, profound insight, willingness to cultivate new ideas, and genuine consideration for my well-being as both a human and scientist, have been invaluable. From "Do you think you could find solar installations using remote sensing?" to now, thank you.

I also want to extend my deepest gratitude to my committee members, Drs. Annick Anctil, David Hyndman, and Rufus Isaacs. In particular, Annick, thank you for years of immeasurable technical, professional, and personal guidance. Thank you for your kindness, openness, and for showing me into a world I did not know I would be so deeply enthralled with. Dave, you are why I am here. It was your time, effort, and conversation in meeting me at my undergraduate research poster at GSA that solidified my choice of MSU. Subsequently, your mentorship and guidance during my Master's degree, laid the foundation for me staying here. Thank you. And to Rufus, thank you deeply for the invaluable guidance and conversation over the last several years, helping me to find the intersection of solar energy research and a personal-turned professional interest in pollinators. I am excited to continue those discussions into the future.

None of this would have been possible without bountiful guidance from a collection of additional mentors here at MSU and beyond. At MSU, Drs. Sherry Martin, Jay Zarnetske, Phoebe Zarnetske, Kyla Dahlin, Ashton Shortridge, and Raechel Portelli all at one point or another, pointed me in a direction I did not yet know I needed. Prior mentors at Hope College were also pivotal in instilling a deep love of Earth and physical sciences, including Drs. Jonathan Peterson, Edward Hansen, Brian Bodenbender, and Suzanne DeVries-Zimmerman. Several mentors from the NASA DEVELOP program also made the COVID-remote DEVELOP term a fruitful one despite the challenges, thank you Sydney Neugebauer, and Drs. Kenton Ross and Neil Ganju.

To my past and present fellow Hydro Lab members, you have made and are making this place the easiest job and office in the world to never leave. Thank you, Brent Heerspink, for being

both a mentor and a dear friend from day one. Beyond the life and work discussions, I am most looking forward to our fishing trip post-defenses. Thank you, Jeremy Rapp, for a deep friendship and countless discussions, ranging from contributing to this dissertation to the logistics of fantasy world building, thank you. Thank you, Behnaz Mirzendehdel, for your never-ending encouragement and sea of kind words. To James Bingaman, Alexis Lanier, Samin Abolmaali, Madeline Sigler, Noah Bohl, and all others, thank you for all that you have added to the department and to my life. To past lab members, specifically Chanse Ford, Alex Kuhl, Ally Brady, and Quercus Hamlin, your support is still bearing fruit, thank you.

An additional thank you is necessary for several others who provided support or guidance over the last several years, including Luis B. Martinetti, Jake Roush, and Drs. Siddharth Shukla, Jill Deines, Erin Hacker, Sam Smidt, and everyone in the EES Department. Special thanks too to the entire Sustainable Energy Systems Lab for continuous feedback and friendship as well. And to Francis Hanna, with whom conference and coffee conversation became a favorite pastime, thank you – that startup will indeed happen one day. Through a variety of avenues, several others have provided a helping hand and word along the way, thank you to Alexis Pascaris, Kirsten Perry, Frank Golbeck, Thomas Hickey, and Drs. Bonnie McGill, Sam Zipper, Matthew Sturchio.

To my wife, Karey Stid, you are a guiding light in the darkness of the world, and a reminder that light is everywhere at all times—enough to install solar. I love you with all my heart and being, thank you for being you, and for loving me into being me throughout this journey and beyond. To my parents, Wesley and Lori Stid, this dissertation and degree are a direct reflection of the compassion, patience, and unwavering support you have given me throughout my life. You have been infinitely supportive of everything it took to get here, doing so with grace and love, I am endlessly grateful. To my sister Aly, thank you for all that you are and all that you will be. To the Crimmins, Frink, and Harbort families, you have all provided a fountain of encouragement and love, thank you. To friends who have provided much needed laughter, support, and grounding, Christian and Sammy Smith, your friendship has meant the world to me, I cannot thank you enough. To the collective friends of “Rum Ham”, Justin and Shelby Fairfield, Steven Hanson, Tyler and Kelsey Gibson, Ian Gorgenson, Mike Miklusicak, and Griffin Weigl, I appreciate you more than I can say. This experience has been challenging, powerful, and inspiring. To all mentioned and anyone I have omitted, thank you all for being a part of this journey with me.

TABLE OF CONTENTS

LIST OF TABLES

LIST OF FIGURES

LIST OF ABBREVIATIONS

US: United States

CONUS: Contiguous United States

PV: Photovoltaic

CSP: Concentrating Solar Power

GW_{DC}: Gigawatt (Direct Current)

GW_{AC}: Gigawatt (Alternating Current)

MWh: Megawatt-hour

TWh: Terawatt-hour

GM-SEUS: Ground-Mounted Solar Energy in the United States Dataset

USPVDB: United States Large-Scale Photovoltaic Database

GCR: Ground Cover Ratio

NAIP: National Agriculture Imagery Program

GEE: Google Earth Engine

RF: Random Forest

CDL: Cropland Data Layer

NLCD: National Land Cover Database

LULC: Land Use Land Cover

AgROE: Agricultural Radius of Effect

LUE: Land Use Efficiency

USWTDB: United States Wind Turbine Database

SCYM: Scalable Satellite-Derived Yield Maps

RLP: Relative Land Productivity

CHAPTER 1: INTRODUCTION AND REVIEW OF HYDROLOGICAL ASSESSMENTS ON SOLAR ENERGY WITH RESULTING KNOWLEDGE GAPS

Abstract

By 2050, the United States (US) is projected to install enough solar photovoltaic (PV) infrastructure to cover ~1% of its contiguous land surface. The construction and operation of ground-mounted solar energy installations can physically change the landscape and energy and water budgets at the surface, which can lead to broader hydrological outcomes. Here, we review the available body of literature on solar energy installations and effects on plot-scale, watershed-scale, and cross-scale hydrological phenomena. We discuss current tendencies in literature focus and identify key areas where solar and hydrology research could better guide a co-beneficial path forward for the future energy and hydrological landscape. We also provide two contributing assessments: 1) current and future solar coverage of HUC10 watersheds to provide context on coverage-based studies and outcomes, and 2) a counterfactual groundwater flow simulation of a high- and low-impact solar installation in a humid, agriculturally dominated watershed in southwest Michigan. Together, these assessments highlight the need for a better understanding of existing practices and for regionally-relevant low-impact construction and management practices that manage groundwater budgets in a high solar coverage future. More research and open data sharing are needed to fill gaps in several frontiers including: location, construction, and design of the existing solar energy landscape, treatment-control studies, before-and-after studies, studies including both direct and indirect water budget reporting, better regional representation, larger-scale agrivoltaic study designs, and studies considering groundwater. We have the opportunity to include management and regeneration of water resources based on a region's water-needs in our path towards net-zero.

1.1: Introduction

To avoid the continued effects of climate change, air pollution, and energy insecurity, global energy systems must transition away from fossil fuel dependency over the next two decades. Both globally and in the United States (US), solar and wind energy will lead the path forward (Ardani et al., 2021; Heath et al., 2022; Jacobson et al., 2017; Victoria et al., 2021), constituting a new energy landscape that will result in significant physical and socioeconomic changes (De Boer & Zuidema, 2015; Preziuso et al., 2023). Achieving this shift without compromising other sustainable development goals (SDG's) will involve careful considerations of tradeoffs and synergies of the solar and wind buildout required to meet the electricity needs of the future (Hernandez et al., 2019, 2020). Given that solar irradiance and wind energy are spatially distributed sources of energy, both technologies require the use of considerable areas of land. What technology is implemented, where they succeed best, and how to manage them to provide more than just electricity, are key challenges for the renewable energy community.

Renewable energies can be regenerative or depletive on the landscape. A few examples of concerns about land use transformation include food security and prime agricultural land loss (Hall et al., 2022; Morris & Blekkenhorst, 2017), permanent land use and degradation (Lambert et al., 2021), changes in hydrological connectivity (Moore-O'Leary et al., 2017), ecological habitat fragmentation and biodiversity loss (Karban et al., 2024; G. C. Wu et al., 2023), insect and avian well-being (Grodsky et al., 2011, 2021), downwind changes in weather and vertical mixing (Baidya Roy & Traiteur, 2010), migration pathway disruption (Levin et al., 2023), and property value reduction (Elmallah et al., 2023). These are all legitimate concerns that need to be addressed as soon as possible given the pace of renewable energy buildout.

There are three primary levers by which the outcomes of renewable energy on the landscape can be swayed: siting, construction (including design), and management. There is evidence that all three levers can be adjusted effectively (C. S. Choi et al., 2023; Hise et al., 2022; Karban et al., 2025; Sorensen et al., 2022) with the co-benefit of increased public and professional support for buildout (Moore et al., 2022; Pascaris et al., 2022). Thus, each of these concerns can be studied and addressed given knowledge of existing infrastructure and how it has impacted its environment. However, many accounts of solar and wind energy spatial, temporal, and design attributes have historically been absent, incomplete, or held by privacy paywalls. This leaves the realized practices of the modern existing renewable energy landscape, and thus outcomes, a

mystery. To address this gap, we need an up to date and comprehensive account of existing solar and wind energy siting, design, and management practices, and how they impact their physical and ecological landscapes. We seek to fill this gap.

Governments, academics, and independent organizations around the world have begun to seek out and create publicly available datasets on renewable energy installation location, design, and electricity generation in order to plan for a renewable future. Examples include the United Kingdom (UK), which has started regular updates to the Renewable Energy Planning Database (REPD) (UK Government, 2024), collecting data on all renewable energy installations >150 kW. One of the purposes of REPD is to protect food security and best and most versatile land (Claire Coutinho, 2024). In the United States (US), the United States Wind Turbine Database (USWTDB) was created in 2018, a multi-institution federal effort to make wind turbine spatiotemporal metadata publicly available (B. D. Hoen et al., 2018; Rand et al., 2020). More recently, the United States Large-Scale Solar Photovoltaic Database (USPVDB) became the first regularly updated, comprehensive, and publicly available dataset characterizing utility-scale (≥1 MW) solar energy installations in the US (Fujita et al., 2023, 2024). Many independent groups have also begun to collect and distribute this information (Byers et al., 2021; Deline et al., 2021; Evans et al., 2021, 2023; GEM, 2024; Global Energy Observatory et al., 2021; NREL, 2025; OpenStreetMap Contributors, 2024; Phillpott et al., 2024b, 2024a; Seel et al., 2024; Stid et al., 2022; Stid, Shukla, et al., 2023; Thonig et al., 2023). Regarding land use, the Protecting Future Farmland Act of 2023 has only recently provided requirements for the USDA to collect and disseminate information on siting, land use, site disturbance, system purpose, and ground cover management, while providing best practice guidance in each category (Protecting Future Farmland Act of 2023, 2023). However, the rapid expansion of renewable energy infrastructure, the recent emergence of these datasets, and the absence of key land-use attributes have limited large-scale analyses of landscape changes. To effectively plan for future energy infrastructure, we need comprehensive and publicly accessible data that accounts for land use trade-offs, synergies, and system design and management decisions.

The aim of this dissertation is to enhance existing knowledge on the land we use for renewable energy infrastructure. We provide an updated assessment of the land use, land management, and impacts of solar and wind energy installations on the US landscape. Importantly, all data, code, and process are made publicly available. One important aspect of this work is a

distinction in the scale of solar energy installations. There are two primary scales of solar energy buildout: small-scale (<1 MW) and large-scale (≥1 MW) (EIA, 2025). Note that these two scales inherently include residential- (<1 MW, rooftop), commercial- (<1 MW, ground-mounted), community- (often, 1 to 5 MW), industrial (range of capacities, use-case definition), and utility- (≥1 MW, ground-mounted) scale installations. Each scale is unique in policy, incentive, and literature coverage (Mamun et al., 2022; O'Shaughnessy, 2022; Stid, Shukla, et al., 2025; Waechter et al., 2024). Within this dissertation, we simplify and filter these to include ground-mounted commercial-scale and utility-scale solar.

1.2: Solar PV energy generation and hydrology

To achieve net-zero energy production, the United States (US) will convert ~1% of its contiguous land surface to solar energy systems over the next 30 years (Ardani et al., 2021; Larson et al., 2021). Similarly, other regions, like China, will require up to 2% of their landscape to meet net-zero requirements (Ji et al., 2022). Despite this rapidly approaching deadline, we know relatively little about how the current solar energy landscape affects local or regional hydrology, much less about how the future landscape will alter hydrology. As we are early in this timeline, we can focus siting (location), installation (construction and design), and management (ground cover) on regeneration and management of water resources that suit a region's water-needs. For instance, the management needs of water-scarce Southern California watersheds differ significantly from the needs of many shallow water table Michigan watersheds, as expressed by developers in qualitative interviews (Pascaris et al., 2023). Therefore, understanding solar installation hydrological dynamics both at the site and regional scale will be essential for focusing siting and management of future infrastructure.

This review builds on a recent review on solar landscape hydrology and stormwater management literature by Yavari et al. (2022) which outlines gaps in our understanding of runoff generation processes at solar array sites. While there are a few studies that employed modified models to represent solar on a landscape, only a few have attempted to scale local impacts to the watershed scale, and none at the time of writing have validated their models with field data (Yavari et al., 2022). Despite this lack of watershed-scale knowledge, there is a vast body of literature, largely focused on agrivoltaics, that provides plot-scale quantifications of solar induced changes to near surface hydrology (Mamun et al., 2022; Walston et al., 2022; Yavari et al., 2022). These studies show that agrivoltaic management enhances soil moisture retention and water use

efficiency (WUE), regulates the microclimate, and reduces evapotranspiration (ET) (Yavari et al., 2022). However, there are few studies which extend predictions to hillslope, catchment, or watershed-scale. Some that theorize watershed-scale impacts posit negative effects such as erosion, prolonged drying of ephemeral bodies, groundwater overdraft from water-intensive solar practices, or extensively grading the land leading to reduced connectivity of drainages, rills, and microwashes (Grippo et al., 2015; Klise et al., 2013; Moore-O'Leary et al., 2017). There is also a very real possibility that solar land use change (~0.5% of contiguous US landscape) may not be extensive enough to impact large scale watershed dynamics depending on distribution, prior land use, and land management (A. Sharma et al., 2011; S. Sharma & Waldman, 2021; Shobe, 2022). If that was the case, however, plot-scale management efforts would still be of significant value given the local benefits described in the literature.

The concept of emergent behavior is the arising of novel and coherent structures of patterns and properties during the process of self-organization in complex systems (Goldstein, 1999). Refined for hydrology, emergent behavior is the occurrence of large-scale (watershed-scale) hydrologic phenomena that are physically linked to changes in small-scale (hillslope- or plot-scale) phenomena. This concept is crucial for understanding how functionally heterogeneous hydrological processes scale from the plot- to watershed-scales (Troch et al., 2009). Thus, measuring plot-scale phenomena alone does not necessarily provide direct insight to hillslope or catchment scale processes without further inspection. There needs to be a pathway towards the emergence of larger-scale behaviors.

As previously suggested (Sivapalan et al., 2003), to explain the simplicity of how solar can impact our hydrologic landscape, we need mechanisms to aggregate necessary processes and remove unnecessary processes to perceive effects of larger hillslope or watershed scales. To help explain this simplicity, we compiled metadata on the various available studies regarding both direct and indirect effects of solar on hydrology across hydrological scales. We collect and assess study design metrics including management practices, Köppen-Geiger climate classification for each study site, scale, and findings, and produce a data table to map the current state of the literature. We go further and attempt to connect distributed plot-scale behavior with watershed-scale using results from the few studies we identify to approach emergent behavior. We also provide a counterfactual numerical simulation of the impact of installation of a 160 MW_{DC} utility-scale solar array on groundwater storage and discharge in a humid, shallow, agricultural watershed

in southwest Michigan to display shortfalls of assumptions required by the lack of available data and gaps in understanding. Also providing watershed (HUC10) maps of solar direct area coverage, we pose the questions: Will solar array build out, both current and projected, alter the landscape enough to induce positive or negative emergent behavior? If so, how can we focus solar siting, installation, and management practices to push the scales towards water security and stability? We discuss how answering these questions will involve extensive and open-access field-data collection efforts and more expansive solar array design characterizations that coincide with focused modeling spanning regions, practices, and technologies.

1.3: Methodology

1.3.1: Review strategy

This study primarily used the Google Scholar, Scopus, and HESS (Hydrology and Earth System Sciences) search engines along with the following search criteria; “solar”, “solar photovoltaics”, “PV”, “solar farm”, “agrivoltaics”, “hydrology”, “hydrogeology”, “runoff”, “recharge”, “water use”, “groundwater”, “stormwater”, “soil moisture”, “water budget”, “evapotranspiration”, “ecosystem services”, “impact analysis”, and “microclimate”. There are a few key study designs that we have decided to omit from this review. To emphasize work in the recent decade, we have attempted to limit the study date range to studies published after 2012 and prior to March 2023, when this review was originally collected. We also update the reviewed literature discussing studies published between March 2023, and December 2024. We have omitted water quality assessments, as this review is focused on processes affecting local and regional hydrological flow or availability. We have omitted solar pumping for irrigation and “floatovoltaics” from this review, both common concepts within the literature search for these criteria. Although, one study pertains to covering canals with solar, which is not floatovoltaics in design but incorporates predominant impacts of the practices. We have also decided to omit wet-cooled, trough, and concentrated solar power (CSP) systems as their water use concerns are different from more common dry-cooled photovoltaics (PV). Although, it should be noted that these systems still change the landscape and that there are legitimate concerns with water-use for these systems (Klise et al., 2013). Finally, though we include agrivoltaics in our search criteria, this is not a review of agrivoltaic effects alone, of which there are several existing reviews for the vast and growing body of literature (Gomez-Casanovas et al., 2023; Mamun et al., 2022; Walston

et al., 2022), and only include those that have a significant water or hydrological component in study design or data collection.

Studies were grouped into their respective hydrological scales of assessment (plot and watershed) based on study design and scope, their management practices, and reported impacts. The hydrological scale (or scope) was plot-scale if the study only concerned shallow vadose-zone effects directly beneath or proximal to solar arrays. Studies that discussed watershed-scale effects (including attribution of indirect changes) of solar but did not collect measurements or use models of plot-scale dynamics leading to those effects were watershed-scale. Studies that went beyond local vadose zone (unsaturated) effects and onto hillslope-, catchment-, or watershed-scale dynamics by discussing lateral flow components including connectivity and alteration to water bodies, change in region water budgets (ET), deeper vertical flow components such as drainage, or general runoff generation processes as a result of plot-scale dynamics, were considered plot- and watershed-scale. We have also coded studies by mode of impacts as either "direct" or "indirect" effects. Direct effects refer to hydrological changes as a direct result of solar PV land use change and operation. Indirect effects refer to life-cycle water use changes (manufacturing, construction, operational cleaning, site irrigation) and the opportunity cost of solar PV including shutting down thermoelectric power and hydroelectric dams.

1.3.2: Watershed zonal analysis of current and future solar infrastructure

We performed a zonal summation of the current and projected solar direct area coverage in HUC10 watersheds. Kruitwagen et al. (2021) provides the most spatially complete and up-to-date dataset of solar array installations across the United States (and globally), and includes arrays installed through 2018. Princeton's Net-Zero America Project (Jenkins et al., 2021; Larson et al., 2021) estimates the extent of solar and wind footprints for 2050 electric-load requirements under six build-out scenarios. We used the 100% Renewable (E+ RE+) scenario for the zonal analysis of the projected solar footprint, as this scenario requires the most land for solar, ensuring that existing arrays from Kruitwagen et al. (2021) were included. The 100% Renewable scenario would lead to the largest potential hydrological impact and could be considered a "worst-case scenario" if sited and managed responsibly. We also excluded rooftop arrays via a building dataset (Heris et al., 2020) filter requiring a 75% overlap with building footprints.

1.3.3: Simulating plot-scale solar management on watershed-scale hydrogeology

As a proof of concept for addressing the knowledge gaps identified in this review, we simulated the change in three-dimensional groundwater storage and discharge due to a counterfactual utility-scale solar installation (Figure 1B) on agricultural land underlain by a Quaternary aquifer system in Michigan's Lower Peninsula. The Augusta Creek Watershed (Figure 1A) in humid southwestern Michigan, part of the Lake Michigan Basin, drains 98 km^2 into the Kalamazoo River and is composed of 47% agricultural land, 23% upland forest, and 20% wetland and marsh complexes (Ruhala et al., 2018). We selected this watershed because of its agricultural land share, given most solar arrays in the United States are installed on agricultural land (Kruitwagen et al., 2021; Stid et al., 2022), on-going data collection efforts in the region (Weidner et al., 2022), and its proximity to Michigan State University's (MSU) W.K. Kellogg Biological Station (KBS), where we are proposing building an experimental solar research laboratory to further address gaps in knowledge and data discussed here. Importantly, this watershed also does not currently contain a ground-mounted solar array.

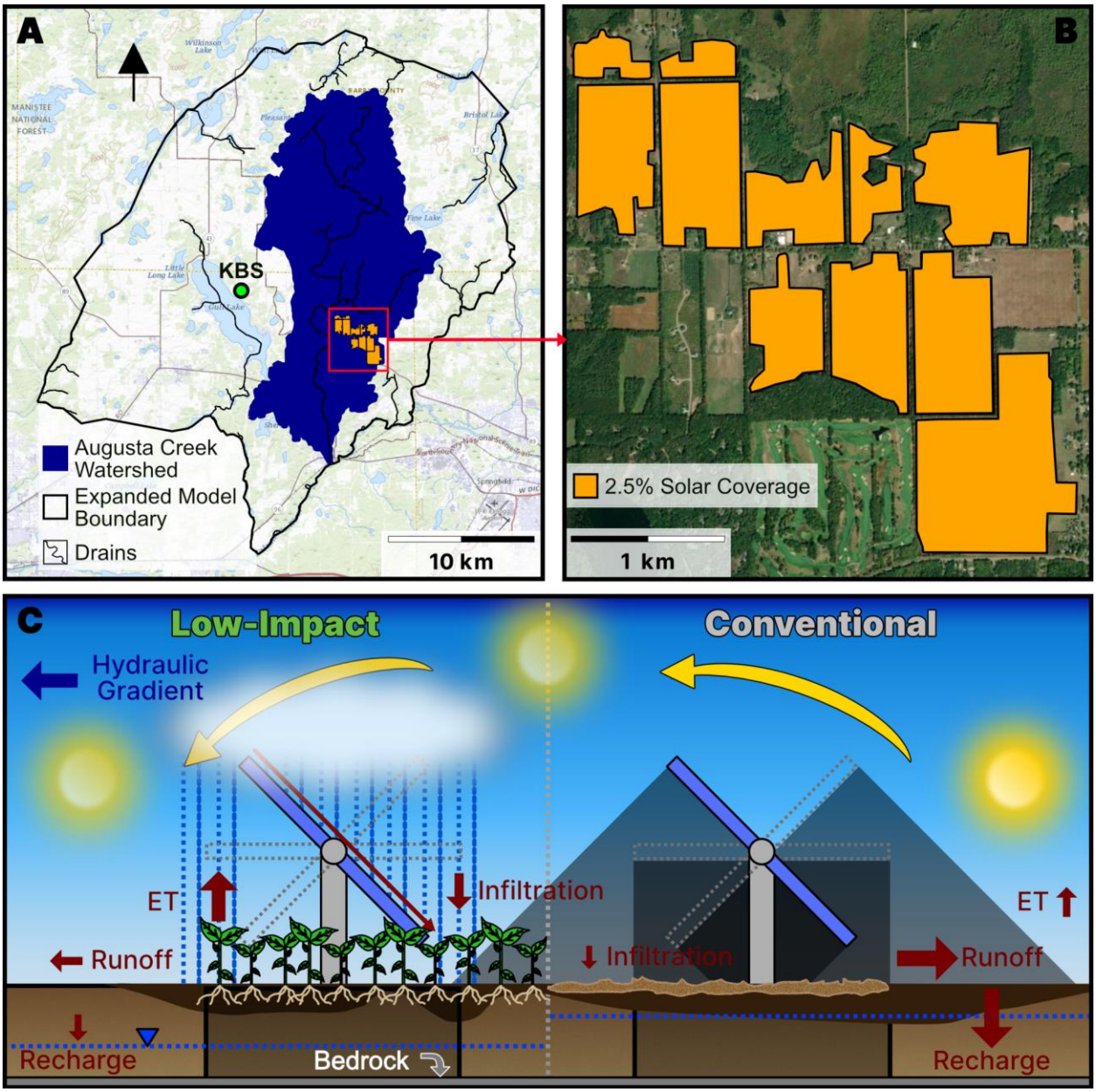

Figure 1. Perceptual model for the Augusta Creek Watershed groundwater simulation. Perceptual flux changes considering a 160 MW_{DC} utility-scale solar installation and two distinct site preparation and management. (A) The Augusta Creek Watershed, manually delineated expanded model boundary, and NHD drains with more than 3 km in connected length. (B) The counterfactual solar installation covering 2.5% of the watershed area and using agricultural land that could be feasible for a solar installation. (C) The perceptual model for a single-axis solar array altering the hydrological budget under two different site preparation and management scenarios: low-impact (left) and high-impact (right).

We used the three-dimensional groundwater flow model MODFLOW 6 version 6.4.4 (Langevin et al., 2017) and flopy version 3.6 (Bakker et al., 2016; Hughes et al., 2023) to construct

a steady-state groundwater flow model for the year 2013 within the model boundary shown in Figure 1. The underlying Quaternary aquifer system is composed of glacial outwash and tills containing a mix of gravel, sand, silt, and clay, ranging in thickness between 40 and 120 m (FTWRC, 2017; Ruhala et al., 2018). Median depth to water within the Augusta Creek Watershed is ~7 m (Zell & Sanford, 2020). Soils in the region are sandy to loamy intermixed with high-organic-containing mucks in wetland and riparian regions (FTWRC, 2017; Ruhala et al., 2018), although we do not model vadose zone dynamics here.

Three layers of equal depth based on aquifer thickness are used to account for known changes in horizontal hydraulic conductivity (HK) and vertical anisotropy with depth (Shepley, 2024). Aquifer thickness was derived from (model top) USGS 3D Elevation Program (3DEP) 10m DEM (USGS, 2023) and (model bottom) USGS bedrock topography (Soler & Garrity, 2018), smoothed with a focal filter of 2,500 m. The model is gridded at 30 m resolution, resulting in 720,000 grid cells in each layer across an extended model boundary of 360 km^2. The area of interest for this model includes the Augusta Creek Watershed, Gull Lake, and MSU KBS. The model boundary was extended to the next assumed no-flow (Neumann) boundary by manually connecting discharge boundaries (streams) and water bodies (lakes). We set the constant head boundary (Dirichlet boundary condition) as a 1 km segment of the Kalamazoo River at the watershed outlet just upstream from the USGS Stream Gauge for Augusta Creek Near Augusta, MI (USGS 04105700) which provided observation of the stream stage.

Our model incorporated the drain (DRN), river (RIV), recharge (RCH), and evapotranspiration (EVT) stress packages (Langevin et al., 2017). Briefly, the following model inputs were used: starting heads derived from Zell and Sanford (2020) depth to water (DTW) and the USGS 3DEP DEM, horizontal hydraulic conductivity from the Michigan Department of Environment, Great Lakes, and Energy (EGLE) Wellogic database (EGLE, 2020), extrapolated using Quaternary geology from Farrand and Bell (1982), and compiled by (Hamlin et al., 2022), and annual recharge from Reitz et al. (2017) for the year 2013. Vertical anisotropy was assumed as a constant of 10 taken from (Shepley, 2024). HK and vertical anisotropy were also varied with depth. HK was decreased by 3-, 3.5-, and 4-times from the top to bottom layer to account for overestimation of HK in the given methods, compaction, alignment, and pore filling with depth. Vertical anisotropy was increased by 0-, 1.2-, and 1.67-times the initial value (10) with depth to account for vertical hydraulic conductivity decreasing faster with depth than horizontal

conductivity. The model year, 2013, was the most recent available recharge year from Reitz et al. (2017). We used the National Hydrography Dataset Plus (NHD+) (USGS, 2020) data for drains, selecting for connected drain segments greater than 3 km in length to remove likely internally drained systems (disconnected drains). Maps of starting heads, recharge, and the DEM are shown in Figure A26, and maps of multi-layered HK, vertical anisotropy, and the model layer bottoms are shown in Figure A27.

We created a counterfactual scenario where a solar array was installed on 2.5% of Augusta Creek Watershed's agricultural area (2.3 km^2–Figure 1B) and considered two site preparation and management scenarios that altered onsite recharge and downstream drain fluxes: low-impact and high-impact (conventional) (Figure 1C). Pisinaras et al. (2014) found that at the sub-basin scale, runoff and recharge significantly increased with solar land use change (from a prior agricultural use) of 1% and 5% watershed area due primarily to a decrease in ET and a reduction in infiltration, with the effect varying depending on site preparation and management (low- and high-impact).

We considered the low-impact scenario as the control, assuming that an intentional reduction in topsoil removal and soil compaction and effective site management with established or maintained vegetation would not result in increased runoff or recharge relative to agricultural land use (i.e., assumed no change in infiltration and ET from a baseline model). Our high-impact scenario was similar to that of Pisinaras et al. (2014), assuming topsoil removal and high compaction during construction, and bare soil ground cover management post-installation. Following Pisinaras et al. (2014), and given theoretical site conditions, we assumed that high-impact construction and management would result in an increase in site runoff of 110 mm yr^{-1} and an increase in onsite recharge of 40 mm yr^{-1}. Importantly for both scenarios, we did not consider additional model controls for a stormwater management plan, essentially assuming that site preparation and management were the only forms of hydrological management and alteration.

To simulate the change in water balance due to high-impact solar construction and operation, we increase recharge within the bounds of the array and within a downstream river segmentation to simulate increased runoff. Accounting for the total effect of the solar area, we distributed 25,700 m^3 yr^{-1} to the ~ 7 km downstream river segment (drain) and 9,300 m^3 yr^{-1} to the solar direct land use (as shown in Figure 2). The MODFLOW cells with redistributed recharge are shown in Figure 2 and the modified recharge layer can also be found in Figure A28.

To evaluate model performance, we compared the residuals of the control scenario model (no solar ~ low-impact solar) to heads at 4,970 observation wells within the model boundary from EGLE (2020), recharge, and HK, and plot residuals spatially. We also computed average annual streamflow and compared to the annual median streamflow of the downstream USGS Stream Gauge. Given that the uncalibrated model performed fairly well and that this approach was conceptual, model calibration was beyond the scope of this effort.

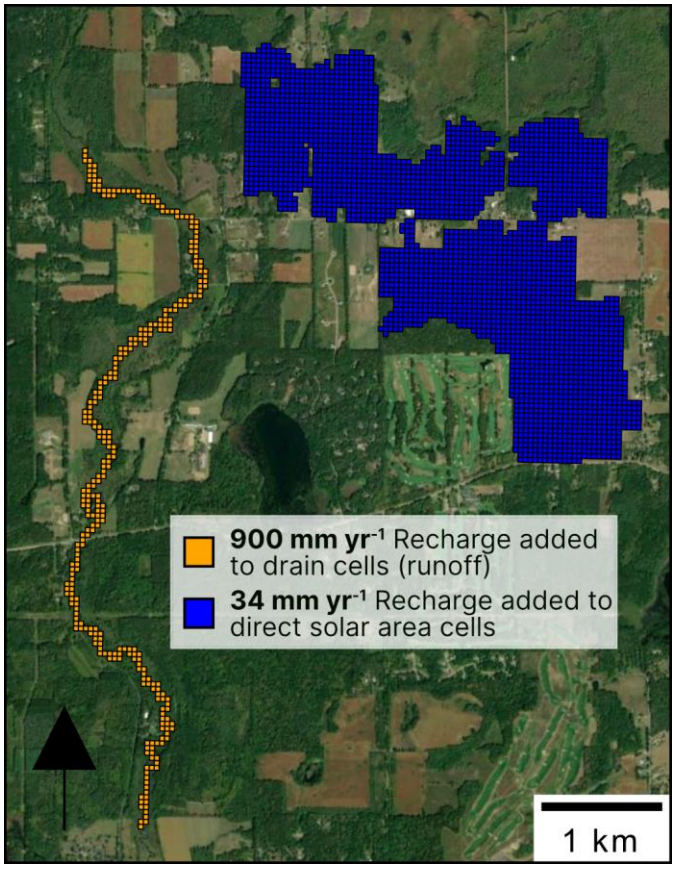

Figure 2. MODFLOW grid cells with redistributed water fluxes due to solar land use. Change in runoff and recharge rates as a result of high-impact solar land use and management from Pisinaras et al. (2014) were estimated for the 2.3 km^2 solar area and redistributed across grid cells of a ~7 km downstream drain segment (900 mm yr^{-1}) and in grid cells within the bounds of the counterfactual solar array (34 mm yr^{-1}).

1.4: A review of solar PV hydrology literature

In total, this review included 68 articles on solar and hydrology. We analyzed 53 peer-reviewed studies (including a paired-study counted only once), one thesis (herein, included in "studies"), seven commentaries, perspectives, and qualitative case studies, four reviews, and one guidance document paired with a report, published between January 2013 January 2025 that

directly or in-directly reported changes in hydrology because of solar PV. Study spatial extent ranged from ~3-4 m^2 experimental plots (Baiamonte et al., 2023; F. Wang & Gao, 2023; Warmann et al., 2024) to global (Parkinson & Hunt, 2020). Our recent work in California's Central Valley (Stid, Shukla, et al., 2025) involved the largest number of existing solar arrays, including 925 unique installations in the analysis, followed 478 unique arrays (S. Curtis et al., 2020) and 276 unique arrays (Walston et al., 2021).

There was a spatial study distribution bias for United States (US) based studies, with US study areas in 28 of 54 studies, five France-based study areas, five Italy-based study areas, four China-based study areas, two Canada-based study areas, several studies with one study area (e.g., Turkey, Germany, India, Greece, United Kingdom), with the remainder global in extent or theoretical and not placed-based.

Regarding studies that reported a referenceable location for the relevance of their results (45 studies, some contained multiple Köppen-Geiger climate classifications), 36% provided results in arid climates, 60% in temperate climates, and 16% in continental climates. Within these primary climate groups, 42% provided results in fully humid regions, 46% in dry summer regions, and 24% in dry winter regions. Five studies crossed climate regions.

For the hydrological scale of assessment, we coded 24 studies as plot-scale, 11 studies as watershed-scale, and 19 studies as plot- and watershed-scale in scope, thus providing insight into emergent behavior. We classified 45 studies as having direct physical hydrological implications (direct impact) and eight studies as attributing indirect hydrological outcomes (indirect impact) as a result of solar PV, and one with shared impacts (reported direct and indirect impacts). Articles are shown in Table 1.

Table 1. Reviewed articles on solar energy impact on hydrology.

Hydrological Scale	*Direct, Indirect, Both*	*AgPV (%)*	*Studies*
Plot	(23), (1), (0)	79%	(H.-E. Adeh et al., 2018; Amaducci et al., 2018; Andrew et al., 2021; Armstrong et al., 2016; Aschale et al., 2022; Barron-Gafford et al., 2019; C. S. Choi et al., 2020, 2023; Elamri, Cheviron, Lopez, et al., 2018; Graham et al., 2021; Kannenberg et al., 2023; Lambert et al., 2021; Meneses et al., 2023; Mengi et al., 2023; Ravi et al., 2016; Semeraro et al., 2024; Şevik & Aktaş, 2022; Sturchio et al., 2022; Sturchio, Kannenberg, & Knapp, 2024; Sturchio, Kannenberg, Pinkowitz, et al., 2024; Valle et al., 2017; Warmann et al., 2024; Weselek et al., 2019; Williams et al., 2023)
Watershed	(3), (7), (1)	9%	(Arent et al., 2014; S. Curtis et al., 2020; Devitt et al., 2020; He et al., 2019; Klise et al., 2013; Macknick & Cohen, 2015; McKuin et al., 2021; Mier-Valderrama et al., 2024; Parkinson & Hunt, 2020; S. Sharma & Waldman, 2021; Stid, Shukla, et al., 2025)
Plot & Watershed	(19), (0), (0)	32%	(Baiamonte et al., 2023; Barnard et al., 2017; Y. Chen, Zhang, et al., 2024; Cook & McCuen, 2013; Edalat, 2017; Elamri, Cheviron, Mange, et al., 2018; Galzki & Mulla, 2024; Gullotta et al., 2023; Jahanfar et al., 2020; H. Liu et al., 2023; Marrou, Dufour, et al., 2013; Marrou, Guilioni, et al., 2013; McCall, Macdonald, et al., 2023; Mulla et al., 2024; Nair et al., 2024; Pisinaras et al., 2014; Tanner et al., 2020; Walston et al., 2021; F. Wang & Gao, 2023; C. Wu et al., 2022; Yavari Bajehbaj et al., 2024)
Review, Commentary, and Report	-	-	(Biggs et al., 2022; Gomez-Casanovas et al., 2023; GPI, 2023; Grippo et al., 2015; Mamun et al., 2022; McCall, Daw, et al., 2023; Moore-O'Leary et al., 2017; Rößner, 2022; Shobe, 2022; Sturchio & Knapp, 2023; Walston et al., 2022; Yavari et al., 2022)

Notes: Articles in the table were published between 2013 and February 2025. AgPV denotes that a study claimed to be or was coded in this review as agrivoltaic in study focus, excluding studies regarding exclusively non-agriculturally productive grasses or more specifically ecovoltaics.

1.4.1: Solar induced heterogeneity at the plot-scale

The most common, and possibly most important concept regarding direct hydrological effects at the plot-scale was that solar of any design, placement, management, or climate, induced heterogeneity in how rain and radiation traverse to the ground's surface and leave it. All 46 direct impact studies discussed spatial heterogeneity of soil moisture, erosion, infiltration, WUE, or ET. Ground-mounted solar panels shade regions of the ground cover for long periods of the day, altering the energy balance under and between array panel-rows, reducing ET, and enhancing WUE, carbon uptake, and net primary productivity (NPP) of vegetation (H.-E. Adeh et al., 2018; Armstrong et al., 2016; Barron-Gafford et al., 2019; C. S. Choi et al., 2023; Jahanfar et al., 2020; Kannenberg et al., 2023; Marrou, Guilioni, et al., 2013; Mengi et al., 2023; Ravi et al., 2016; Semeraro et al., 2024; Sturchio, Kannenberg, Pinkowitz, et al., 2024; Tanner et al., 2020). Change in ET dominates the change in the hydrological budget, and has been shown to moderately decrease, -1.3% (Kannenberg et al., 2023)) or more significantly decrease -37% to -67% (PET)

under-panel during the summer (Yavari Bajehbaj et al., 2024). Although ET is reduced, it should be noted that ET-cooling is also a driver for enhanced panel-efficiency and thus electricity generation, with some (Williams et al., 2023) showing as much as a 10°C decrease in panel temperature of vegetated ground cover as opposed to bare soils.

Rainwater is also redistributed (H.-E. Adeh et al., 2018; Edalat, 2017; Elamri, Cheviron, Mange, et al., 2018; Galzki & Mulla, 2024; Yavari Bajehbaj et al., 2024) creating unique zones of increased infiltration and soil moisture (Sturchio, Kannenberg, Pinkowitz, et al., 2024; C. Wu et al., 2022; Yavari Bajehbaj et al., 2024), hydraulic conductivity (C. S. Choi et al., 2020), increased infiltration-excess overland flow (F. Wang & Gao, 2023), and potential for erosion (Barnard et al., 2017; Elamri, Cheviron, Mange, et al., 2018; H. Liu et al., 2023; Meneses et al., 2023; F. Wang & Gao, 2023), primarily at the solar dripline. Yavari Bajehbaj et al. (2024) found that soil moisture was 19% higher than reference at the panel-row dripline (fixed-tilt) and 25% lower than reference under the panel-row. For single-axis tracking arrays, the dripline transitions from east to west throughout the day, mitigating some of this heterogeneity (Sturchio et al., 2022). However, within single-axis tracking arrays, vapor pressure deficit (VPD) and air temperature are lower in the morning causing vegetation within the east-edge dripline to have greater stomatal conductance and thus greater ET compared to the western edge (shaded in the morning) (Sturchio, Kannenberg, Pinkowitz, et al., 2024). Thus, even at the panel-row scale, there are distinct heterogeneous effects of solar PV installations on water movement through the landscape.

The kinetic energy and velocity of water droplets also change (both in magnitude and in distribution) as a result of solar cover. The angled panel-rows create a “rooftop effect” at the dripline region, focusing precipitation and kinetic energy into a much smaller area than what it would have fallen. Depending on ground cover, scours or depressions can be created that raise concerns for sediment loss and stormwater runoff (Baiamonte et al., 2023; C. S. Choi et al., 2020; Devitt et al., 2020; Elamri, Cheviron, Mange, et al., 2018; H. Liu et al., 2023; Shobe, 2022; Walston et al., 2021; F. Wang & Gao, 2023). This effect can worsen if topsoil has been removed (grading) and site construction has led to compaction and thus loss in soil structure and macropores (C. S. Choi et al., 2020; Lambert et al., 2021) and if panel-row faces are aligned with runoff flow direction (Baiamonte et al., 2023; Edalat, 2017). These erosional forces are largely mitigated by retention of topsoil and soil structure (C. S. Choi et al., 2023), retaining or establishing vegetation (often deeply rooted vegetation such as native grasses) (Cook & McCuen, 2013; GPI, 2023;

Walston et al., 2021; Yavari Bajehbaj et al., 2024), and by effective stormwater management plans that reduce surficial hydrological connectivity (Baiamonte et al., 2023; GPI, 2023; H. Liu et al., 2023; Yavari et al., 2022). Although distinct from vegetation establishment or retention, revegetation may not mitigate effects of site construction for many years if at all, suggesting that the best practice in stormwater runoff and erosional management is low-impact site development and vegetation retention if available (C. S. Choi et al., 2020, 2023). It is also important to note, regarding concerns for stormwater runoff, at least 12 US states have solar-specific required stormwater management plans, with the remainder most often deferring to general stormwater management plans for any construction related operation under the US Environmental Protection Agency (EPA) (US EPA, 2015) and the EPA's National Pollution Discharge Elimination System (NPDES) (Yavari et al., 2022). These unique water and energy balance regimes created by different mount technologies are conceptually depicted as distinct "model" regions in Figure 1.

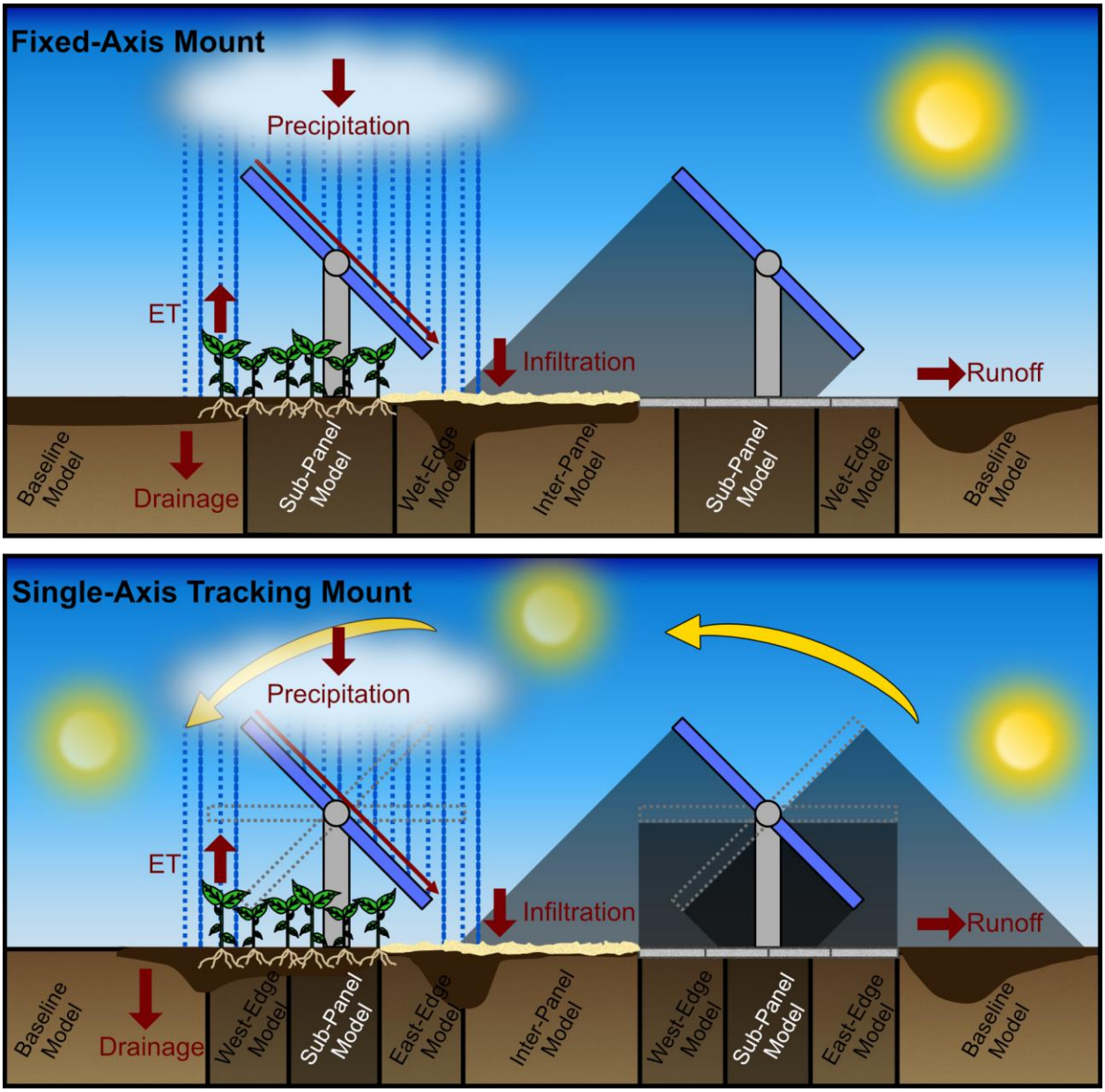

Figure 3. Conceptual water and energy balance regimes by mount. Distinctions in water and energy balance regimes between fixed- and single-axis mounts are empirically affirmed by studies (C. S. Choi et al., 2023; Sturchio, Kannenberg, Pinkowitz, et al., 2024; Yavari Bajehbaj et al., 2024). Note that East-Edge zone indicates a region of higher stomatal conductance compared to the West-Edge zone as reported in existing studies (Sturchio et al., 2022; Sturchio, Kannenberg, Pinkowitz, et al., 2024). Both mount configurations depict variations in ground cover from left to right: vegetated, barren, impervious.

1.4.2: Attributing changes in hydrology to solar at the watershed-scale

While several hydrological impacts of solar energy have been conceptually scaled from plot- to watershed-scale, few studies have measured or modeled impacts based on emergent

behavior with clearly defined mechanisms for scaling. As a result, many of these effects remain theoretical. Regardless, it is important to consider both the direct and indirect impacts of a shifting energy landscape and how those effects might accumulate at larger scales.

In addition to altering the physical landscape, solar energy installations can create regional hydrology and water use opportunity costs, which are not often discussed in water use reviews of solar energy (Moore-O'Leary et al., 2017). In water scarce regions, several approaches with transformative hydrological potential have been proposed. For example, if irrigated farmlands sourcing groundwater from agriculturally impaired watersheds are converted, there is significant potential for water use savings (S. Curtis et al., 2020). This practice has already been observed in California, where we recently (Stid, Shukla, et al., 2025) quantified the potential reduction in irrigation water use (~6,000 m^3 ha^{-1} yr^{-1}) through the adoption of agriculturally co-located solar installations (agrisolar) and more broadly agrisolar-moderated (in regard to farmland owner income) following irrigated land. Additionally, recent landowner interviews have affirmed that this is indeed a consideration for farmers, who are operating under legislation requiring significant water use reduction within the next two decades (Biggs et al., 2022). Even if crop-production persists on the converted land (agrivoltaics), reduced crop water requirements and focused or collected precipitation can turn irrigated agriculture into rainfed agriculture in some regions for some crop types (Parkinson & Hunt, 2020; Şevik & Aktaş, 2022; Warmann et al., 2024).

Beyond offsetting irrigation water use, recent work (McKuin et al., 2021) has suggested that covering California's extensive canal system (6,350 km) of transported surface water with solar could result in reduced evaporative losses of 39,000 m^3 km^{-1} yr^{-1} of canal covered. Another exciting management opportunity is employing solar land use for managed aquifer recharge (MAR) (Rößner, 2022) MAR is a relatively new water security pathway by which excess stream and flood waters are artificially stored in aquifers with immense storage capacity, often a result of intensive irrigation and water use (Dahlke et al., 2018). In California, a severe multi-decadal drought followed by the 2023 flooding events have gained this artificial storage method attention and now may be an opportune time to begin implementation of Solar-MAR study sites.

There is also a significant potential for water-use offset if the shut off water-intense thermoelectric electricity production is attributed to solar (Arent et al., 2014; Macknick & Cohen, 2015). Attributing the shut-off of hydroelectric dams to solar might also conserve groundwater because of an increase in surface water supply for irrigation (He et al., 2019) and may even lead

to enhanced stream connectivity restoring stream sediment fluxes and unblocking fish migration (S. Sharma & Waldman, 2021). S. Sharma & Waldman (2021) showed that replacing all of the hydroelectric dams in Maine with solar would be feasible by converting only 22% of current reservoir area to solar, leading to no new land use and 78% of reservoir land area returned to what it was prior to damming.

Concerns over runoff-induced erosion and sediment entrainment have been posed beyond local (site-scale) degradation. The greatest concern is regarding grading and compaction (also called earthworks) of large swaths of land for the installation of solar, and the resulting possible loss in ephemeral streams, disturbances to downstream riparian habitats, and connectivity of drainages, rills and microwashes (Grippo et al., 2015; Moore-O'Leary et al., 2017). Grading and compaction removes preferential flow paths that contribute to hydrologic connectivity and reduces infiltration capacity leading to increased Hortonian overland flow (Baiamonte et al., 2023; Barnard et al., 2017; H. Liu et al., 2023; C. Wu et al., 2022).

Many studies and commentaries reporting the concerns described above proposed them as "possible, but in need of further validation and study" (Grippo et al., 2015; Moore-O'Leary et al., 2017; Shobe, 2022). Mier-Valderrama et al. (2024) was one of the first to directly model the effect of site preparation on a watershed actively undergoing preparation and within a potentially high-solar coverage basin (15-30% estimated coverage). Current site conditions reported were loss of vegetation in and around proposed solar sites, grading and topsoil removal, and the presence of generally bare soil. They found that 15-30% solar coverage under these conditions did not significantly change watershed discharge but significantly increased cumulative sediment load (+12 to +30%) and erosion rates relative to assumed soil loss tolerance values (+2.29 tons ha^{-1} yr^{-1}). These effects were due to changes in vegetative cover, land management practices, and agriculturally-relevant runoff potential (curve number) (Mier-Valderrama et al., 2024). Despite these concerns and evidence behind them, there are not yet legally binding requirements requiring low-impact site development beyond guidance documents (GPI, 2023; McCall, Daw, et al., 2023; McCall, Macdonald, et al., 2023; NREL, 2020; USDA NRCS, 2024).

1.4.3: Studies approaching emergent behavior in solar hydrology

We coded 19 studies and two reports as approaching emergent behavior in study design, methods, results, and/or discussion (Table 1). Common approaches in these studies included existing or experimental plot-scale field data collection and hydrological model calibration using

SWAT (Pisinaras et al., 2014), HEC-HMS (Barnard et al., 2017; Edalat, 2017), HYDRUS (Elamri, Cheviron, Mange, et al., 2018; Galzki & Mulla, 2024; GPI, 2023; McCall, Daw, et al., 2023; Mulla et al., 2024), EPA SWMM (Gullotta et al., 2023; Nair et al., 2024), or experimental models (Baiamonte et al., 2023; Cook & McCuen, 2013; Elamri, Cheviron, Mange, et al., 2018; H. Liu et al., 2023). We have included results from these studies independently in plot or watershed-scale sections where relevant, and synthesize important concepts approaching emergent behavior here.

Cook & McCuen (2013) is the earliest and one of the most comprehensive hydrological study designs to-date. Cook & McCuen (2013) produced a theoretical rainfall-runoff model in MATLAB numerically solving for the water balance for pre- and post-solar conditions. The model accounts for the increased kinetic energy as a function of rainfall velocity and panel slope and a range of ground covers (gravel, native vegetation, and a down-slope buffer strip). If a native grass was retained as ground cover, Cook & McCuen (2013) found no significant effect on runoff volume, peak discharge, or time to peak. Although peak discharge was higher and quicker, the increment of change was not enough to warrant stormwater management (Cook & McCuen, 2013). However, for bare ground and gravel ground covers, peak discharge increased by 100% compared to native grass ground cover.

Elamri, Cheviron, Mange, et al. (2018) developed a rain redistribution model called AVrain to route rainwater to the ground and used the Hydrus-2D unsaturated zone model to route water in the soil. They showed that lateral dispersion resulted in lower soil moisture heterogeneity than the heterogeneity in rainwater distribution. Importantly, Elamri, Cheviron, Mange, et al. (2018) agreed with Cook & McCuen (2013) that under bare soil conditions, splash erosion from the increased rainfall intensity and kinetic energy creates preferential pathways for increased overland flow.

Barnard et al. (2017) used HEC-HMS and FLO-2D models to simulate infiltration, overland flow, and runoff in two proposed solar sites in Texas and Georgia. They emphasize the importance of 2D models in representing flow paths and velocities associated with solar land use change, but importantly report worst case scenarios for scour depths of 0.6 to 0.7 ft (Barnard et al., 2017). Bringing those concepts together, Edalat (2017) showed that if those erosion pathways were parallel with the hillslope, there is a possibility that the overland flow may lead to increased runoff and stream discharge.

Jahanfar et al. (2020) conducted a green roof solar study and found that solar-integrated green roofs were less effective at reducing stormwater discharge and peak runoff due to rainwater

redistribution at the dripline. Wang & Gao (2023) also noted the erosion pathways with splash sediment deposition behind the dripline, and erosion in-front of the dripline. At the experimental slope's outlet however, the PV slope in Wang & Gao (2023) study produced drastically less erosion and delayed runoff and "flood" timing due to overland flow attenuation within the dripline depression. This agreed with Elamri, Cheviron, Mange, et al. (2018), showing that PV rainfall interception reduced under-panel erosion. A concern of the Wang & Gao (2023) study design (which they point out) is their small-experimental scale (4 m^2 "hillslope"). Additionally, numerous studies used runoff coefficients (curve numbers) and explained their logic in CN selection (Barnard et al., 2017; Galzki & Mulla, 2024; Jahanfar et al., 2020; Mier-Valderrama et al., 2024; Pisinaras et al., 2014; Walston et al., 2021).

At the same agrivoltaic site as Elamri, Cheviron, Mange, et al. (2018), Marrou, Dufour, et al. (2013) and Marrou, Guilioni, et al. (2013) calculated "deep fluxes" as capillary rise or drainage. Although they report no significant drainage losses across the growing season, early season increased irrigation did lead to increased drainage. Capillary rise, however, significantly contributed to the crop water balance. C. Wu et al. (2022) accounted for this drainage in physical models of the hydrologic budget, explaining the field capacity exceedance leading to drainage losses.

Tanner et al. (2020) performed PV-analog data collection for several semi-arid desert sites and quantifying effects on plant communities. In well-drained high conductivity soils, soil moisture retention was extremely low (and thus non-beneficial for plants) due to drainage and deep percolation (Tanner et al., 2020). Merging these concepts together with the highly studied field of agrivoltaics, vegetative ground cover is a double-edged sword when it comes to drainage. More drainage means more return to groundwater systems, which would be beneficial in overdrawn agricultural lands. However, since drainage directly impacts water yield for sub-array plants (Walston et al., 2021) well-drained coarse texture soils are not optimal for vegetative growth.

Although change in terrestrial ET has been discussed as a plot-scale dynamic, Chen et al. (2024) was the first to empirically measure a regional change in water balance (ET) as a result of ten utility-scale solar arrays in China. Using MOD16 satellite data and the Penman-Monteith method for estimating potential ET (PET), Chen et al. (2024) found that solar significantly reduced ET by 3% to 18% post-installation. They up-scaled their approach to estimate the change in PET due to potential future solar coverages of 10, 30, and 50%, albeit these are considerably higher

than the 1.8% of China's land surface likely required to meet net-zero requirements (Ji et al., 2022).

A recent collaboration between the Great Plains Institute (GPI), the National Renewable Energy Laboratory (NREL), the University of Minnesota, and Fresh Energy has created the PV Stormwater Management Research and Testing (PV-SMaRT) project with the aim of creating and disseminating tools and best practices for stormwater management at ground-mounted PV sites (GPI, 2023). The backbone of the technical component of this project is the vadose zone modeling software HYDRUS-2D/3D, which the team uses along with experimental site data from five existing arrays (soil moisture, rain gauge) to model soil moisture and stormwater runoff accounting redistribution of precipitation and site specific physical characteristics such as soil texture, soil depth, bulk density, vegetative cover, solar panel designs, and climatic factors (Galzki & Mulla, 2024; Mulla et al., 2024). They also emphasize that solar is not a continuous impervious surface but is a discontinuous impervious surface and should thus be planned for and managed differently (Mulla et al., 2024). The team has created and shared a publicly available and easy to use stormwater runoff calculator allowing for rapid estimation of NRCS stormwater runoff curve numbers (CN) (Galzki & Mulla, 2024).

The PV-SMaRT team also compared their modeled stormwater runoff outcomes with another critical modeling effort that used the US Environmental Protection Agency's storm water management model (SWMM), which was used to simulate 100-year storm runoff events (and others) and change in runoff as a result of a solar installation (Gullotta et al., 2023; Mulla et al., 2024; Nair et al., 2024). Although fundamentally different, both modeling efforts found that solar increased modeled runoff or outflow by ~14% during large storm events, with the EPA SWMM studies finding no runoff impact during smaller events. Both also noted that antecedent and post-construction physical soil properties (e.g., soil depth, bulk density, and texture) and array design (e.g., panel-row orientation in regard to topographical slope) play a critical role in generating runoff (Galzki & Mulla, 2024; Gullotta et al., 2023; Mulla et al., 2024; Nair et al., 2024). Thus, these dynamics should be key considerations for future solar siting and construction. One takeaway is clear from both groups, better (and freely available) models of stormwater runoff can help reduce project costs, both before construction and during operation, of stormwater management design.

Before Yavari Bajehbaj et al. (2024), there were no studies that directly measured or validated with field data on the hillslope, catchment, or watershed-scale impacts of existing solar energy installations regarding the proposed benefits or concerns of this section. There are a few

preceding studies with small-scale experimental results (Baiamonte et al., 2023) and modeled behavior calibrated with plot-scale field measurements (Mulla et al., 2024), but none had directly measured change in the connected hydrological landscape beyond the solar site as a result of solar installation. Yavari Bajehbaj et al. (2024) collected field data on soil moisture, ET, and runoff at two existing solar farms with vegetation and infiltration basins (trenches). Conferring existing plot-scale findings, the study reported that solar arrays redistribute water and energy resulting in unique zones of altered soil moisture, with the drip edge being the most important (greatest increase in soil moisture) for understanding runoff generation at a site. Vegetation at their array was established by perennial grasses that were taller in the inter-row spacing than the under-panel region. The infiltration basins successfully conveyed runoff from the sites, although the lack of control prevents comparison of basin effectiveness and relative runoff volume.

Baiamonte et al. (2023) was also innovative, using physical models to characterize a suite of runoff generating processes, although within a small experimental test-plot (two small proxy panels) and a rainfall simulator. Baiamonte et al. (2023) compared a control bare soil slope (14%) with solar panel-rows perpendicular and parallel (panel-row faces) to slope direction. Key insights from this were that both panel-row orientations increased runoff comparably (11.7- and 11.5-times control slope for panel-row facing perpendicular and parallel to surface slope respectively) and that time to runoff is shorted by 50% to 25% relative to bare soil for the orientations respectively. This was also the first study to use physically-based models to extend (up-scale) these micro-hillslope measured effects to a longer hillslope, finding increased change in runoff volume and time to runoff (except for parallel panel-row alignment) with longer hillslopes.

Liu et al. (2023) was the first to directly address the concept of hydrological connectivity (HC), defined as water-mediated transport of matter, energy and/or organisms within or between elements of the hydrological cycle at an existing utility-scale solar array in Wuzhong, China. Essentially, HC is a form of emergent behavior. Liu et al. (2023) introduced a novel model, the Solar-Farm model (SOFAR), to simulate the ecohydrological effects of large-scale solar arrays on HC and soil erosion. The study found that runoff (99%–154%) and erosion (21%–76%) were both significantly increased during construction and operation of solar arrays, with the greatest effect occurring near river channels and with lower vegetative cover. Liu et al. (2023) posit a positive feedback loop, whereby enhanced runoff from increased soil erosion and sediment transport to river networks, increasing HC, leading to more runoff.

1.4.4: Current and future solar coverage of watersheds in the US

Pisinaras et al. (2014) used the SWAT Model to and climate projections to simulate long-term (90-years) changes in surface runoff as a function of solar-watershed coverage. While more solar coverage (1 to 5%) within watersheds did lead to increased runoff and percolation potential, the impact of reductions in site preparation intensity decreased with more solar coverage (Pisinaras et al., 2014). This begs the question, to what extent does current or future solar impact watersheds? Figs 2 and 3 show the solar watershed (HUC10) coverage of current (through 2018) solar direct area and a possible solar buildout for net-zero electricity needs by 2050 respectively. As of 2018, the Kruitwagen et al. (2021) solar dataset contained 6,342 ground-mounted solar arrays ranging in size from 379 m^2 to 23 km^2 with a total land cover area of 654 km^2. The Net-Zero American (Jenkins et al., 2021) solar dataset contained 9,294 ground-mounted solar arrays ranging in size from 2,752 m^2 to 352 km^2 with a total land cover area of 61,200 km^2. The median watershed solar coverage of existing installations was 0.016% with a max of 3.4%. The median watershed solar coverage for the highest projected solar coverage (100% renewable by 2050) was 2.0% with a max of 56%. Albeit the high values for the projected solar coverage seem extreme given existing infrastructure, Mier-Valderrama et al. (2024) provide an already under construction example of a watershed with 15% to potentially 30% of a watershed being covered with solar energy land use. Some future watersheds will experience high solar coverage.

The purpose of creating these maps is two-fold. First, watersheds with intensive existing solar coverage (>1%) can be the first to develop management plans to optimize stormwater management and recharge management. Monitoring and modeling results of these management plans (pre- and post-treatment) will provide insight into which plan works best for a given region's water needs. Second, watersheds with extensive future coverage (>5%) can be the focus of pre- and post-solar installation data collection and models. Performing such models may inform placement prior to the installation of the systems themselves to suit a region's needs.

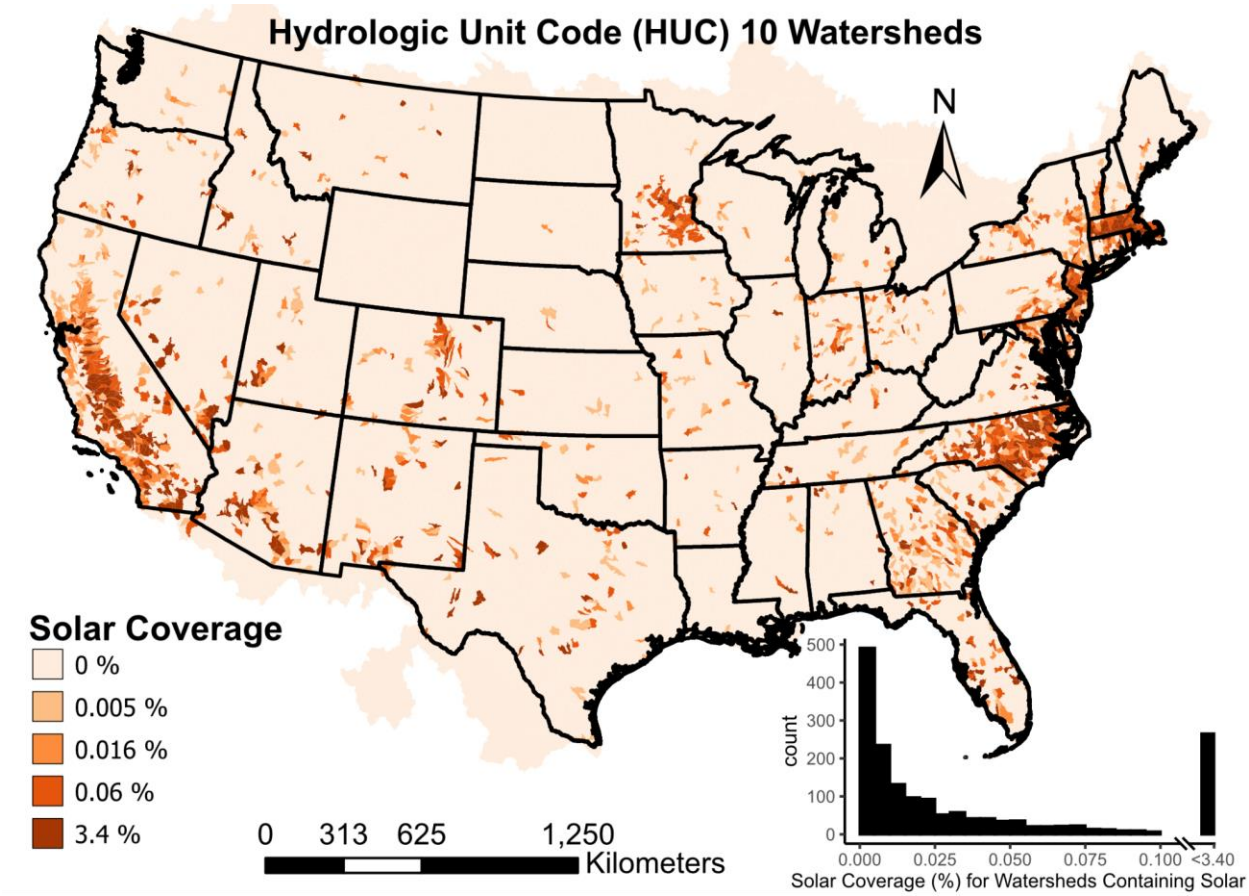

Figure 4. Solar land footprint of HUC10 watershed area through 2018. Current solar areas were downloaded from Kruitwagen et al. (2021) reported solar shapes and watershed boundaries were downloaded from USGS Hydrologic Unit maps. Note that the histogram contains solar coverage for only the 1,719 (of 18,853) watersheds containing ground-mounted solar.

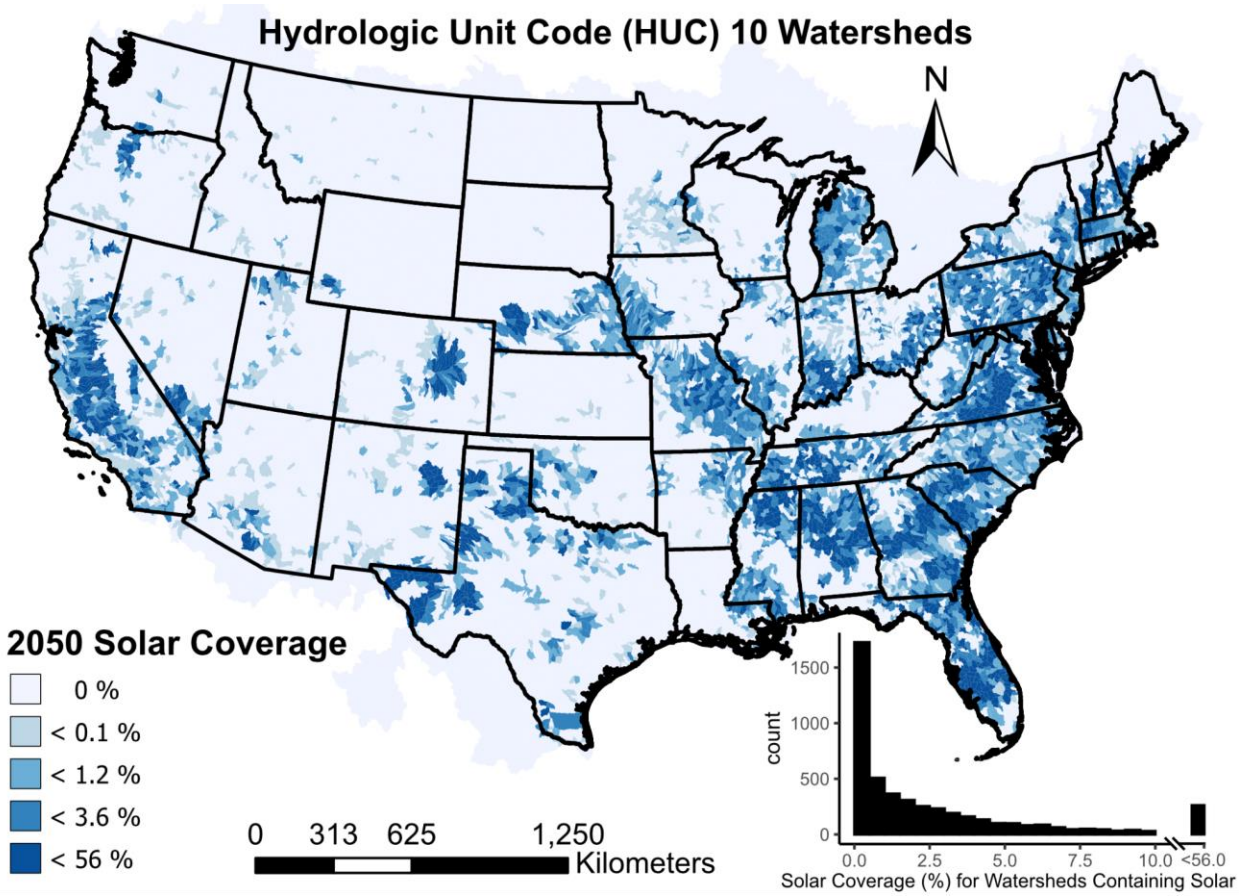

Figure 5. Future solar area coverage of HUC10 watershed area. The future solar land footprint was downloaded from Net-Zero America (Jenkins et al., 2021) reported solar shapes for the 100% renewable (RE+ E+) scenario, current solar land footprint from Kruitwagen et al. (2021), and watershed boundaries were downloaded from USGS Hydrologic Unit maps. Note that the histogram contains solar coverage for only the 3,535 (of 18,853) watersheds containing ground-mounted solar.

1.5: Simulating hydrological fluxes with limited information: A thought experiment

A 2.3 km^2 utility-scale single-axis solar array would equate to approximately 160 MW_{DC} based on a simple area to capacity relationship from Fujita et al. (2023). An array this size in Michigan could supply electricity to between 30- and 40,000 homes assuming a household average electricity use of 10.6 MWh yr^{-1}. Regarding control model performance (low-impact scenario, assuming no change in model inputs from solar coverage), head residual (simulated minus observed hydraulic head) root mean square error (RMSE) and mean absolute error (MAE) were 5.47 m and 3.87 m respectively. Residuals were spatially random, except for a clustering of high head residuals in the southwest portion of the extended model boundary (Figure A29). This may be due to erroneously high starting head biases derived from the DTW product (Zell & Sanford,

2020) (shown in Figure A30), or inaccurate low HK values on the border of this region (Figure A1.2). Residuals relative to recharge (Figure A31) and HK (Figure A32) were homoscedastic. Residuals at observation wells were high for low observed heads and low for high observed heads, possibly contributing to the assumption that starting heads in the southwestern portion of the model boundary were too high (Figure A33). Since this region was outside our area of interest, these residuals are not of concern for our modeling purposes. The average streamflow in the model year 2013 at the downstream USGS Stream Gauge for the Kalamazoo River at Comstock was 37.39 cubic feet second^{-1} (cfs), while computing modeled streamflow resulted in an annual average streamflow of 35.41 cfs, well within the quartiles for the stream gauge (Figure A34).

We simulated the change in heads and streamflow as a result of two different installation and management scenarios described by the literature: low- and high-impact. We use this model to provide an estimate on the potential consequences of improperly managed utility-scale solar in humid, high-water table, potentially flood-prone regions like Michigan's southwestern Lower Peninsula. This model is one of the first to consider groundwater fluxes in relation to solar installation and design practices. It is essential to note that this is an uncalibrated, single-year, steady-state groundwater model for a counterfactual solar installation with inherently erroneous assumptions, specifically regarding the redistribution of recharge due to solar practices (Figure 2 and Figure A26). We did not consider any surficial processes, applying literature values from one study for the change in runoff and recharge as a result of high-impact solar design and management. We also assumed there were no stormwater management controls outside of site preparation and management, which is also counterfactual given that most states, including Michigan, require stormwater management plans at utility-scale solar installations such as infiltration basins (PA 233 of 2023, 2024; Yavari et al., 2022).

We also made several assumptions about the low-impact and high-impact site preparation and management scenarios. While the assumed preparation and management variables are conceptually reasonable (e.g., high-impact: soil compaction and topsoil removal leading to reduced infiltration, shading and vegetation removal leading to decreased ET, low-impact: topsoil conservation efforts and vegetation lead to maintained ET and infiltration), how those variables manifest in quantitative changes in infiltration, ET, and drainage are not well understood or constrained by available studies and data. We have also not considered system design (aside from single-axis tracking mounting).

With these constraints in mind, covering 2.5% of the Augusta Creek Watershed's area with high-impact solar land use resulted in an estimated change in the hydrologic budget of 35,000 m^3 yr^{-1}. This change in budget created up to a 5% (18 m^3 day^{-1}) increase in downstream flows (Figure 6B), a 0.07 m increase in onsite heads (Figure 6A), and a 1-3% decrease in upstream depth to water (DTW) (Figure 7). Note that the average DTW in the watershed was ~7 m.

Thus, a takeaway from this simulation is that high-impact solar management may not lead to a significant change in absolute head but could lead to increased instances of upstream or downstream flooding in shallow flood-prone systems, an effect that could worsen with the alteration of rainfall intensity under a changing climate. Importantly, Liu et al. (2023) also found the greatest potential for increased erosion rates and hydrological connectivity occurred closer to river channels. Our counterfactual array was within 500 m of both the upstream and downstream segments of Augusta Creek.

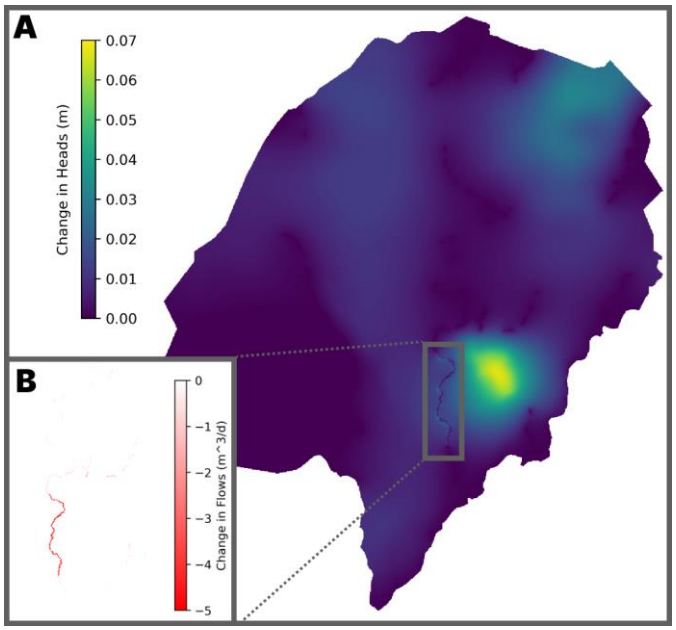

Figure 6. Comparison of development scenarios on hydraulic heads and streamflow. Change was considerd high-impact minus low-impact. Note that negative changes in streamflow indicate a greater flux out (negative) of the model region for the high-impact scenario (B). Heads displayed here are from the first (top) layer of both simulations.

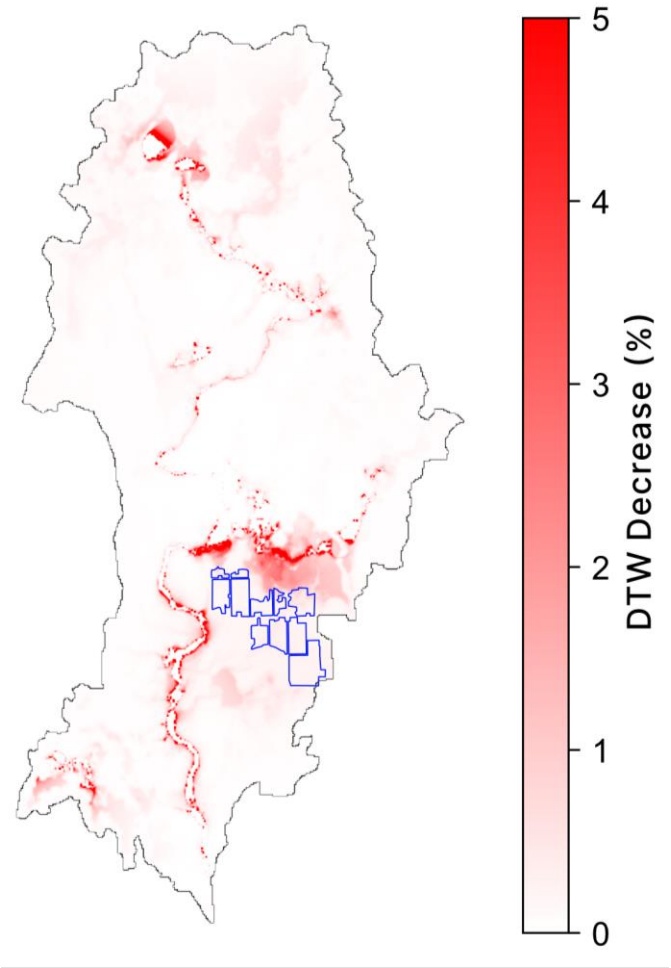

Figure 7. Change in DTW within the Augusta Creek Watershed across scenarios. Change is the depth to water (DTW) with the high-impact scneario reltaive to the low-impact scenario. Note that change in depth to water (DTW) is in percent (%).

Although we did not attempt to incorporate surficial and vadose zone hydrology, the lack of available data and knowledge on how solar coverage affects vadose zone hydrology and how those effects emerge in groundwater hydrology prevents the inclusion of such models, at least in a simple thought experiment simulation such as this. Importantly, no studies have incorporated groundwater flow in their measurement or modeling efforts, making it impossible to compare results and limitations of this thought experiment.

To properly represent how low-impact and high-impact solar land use alters surficial and vadose zone hydrology in the region, we would need a physical model of rainwater and energy redistribution based on more developed design information (e.g., mount technology, panel-row spacing, panel-row orientation in respect to topographical slope). We would also need to better

understand variation in soil texture across the region (sandy to loamy) would respond to greater instances of saturation and hydrological conductivity to reveal if downstream runoff could increase to the rate that Pisinaras et al. (2014) predicts. Importantly, data available for vadose zone hydrological responses (e.g., soil moisture) to solar do not broadly exist beyond initial data provided by a few innovative groups (Kannenberg et al., 2023; Sturchio et al., 2022; Sturchio, Kannenberg, Pinkowitz, et al., 2024; Yavari Bajehbaj et al., 2024). Although these groups are filling an essential gap, there is not yet enough available data or knowledge to calibrate a process-based model using existing resources. Additionally, stormwater management plans would be required by EPA's NPDES and more recently in Michigan, PA 233 of 2023 (PA 233 of 2023, 2024) meaning runoff would be captured and rerouted to recharge (likely within an infiltration basin). Ultimately, we need to better understand how the change in surficial water balance at existing solar facilities materializes in groundwater heads and streamflows, across a variety of landscapes and climate zones.

1.6: Frontiers in solar hydrology and knowledge gaps preventing large-scale assessments

Solar hydrology is a rapidly evolving field. More than a third of the peer-reviewed studies in this review have been published since 2023. Rapid scientific exploration and understanding are critical given the pace of installation required to achieve net-zero by 2050. However, there remain key knowledge gaps in the field preventing a comprehensive understanding of how solar energy landscapes alter hydrological cycles, particularly across scales. There are also new technologies, designs, and management practices that go beyond mitigating the negative effects of land use change to restore or manage existing natural resources and ecosystem services. For example, MAR is an exciting new technique for mitigating flood concerns and regenerating storage in overdrawn aquifers and should be further explored within solar landscapes. Thorough investigation of these opportunities can enhance adoption and speed the transition to net-zero.

1.6.1: Limitations of solar infrastructure metadata and open hydrological data

The articles assessed in this review make clear that the solar energy landscapes cannot be simplified to impervious surfaces. Solar creates a unique disconnected impervious surface that fundamentally alters where and how water and energy traverse to the ground surface. This alteration is highly dependent on solar infrastructure design. A lack of solar design metadata prevents the upscaling, comparison, and generalization of many of the hydrological effects shared

here. Key design metadata includes site location, extent, total area transformed, total panel-row area, orientation, tilt, packing, height, mount technology, prior land use, ground cover practices, soil types, construction practices, stormwater management plans, and numerous other place-based metrics that will vary from region to region. Acquiring comprehensive and high-quality metadata on these attributes and sharing them publicly as an open access database is important to a scalable real world understanding of how the solar energy landscape alters hydrological functioning. There would also be value in standardizing reporting of these metrics in studies on individuals or groups of arrays. There is a need for an open and regularly updated database and literature knowledgebase on many of these attributes to fully realize the benefits of the solar buildout and minimize potential negative consequences.

In addition to reporting solar design attributes, we see the need for focused in situ data collection of solar treatment hydrological data and sharing amongst a shared global database. The Innovative Solar Practices Integrated with Rural Economies and Ecosystems (InSPIRE) initiative through the DOE and NREL initiated a project like this for agrivoltaics specifically (NREL, 2025). The InSPIRE group's mission should be broadly accepted, deployed across numerous solar sites across the U.S. and internationally, and should be a database for agrivoltaic and non-agrivoltaic hydrologic datasets. As mentioned, there are a few key groups participating in open data sharing for metrics like soil moisture and soil physical characteristics (Kannenberg et al., 2023; Sturchio et al., 2022; Sturchio, Kannenberg, Pinkowitz, et al., 2024; Yavari Bajehbaj et al., 2024). Once these data are available, we will need scalable and reproducible approaches to model a suite of existing and future design scenarios (Gullotta et al., 2023; Warmann et al., 2024; Williams et al., 2025). These gaps prevent high-fidelity modeling and calibration efforts, as displayed with our thought experiment using MODFLOW.

1.6.2: The value of comparative assessments and treatment-control replicate study designs

Studies that compare solar siting, design, management practices, or spatial effects (e.g., unique soil moisture zones–Figure 3) treatments provide the capability of attributing hydrological changes to the treatment itself as opposed to another confounding variable. Several studies in this review compared hydrology components under different experimental treatments. Walston et al. (2021) was the largest agrivoltaic study assessing the ground cover consequences of 276 solar arrays across the Midwestern United States. Specifically, Walston et al. (2021) modeled soil moisture, surface runoff, and erosion consequences between pre-solar agricultural land use, with

post-solar turfgrass ground cover, and native grass ground cover. C. S. Choi et al. (2020) and Jahanfar et al. (2020) compared hydrologic conditions under different antecedent conditions. Baiamonte et al. (2023) was the first to empirically compare the effect of panel-row orientation on infiltration-excess overland flow while controlling slope and ground cover. Several studies (C. S. Choi et al., 2023; Cook & McCuen, 2013; Pisinaras et al., 2014; Williams et al., 2023) compared surface hydrology dynamics (ET, surface runoff, and percolation) between agrivoltaic or native grass ground covers and bare soil. This is of particular value given that a vast majority of solar in the US is likely barren or sparsely vegetated given the cost of management (Feuerbacher et al., 2021; Fujita et al., 2023; McCall, Macdonald, et al., 2023; NREL, 2025; Stid, Kendall, et al., 2023) and lack of policy direction or cost support to vegetate these sites. Displaying the costs of bare soil, gravel, and impervious surface ground cover relative to agrivoltaics from the lens of hydrology may be a pathway to motivate acceptance of agrivoltaic management practices to reduce stormwater runoff both at the local and national scales.

One further suggestion for future comparative studies is to employ a treatment, treatment control, and a control (non-solar or pre-solar). Several studies use a nearby plot of land that is non-solar as a control, which still provides valuable insight, but it becomes difficult to attribute hydrological impacts to how solar changes the landscape vs. how the treatment (e.g., graded vs. non-graded, vegetation vs. bare soil, fixed- vs. single-axis, full-density vs. half-density packing, arid vs. humid climates) affects the landscape and hydrology. One type of treatment-control study design that is sparse in the reviewed literature is before-and-after (solar installation) studies. For example, Edalat (2017) was able to compare pre- and post-installation effects on peak flow and peak flow time relative to the impacts of site preparation and antecedent soil moisture in their theoretical solar watershed in Nevada. Studies like Yavari Bajehbaj et al. (2024) fill some of the most critical gaps in data acquisition, availability, and a real physical understanding of mechanisms (like saturation at the dripline) leading to hydrological processes. However, Yavari Bajehbaj et al. (2024) did not compare watershed-scale dynamics pre- and post-solar installation or with bare soil and vegetation.

There is a clear need for foundational experimental solar facilities with plot-replicate treatment and control study designs and comprehensive pre-installation characterization to compare various solar construction and management practices. Additional common catchment and watershed study designs to inform our understanding of solar energy implications for hydrology

are paired-watershed studies (McDonnell et al., 2018), v-notch or rectangular weir installation to monitor runoff and changes in hydrograph function (Dunne & Black, 1970), and isotope tracers to artificially enrich panel-intercepted waters and determine how rainfall redistribution alters runoff in a given storm event (Sklash & Farvolden, 1979). While a simple pre- and post-installation remote sensing study of the persistence of ephemeral streams may also give insight to prolonged drying, extensive modeling approaches may be needed to pick apart causality between solar being installed and climate change induced reductions in stream connectivity (Ward et al., 2020).

1.6.3: A holistic understanding of direct and indirect effects

Most of the existing literature on solar and hydrology reports a change in water balance via direct or indirect impacts, rather than reporting both. Without both, we cannot have a holistic understanding of how solar alters hydrologic functioning. For example, in Stid et al., (2025), we reported that solar arrays converting irrigated cropland (agrisolar) in California's Central Valley resulted in an estimated reduction in irrigation water use of ~6,000 m^3 ha^{-1} yr^{-1}. When extrapolated, Chen et al. (2024) reports a measured change in ET of ~35 mm across ~38 km^2 of ground mounted solar at solar sites of 350 m^3 ha^{-1} yr^{-1}. Although irrigation and ET are inherently interlinked in cropland water balance, future studies should seek to report both direct and indirect changes in inputs and land use opportunity costs to better understand where the water is within this land use change.

1.6.4: Opportunities to expand study design and regional representation

There is a need for more representative study design and more diverse regionality of solar and hydrological studies. Regarding regionality, the study area bias of US landscapes could benefit from a more diverse selection of study sites. More data from more diverse physical conditions across the US will aid in constraining the physical explanation of reported effects. Additionally, arid and semi-arid climates seem to dominate much of the literature, with continental climates only represent 16% of the study distribution and humid climates representing 42%. Solar will be installed in nearly every climate; it is critical to understand how these effects scale under those varying meteorological conditions. For example, the solar arrays assessed by Yavari Bajehbaj et al. (2024) were in a humid continental climate (Dfa), with 84 storm events over just 247 days, making this one of the only studies to collect such data.

Regarding the representation of the complete solar energy landscape, only a few studies

considered regional solar deployment and changes in water balance, with fewer considering more than a few installations (S. Curtis et al., 2020; Stid, Shukla, et al., 2025; Walston et al., 2021). In most regions, solar arrays are numerous beyond this representation of the landscape, potentially underestimating the net effects on a larger landscape. Again, this makes having an openly accessible database of ground-mounted solar installations an incredibly powerful tool to standardize outcome upscaling. Although plot and watershed scale studies typically provide the most insight for emergent behavior, the scale of assessment (plot-, watershed-, and plot- and watershed-scale) was relatively well-distributed (Table 1).

Agrivoltaic solar management is an incredibly powerful method to retain many of the ecosystem services that agricultural land provides while also benefiting solar energy production and farmer economic well-being (Barron-Gafford et al., 2019; Mamun et al., 2022; Walston et al., 2022). Additionally, vegetated ground cover, especially deeply rooted vegetation, reduces potential erosion and sediment loss and may in general mitigate runoff concerns (Cook & McCuen, 2013; Walston et al., 2021). However, much of the existing body of literature has focused only on plot-scale vadose-zone effects (79%) of agrivoltaics. Agrivoltaics are much less represented in watershed (9%) and plot and watershed-scale (32%) studies (Table 1). Thus, more studies on agrivoltaics could include expanding the assessment, measuring, or modeling of plot-scale effects to the hillslope, catchment, and watershed-scale effects as a result of agrivoltaic production.

1.6.5: Considering groundwater and more runoff generation processes

It is clear from the plot-scale studies discussed previously that the energy and water balances of the surface are altered by solar land cover. However, one runoff generation process, infiltration-excess (Hortonian) overland flow, dominated the studies approaching emergent behavior discussed here, with drainage or percolation discussed in part in a few studies. Notably, none directly discussed saturation-excess overland flow (although Yavari Bajehbaj et al. (2024)reported on incidence of saturation and runoff), recharge and flow in groundwater aquifers, or lateral subsurface stormflow, which we have known to be the dominant runoff process for over 50-years (Weyman, 1970). Groundwater dynamics are left out of nearly every study and model design. Groundwater dynamics have long been omitted from hydrological modeling studies and are invaluable to understanding water balances in almost any region of the world (Singha & Navarre-Sitchler, 2022).

1.7: Conclusions

Solar energy will dominate new energy infrastructure in the next three decades. Ground mounted solar arrays change the pathways through which water and energy reach the ground surface and leave it, lettering local, regional, and global water balance. Depending on a suite of site-, construction-, design-, and management-specific conditions, solar energy landscapes can both increase and decrease soil moisture, hydrological connectivity, runoff, time to runoff, erosion, sediment load, streamflow, percolation, peak flow, peak flow time, net primary productivity (of ground vegetation), and ultimately, management of water resources. A large and rapidly growing body of literature has sought to measure and model these effects, yet knowledge gaps remain that need to be addressed early in this energy landscape transition. Filling these gaps is critical, seeing that much of the world's watersheds (in the US, Figure 5) will contain a significant portion of solar coverage in the near future.

Acknowledgements

This chapter was supported by the USDA National Institute of Food and Agriculture INFEWS grant number 2018-67003-27406 (accession No. 1013707). The concepts, approach, and motivation for this chapter originated in discussions and support from Anthony D. Kendall and were further developed in a course project and guidance from Jay P. Zarnetske. Any opinions, findings, and conclusions or recommendations expressed in this publication are those of the authors and do not necessarily reflect the views of the USDA.

CHAPTER 2: A COMPREHENSIVE GROUND-MOUNTED SOLAR ENERGY DATASET WITH SUB-ARRAY DESIGN METADATA IN THE UNITED STATES

Abstract

Solar energy generating systems are critical components of our expanding energy infrastructure, yet available datasets remain incomplete or not publicly available–particularly at the sub-array level. Combining the best freely available datasets in the US with object-based image analysis and machine learning, we present the Ground-Mounted Solar Energy in the United States (GM-SEUS) dataset, a harmonized, open access geospatial and temporal repository of solar energy arrays and panel-rows. GM-SEUS v1.0 includes over 15,000 commercial- and utility-scale ground-mounted solar photovoltaic and concentrating solar energy arrays (186 GW_{DC}) covering 2,950 km^2 and includes 2.92 million unique solar panel-rows (466 km^2). We use these newly compiled and delineated solar arrays and panel-rows to harmonize and independently estimate value-added attributes to existing datasets including installation year, azimuth, mount technology, panel-row area and dimensions, inter-row spacing, ground cover ratio, tilt, and installed capacity. By estimating and harmonizing these attributes of the distributed US solar energy landscape, GM-SEUS supports diverse applications in renewable energy modeling, ecosystem service assessment, and infrastructure planning.

2.1: Background and Summary

High-quality spatiotemporal characterization of solar energy systems (photovoltaic–PV and concentrating solar power–CSP) has historically been sparse, incomplete, or held behind privacy barriers or paywalls. This gap in data availability has hindered regional- and global-scale analysis on a key component of the growing and diversifying energy landscape, and inhibits vigorous solar energy design, distribution, and monitoring investigation. Recently, numerous groups have attempted to fill this gap using remote sensing, manual digitization, crowdsourcing, and machine learning techniques to spatiotemporally characterize solar energy across the globe (Arnaudo et al., 2023; Bradbury et al., 2016; Camilo et al., 2018; Carr et al., 2016; D. Chen et al., 2024; Y. Chen, Zhou, et al., 2024; Clark & Pacifici, 2023; Costa et al., 2021; Dunnett et al., 2020; Evans et al., 2023; Q. Feng et al., 2024; Fujita et al., 2023; Ge et al., 2022; Hou et al., 2019; Hu et al., 2022; Imamoglu et al., 2017; H. Jiang et al., 2021, 2022; Kasmi et al., 2023; Kausika et al., 2021; Kruitwagen et al., 2021; J. Liu et al., 2024; Malof et al., 2016; Mayer et al., 2022; Ortiz et al., 2022; Phillpott et al., 2024a; Plakman et al., 2022; Ravishankar et al., 2022; Stid et al., 2022; Stowell, Kelly, Tanner, Taylor, Jones, Geddes, & Chalstrey, 2020; Tao et al., 2023; J. Wang et al., 2023, 2024; Xia et al., 2023; Yu et al., 2018; X. Zhang et al., 2022; Zhuang et al., 2020). There are also others maintaining databases of value-added attributes for a variety of applications (Barbose et al., 2024; Deline et al., 2020, 2021; EPA, 2024; GEM, 2024; Global Energy Observatory et al., 2021; NREL, 2025; Seel et al., 2024; Thonig et al., 2023; Wolfe, 2012; Xu et al., 2024). However, dataset availability, quality, and completeness (scale exclusivity and metadata coverage) vary widely, leaving key solar energy design information unknown for the broader scientific community. We aim to fill this gap by compiling a harmonized spatiotemporal dataset of ground-mounted solar energy arrays in the United States (US). We go further using high-spatial resolution aerial imagery alongside high-temporal resolution satellite imagery to independently estimate a suite of installation design metadata that contribute new knowledge on the solar energy landscape.

Understanding the location and design of current renewable energy infrastructure allows for more effective modeling, monitoring, and planning efforts for future infrastructure. The United States Large-Scale Solar Photovoltaic Database (USPVDB) is the most comprehensive publicly available, regularly updated, and standardized dataset of georectified utility-scale solar arrays in the US (Fujita et al., 2023, 2024). Importantly, this database contains valuable high-quality

permitting data from US Energy Information Administration (EIA) Form 860 including installation year, installed capacity, mount technology (fixed-axis, single-axis tracking, or dual-axis tracking), tilt, prior land use, agrivoltaic acceptance, and more. Although USPVDB is the current best available solar metadata asset in the US, it does have limitations. USPVDB reports utility-scale ($\geq$1 MW_{DC}) solar PV installations, which comprise the majority of installed capacity in the US (Fujita et al., 2023). However, this database omits the more numerous and distributed commercial-scale (<1 MW_{DC}) solar PV projects (Perry et al., 2024; SEIA & Wood Mackenzie, 2024) and concentrating solar power (CSP) installations. These limitations leave critical data gaps in our understanding of distributed energy resources and the solar energy landscape. There are key differences in the ecosystem service and economic land use trade-offs between commercial- and utility-scale installations (Stid, Shukla, et al., 2025). Proportionally, commercial-scale systems tend to reside more often on cropland than utility-scale installations (Kruitwagen et al., 2021) and experience less regulation and oversight (Gómez-Catasús et al., 2024). Recent work has also shown that EIA Form 860 permitting data can be incomplete or contain errors (Perry et al., 2024) and underestimates the total extent of installed solar energy (Phillpott et al., 2024a) us there is a need for a comprehensive and independent metadata characterization of this rapidly deployed technology.

Kruitwagen et al. (2021) produced the first global and publicly available geospatial dataset of solar energy installations. The follow-on product, the TransitionZero Solar Asset Mapper (TZ-SAM), is an open-access, global, and regularly updated dataset of commercial- and utility-scale solar facilities, derived using machine learning with Copernicus Sentinel-2 imagery (10 m), trained and validated on existing and hand annotated datasets (Phillpott et al., 2024a). OpenStreetMap (OSM), one of the richest geographical databases in existence, also provides access to commercial-scale and utility-scale solar arrays and panel-row data generated by open collaboration–crowd-sourced hand annotation of aerial and satellite imagery (OpenStreetMap Contributors, 2024) that has been used in a number of previous solar data acquisition efforts (Dunnett et al., 2020; Kruitwagen et al., 2021; Phillpott et al., 2024a; Stowell, Kelly, Tanner, Taylor, Jones, Geddes, & Chalstrey, 2020). There are concerns about the spatial quality and consistency of medium-coarse resolution remote sensing and crowd-sourced solar array delineation (Fujita et al., 2023; Hu et al., 2022; Phillpott et al., 2024b). For example, remote sensing and crowd-sourced datasets are known to overestimate the total area of an array due to ambiguous array definitions or to classification of

10 to 30 m satellite imagery (Fujita et al., 2023; Hu et al., 2022; Stowell, Kelly, Tanner, Taylor, Jones, Geddes, & Chalstrey, 2020). Yet, datasets like TZ-SAM and OSM are critical for filling temporal, scale, and reporting bias limitations. Together, USPVDB, TZ-SAM, OSM, and similar high-fidelity spatial delineation and metadata acquisition efforts provide the foundation for understanding the renewable energy landscape and for the dataset presented here.

Solar array siting, management, and design choices have long-term impacts on electricity production, the physical landscape, and related ecosystem services. Most often, available datasets derived on permitting data, remote sensing, or even manual annotation stop at the project or array-scale. However, sub-array design metadata would allow for the scaling of in-depth design and design-impact analyses that are often completed at a single system level (Gómez-Catasús et al., 2024) and thus limited by a lack of high-resolution data. Several modern tools and approaches have been published working to optimize solar designs for electricity production (Gilman et al., 2018; Holmgren et al., 2018; Prilliman et al., 2022; Wagner & Wendelin, 2018), co-production of electricity and vegetation (Jamil et al., 2023; Warmann et al., 2024; Williams et al., 2025) and stormwater runoff (Galzki & Mulla, 2024; Gullotta et al., 2023; McCall, Daw, et al., 2023; Mulla et al., 2024; Nair et al., 2024). Along with numerous other tools, these models are dependent on array location, sub-array panel-row geometry information, mount technology, tilt, ground cover ratio (GCR), and temporal information which have not been widely available collectively prior to this work.

Here, we leverage the best available datasets and databases to compile a comprehensive ground-mounted solar array dataset that is up to date, open access, and not limited to utility-scale capacity. We also compile existing sub-array panel-row datasets and, where available, use high spatial-resolution imagery to delineate new sub-array row objects within solar array bounds. We use this new panel-row delineation to improve existing array and panel-row boundaries, addressing concerns about accuracy and harmonization of manually digitized datasets and coarse remote sensing-derived datasets (Fujita et al., 2023; Hu et al., 2022; Phillpott et al., 2024b). We add value to the dataset by independently estimating several array- and sub-array attributes including installation year, module efficiency, estimated tilt (fixed-axis) for all arrays, inter-row spacing, panel-row width and length, and azimuth, for arrays with harmonized or panel-row information.

The Ground-Mounted Solar Energy in the United States (GM-SEUS) v1.0 dataset contains 15,017 ground-mounted solar PV and CSP arrays covering 2,944 km^2. The dataset includes 9,631

utility-scale arrays composing an estimated 184.2 GW_{DC} and 5,386 commercial-scale arrays composing an estimated 2.1 GWDC, making this the largest publicly available US solar repository to date (Figure 8). For 9,042 arrays (83.1 GW_{DC}), we delineated 2.92 million high-quality solar panel-rows, thus improving array geometries and providing sub-array design metadata. Collectively, the solar panel-row geometries compose 466 km^2 in total panel-row area. Including harmonized metadata, 42% of arrays were fixed-axis, 21% were single-axis, 2.1% were dual-axis, 2.6% were mixed, and 33% were unknown. Solar PV GCR varies with mount type, and on average was 53% for fixed-axis, 42% for single-axis tracking, 50% for dual-axis tracking, and 63% for arrays with mixed mounts (GCR_1). By standardizing the array definition and independently collecting and delineating panel-row information to derive new array boundaries, we also addressed several concerns about coarse remote sensing and crowd-sourced dataset boundary quality.

Several efforts have extracted sub-array design metadata (Arnaudo et al., 2023; Edun et al., 2021; Perry et al., 2024; Perry & Campos, 2023; Ravishankar et al., 2022; Stid et al., 2022), but this is the first endeavor to provide a publicly-available dataset of this magnitude and spatial coverage. Importantly, the dataset is open access with all code and data available for training and acquisition of new array datasets both in the US and other countries. Greater knowledge on global solar PV panel-level distribution would enhance use cases reported here to the global PV market and all impacted landscapes. We intend to update this dataset annually and invite others and endeavor ourselves to continue to introduce new value-added attributes to this dataset.

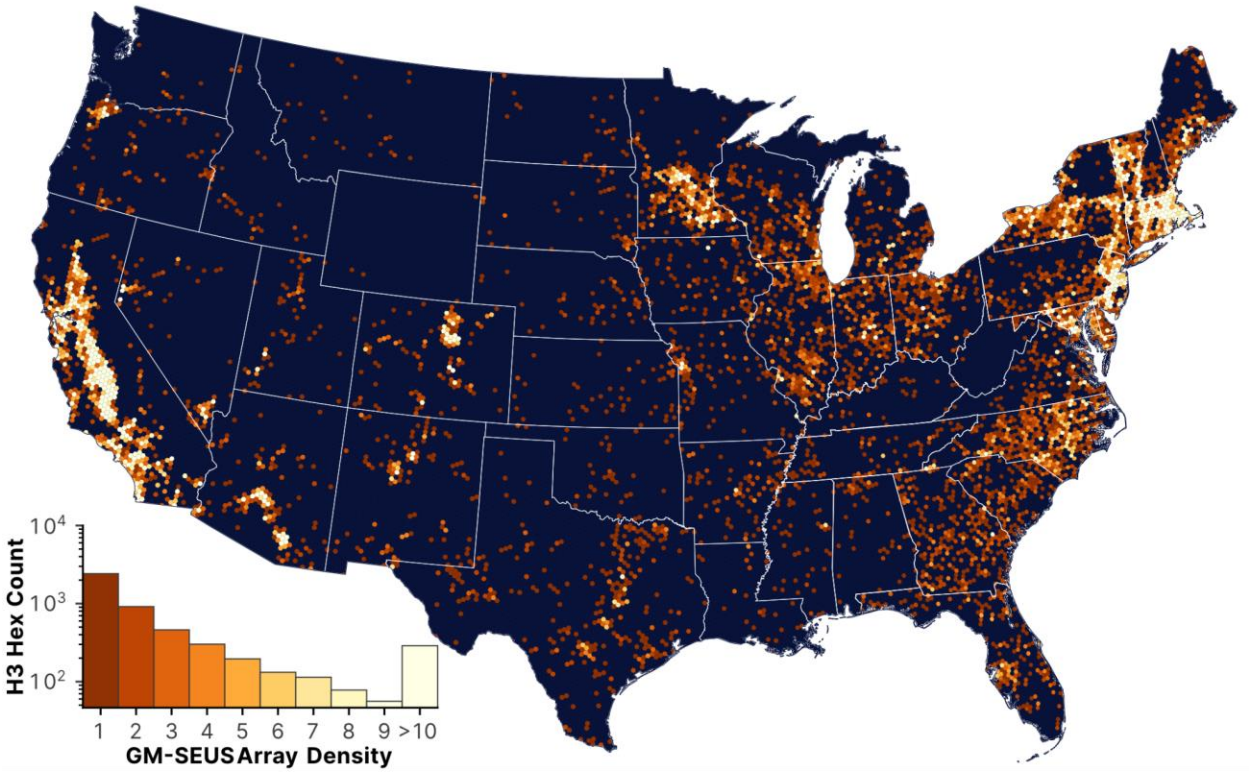

Figure 8. GM-SEUS solar array distribution. GM-SEUS arrays are zonally grouped by number of solar installations within Uber H3 hexagons (resolution 5). H3 hexagons at this resolution have an average area of 253 km^2.

2.2: Methodology

2.2.1: Compiling existing ground-mounted solar datasets in the US

2.2.1.1: Existing solar array data

We compiled a dataset of distributed multi-scale ground-mounted solar arrays across the contiguous US (CONUS) through December 2024. We chose to only use freely available datasets to ensure availability of our results. We used existing ground-mounted solar array datasets in the US that contained explicit array polygons. Each dataset is unique in coverage and metadata completeness and was created for a distinct purpose. We collected data from the following open repositories: The United States Large-Scale Photovoltaic Database v2.0 (USPVDB) (Fujita et al., 2023, 2024), project and panel-row annotations from OpenStreetMap (OSM) (OpenStreetMap Contributors, 2024), the TransitionZero Global Solar Asset Mapper Q3-2024 (TZ-SAM) (Phillpott et al., 2024b, 2024a), a California Central Valley solar PV dataset (CCVPV) (Stid et al., 2022;

Stid, Shukla, et al., 2023), and a Chesapeake Watershed solar dataset (CWSD) (Evans et al., 2021, 2023).

We defined a solar array footprint or boundary as *adjacent, existing, and connected solar panel-rows (PV or CSP) of the same installation year including the inter-row spacing between them* (Figure 9). We spatially joined existing datasets saving geometry information in the order of compliance with this definition: USPVDB, CCVPV, CWSD, OSM, and TZ-SAM, with USPVDB, CCVPV, and CWSD most closely following the provided definition of an array.

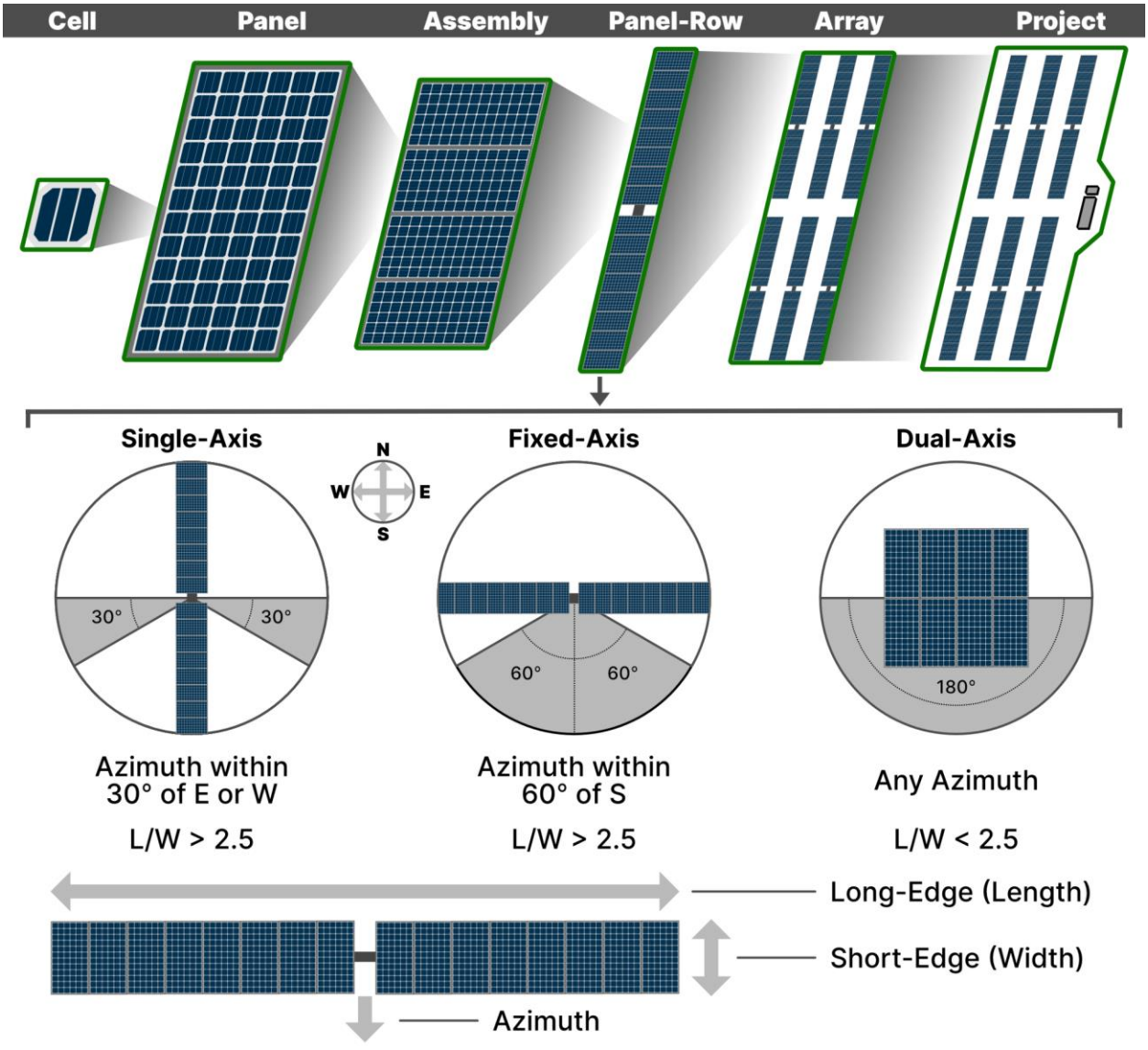

Figure 9. Conceptual hierarchical system boundaries and panel-row metadata logic. Green boundaries indicate the conceptual boundary for each term. This study reports the geospatial and temporal characteristics of panel-rows and arrays. A **panel-row** a spatially-unique collection of one or more panel-assemblies connected by proximity and often sharing one mount, but not

Figure 9 (cont'd)

necessarily electrically connected. An **array** is composed of one or more adjacent rows of the same installation year, and the row-spacing between them. The **cell**, **panel**, **assembly**, and **project** are not the system boundaries focused on in this study. The ratio of the long-edge to the short-edge is the L/W ratio. Azimuth is initially defined as the primary cardinal direction of the short-edge vector (face of the panel-row) in the minimum bounding rectangle in south facing angles given that all solar arrays were in the northern hemisphere.

We also compiled existing value-added solar energy datasets that contained location (latitude and longitude) spatial data without georectified array boundaries. These data were from the following open repositories: the NREL Agrivoltaic Map from the InSPIRE initiative (NREL, 2025), the LBNL Utility-Scale Solar (USS), 2024 Edition report (Seel et al., 2024), the NREL Photovoltaic Data Acquisition initiative (PVDAQ) (Deline et al., 2021), the International Energy Agency and NREL hosted Solar Solar Power and Chemical Energy Systems (SolarPACES) initiative CSP.guru data product (Thonig et al., 2023), Global Energy Monitor's (GEM) Global Solar Power Tracker (GSPT) (GEM, 2024), and The World Resources Institute's (WRI) Global Power Plant Database v1.3.0 (GPPDB) (Byers et al., 2021; Global Energy Observatory et al., 2021). Some of these datasets are also compilations of each other and various existing datasets including the EIA Form 860, Wiki-Solar (Wolfe, 2012), and various other regional and global sources including those used here. We joined these locations with existing array boundaries using a 190 m radius, the distance at which ~75% of solar location data is associated with an existing array (Perry et al., 2024). Again, these input datasets were generated for different purposes and have distinct coverage and metadata completeness and quality.

Table 2. Existing and publicly available datasets of solar energy systems.

Source	Array Info	Row Info	CONUS Count	Region	Scale	Tech	Install Year	Az	Tilt	Mount	GCR	Cap
GM-SEUS	**Poly**	**Poly**	**15,017**	**CONUS**	**Comm & Util**	**PV & CSP**	☑	☑	☑	☑	☑	☑
USPVDB	Poly	✕	4,185	US	Util	PV	☑	☑	☑	☑	✕	☑
CCVPV	Poly	Poly	1,006	CA, US	Comm & Util	PV	☑	✕	✕	☑	☑	☑
CWSD	Poly	✕	1,352	Eastern States, US	Comm & Util	PV	○	✕	✕	✕	✕	✕
TZ-SAM	Poly	✕	12,208	Global	Comm & Util	PV & CSP	○	✕	✕	✕	○	☑
OSM	Poly	Poly	10,531	Global	Comm & Util	PV & CSP	○	✕	✕	✕	✕	○
InSPIRE	Point	✕	571	US	Comm & Util	PV	☑	✕	✕	☑	✕	☑
USS	Point	✕	1,503	US	Util	PV & CSP	☑	☑	✕	☑	✕	☑
SolarPACES	Point	✕	13	Global	Util	CSP	☑	✕	✕	○	✕	☑
PVDAQ	Point	✕	16	CONUS	Comm & Util	PV	✕	✕	✕	✕	✕	☑
GSPT	Point	✕	5,524	Global	Util	PV & CSP	☑	✕	✕	✕	✕	☑
GPPDB	Point	✕	3,248	Global	Util	PV	○	✕	✕	✕	✕	☑

Notes: A ☑ indicates that the reference dataset contains the attribute for a majority of arrays. An ✕ indicates the absence of the attribute in the reference dataset for a majority of arrays. A ○ indicates that the reference dataset contains partial or limited attribute information (see Appendix B Text A2.2). Datasets contain commercial-scale arrays if capacity information exists and at least one array with a capacity of below 1 MW_{DC}, and utility-scale 1 MW_{DC} or above, or if otherwise specified. *Az* indicates the presence of azimuthal direction and *Cap* indicates the presence of capacity information. Note that *Comm* and *Util* are shorthand for commercial-scale and utility-scale solar respectively.

2.2.1.2: Georectifying missing solar array boundaries and metadata

The 190 m georectification distance for missing boundary and metadata attribution is shorter than distances used in similar studies using between 300 m (Stowell, Kelly, Tanner, Taylor, Jones, Geddes, & Chalstrey, 2020) to 400 m (Dunnett et al., 2020). There were 1,616 arrays with value-added reference point data and without georeferenced solar array boundary data within 190 m. For the initial GM-SEUS v1.0, we manually digitized and georectified 126 missing array

boundaries from the NREL Agrivoltaic Map using the most recently available imagery including National Agricultural Imagery Program (NAIP) aerial imagery (USDA FPAC-BC-GEO, 2023), Copernicus Sentinel-2 imagery (ESA, 2024), Google Maps basemap imagery (Google Maps, 2024). We followed digitization logic from Fujita et al. (2023) and our array definition, creating new boundaries that encompass panel-rows and the space between them. If the array geometry was present in the existing solar array datasets but was outside the 190 m radius, we georeferenced information to that shape, and added omitted array boundaries where necessary. Where possible, we investigated context using the array name (when given) in a Google search (which often pointed to InSPIRE, OSM, and GSPT repositories), leading to georeferencing and value-added attribute joining of new and existing objects between 191 m and ~50 km from the provided coordinates. We omitted 27 solar arrays installed after available reference imagery, or without available imagery and context. In total, we added 4.26 km2 of new array area for 34 arrays. We intend to fully delineate and georeference new and remaining 1,490 point data arrays in future version updates.

2.2.1.3: Existing solar panel-row data

To our knowledge, only two data repositories contain large quantities of freely available ground-mounted solar panel-row geospatial data in the US, our recently published dataset of panel-row geometries California's Central Valley (Stid et al., 2022; Stid, Shukla, et al., 2023), and mixed array and panel-row data within OSM, most often tagged with *generator:source = solar* (Dunnett et al., 2020; OpenStreetMap Contributors, 2024). We took guidance and motivation from existing OSM solar data extraction methods to extract and process current solar array and panel-row data from OSM (Dunnett, 2020; Dunnett et al., 2020), although we developed our own independent workflow. Complete polygon data was extracted from both *generator:source = solar* (likely panel-rows) and *plant:source = solar* (likely arrays) from OSM. We separated panel-rows from arrays within both tags by checking geometries with comparable panel-row area and perimeter to area ratios to those panel-rows reported in (Stid et al., 2022). We removed repeat panel objects prioritizing OSM over CCVPV to remove imagery classification biases.

2.2.1.4: A complete reference dataset of existing ground-mounted panel-row and array data

We excluded rooftop solar arrays by removing existing and digitized array boundaries that had more than a 50% areal intersection with the Global Google-Microsoft Open Buildings Dataset

(VIDA et al., 2023), and panel-rows within those array boundaries. Within existing datasets, 1,786 solar arrays and 5,714 panel-row objects were considered roof-mounted and thus removed. The resulting preliminary dataset composed of existing ground-mounted solar arrays and panel-rows contained 14,905 array objects with over 3,056 km^2 in original direct land use area and 1.07 million unique panel-row objects composing 137.3 km^2 in direct panel-row area and 4,470 existing arrays. Prior to enhancing this data, this is the largest freely available dataset of panel-row objects compiled to date.

2.2.2: Deriving new solar panel-row geometries and attributes

We used unsupervised object-based image segmentation and supervised machine learning approaches to acquire a high-quality panel-row delineation within solar array boundaries. NAIP 4-band imagery is the only free and widely available imagery with spatial resolution capable of delineating individual solar PV and CSP panel-rows. NAIP is collected during the primary regional growing season every two to three years at the state-level at 0.3 to 0.6 m resolution (see Figure 10). NAIP digital ortho quarter quads (DOQQ) mosaics are made available in GEE. At the time we wrote this paper, the most recent NAIP DOQQ imagery ranges from 2021 to 2023, depending on the state, flight contracts for specific years, and upload timeline to GEE. During GM-SEUS processing, NAIP 2023 was actively being uploaded to GEE, replacing 2021 imagery in some states. We intend to fully reprocess new imagery and update the product later in 2025. NAIP imagery dates used in the development of GM-SEUS are shown in Figure 10.

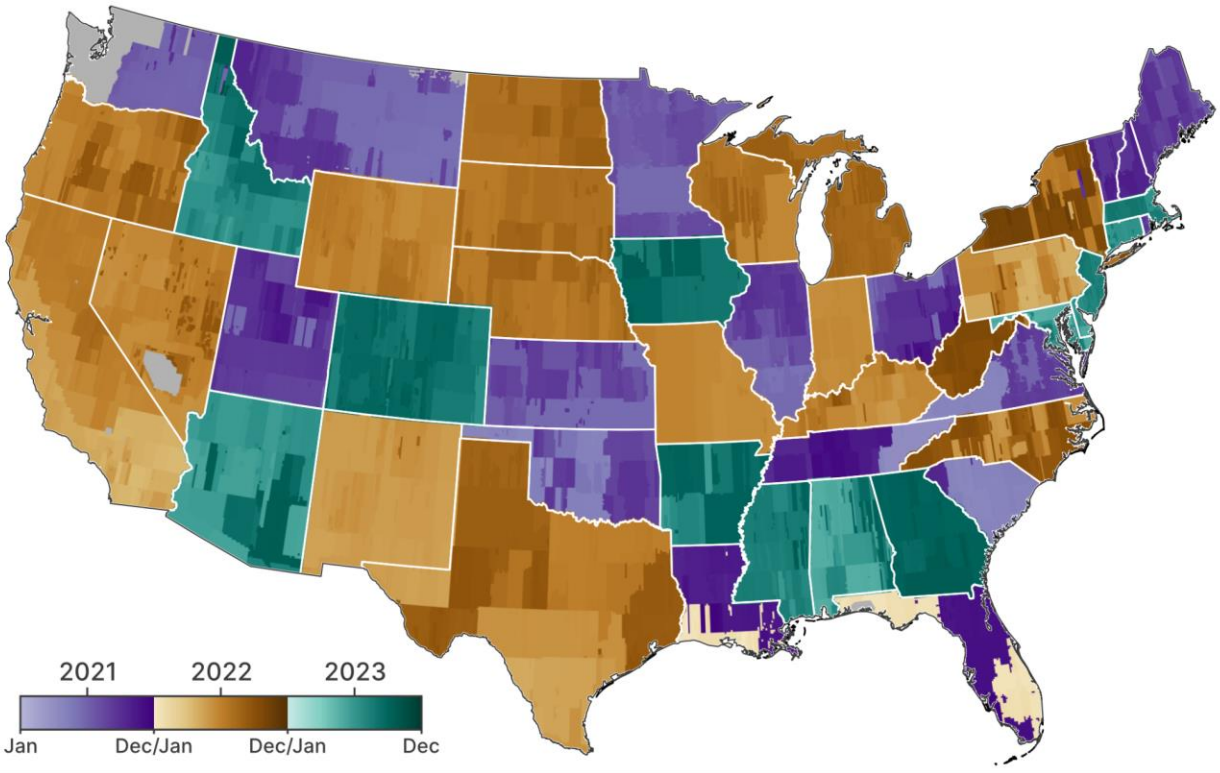

Figure 10. The most recently available NAIP imagery within Google Earth Engine. The color gradient indicates the within-year acquisition date, ranging from earlier (lighter shade) to later (darker shades) in the calendar year. These dates represent the temporal limitation of panel-row delineation and array boundary enhancement based on available imagery (through 2023). Note that NAIP 2023 was being processed at the time of writing, and has been included for states made available in GEE by December 2024. Grey areas are either prohibited flight spaces for national security (e.g., S. Nevada), or where the most recent imagery was prior to January 2021 (e.g., W. Washington).

2.2.2.1: Panel-row image and object classification

Solar PV and CSP panels and panel-rows are spectrally and geometrically distinct from other landscapes due to the unique composition, purpose, and design of solar generating units. We used five spectral indices with reported utility in classifying solar PV panel-rows (Stid et al., 2022) and solar arrays (Plakman et al., 2022) to train and run a Random Forest (RF) model (Breiman, 2001), a simple non-iterative clustering (SNIC) algorithm, and a X-means clustering model for solar panel-row classification. The indices were the normalized difference photovoltaic index (*NDPVI*) (Stid et al., 2022), the normalized blue deviation (*NBD*) (Stid et al., 2022), 4-band brightness (Br), the normalized difference vegetation index (*NDVI*) (Kriegler et al., 1969; Rouse et al., 1974), and the normalized difference water index (*NDWI*) (McFeeters, 1996). These indices are calculated by:

$$NDPVI = \frac{(\alpha * B - NIR)}{(\alpha * B + NIR)} \quad \textbf{Eq. 1}$$

$$NBD = \frac{B - \frac{R + G}{2}}{B + \frac{R + G}{2}} \quad \textbf{Eq. 2}$$

$$Br = \frac{R + G + B + NIR}{4} \quad \textbf{Eq. 3}$$

$$NDVI = \frac{(NIR - R)}{(NIR + R)} \quad \textbf{Eq. 4}$$

$$NDWI = \frac{(G - NIR)}{(G + NIR)} \quad \textbf{Eq. 5}$$

where α is a weighting coefficient (0.5) to reduce the importance of variations in the blue band when differentiating impervious surfaces from the rest of the landscape (Stid et al., 2022).

Although generally unique, the spectral signature of solar panel-rows varies across regions, technologies, and imagery timing, and atmospheric conditions (Stid et al., 2022). Shadows, water, and impervious surfaces also generally have low brightness and moderate blue reflectance. This presents an issue of spectral confusion (noise) in using pixel-based classification techniques alone, which fail to capture spatial relationships between neighborhood pixels, resulting in considerable commission error. However, nearly all ground-mounted solar panel-row objects are distinctly linear and square or rectangular objects with a relatively constrained set of possible sizes and array layouts. This makes geographic object-based image analysis (GEOBIA), a subset of computer vision, an ideal approach for improving traditional image classifications of solar energy systems (Blaschke et al., 2014).

To incorporate spatial context, we clustered imagery within array boundaries using SNIC of the given spectral indices and a gray-level co-occurrence matrix (GLCM) textural measure (sum average) of each index. SNIC is a polygonization segmentation approach that generates superpixel objects across a seed grid based on spatial-spectral context parameters such as compactness, connectivity, and neighborhood (Achanta & Susstrunk, 2017). SNIC has shown promise in delineating solar arrays, with Plakman et al. (2022) also using SNIC and RF approach to classify solar array boundaries in the Netherlands using Sentinel-2 imagery. GLCM textural metrics,

specifically the sum average, further capture the unique spatial-neighborhood relationships between proximal panel-row-like pixels. GLCM has demonstrated utility in mapping high-resolution land cover (NAIP) in combination with RF (Maxwell et al., 2019) and in solar classification (Q. Feng et al., 2024). SNIC was performed using GEE's native ee.Algorithms.Image.Segmentation.SNIC algorithm, and the GLCM sum average (Haralick et al., 1973; Haralick & Shanmugam, 1974) was calculated for each index using GEE's native ee.Image.glcmTexture function and is represented by:

$$Sum\ Average = \sum_{i=2}^{2N_g} ip_{x+y}(i) \quad \textbf{Eq. 6}$$

where i is the gray-level intensity of the index, N_g is the range in gray-level intensities within an image, and $px+y$ is the sum probability of co-occurring pixels in the matrix having the sum intensity value i. We then randomly sampled the SNIC superpixel clusters of the five spectral indices and the sum average for each index at 1000 points within each array boundary to train a locally-relevant X-means clustering algorithm. We used a minimum number of clusters of 2 (solar and non-solar) and a maximum of 4 clusters, allowing one level of variability in solar and non-solar supercluster averages (e.g., two module types or two ground covers). For large arrays (>5 ha) and arrays with multi-polygon boundaries, we split imagery within the array sub-boundary into equal area chunks (no greater than 5 ha) to enhance computational efficiency and to allow large arrays to have greater X-means variability.

To classify the unsupervised X-means clusters, we trained and ran a Random Forest (RF) model to identify panels (distinct from other land covers) within each array. We generated a new CONUS NAIP training dataset with 12,000 training points composed of 6 classes and 2,000 sample points per class (solar: 0, developed: 1, vegetated: 2, water: 3, snow/ice: 4, barren/sparse vegetation: 5). This training dataset is distributed along with the GM-SEUS data to facilitate others doing land use classification with NAIP data. To generate solar samples, we randomly sampled 2,000 panel-row centroids in existing solar panel-row data that were installed across CONUS prior to 2023. We acquired land cover samples from 2018 and 2019 NAIP imagery random sampling within 25,000 Land Change Monitoring, Assessment, and Projection (LCMAP) validated reference plots from Pengra et al. (2020), acquiring up to 90 points within each 900 m^2 plot (max of 10% of the plot sampled), ensuring each class had the closest to 2,000 samples as possible given

class limitations. Given that LCMAP contains few examples of snow/ice plots, we also randomly sampled ~2,000 snow/ice points from the Randolph Glacial Inventory (RGI Consortium, 2023) within CONUS. Qualitatively, we observed that within array bounds where existing ground cover is relatively constrained to vegetation, barren surfaces, and impervious surfaces, known CSP panel-rows were often spectrally similar to snow/ice due to the high reflectance of CSP reflectors, and CdTe/thin-film panel-rows could be spectrally similar to water because of the high absorbance of the visible and NIR spectrum. Thus, the final solar classification image included those respective classes for CSP and thin-film module type installations.

We classified the original NAIP imagery using the five spectral indices and the new NAIP training dataset with 200 trees and a bag fraction of 0.5. The RF model had an overall accuracy of 99.6% based on the aggregated performance per tree and an out of the bag error estimate of 0.35. Each cluster with the majority of its area classified as solar (or water and snow/ice in the respective cases), was assigned to the solar class. We then eroded small islands (commission errors) and filled holes (omission errors). Panel-rows were then vectorized and negative-buffered by a single pixel width to dissolve single-pixel inter-row connections. Given the large number of vertices captured by sub-meter image classification, we improved processing and storage efficiency by saving the convex-hull of each pixel-based panel-row as the final geometry. Panel-rows with an area greater than three-times the median within-array panel-row area (likely inter-row connections could not be dissolved) were allowed to maintain their pixel-based geometry. Arrays without newly generated panel-rows, or with new total array areas that were less than 15% of the initial array area were omitted. All imagery and data were accessed, trained, classified, and analyzed in GEE.

2.2.2.2: Estimating panel-row azimuth, mount technology, inter-row spacing, and tilt

We estimated the azimuth and mount technology for each panel-row object. We defined the azimuth as the primary cardinal direction of the short-edge vector in the minimum bounding rectangle (±180°). In the northern hemisphere, the azimuth of a solar panel-row is not likely to be north facing (270° to 360° and 0° to 90°), thus, we added 180° to any short-edge vector with a cardinal direction classified in these ranges. In the final GM-SEUS dataset, the average azimuth (*avgAzimuth*) for single-axis mounted solar arrays was corrected to the southward-normal (perpendicular) angle to the panel-row face direction to follow azimuth definitions in existing

datasets (Fujita et al., 2023; Seel et al., 2024). The final panel-row dataset maintains azimuth (*rowAzimuth*) as the primary direction of the short-edge vector (panel-row face).

To classify mount technology, we also calculated the length ratio of the long vector to the short vector and the ratio of panel-row area to bounding box area. The conditions for classifying mount technology were: single-axis–azimuth is within 30° of east or west and length ratio is greater than 2.5, fixed-axis–azimuth is within 60° of south and length ratio is greater than 2.5, dual-axis–the length ratio is less than 2.5. We also calculated the distance between each panel-row and the nearest panel-row (*rowSpace*) in the azimuthal direction for fixed- and single-axis panel-rows and all directions for dual-axis panel-rows. Azimuth and mount classification logic is similar to other studies (Edun et al., 2021; Perry & Campos, 2023) shown in Figure 9.

Optimal fixed-axis tilt (*tiltEst*) is generally considered directly correlated with array latitude, with slight deviations at higher latitudes (Martín-Chivelet, 2016). However, local climate and topography also play an important role (Al Garni et al., 2019). Using newly acquired azimuth and mount metadata, we estimated optimum tilt angle (*tiltEst*) for fixed-axis solar PV arrays (and mixed-mounted arrays) using the pvlib iotools package (Holmgren et al., 2018; Jensen et al., 2023). The latitude and longitude of each array was used to retrieve local typical meteorological year (TMY) data from the PVGIS-ERA5 v5.3 database (European Commission, 2024). The TMY data provided location specific irradiance data that incorporates shading from local topography. Global plane of array irradiance for orientations between 10 and 70 degrees from horizontal facing the *avgAzimuth* were modeled using the TMY and an isotropic model in python. The tilt with the greatest annual modeled global plane of array irradiance was selected for *tiltEst*.

2.2.2.3: Quality control with panel-row object-based knowledge

To ensure high-quality reporting of solar panel-row and array metadata, we retained only panel-rows that were geometrically consistent and produced reasonable array boundaries. This means that the final datasets are spatially conservative, omitting array and panel-row area (and at times, panel-rows within an entire array) thus under-representing the actual spatial footprint of the array (see Figure 12). Thus, in addition to the quality-controlled dataset of array and panel-row boundaries, the data repository contains the raw GEE output for all NAIP classified panel rows.

The vectorized panel-row dataset contained commissions that were geometrically dissimilar to true positives within the dataset (universally) and within the array (locally). Thus, we

universally removed panel-rows based on several criteria. First, we removed panel-row objects that were outside a minimum (15 m^2) and maximum (2000 m^2) panel-row area based on the minimum and maximum panel-row areas of the existing panel-rows dataset. We then universally removed any panel-row object with a perimeter to area ratio less than the minimum of the existing panel-row dataset (0.18).

Locally (within each array) we removed panels in which two or more of five geometric similarity measures failed: (1) mount technology of the panel composed less than 10% of the array, (2) ratio of the long-edge to the short-edge (length ratio) more than three standard deviations from the array mean, (3) the ratio of the panel-row area to the bounding box area more than three standard deviations from the array mean, (4) the perimeter to area ratio more than three standard deviations from the array mean, and (5) the Polsby-Popper ratio of Compactness more than three standard deviations from the array mean. The Polsby-Popper ratio, first used to defend against gerrymandering (Polsby & Popper, 1991), is defined by:

$$Compactness = \frac{4 * \pi * rowArea}{rowPerimeter^2} \quad \textbf{Eq. 7}$$

While removing universal and within array outliers removed a considerable quantity of commissions, some arrays contained overall low-quality classifications leading to retention of low-quality panel-rows objects. To address this, we created temporary solar array boundaries from the panel row objects (see *Enhancing existing array boundaries with panel-rows*). We then calculated the new array area and the perimeter to area ratio of the new array and the original existing array shape. We remove array-wide panel-row objects that were less than 25% of the original array area and greater than 99th percentile of the existing arrays perimeter to area ratio.

In total, we removed 36,000 panel-row objects due to within-array geometry quality control concerns and 48,000 panel-row objects due to poor array-boundary delineation. We also removed 4,000 panel-rows where the disconnected area composed less than 1% of the total array area. To create the final GM-SEUS panel-row dataset, newly derived panel-rows were merged with existing panel-rows giving preference to existing panel-rows. The result was 1.07 million panel-rows from existing sources, and 1.85 million newly delineated panel-rows. The panel-row and enhanced array boundary delineation workflow is shown in Figure 11.

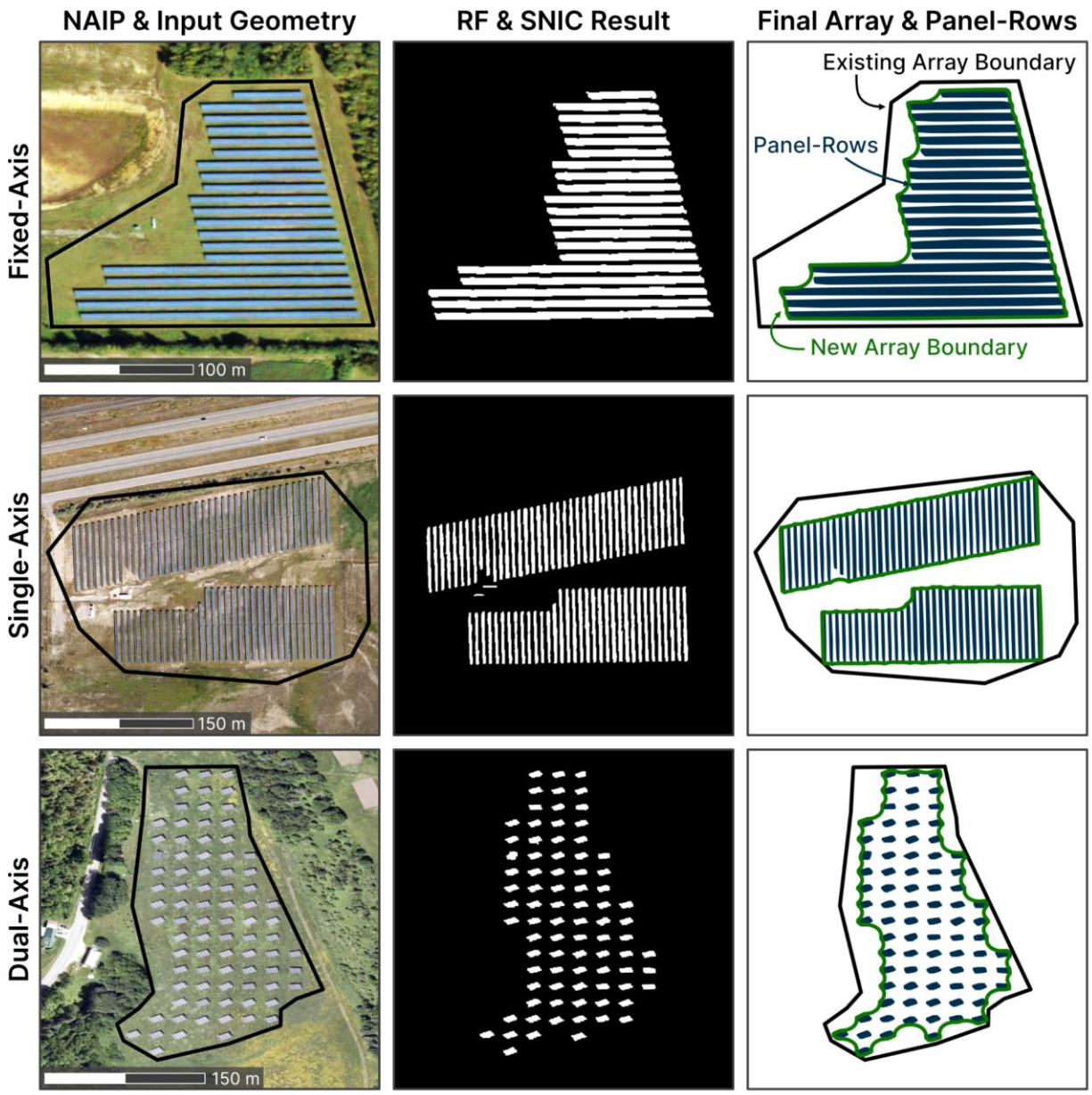

Figure 11. Example panel-row and array boundary delineation by mount technology. The left column contains NAIP aerial imagery and input geometries originating from the Source dataset of greatest spatial quality for that array.

2.2.3: Deriving new solar array geometries and attributes

2.2.3.1: Enhancing existing array boundaries with panel-rows

We created new solar array geometries from GM-SEUS panel-rows using a buffer, dissolve, and erode approach. The selected buffer distance was 10 m, allowing for large panel-assemblies in panel-rows and high-latitude panel-rows to both have large (up to 20 m) spacing.

This is similar to our previous approach where we used a five-meter buffer to group panel-rows into an array (Stid et al., 2022) and to (Hu et al., 2022) who used a three meter buffer to assign an array group for rooftop solar. Importantly, the erosion used here removes the area external to the panel-rows and the space between. Thus, this process inherently aligns with our definition of a solar array spatial footprint.

The GM-SEUS repository contains a version of all newly created array boundaries from the final panel-row dataset and a version of all existing array boundaries replaced with newly delineated array boundaries where available. We maintain USPVDB and CCVPV array boundaries due to their completeness (see Figure 12) and match our definition of an array. OSM, CWSD, and TZ-SAM arrays do not inherently follow our definition of an array and contain manual delineation (OSM and CWSD) and coarse resolution remote sensing (CWSD and TZ-SAM) biases (Fujita et al., 2023; Phillpott et al., 2024a). Additionally, given that CWSD and TZ-SAM arrays are independent of project-level metadata, we allowed newly delineated disconnected array shapes to be considered as separate arrays in this source dataset. For these arrays, we grouped newly created sub-array geometries by the same installation year (see *Estimating installation year*), allowing arrays installed in different years to be their own installation. In total, 5,017 arrays (174 km^2) received a new array boundary delineation. The original area of these arrays was 281 km^2.

2.2.3.2: Estimating ground cover ratio (GCR)

Ground cover ratio (GCR), sometimes referred to as packing factor (PF), has previously been defined by two different relationships. We calculate and report both by:

$$GCR_1 = \frac{totRowArea}{totArea^*} \quad \textbf{Eq. 8}$$

$$GCR_2 = \frac{rowWidth}{rowWidth + rowSpace} \quad \textbf{Eq. 9}$$

where *totRowArea* is the top-down or apparent total panel-row area within an array at peak solar inclination (for tracking arrays), $totArea^*$ is the total land area of the panel-rows and the spacing between them (Cagle et al., 2023; Gordon & Wenger, 1991; Martín-Chivelet, 2016; Narvarte & Lorenzo, 2008; Ong et al., 2013; Stid et al., 2022), which is equivalent to *totArea* for arrays with complete panel-row delineation and arrays were a new boundary was delineated and replaced an original boundary, *rowWidth* is distance from the bottom edge to the top edge of a row along the

short edge, and *rowSpace* is the distance (azimuthal distance fixed- and single-axis) from an array edge to the nearest panel-row edge. The sum of *rowWidth* and *rowSpace* is the horizontal ground distance between any identical point of a module in a directly adjacent row (Gilman et al., 2018; Prilliman et al., 2022; Tonita et al., 2023). We fill in gaps with available CCVPV packing factor reported values and estimate GCR for arrays without panel-row information using a multiple linear regression between latitude and longitude in relation to GCR_1 and GCR_2 from arrays with panel-row information for each mount technology and for PV and CSP arrays independently.

2.2.3.3: Estimating installation year

Solar array installation year is often acquired by change detection and manual validation of aerial and satellite remote sensing imagery where permitting data is not available (D. Chen et al., 2024; Kruitwagen et al., 2021; Phillpott et al., 2024a; Stid et al., 2022; Tao et al., 2023). Given the lack of permit data for most of GM-SEUS and the quantity of installations, we needed a way to independently and automatically estimate the year of completed installation. We used the GEE implementation of Landsat-based detection of trends in disturbance and recovery (LandTrendr) algorithms (Kennedy et al., 2018) to estimate the solar array installation year. LandTrendr is a suite of temporal segmentation algorithms tailored to detecting changes in forested areas at 30 m resolution, but with broader applications. We previously used LandTrendr and *NDPVI* to detect solar installation years between 2008 and 2018 in California with a 79% accuracy within one year of the manually validated installation year (Stid et al., 2022).

Temporal segmentation requires a significant change in pixel spectral trajectory, which is dependent on the historical land use and land cover, and the subsequent land management between the arrays. Landsat pixels (30 m) contain mixed land cover of panel-rows and the space between them, meaning the post-installation reflectance is dependent on GCR, panel-row area, and ground cover management. Given the broader spectrum of possible spectral histories and variables affecting solar reflectance across the US and reported utility in employing multiple indices for LandTrendr disturbance detection (W. B. Cohen et al., 2020), we modified our original approach to include a multi-index performance-weighted average of LandTrendr years of disturbance across twelve spectral indices. These were the indices with reported utility in solar detection (*NDPVI*, *NBD*, *Br*, *NDVI*, and *NDWI*) along with seven land use change indices built into LandTrendr including the enhanced vegetation index (EVI) (Huete et al., 2002), the normalized burn ratio (NBR) (García & Caselles, 1991), the normalized difference moisture index (NDMI) (Gao, 1996),

and the Tasseled Cap-Transformations (greenness, brightness, wetness, and angle) (Crist & Cicone, 1984; Kauth & Thomas, 1976). All built-in indices except EVI take advantage of short-wave infrared bands that Landsat includes but NAIP does not.

We used LandTrendr and these indices to estimate the year of newest disturbance, or land use change, within the boundaries of each array polygon between 2009 and 2023, noting that a significant amount of existing solar has been installed in the last decade (Fujita et al., 2023). We break each array into composing polygons to allow for multiple installation years within an array area. We also remove segmented boundary years (2008 and 2024) to address known biases in the LandTrendr segmentation at edge years (Stid et al., 2022). To promote accuracy, we subset LandTrendr indices where the mean absolute error (MAE) between the USPVDB permitted installation year and LandTrendr estimated installation year (~4,000 arrays) was less than 2 years (*NBD*, *NDPVI*, *NDWI*, TCG, and NDMI). For these indices, we applied an inverse variance-weighted (IVW) average to calculate the installation year. Similar performance-weighted average approaches are common for various applications (W. B. Cohen et al., 2020; Comte & Olden, 2017; Merrifield et al., 2020). We then include indices with greater MAE to fill in non-detect installation years (TCA, *NDVI*, NBR, *Br*, TCW, EVI, and TCB). Of the over 16,000 input array polygon boundaries, this LandTrendr method only omitted an installation year estimation for 41 array polygons, only 2 of which did not have installation years from other sources.

We independently estimated the installation year for all arrays. However, we also retain installation years from existing datasets in the following order: USPVDB, InSPIRE, USS, SolarPACES, GSPT, GPPDB, TZ-SAM, CWSD, and OSM. We omitted CCVPV since the multi-index performance-weighted average method is more robust than our original single index approach. We also only included installation year from TZ-SAM and CWSD for 2018 or later, since these approaches are based on Sentinel-2 availability. When LandTrendr did not result in a year of detected disturbance, we manually analyzed the installation year using available historical satellite and aerial imagery for each array and LandTrendr time series plots from methods from Stid et al. (2022) an Stid et al. (2025). We allowed new array shapes derived within TZ-SAM array boundaries to be considered their own array and regrouped them if they were installed in the same year. We provide both a compiled existing installation year (*instYr*) and the new LandTrendr-derived installation year (*instYrLT*) in the final GM-SEUS dataset.

2.2.3.4: Estimating module efficiency and installed capacity

Installed solar capacity is generally assumed to be directly correlated with panel-row surface area. Others have used statistical regression relationships between known solar PV capacity and panel-row surface area (Mayer et al., 2022), along with several adjustable parameters such as the spectral-intensity of the module surface area (Hu et al., 2022; So et al., 2017). With temporal information and module composition, we were able to estimate module efficiency and thus installed capacity for solar PV arrays with (Eq. 10) and without (Eq. 11) panel-row information. We thus used the following relationships modified from Martín-Chivelet (2016) and Phillpott et al. (2024) to estimate peak installed capacity for solar PV arrays (power, MW_{DC}):

$$capMWest_{PV} = totRowArea * \eta * G_{STC} \quad \textbf{Eq. 10}$$

$$capMWest_{PV} = (totArea^{**} * GCR_{local}) * \eta * G_{STC} \quad \textbf{Eq. 11}$$

where η is the annual average value for ground-mounted systems from Lawrence Berkeley National Lab's (LBNL) Tracking the Sun 2024 Report (Barbose et al., 2024) for each technology (c-Si or thin-film), G_{STC} is the irradiance at standard test conditions (0.001 MW_{DC} m^{-2}), totArea** is the total array area adjusted for area bias of the input dataset relative to USPVDB array area, and GCR_{local} is the estimated GCR_1 for arrays without panel-row information in relation to latitude and longitude by mount technology and module type. Note that Eq. 11 and 12 are effectively the same, because GCR_{local} is equivalent to the mount and spatially relevant average ratio of *totRowArea* to *totArea*. Area bias was determined by intersecting array shapes from input datasets with USPVDB arrays and acquiring the average percent-difference in array polygon area (Figure 12B and 12C). This corrects for array datasets that tend to over or underestimate total array area (by our definition), reducing erroneous *totRowArea* estimates when multiplying by GCR_{local}.

After dataset harmonization, 59 of 74 CSP arrays were missing a reported installed capacity. For these arrays, we estimated thermal capacity (MWth) for solar CSP arrays with (Eq. 12) and without (Eq. 13) panel-row information by:

$$capMWest_{CSP} = totRowArea_{effective} * C_f \quad \textbf{Eq. 12}$$

$$capMWest_{CSP} = (totArea * GCR_{local})_{effective} * C_f \quad \textbf{Eq. 13}$$

where $totRowArea_{effective}$ is the effective panel-row (for CSP, collector) area, estimated for parabolic trough, linear fresnel, and dish-CSP systems as the half of the circumference of a circle with a diameter of *rowWidth*, and for power tower, beam down tower and hybrid-CSP systems as the *totRowArea*, Cf is the recommended conversion factor 0.0007 MWth m^{-2} of aperture collector area to installed thermal capacity (IEA SHC, 2023). Again, $totArea * GCR_{local}$ is a spatial regression of GCR1 as it relates to *totRowArea*. Although this technical recommendation does not extend to tower-CSP plants, we use it for tower-CSP plants due to the lack of available recommendations. This is a vastly simplified approach, with more robust methods available (Dobos et al., 2014; Wagner & Zhu, 2011), but beyond the scope of this GM-SEUS initial version.

Similar to other new solar array attributes, we estimate installed capacity for all arrays and retain capacity attributes from existing datasets with a capacity attribute in order of perceived quality: USPVDB, InSPIRE, USS, SolarPACES, PVDAQ, GSPT, GPPDB. We chose to estimate capacity for all CCVPV, TZ-SAM, and OSM datasets using Eq.'s 10-13 (CWSD did not report capacity).

2.3: Data Records

GM-SEUS v1.0 is available for public use and is provided in the Zenodo Repository (Stid et al., 2025). The final data repository provides all geospatial files as geopackage, shapefile, and as CSV. We also provide 17,500 input and target images derived from GM-SEUS and recent NAIP imagery for direct application in deep learning and pattern recognition use cases. When using these products, please cite the original data sources and articles (Byers et al., 2021; Deline et al., 2021; Evans et al., 2021, 2023; Fujita et al., 2023, 2024; GEM, 2024; Global Energy Observatory et al., 2021; NREL, 2025; OpenStreetMap Contributors, 2024; Phillpott et al., 2024b, 2024a; Seel et al., 2024; Stid et al., 2022; Stid, Shukla, et al., 2023; Thonig et al., 2023) along with this work. All arrays and panel-rows contain a "Source" attribute, which references the data source of the original spatial information (see README in the data repository for more detail). See Table 1 for attribute-level information in each dataset. Data records are up to date through December 2024. The USPVDB, TZ-SAM, and OSM datasets intend on updating their completeness on a regular basis. We intend on providing annual updates to this dataset. A complete list of repository file descriptions and attributes can be found in Appendix B Text A2.1.

2.4: Technical Validation

2.4.1: GM-SEUS completeness compared to other datasets

Through the end of Q3 2024, the Solar Energy Industries Association (SEIA) and Woods Mackenzie reported that the US had installed 5.3 million solar systems with a total solar capacity of ~220 GW_{DC} (SEIA & Wood Mackenzie, 2024). Given available information, ~18% is residential-scale solar (~40 GW_{DC}), ~12% is commercial- or community-scale (~25 GW_{DC}), and ~70% is utility-scale (~150 GW_{DC}), with more than 80 GW_{DC} installed since 2023 alone (SEIA & Wood Mackenzie, 2024).

GM-SEUS reports an estimated 186 GW_{DC} installed through December 2024 (TZ-SAM and OSM provide the most recent data), or ~107% of non-residential solar capacity (~85% of all solar capacity) through 2024. We also provide new sub-array metadata for 9,042 arrays (83.1 GWDC), 5,858 (16.7 GW_{DC}) of which are not contained within USPVDB. Note that we include all arrays from USPVDB and TZ-SAM but refine the TZ-SAM array area where panel-row information is available and independently estimate installed capacity using site-level information. It is important to consider that due to quality control and inspection requirements, NAIP imagery is always at least a year behind. This means that we are not able to directly determine commission error (non-solar) in the existing dataset compilation. However, if we only consider arrays verifiable with recent imagery (USPVDB, CCVPV, OSM, and georectified arrays, and arrays with compile or identified panel-rows), total GM-SEUS installed capacity is 125 GW_{DC}, 72% of reported non-residential capacity through 2024. Though high-resolution imagery is temporally limiting, it is thus likely that some arrays derived with moderate resolution remote sensing (CWSD, TZ-SAM) contain non-solar commissions.

For reference, within CONUS, the USPVDB v2.0 is complete through Q3 2023 and represents a permitted 90.4 GW_{DC} (Fujita et al., 2024), or ~65% of non-residential solar capacity through 2023. TZ-SAM Q3 2024 estimates capacity by array area and country-wide values for GCR and inverter-loading ratio (ILR) and represents 197 GW_{AC} within the CONUS (~253 GW_{DC} assuming a median ILR of 0.22 from USPVDB), or ~145% of non-residential solar capacity (~115% of all solar capacity) through Q3 2024 (Phillpott et al., 2024b). Though, note that coarse GCR estimates, and medium-coarse satellite imagery generated array geometries may overestimate encompassed area and thus estimated capacity (Fujita et al., 2023). This is evident in

the TZ-SAM arrays that intersect USPVDB arrays, which overestimate total array area on average by ~45% (by our definition of an array – Figure 9 and Figure 12) and installed capacity by ~27% (assuming 0.22 ILR) for the same arrays.

Many of the input datasets report being the most complete or comprehensive for their scope at the time of publication. We have compiled these data repositories, removed repeat information preferencing quality, acquired updated data from OSM, and improved spatiotemporal characterization for several existing array datasets. GM-SEUS is thus a harmonization and enhancement of the most comprehensive publicly available ground-mounted solar energy datasets available in the US given (see Table 2). However, we exclude non-contiguous US regions and residential and rooftop systems. The most comprehensive residential and rooftop datasets to-date are Bradbury et al. (2016) in the US (data: (Bradbury et al., 2020)) and Stowell, Kelly, Tanner, Taylor, Jones, Geddes, & Chalstrey (2020) in the United Kingdom (data: (Stowell, Kelly, Tanner, Taylor, Jones, Geddes, Chalstrey, et al., 2020)).

We have inevitably omitted existing ground-mounted solar energy systems and likely included commissions (non-solar objects). We have no way of knowing the extent of omission error beyond comparing against broad solar industry trends and acknowledging the 1,490 point data sources that we still need to manually georeference and digitize. Commission error is also difficult to quantify given high-resolution imagery temporal limitations. For example, we have no way of knowing if arrays without available NAIP imagery including panel-rows are: 1) arrays installed after the most recent NAIP imagery or 2) inclusive of non-solar objects. There may also be situations where erroneous classifications of non-solar objects passed the panel-row quality control. In general, validation of completeness is limited by our reliance on freely available data and our decision to not include additional existing data held behind paywalls. The difficulty in validating GM-SEUS underscores the motivation to create this product along with similar efforts.

2.4.2: Spatial confidence in array and panel-row delineation

The EIA Form 860 and USPVDB is the most rigorous, robust, and widely available data from which to compare our results and is often the source for metadata on other existing datasets. The hand delineated array boundaries in USPVDB ensure completeness also match our definition of an array (Figure 9). Thus, for both spatial confidence and attribution technical validation, we compare our results to USPVDB alone.

We generated panel-row geometries for 9,042 arrays. Although we maintain USPVDB

boundaries in the final dataset, we use these high-fidelity hand delineated boundaries to validate our NAIP array delineation approach for other existing array datasets. To evaluate confidence in newly generated array geometries, we use the Jaccard Similarity Index, also known as the Intersection over Union (*IoU*) (Levandowsky & Winter, 1971). *IoU* is bound by 0 and 1, where zero indicates no overlap and 1 indicates identical overlap of input geometries (A, B). *IoU* was calculated by:

$$IoU(A,B) = \frac{A \cap B}{A \cup B} \quad \textbf{Eq. 14}$$

We generated panel-rows using NAIP imagery and created array boundaries for 2,871 of 4,185 USPVDB arrays (52.9% of total USPVDB area). We calculated the *IoU* for all NAIP panel-row delineated array boundaries that intersected with any USPVDB array polygon. Due to USPVDB multi-polygons and connected array shapes, we dissolved all boundaries and considered any individual polygon where boundaries overlapped. The 1,314 array omissions were due either to poor quality panel-row or array delineation or outdated imagery compared to the installation of the array. Though, note that this partial coverage is only for array boundary delineation method validation and that we include all USPVDB arrays and array area in GM-SEUS.

The median IoU for array GM-SEUS boundaries was 0.88 (Figure 12A), which is comparable and even superior to numerous instances of *IoU* being used to validate solar array boundary delineation (Bradbury et al., 2016; Kruitwagen et al., 2021; Plakman et al., 2022; Ravishankar et al., 2022; Tao et al., 2023). The NAIP panel-row delineation method underestimates USPVDB area on average by ~12% (Figure 12B and 12C). This makes sense, given our highly-conservative panel-row selection for high-quality sub-array metadata and that we only consider array area within the existing array boundary. We also compared the spatial array delineation of existing datasets to USPVDB using *IoU* resulting in median values of 0.95 for CCVPV, 0.85 for CWSD, 0.83 for OSM, and 0.69 for TZ-SAM, with proportional coverage of USPVDB area being 3.5% for CCVPV and CWSD, 93.0% for OSM, and 99.6% for TZ-SAM. Note that CCVPV and CWD more closely follow the array definition used here (and in USPVDB), where OSM and TZ-SAM more closely correspond to project area (Figure 9).

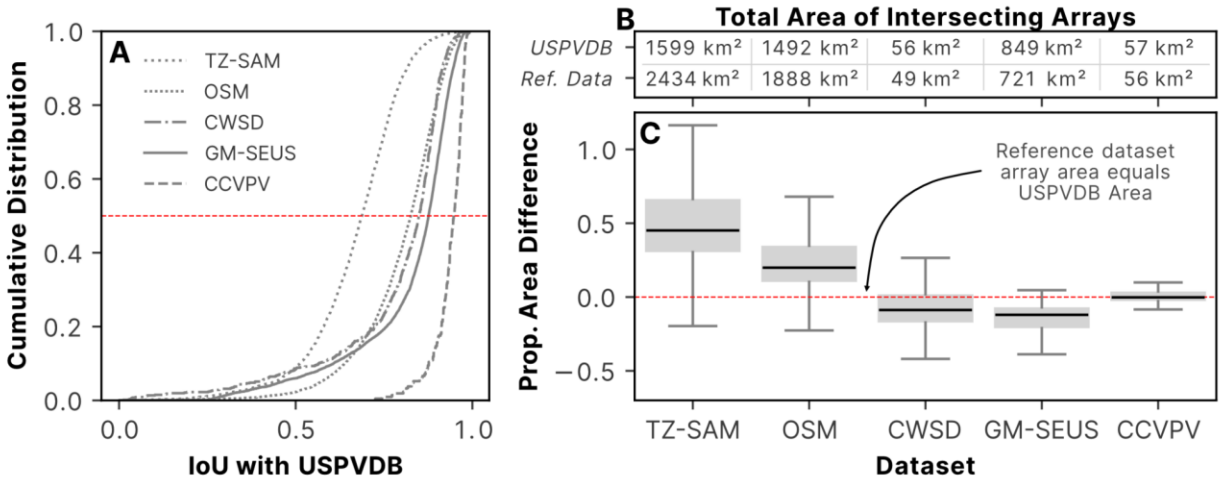

Figure 12. Spatial validation compared to USPVDB. GM-SEUS array boundaries considered here are all those newly derived by the NAIP segmentation approach. (A) Cumulative distribution function of the *IoU* for each existing (TZ-SAM, OSM, CWSD, CCVPV) and new (GM-SEUS) array dataset relative to USPVDB. (B) Total area of intersecting arrays with USPVDB representing the USPVDB area intersecting with array area and Ref. Data representing the intersecting reference dataset array area. from other existing and new datasets. (C) Proportional array area difference for existing and new array dataset boundaries intersecting USPVDB.

We also used *IoU* to compare newly generated GM-SEUS panel-rows to existing OSM and CCVPV panel-row datasets, given that USPVDB does not provide panel-row spatial data. The median *IoU* for GM-SEUS panel-row boundaries was 0.48 (Figure 13A). This is considerably lower than the array boundary *IoU*, though comparing high-spatial resolution individual panel-rows is similar to pixel-wise *IoU*, which are known to have lower scores than array-wise *IoU* (Hu et al., 2022). Additionally, OSM contributors most often use Bing or Maxar imagery to delineate panel-rows in the OSM user-interface (OpenStreeMap Wiki, 2024). Horizontal accuracy standards for NAIP rectification require 95% confidence within 4-meters of true ground (Maxwell et al., 2017). At the scale of panel-rows, ground sample errors of up to a few meters can mean entirely missing or missing in part panel-row overlap with panel-rows hand delineated by OSM. Thus, what is more spatially important than panel-row geometric alignment is the correlation between total estimated panel-row area within each array (Figure 13B) and the difference in total panel-row for each individual intersection (Figure 13C and 13D). Figure 6B shows that array-total panel-row area is highly correlated (log-log transform $R^2 = 0.95$) between existing panel-rows and GM-SEUS NAIP-generated panel-rows, and that NAIP-panel-rows area ~15% larger than hand delineated panel-rows (Figure 13C and 13D).

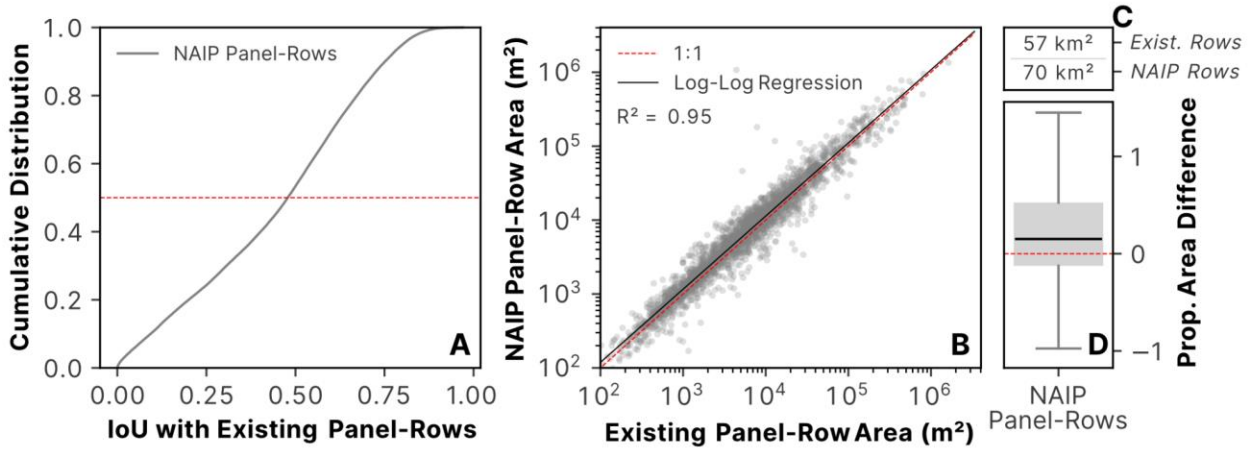

Figure 13. Spatial validation compared to input existing panel-row datasets. GM-SEUS panel-row boundaries considered here are all those newly derived by the NAIP segmentation approach. (A) Cumulative distribution function of the IoU for GM-SEUS NAIP panel-rows and existing panel rows. (B) Log-Log transformed relationship between total panel-row area within a unique array for existing GM-SEUS NAIP panel-rows. (C) Total area of intersecting panel-rows with Exist. Rows representing the existing panel-row area intersecting with panel-row area of NAIP Rows, representing the intersecting GM-SEUS NAIP panel-row area. (D) Proportional panel-row area difference for GM-SEUS NAIP panel-row boundaries intersecting existing panel-row boundaries.

2.4.3: Attribute validation

We estimated several solar array and sub-array characteristics that have available reference data for validation. We estimated the array installation year based on the LandTrendr-derived year of greatest spectral change, module efficiency based on installation year and module type, GCR based on new and existing panel-row delineation, installed capacity based on panel-row area or local GCR, predominant array mount technologies and azimuth based on panel-rows, and panel-row tilt based on latitude. We are not aware of validation datasets for other sub-array metadata metrics.

We harmonized and estimated the installation year for all arrays in GM-SEUS. Comparing GM-SEUS to the utility-scale solar arrays in USPVDB v2.0, the estimated installation year MAE was 1.52 years (Figure 14). Error was skewed high in early installation years and low in late installation years, displaying limitations in this short-year-range and high spatial-resolution application of LandTrendr temporal segmentation. However, the more available years to segment, the less impact this error will have. Additionally, some indices (*NDB* and *NDPVI*) did not have the early installation year bias. For the individual indices used in estimating installation year, *NBD* had the lowest MAE (1.53 years) and TCB had the greatest MAE (4.07 years). Within USPVDB,

individual indices omitted installation years for between 113 arrays (TCG) and 551 arrays (TCB). In total, 66% of estimated installation years were within one year of permitted installation year, and 80% were within two years.

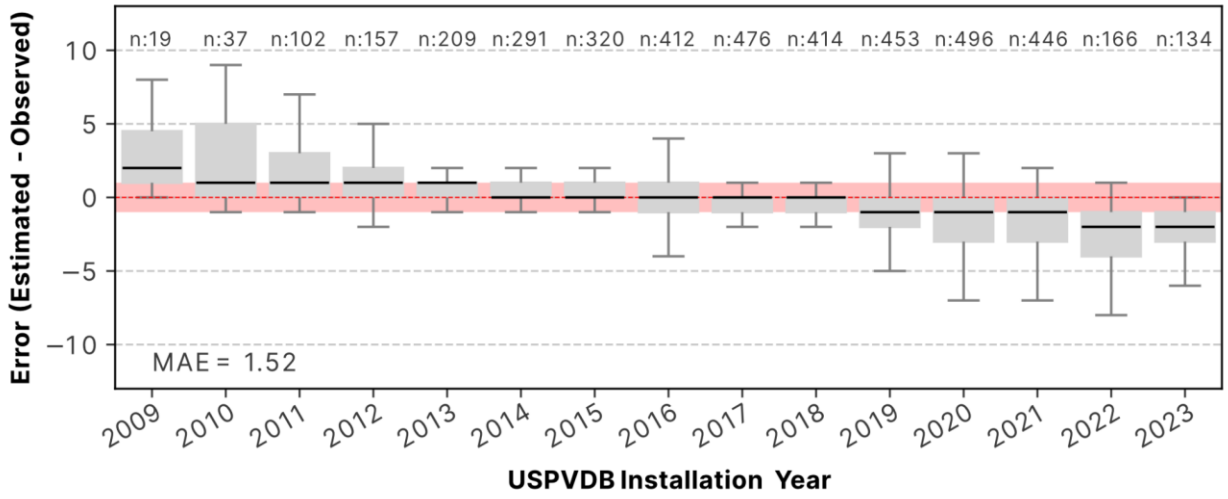

Figure 14. Estimated installation year validation compared to USPVDB. Boxplots show quartiles and median installation year deviation, with high values indicated an overestimate of installation year. The dotted red line indicates no deviation, and the red alpha range displays a ±1 year deviation range.

We acquired permitted peak capacity from existing data sources for 4,894 arrays and estimated capacity for the remaining 10,123 arrays in GM-SEUS. Compared to USPVDB, estimated installed capacity log-log transform R^2 of 0.84 for solar PV arrays (c-Si and thin-film). We did not perform a statistical analysis for CSP estimated capacity given the small number of available validation data and difficulty in estimating capacity using estimated aperture area alone (Eq. 12 and 13). Estimated capacity error is shown in Figure 15.

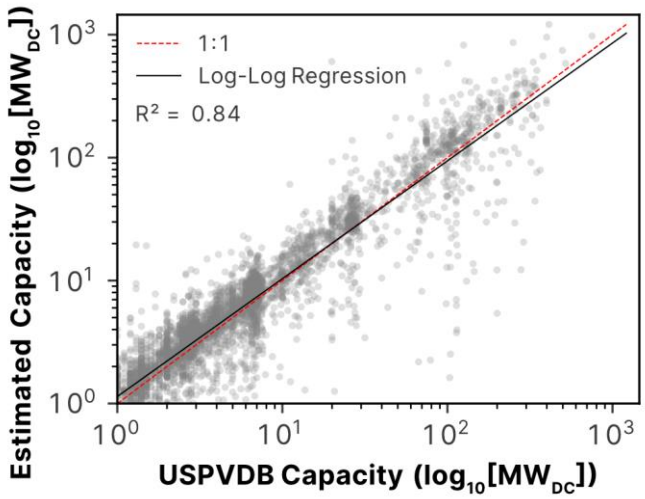

Figure 15. Estimated installed capacity validation. Note that the plot and regression are Log-Log transformed.

Relative to USPVDB, GM-SEUS mount types were correct 92% of the time. Regarding azimuth and tilt, Perry et al. (2024) reported accuracy of permitted azimuths within 15 degrees of ground truth (64%) and of permitted tilt within 5 degrees of ground truth (63%). For GM-SEUS, 89% of reported azimuth values and 12% of reported optimal tilt values were within 15 and 5 degrees of permit-reported azimuth and tilt respectively. Note that rather than estimating actual tilt, we estimate optimal tilt for an array using local TMY and topography data. Expanding the threshold, estimated optimum tilt was within 10 degrees of permitted tilt for 41% of arrays with permitted tilt, and 80% within 15 degrees of permitted tilt.

Median GM-SEUS Solar PV GCR_1 values were 53% for fixed-axis, 42% for single-axis tracking, 50% for dual-axis tracking, and 63% for arrays with mixed mounts. We compared GM-SEUS GCR (GCR_1) estimates with CCVPV packing factor estimates (Stid et al., 2022), estimates from Ong et al. (2013), and USA-wide estimates from Phillpott et al. (2024). Although, Phillpott et al. (2024) reports GCR for small (43%), medium (36%), and large (30%) arrays, rather than by mount technology. Fixed-axis and single-axis tracking GCR_1 values are comparable across GM-SEUS, CCVPV, and Ong et al. (2013), and for "small" array GCR (43%) reported in Phillbott et al. (2024). GM-SEUS dual-axis GCR_1 is more than twice (50% vs. 22%) what is reported by Ong et al. (2013). However, Ong et al. (2013) reported only 9 dual-axis arrays (and only 83 systems in total). We considered 230 dual-axis systems, 5,282 fixed-axis systems, 2,583 single-axis systems, and 298 mixed-mount systems. GCR_1 and GCR_2 distribution and comparison to validation data is shown in Figure 16.

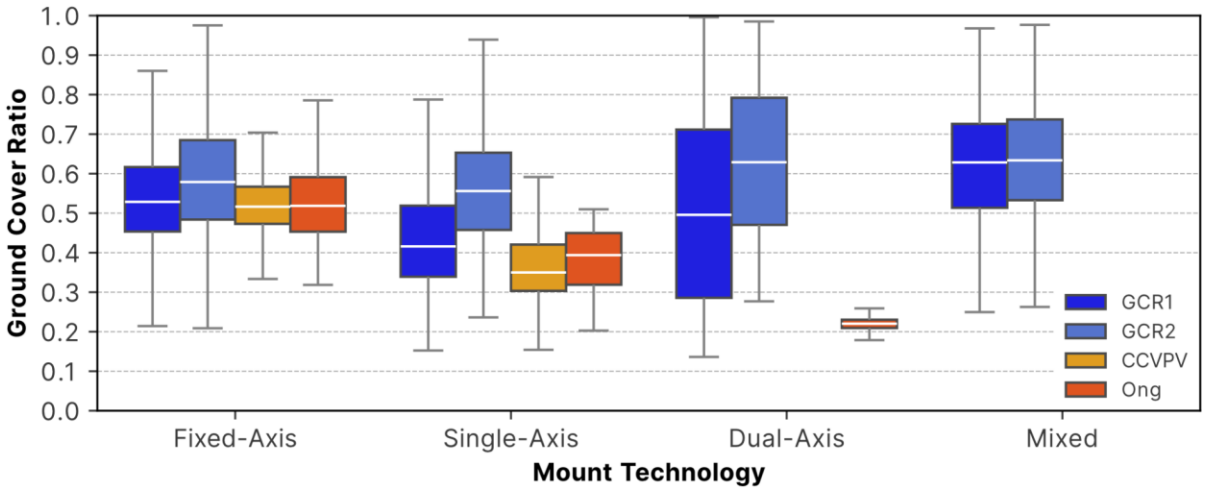

Figure 16. Ground cover ratio distribution compared to existing sources. *GCR_1* and *GCR_2* are newly derived metrics described by Eqs. 8 and 9. CCVPV is the packing factor for only fixed- and single-axis tracking arrays from Stid et al. (2022), and Ong represents reported packing factor values from Ong et al. (2013). Although not included in the graph, Phillbott et al. (2024) reports GCR for small (43%), medium (36%), and large (30%) arrays.

2.4.4: Additional limitations of GM-SEUS Version 1.0

Despite our best efforts, we acknowledge limitations in the creation of GM-SEUS. We already noted several limitations including reported attribute error, potential omission of existing arrays, evaluation issues due to imagery horizontal accuracy, and potential inclusion of non-solar objects. Hu et al. (2022) defines several additional cautions when performing solar energy characterization using overhead imagery. These include issues with distribution shift, availability of testing data, standardization of comparison metrics, and the scale of evaluation impacting reported performance. Where possible, we mitigate these pitfalls by evaluating performance with data of similar scope and coverage (USPVDB) and at the array or panel-row level, rather than aggregating (Hu et al., 2022). We also make our dataset publicly available and use common evaluation metrics (e.g., IoU).

There are additional challenges when using NAIP for image classification due to high-resolution aerial imagery metadata variability. These include timing of acquisition (season, date, time of day), camera tilt, look angle, flight path mosaic and georectification artifacts, and low-radiometric resolution (Maxwell et al., 2017). On a pixel-wise basis, for example, these challenges could lead to underestimating the panel-row area of a single-axis tracking system if imagery was acquired at the start or end of contracted flight time (Bunis & Mootz, 2007). We have accounted

for this bias in the past by trigonometrically correcting panel-row area based on the maximum estimated tilt angle of the tracking mount at the timing of imagery (Stid et al., 2022). Though, even at sub-meter resolution, this correction could overestimate panel-row area if edge-pixels (or shadows) were included in the classification or if tilt is lower than expected. In fact, we know that in some arrays, GM-SEUS overestimates panel-row area due to convex-hull operation and commissions including shadows and access roads (Figure 13C-13D and Figure A35). This example may also explain some uncharacteristically high GCR values, particularly for dual-axis installations (Figure 16).

Conversely, we also underestimate total array area compared to USPVDB (Figure 12B and 12C), in part due to correcting inconsistencies with hand annotation (Figure 4), but also due to conservative panel-row quality control resulting in holes and disconnected array boundaries (Figure A35). We accept this limitation here because we valued high-quality panel-row metadata over within-array panel-row completeness. Ultimately, panel-row area (Figure 13B-13D) and GCR (Figure 16) estimates indicate that panel-row area and packing layout are generally consistent with prior findings and data, with a slight overestimation of panel-row area. Additionally, at the time of writing, TZ-SAM released a new version of their data product (Q4 2024) that is not included here but will be included in a version update.

2.5: Usage Notes

The goal of this effort is to provide researchers and policymakers with a distributed ground-mounted solar array dataset and sub-array design metadata on the existing US solar energy landscape. Additional examples of applications for a harmonized and more comprehensive dataset of ground-mounted solar energy installations with sub-array design information, capacity- and technology-inclusive array data, and installation year, may include: high resolution nowcast modeling and grid/transmission planning (Bright et al., 2018; Buster et al., 2024; Price et al., 2025; Samu et al., 2021; US DOE, 2024); grid pricing and incentive planning (Laws et al., 2017); tracking policy effectiveness (Crago & Chernyakhovskiy, 2017); evaluating property value impacts (Elmallah et al., 2023; Hao & Michaud, 2024); assessing public perception towards projects with varying scale and levels of community engagement (Hoesch et al., 2025); tracking agricultural production opportunity costs (Stid, Shukla, et al., 2025); modeling carbon storage and sequestration potential (Krasner et al., 2025); modeling potential for habitat connectivity and pollination services (Walston et al., 2018); pattern recognition and training deep learning semantic

segmentation models–see Appendix B Text A2.2 (Malof et al., 2016; Phillpott et al., 2024a); soiling and performance monitoring (Cardoso et al., 2024; Oulefki et al., 2024; Supe et al., 2020); repowering preparation (T. Curtis et al., 2021); estimating losses due to sub-optimal tilt (Al Garni et al., 2019); and tracking spatiotemporal material stock in existing infrastructure using historical material intensity for recycling facility siting and planning (J.-K. Choi & Fthenakis, 2014; Farina & Anctil, 2022; Hanna et al., 2024; Yuan et al., 2024).

This dataset provides a broad characterization of solar array design practices. Any characterization of solar array design and management derived from remote sensing imagery should be considered with extreme scrutiny given the limitations of such approaches (Hu et al., 2022). While our work fills a critical data gap and compiles and enhances existing high-fidelity datasets, the design practices reported here are thus subject to uncertainty and should not be used to represent actual conditions at individual sites. No warranty is expressed or implied regarding accuracy, completeness or fitness for a specific purpose. We publish this dataset in open access, for the broader science community, policy makers, and stakeholders in addressing questions about the existing renewable energy landscape and do not consent to this data being used to target, identify, or make claims about individual arrays, properties, or entities. Any such use case is strictly prohibited.

Similar to the results reported in Fujita et al. (2023), these array boundaries do not represent total project area and thus total land transformation (see Figure 9). Any calculation of solar energy-land interactions (e.g., land-use efficiency, land transformation, or footprint) should consider this knowledge and report limitations accordingly (Cagle et al., 2023).

2.6: Code Availability

The codebase for data acquisition, harmonization, and processing are available via Github (https://github.com/stidjaco/GMSEUS) and a Zenodo release (Stid, Kendall, et al., 2025). Intermediate data products are available upon request, and the data repository README contains links to all source data portals. The code provided in the Github repository includes both IPython notebooks and GEE JavaScript files. These GEE files are intended to be uploaded and processed in the GEE Code Editor (https://code.earthengine.google.com/), requiring an account and attached cloud repository.

We intend to update this work annually, adding new or updated source datasets, re-running metadata extraction with updated NAIP imagery, and selecting the highest-quality array delineation from each version.

Acknowledgements

This chapter was co-authored by Anthony D. Kendall, Annick Anctil, Jeremy Rapp, James C. Bingaman, and David W. Hyndman. Funding support was provided by the USDA National Institute of Food and Agriculture INFEWS grant number 2018-67003-27406 (accession No. 1013707). Additional funding came from the Michigan State University Climate Change Research Support Program and the Foundation for Food and Agriculture Seeding Solutions grant program. The authors thank the contributors of source datasets as well as all OpenStreetMap contributors and community members. Any opinions, findings, and conclusions or recommendations expressed in this publication are those of the authors and do not necessarily reflect the views of the USDA, Michigan State University, or the Foundation for Food and Agriculture.

CHAPTER 3: IDENTIFYING NEW OPPORTUNITIES FOR DUAL-USE SOLAR ENERGY PRACTICES ON AGRICULTURAL LANDS IN THE US

Abstract

We are in the midst of a rapid shift in energy landscapes, with solar energy generation likely to lead the transition in the United States (US). Although necessary, the expansion of solar energy infrastructure raises concerns about land use tradeoffs, particularly regarding agricultural and natural ecosystems. In this study, we analyze the current state of US solar siting and management using a comprehensive national dataset of ground-mounted solar installation.

We use this dataset to quantify prior land use preferences and current prevalence of vegetated, barren, and impervious ground cover management practices. We find that 61% of solar installations by area are co-located with agricultural land, yet a large portion (46% of agricultural solar area) of sites are managed with barren ground cover (57% of all solar area), highlighting new opportunities for regenerative land management and various co-benefits. Utility-scale installations dominate overall land transformation, but we find commercial-scale solar is more distributed and more likely to be sited on marginal farmland and managed with vegetative cover. Our results underscore the need for improved incentives and policies to promote ecologically beneficial solar siting and management, ensuring that the US renewable energy transition supports both energy security and sustainable land stewardship.

3.1: Introduction

Eliminating global dependence on fossil fuels by achieving net-zero energy generation is a critical challenge of this century. Solar energy technologies (photovoltaics–PV and concentrating solar power–CSP) are particularly well-positioned to address this challenge, offering the greatest potential for rapid expansion in most countries alongside with battery storage (Breyer et al., 2018; Haegel et al., 2019; Victoria et al., 2021). Solar PV has become the most cost-effective source of new power (IEA, 2024; IRENA, 2024; Pathak et al., 2023) these can achieve lifecycle carbon, energy, and economic payback in the United States (US) within just a few years (Roy & Pearce, 2024; Smith et al., 2024; Stid, Shukla, et al., 2025). Although the benefits are clear, the land use demand of solar power installations remains a challenge (Lovering et al., 2022; Ritchie, 2022; Trainor et al., 2016), creating competition with natural and anthropogenic ecosystem services (Hernandez, Easter, et al., 2014).

The opportunity costs of solar energy land transformation depend on the current and future ecosystem services provided by the sited land (Moore-O'Leary et al., 2017). Effected ecosystem services can include food production, energy security, water resource management, nutrient stores, ecological habitat and connectivity, and social or community conditions (e.g., property value). In an effort to mitigate these tradeoffs, numerous studies have identified the potential for low-impact or marginal land to satisfy a portion of net-zero land requirements (Cunningham & Seidman, 2024; Hernandez, Hoffacker, & Field, 2015; Hoffacker et al., 2017; Joshi et al., 2021; Katkar et al., 2021; Macknick et al., 2013; Markwith, 2025; Milbrandt et al., 2014; G. C. Wu et al., 2020; Yang et al., 2020). Marginal land uses, such as rooftops, parking lots, landfills, and barren landscapes, have low opportunity costs because they are unlikely to provide critical ecosystem services that would be reduced by solar installation.

Agricultural covers nearly half of the US land area (Winters-Michaud et al., 2024) and has the greatest potential for solar energy generation (E. H. Adeh et al., 2019). It has become one of the predominant solar land uses globally (Kruitwagen et al., 2021; Maguire et al., 2024), but this has created a concern that continued solar energy buildout will threaten global food and agricultural security (Curioni et al., 2025; N. Zhang et al., 2023). Simultaneously, some argue that solar and agricultural co-location (herein, agrisolar) can enhance food and broader agricultural security depending on management and financial incentive structures (Cuppari et al., 2024; Stid, Shukla, et al., 2025). Marginal agricultural land, land with consistently low yields or productivity

due to physical or nutrient limitations, provides an opportunity for a low-impact land use with additional co-benefits.

Conversion of natural lands could also disrupt crucial ecological functioning due to habitat fragmentation, loss, and migration pathway disruption (Cameron et al., 2012; Grodsky et al., 2021; Grodsky & Hernandez, 2020; Karban et al., 2024; Levin et al., 2023; Rehbein et al., 2020). At the same time, others suggest renewable energy buildout is not as much a threat as previously believed, especially with informed siting (Ashraf et al., 2024; Dunnett et al., 2022). Within the US, the most recent projections suggest that up to 0.7% of natural land and 2.4% of cropland may be required to meet net-zero targets for 2050 (Diffendorfer et al., 2024). Despite this discourse, there has been limited analysis of whether solar energy installations in the US are actively converting prime ecological and agricultural lands, or the outcomes of the realized siting practices (Gómez-Catasús et al., 2024). Thus, a comprehensive national account of current land use practices for solar installations is necessary to address these debates and understand potential benefits, consequences, and opportunities of the realized solar energy landscape.

Siting decisions are a key component in determining the effect of the installation on natural and anthropogenic resource. Once the site is decided, site management decisions provide another opportunity to control the impact of the installation on land use. Dual-use designs, like ecovoltaic and agrisolar practices, have been shown to mitigate negative impacts of solar land use, and can even regenerate some natural resources (Knapp & Sturchio, 2024; Stid, Shukla, et al., 2025; Walston et al., 2022). These practices involve the intentional co-prioritization of the site's physical, ecological, and anthropogenic needs with electricity generation. This often involves informed vegetation retention, establishment, or re-establishment depending on the prior conditions of the site and the surrounding landscape (C. S. Choi et al., 2020, 2023; McCall, Macdonald, et al., 2023). Relative to conventional solar installations managed with bare soils or gravels, the benefits of these practices are substantial. Depending on the goal of the site, solar installations can be managed with native grasses, pollinator habitat, grazing habitat, or crop production within an agrivoltaic site (Walston et al., 2022).

Although the benefits of vegetation ground cover are clear for stormwater management, soil health, and habitat, little is known about the actual ground cover practices across the US solar industry beyond voluntary contributions to the National Renewable Energy Laboratory (NREL) InSPIRE database (NREL, 2025). Although this is the largest agrivoltaic database in the world

containing ~600 solar installations with documented vegetated ground cover, these installations represent a small portion of the total existing solar capacity. These installations may also be biased towards effective management practices since many are active research sites. The unreported solar energy landscape and future management practices may fall short of their "green" potential without additional and clear incentives for establishing and maintaining dual-use practices.

In this study, we used the largest available and most up to date ground-mounted solar installation dataset in the US to acquire information on the land use and land management practices of existing solar energy instalaltions. The spatiotemporal granularity of this dataset allowed us to estimate prior land use practices and current ground cover management practices across the entirety of the contiguous United States. We first provide a country-wide perspective, then present results by state and installation year. Finally, we compare commercial- and utility-scale solar energy practices. Given the pace of buildout, these results are a necessary modern complement to outdated or underrepresented understandings about where and how the solar energy landscape has been installed and managed in the US.

3.2: Methodology

3.2.1: Data sources

We used the Ground-Mounted Solar Energy in the United States (GM-SEUS) dataset developed in Chapter 2 of this dissertation to assess land use and land management practices of the existing solar energy landscape. GM-SEUS is a spatiotemporally complete dataset containing array and panel-row boundary information, installation year, and a suite of other design metadata attributes that is up to date with installations through the end of 2024. Importantly, GM-SEUS contains information on both commercial- (<1 MW_{DC}) and utility-scale (≥ 1 MW_{DC}) solar installations. This dataset compiles, harmonizes, and enhances information from a variety of solar energy data sources (Byers et al., 2021; Deline et al., 2021; Evans et al., 2021, 2023; Fujita et al., 2023, 2024; GEM, 2024; Global Energy Observatory et al., 2021; NREL, 2025; OpenStreetMap Contributors, 2024; Phillpott et al., 2024b, 2024a; Seel et al., 2024; Stid et al., 2022; Stid, Shukla, et al., 2023; Thonig et al., 2023).

Prior land use and management practices were acquired from a collection of remote sensing and remote sensing derived datasets as well as several data repositories. We used the United States Department of Agriculture (USDA) National Agricultural Statistics Service (NASS) Cropland

Data Layer (CDL) to derive prior land use practices (Boryan et al., 2011; USDA NASS, 2024). Gaps in CDL availability (pre-2008) were filled in with classes from the National Land Cover Database (NLCD) from the United States Geological Survey (USGS) (USGS, 2024). We acquired facility type information from the United States Large-Scale Photovoltaic Database (USPVDB) to include known brownfields and marginal land uses that are not likely to be represented in CDL (Fujita et al., 2023).

We used the high-spatial resolution aerial imagery (0.3-0.6 m, 2-3 year revisit cycle) from the USDA National Agriculture Imagery Program (NAIP) to classify ground cover practices within the most recently available imagery between 2021 and 2023 depending on the state (USDA FPAC-BC-GEO, 2023). Ground cover validation data was collected for 599 sites in the US from the National Renewable Energy Laboratory (NREL) Innovative Solar Practices Integrated with Rural Economies and Ecosystems (InSPIRE) Agrivoltaics Map (NREL, 2025). Marginal land classification and land productivity were from Jiang et al. (2021) and were downloaded from the Illinois Data Bank (C. Jiang et al., 2022). All remote sensing datasets were obtained (excluding land marginality) and processed using Google Earth Engine (GEE) JavaScript API, with all other analysis performed in R and Python.

3.2.2: Classifying prior land use and productivity for solar energy installations

GM-SEUS array boundaries (panel-rows and the inter-row spacing) were used to extract the spatially predominant (most common) land use land cover (LULC) for five years prior to solar installation. We aggregated CDL classes (and NLCD classes where necessary) into generalized superclass categories, which has been shown to enhance overall class accuracy (Lark et al., 2021). These superclass categories were Cropland, Grassland and Pasture, Natural, and Other LULC. Similar to the CDL cultivated classification (USDA NASS, 2025), the most common superclass category over five years prior to installation was considered the prior land use for that array.

There are several key assumptions made with CDL class aggregation. Importantly, the fallow and idle class (CDL class: 61) was included in the Cropland superclass (Lark et al., 2021). Additionally, CDL does not differentiate between cultivated pasture and natural grasslands. Thus, the CDL Grassland/Pasture (CDL class: 176) contained both natural and cultivated grasslands and composes the entirety of the Grassland and Pasture superclass. The Other LULC category represents all non-natural or cultivated land covers encompassing mostly land that is considered low-impact and marginal in use. This category includes predominantly developed and barren land,

and all brownfield facility types from USPVDB.

Productivity, or marginality, of converted land was estimated using spatially explicit marginal land classification maps, and maps of land productivity derived from physical landscape characteristics (C. Jiang et al., 2021). Here, marginality was defined as economically marginal, and derived by integration of physical datasets and models, climate data, crop models and maps, and census data, to elicit land productivity, vulnerability, and profitability at 30 m resolution (C. Jiang et al., 2021). The modal marginality classification for confident and unconfident marginality and the mean land productivity were extracted within the GM-SEUS array boundaries.

3.2.3: Differentiating ground cover management practices

We differentiated general ground cover practices between the three end member ground covers thought to be most common within the existing landscape: vegetation, barren (bare soil or sparsely vegetated), and impervious surfaces. Note that real ground cover practices likely contain a mix of these ground covers, and that several ground covers are not represented by these classes (e.g., water, gravels, and mulches).

The brightness-darkness-greenness (B-D-G) model is an effective approach for generalized land surface classification (Qiu et al., 2017). Given that the end member ground covers conceptually follow a brightness (barren), darkness (impervious surfaces), and greenness (vegetation), the B-D-G approach was used to logically cluster ground cover pixels within array bounds. Spectral indices used to represent this approach were 4-band brightness (Br), the normalized difference photovoltaic index (*NDPVI*) (Stid et al., 2022), and the normalized difference vegetation index (*NDVI*) (Kriegler et al., 1969; Rouse et al., 1974), representing brightness, darkness, and greenness respectively. *NDPVI* and *NDVI* are calculated by Eq.'s 1 and 4.

NAIP imagery was masked by GM-SEUS solar array boundaries buffered by 5 m to include the fenced-in area. GM-SEUS panel-rows were used to mask pixels containing solar modules, resulting in a top-down aerial representation of only ground cover pixels. Ground cover pixels were then locally (within-array) clustered using GEE implementation of unsupervised K-means clustering (wekaKmeans) using Br, NDPVI, and NDVI into four clusters including one for each general ground cover, and one to account for solar panel-row pixels remaining after being masked (GM-SEUS omission error). This gave each array the opportunity to have each ground cover type. The corresponding mean, maximum, and minimum index values for each index and

cluster were exported and globally (across all arrays) clustered using K-means clustering in R (Maechler et al., 2024) into three clusters. Global cluster number selection was evaluated by maximizing the overall silhouette coefficient. Silhouette values range from -1 to 1, where higher values indicate stronger clustering structure (Kaufman & Rousseeuw, 1990). We considered the brightest cluster as barren, the darkest cluster as impervious surfaces, and the greenest cluster as vegetation.

Within each array, a dominant ground cover type was assigned based on the proportional coverage of each ground cover and several conditions. We considered arrays with more than 50% vegetation coverage as Highly-Vegetated and between 25% and 50% vegetation coverage as Low-Coverage Vegetated. Given GM-SEUS panel-row omission error, which would result in greater estimated impervious cover than reality, we required an array to have 75% impervious cluster coverage to be considered Impervious. Otherwise, arrays were considered Barren or Low-Coverage Vegetated based on the dominant remaining coverage.

To evaluate clustering results, we used the ratio of the Between-Cluster Sum of Squares (BCSS) to the Total Sum of Squares (TSS), where TSS is equal to the sum of BCSS and the Within-Cluster Sum of Squares (WCSS). A higher BCSS/TSS ratio (ranging from 0 to 1) indicates clusters that are more compact within clusters and more heterogeneous between clusters. Additionally, we report both overall and between-cluster silhouette scores, which measure the relative similarity of points within a cluster compared to other clusters.

3.2.4: Statistical evaluation

We used the Wilcoxon Ranked-Sum significance test to determine significance in the land productivity distribution mean from the global mean of 0.5 (Wilcoxon, 1945). Given that our sample size was large (~8,000 to 15,000), we used Cohen's d to measure the effect size between the two means (J. Cohen, 1988). Generally, Cohen's d effect sizes indicate a small effect (~0.2), medium effect (~0.5) or large effect (~0.8).

3.3: Results

3.3.1: Solar energy installations are sited on agricultural and natural lands

We estimated prior land use by area and number of installations through time for 15,017 solar energy installations (2,944 km^2 and 186 GW_{DC}). By area, prior solar land use total share was 44% Cropland, 36% Natural, 17% Grassland and Pasture, and 3% Other LULC (Figure 17 and

18). By number of installations, prior land use share was 44% Cropland, 19% Natural, 14% Grassland and Pasture, and 23% Other LULC (Figure A37). If we consider Cropland and Grassland and Pasture agricultural land, 61% of solar by area and 59% of solar by number of installations resides on land that was previously or is still used for agricultural purposes (agrisolar co-location).

Spatially, the areal share of prior land use varied regionally, with as little as 0% agricultural land use in Washington DC, to 99.8% in South Dakota and Oklahoma (Figure 17). Though, note that total solar area varies regionally as well, with Texas transforming the most agricultural land (433 km^2), followed by California (239 km^2) and Florida (131 km^2). Excluding agricultural land uses, Natural land prior use was the second most prominent use, with California transforming 238 km^2, Texas 229 km^2, and Nevada 91 km^2.

Considering agrisolar installations across the US, 14% of solar array area (22% by number of installations) resides on confidently or potential marginal cropland land. Average land productivity, based on soil inventory, terrain, climate data, and several iterations of the National Commodity Crop Productivity Index (NCCPI) model, was 0.45, indicating average use of land with slightly lower than average productivity. This was significantly different from 0.5 ($p<2.2e^{-16}$), though had a small effect size (Cohen's d = 0.31).

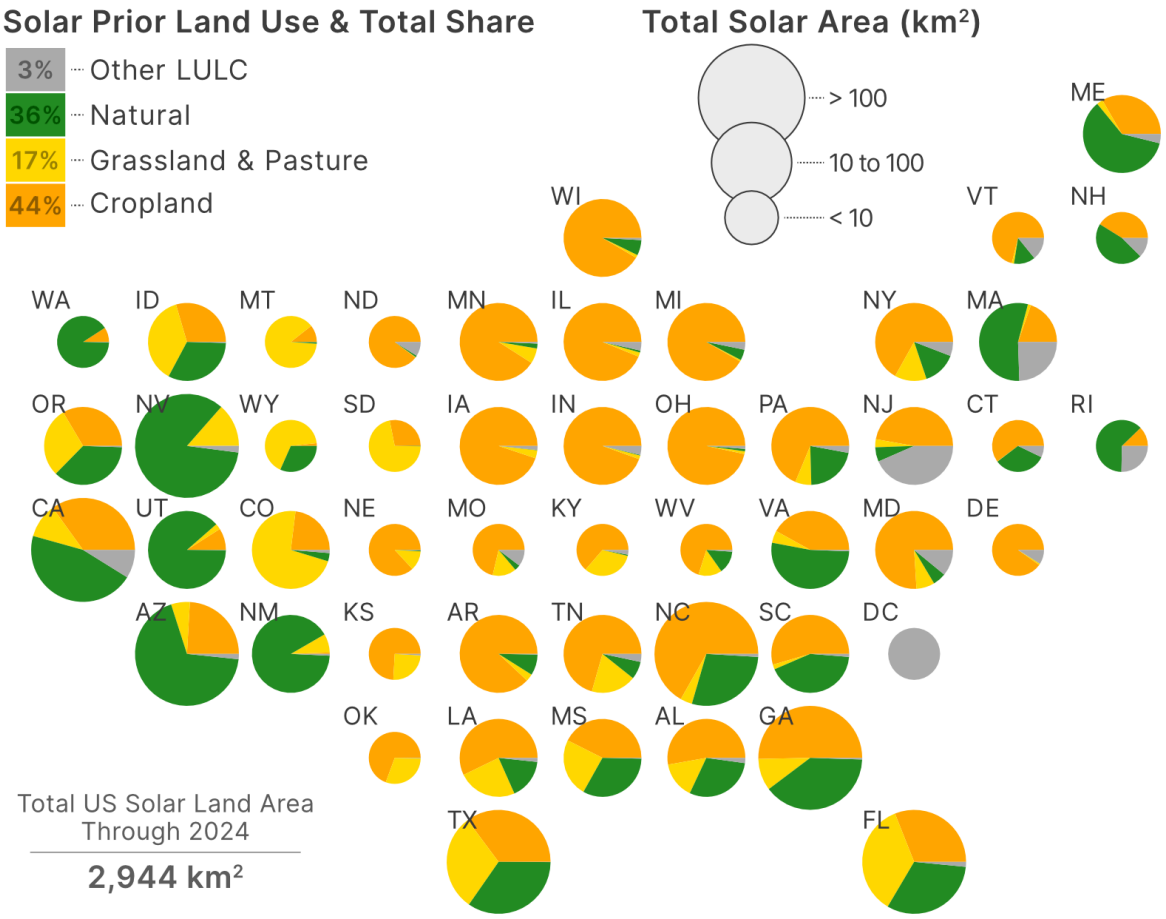

Figure 17. Solar energy prior land use proportion by area at the state-level. Prior land use delineated by state total proportion, with pie chart size representative of the total solar area within the state. Context for state shorthand names can be found in Figure 38.

By age of installation, land use change preferences by area have generally been consistent, though 2024 showed a peak in agrisolar co-location of 81% of total area converted (Figure 2). By number of installations, the proportion of agrisolar co-location indicates the same relationship, with a steadier increase from ~53% before 2010 to 82% in 2024 (Figure A37). Other LULC proportion by installation is primarily responsible for this decrease. Though, note that GM-SEUS uncertainty is greater for arrays installed in 2024, given that these arrays have yet to be quality controlled within GM-SEUS or existing datasets due to the lack of up-to-date imagery.

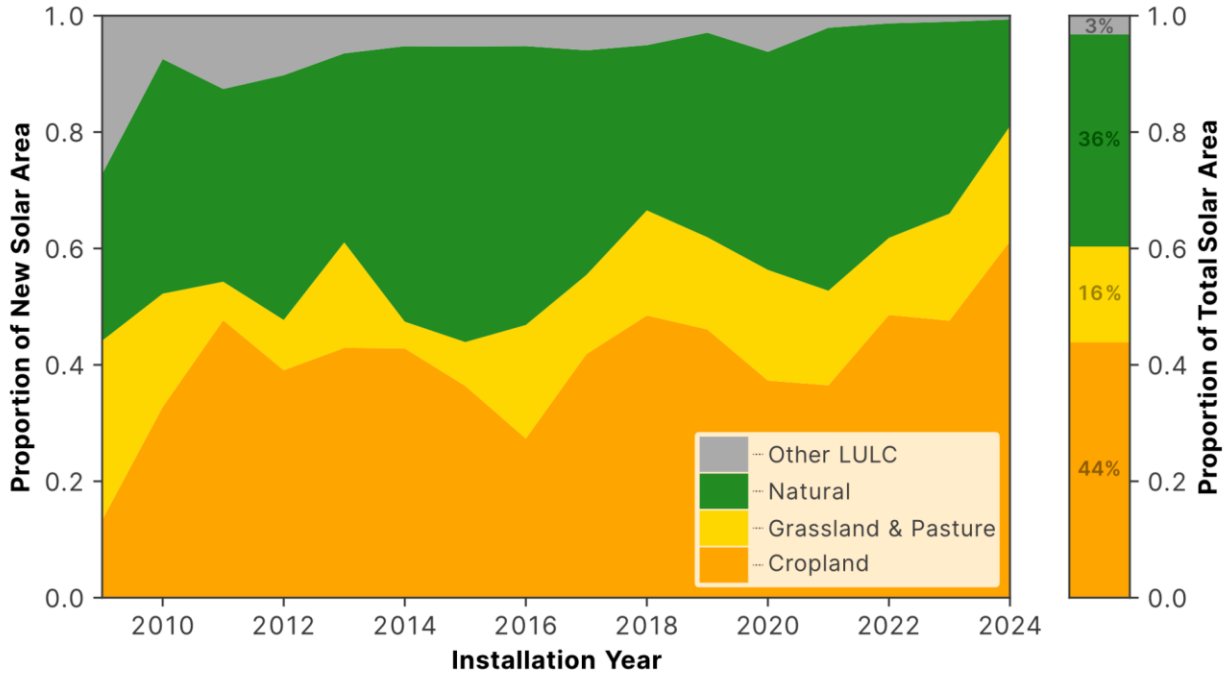

Figure 18. United States solar energy prior land use proportion by area through time. Prior land use was derived from the Cropland Data Layer predominant land use within the array bounds for five years prior to installation. Land cover classes were grouped into representative superclusters. Note that this figure does not indicate temporal changes within arrays, but across arrays of different installation years. Compare to Figure A37 by number of installations.

Several CDL classes could be critiqued as non-active agriculture land that are encompassed by the agricultural superclasses. Within the Cropland superclass, 5% of area was fallow or idle cropland. Within the Grassland and Pasture CDL class that includes both cultivated and natural grasslands, 57% of the arrays by area were Pasture/Hay or Cultivated Crops in NLCD classification, 40% were Grassland/Herbaceous and Shrublands. Though these two classifications have some of the lowest CDL certainty and are often mislabeled active cropland (Lark et al., 2021), removing them still results in 50% of solar by area having an agricultural prior land use.

3.3.2: Solar energy ground cover is predominantly barren

We differentiated general solar array ground cover practices for 8,834 solar energy installations (1,363 km^2 and 82 GW_{DC}) that contained panel-row information and where NAIP imagery of the array was available. Global clustering resulted in three end member ground cover types with 61% of ground cover area classified as barren, 24% classified as vegetation, and 15% classified as impervious. Note, that impervious area likely includes any solar panel-row area that was omitted in GM-SEUS, and potentially water for floatovoltaic practices, given water's high

NDPVI value (Stid et al., 2022). Bare soils may also include highly reflective gravels and concrete, and dry or sparse vegetation. Across 35,000 unique ground cover clusters, the BCSS/TSS ratio was 0.48, indicating moderate cluster separation. The median silhouette score across all clusters was 0.36. Median silhouette scores for specific class boundaries were 0.40 between vegetation and barren, 0.27 between vegetation and impervious, and 0.29 between barren and impervious, again indicating low to moderate separation. Cluster distributions and a ternary visualization are found in Figure 39.

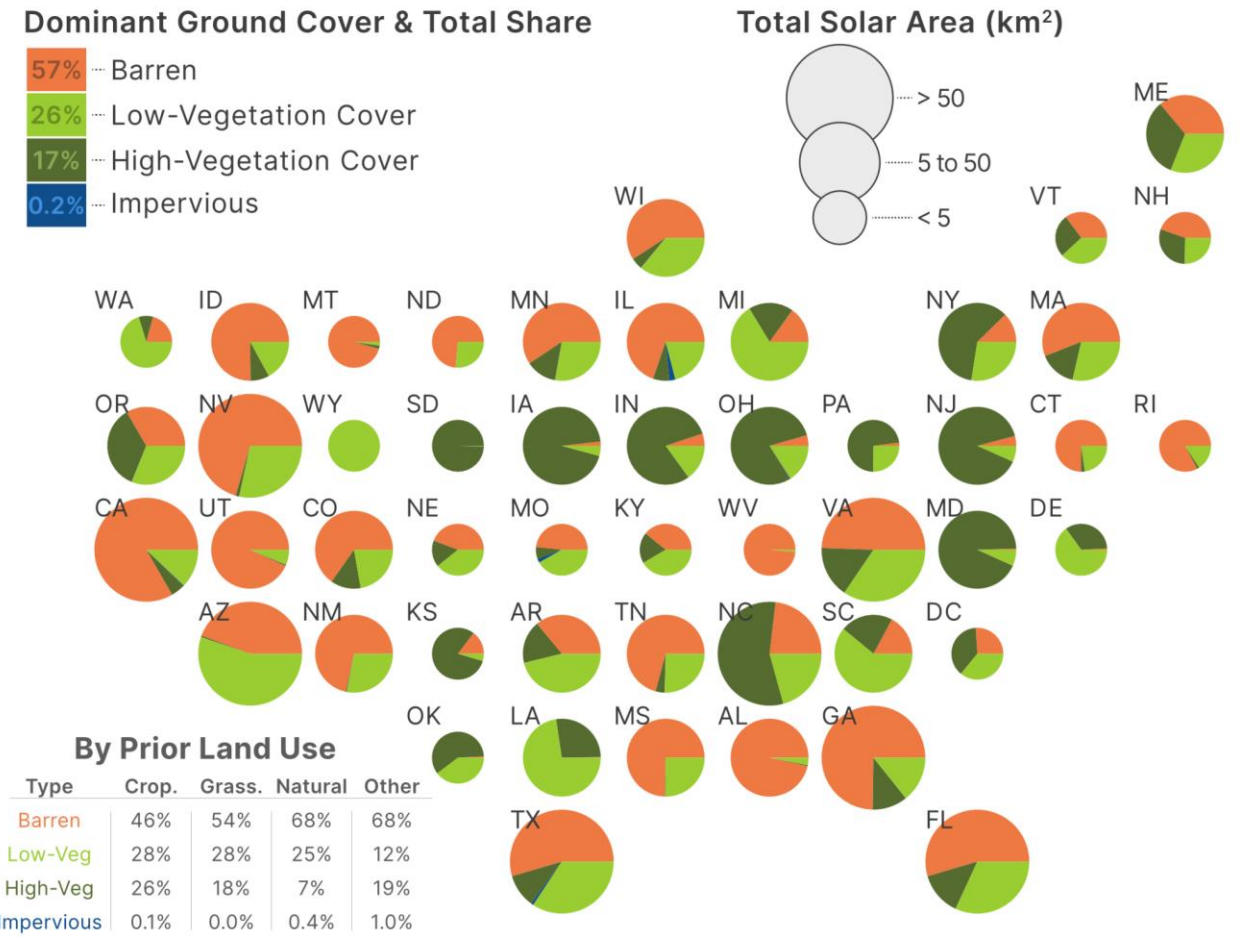

Figure 19. Solar energy prior land use proportion by area at the state-level. Prior land use delineated by state total proportion, with pie chart size representative of the total solar area within the state. Context for state shorthand names can be found in Figure 38. Note that relative to Figure 17, the pie chart scale is halved, due to the filtered number of installations considered for the ground cover analysis.

Considering the dominant ground cover management practice within each array (and our conditions), 57% of solar arrays by area in the US are predominantly managed with bare soil (or sparse vegetation), 26% are managed with some vegetative cover, 17% are managed with a

majority vegetative cover, and less than 1% are managed with impervious cover (Figure 19). When broken down by prior land use (Figure 19), agricultural land has the highest percentage of array area managed with vegetation (54% for Cropland, 46% for Grassland and Pasture). Spatially, midwestern and eastern US states tended to have a greater proportion of vegetated array area, though some states in other regions maintained high cover (e.g., Oregon, Louisiana) potentially as a result of effective policy guidance. Temporally (Figure 20), ground cover practices have remained relatively consistent relative to the global average.

We compared our ground cover estimates to the NREL InSPIRE Agrivoltaics Map array database of reported agrivoltaic installations. Of the 600 agrivoltaic installations in the database, we generated ground cover estimates for only 253 that contained a reported agrivoltaic type (mostly pollinator). Omissions were either due to the non-availability of GM-SEUS panel-row information or temporal limitations of NAIP. We estimated that 144 of these arrays were vegetated, 106 were barren, and three were impervious. We qualitatively observed the ground cover of the three impervious classified arrays and found them to contain predominantly bright dry grasses and impervious or barren access roads.

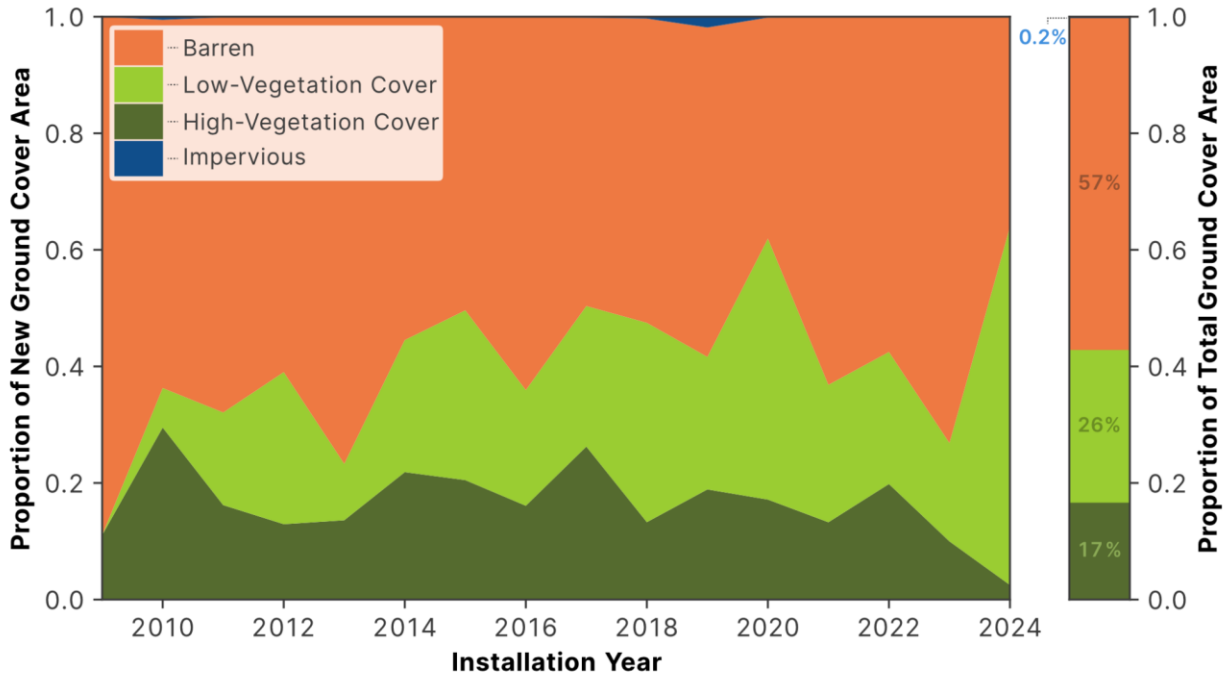

Figure 20. United States solar energy prior land use proportion by area through time. Ground cover management practices were derived from logical clustering of the most recent NAIP imagery. Note that only 8,834 arrays are represented here given availability of panel-row

Figure 20 (cont'd)

information and NAIP imagery. Also, this figure does not indicate temporal changes within arrays, but across arrays of different installation years. Compare to Figure A40 by number of installations.

3.3.3: Variability exists across scales of solar installation

We separated land use and management practices into commercial- (<1 MW_{DC}) and utility-scale (≥1 MW_{DC}) solar installations. For land use, we assessed 5,386 commercial-scale (2.1 GW_{DC}, 26.3 km^2) and 9,631 utility-scale arrays (184 GW_{DC}, 2,918 km^2). For ground cover, we compare 3,794 commercial-scale (1.3 GW_{DC}, 16 km^2) and 5,040 utility-scale arrays (80 GW_{DC}, 1,346 km^2). For marginality, we compared only agrisolar arrays with 2,358 commercial-scale (1 GW_{DC}, 14 km^2) and 6,282 utility-scale arrays (115 GW_{DC}, 1,763 km^2).

Both commercial- and utility-scale solar installations in the US occupy mostly agricultural land and are roughly half managed with barren ground covers (Figure 21). However, a few interesting distinctions emerged. Utility-scale arrays are responsible for a vast majority of land use transformation (99%) and tend to convert more agricultural (61%) and natural (37%) lands by proportion than commercial-scale solar. Though roughly the same proportion of area contains some form of vegetation, commercial-scale arrays were qualitatively more often managed with high-density vegetation.

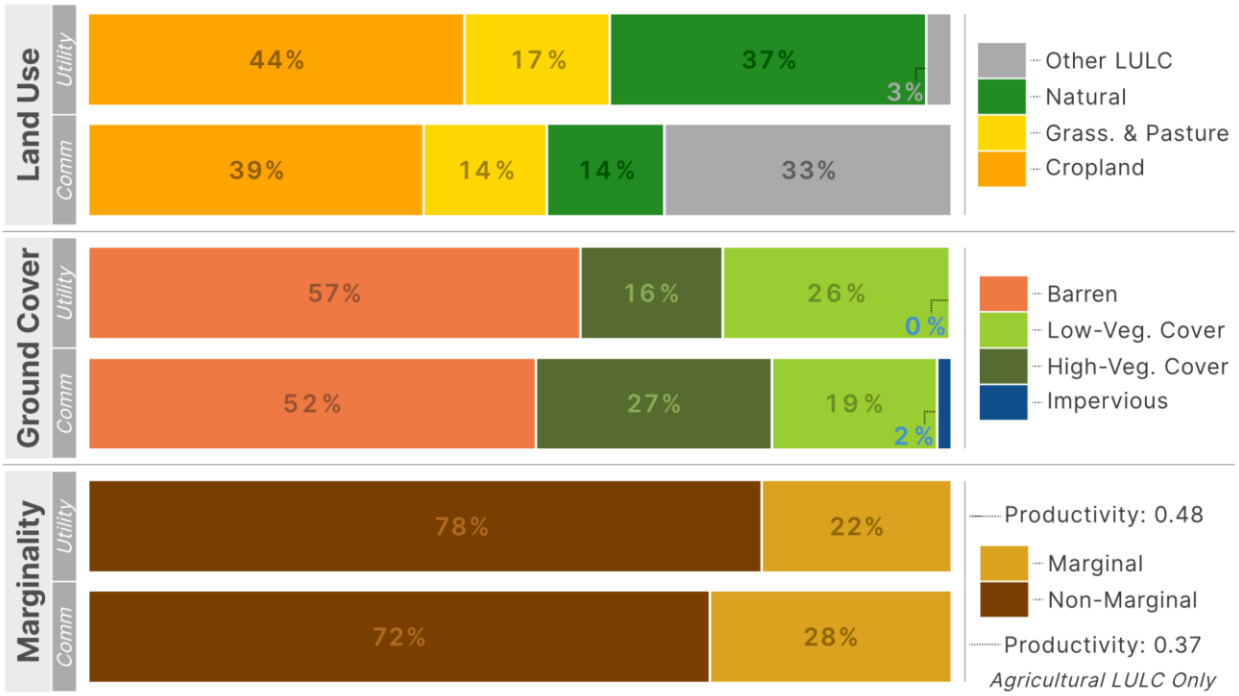

Figure 21. Proportional land use, ground cover, and marginality by scale. Proportions are a function of total area. Commercial-scale solar is defined as peak rated capacity <1 MW_{DC}. Utility-scale solar is defined as having a peak rated capacity of ≥1 MW_{DC}.

Roughly one quarter of cropland occupied by both commercial- and utility-scale solar installations is economically marginal. Additionally, agricultural land productivity was significantly lower than average (assuming a global average of 0.5) for both commercial-scale (0.37) and utility-scale (0.48) installations ($p<2.2e^{-16}$). However, for utility-scale installations, the effect size was 0.14, indicating none to small practical impact. For commercial-scale installations, the effect size was 0.79, representing a large effect. This suggests that commercial-scale solar installations across the U.S. tend to be placed on physically marginal (-13%) croplands.

3.4: Discussion

3.4.1: Solar energy is an agricultural commodity

Regardless of region, time period, or scale of installation, solar energy in the US is installed on agricultural lands. Several studies have identified that cropland and rangelands (together, agricultural land) compose a considerable (Curioni et al., 2025; Kruitwagen et al., 2021; Maguire et al., 2024) yet regionally varying (Evans et al., 2023; Hernandez, Hoffacker, Murphy-Mariscal, et al., 2015; Katkar et al., 2021; Leskova et al., 2022; Maguire et al., 2024; Pitt et al., 2024; Stid et

al., 2022) proportion of existing US solar land use. Our results support this regional variability (Figure 17) yet also display a country-wide preference for converting agricultural (61%) and natural (36%) lands to solar energy infrastructure (Figure 18). Importantly, land use information derived here is more complete than existing studies, including both commercial- and utility-scale solar, and is up to date (through 2024), with the most recent year indicating that 81% of new solar energy areas were agricultural in use prior to installation. Regardless, both by area and by number of installations, a majority of US solar land use is agricultural, indicating that solar energy has become an agricultural commodity.

In some regions of the world, new policies have discouraged or even prohibited the use of prime agricultural land for solar energy (IESO, 2025; UK Government, 2024) despite the productive potential of those regions (Jamil et al., 2023; Neesham-McTiernan et al., 2025). These restrictions often stem from fear over permanent loss or degradation of prime agricultural land and fear of cultural losses as agricultural communities become agroenergy communities (J. Crawford et al., 2022; Pascaris et al., 2020). Improper management of large-scale solar energy projects (utility-scale) in particular has driven much of this concern, creating the food vs. fuel conflict (Berryhill, 2021; Bessette et al., 2024; J. Crawford et al., 2022).

There is little evidence that these concerns cross into smaller-scale solar projects (Nilson & Stedman, 2022). In some regions, negative impacts are dominated by a few large-scale facilities (Pitt et al., 2024). More than a third of US solar capacity is commercial-scale (EIA, 2025) and policies and incentives for siting and management differ greatly between these two scales, along with varying tradeoffs of land use transformation (Crago & Koegler, 2018; Gómez-Catasús et al., 2024; Nilson & Stedman, 2022; Stid, Shukla, et al., 2025). Recent work even shows evidence that together, agrivoltaic practices and small-scale solar enhance the acceptance of agricultural co-location in conservationist surveys (Hilker et al., 2024). Our previous work has also shown that effective incentives and resource management can provide an opportunity to enhance agricultural security in some regions despite crop displacement, and that commercial-scale solar farmland owners stand to benefit more than utility-scale owners per hectare (Stid, Shukla, et al., 2025). Broad-sweeping policies that outright prohibit solar development on farmland could restrict these resource and economic opportunities for farmland owners seeking to install small-scale solar (Pascaris et al., 2021).

There is ample evidence that marginal or non-agricultural lands can contribute a

considerable portion of the renewable energy landscape (Cunningham & Seidman, 2024; Hernandez, Hoffacker, & Field, 2015; Hoffacker et al., 2017; Joshi et al., 2021; Katkar et al., 2021; Markwith, 2025; Milbrandt et al., 2014; G. C. Wu et al., 2020; Yang et al., 2020). However, few studies have identified the realized use of marginal lands beyond its potential (Berryhill, 2021; Katkar et al., 2021; Stid et al., 2022) and this study indicates that non-agricultural lands make up a shrinking non-majority of solar array area in the US. Here, we consider marginal land as agricultural land that is below average productivity and economic value (C. Jiang et al., 2021) and find that about 22% of utility-scale array area and 28% of commercial-scale array area occupies economically marginal cropland. Importantly, we found that commercial-scale arrays tend to be sited on physically marginal land (low productivity) across the US. Though, we acknowledge the limitations of this data product that is not validated with ground-truthed data, and importantly, that marginality is highly-variable based on the scope and scale of interest (Csikós & Tóth, 2023).

3.4.2: New dual-use opportunities for regenerative practices

We estimate that most of the ground cover management in the US is barren, bare soil, or sparsely vegetated, with 43% of solar arrays having some amount of vegetation coverage. This was relatively consistent across installation age (Figure 20) but varied considerably by state and region (Figure 19). Ground cover practices also varied with prior land use, with agricultural land containing more vegetated array area than arrays on Natural and Other LULC (Figure 19). Commercial-scale installations were also estimated to be managed with more high-density vegetation than utility-scale arrays. There is also some evidence that states with mandated solar pollinator scorecards have considerably greater vegetation coverage than states with opt-in or no scorecard (Figure A41), though, more work is needed to understand this relationship across timescales and regions.

Agricultural lands in the US have historically experienced carbon depletion (Drewniak et al., 2015) and create an ongoing threat to biodiversity (Molotoks et al., 2018). Siting solar energy installations on already degraded lands (in carbon and biodiversity) presents an opportunity to minimize conversion of new land crucial for existing diversity and migration pathways (Rehbein et al., 2020) and to regenerate depleted ecosystems and resources (Aragon et al., 2024; Carvalho, Healing, et al., 2024; Frank et al., 2024; Knapp & Sturchio, 2024; Stid, Shukla, et al., 2025; Walston et al., 2022). Recent evidence suggests that compared to the prior agricultural land use, informed ground cover habitats can also lead to enhanced pollinator forage quality, abundance,

and richness (Blaydes et al., 2022; Graham et al., 2021; Walston et al., 2021, 2024). Various studies also provide evidence of enhanced carbon and nutrient stores at ecovoltaic and agrivoltaic dual-use sites (C. S. Choi et al., 2023; Krasner et al., 2025). Given the depleted soil carbon, nutrient stores, and ecological productivity of agricultural land in many regions, these lands hold significant potential to act as carbon and biodiversity sinks.

We found that roughly half of solar arrays installed on agricultural lands (46%) have no form of productive ground cover. Further, of the agriculturally co-located solar arrays not managed with vegetation in our analysis, 300 km^2 are on economically marginal land and 850 km^2 are on land of below average physical productivity. A few additional key advantages of dual-use practices across landscapes include effective stormwater management (Yavari Bajehbaj et al., 2024), enhanced crop yield (Barron-Gafford et al., 2019), improved module efficiency (Williams et al., 2023), broad benefits to ecological functioning (Knapp & Sturchio, 2024), and enhanced public support (Pascaris et al., 2022), though many of these effects are regionally varying and site dependent (C. S. Choi et al., 2024). Our results suggest new opportunities for achieving the benefits of newly vegetated solar landscapes, particularly on marginal lands.

3.4.3: Limitations and future work

There is limited validation data available for ground cover practices at this scale. A few key studies have also indicated that even with highly-robust management practices, vegetation coverage can vary across the year (Li et al., 2025) and can take several years to establish and reach majority cover (McCall et al., 2024).

We identified agrivoltaic arrays (pollinators, native grass, naturalized) as vegetated with an accuracy of 60% relative to the NREL InSPIRE Agrivoltaic database, where accuracy is defined as True Positives / Total Predictions. However, due to the lack of validation data for other ground cover types (e.g., barren, impervious surfaces), we are unable to report class-specific accuracy metrics for those categories. Most of the 40% False Negative error was a misclassification of the barren category. However, agrivoltaic status is not necessarily representative of whole-array ground cover, and practices may change within and across years (Li et al., 2025; McCall et al., 2024).

There are several additional limitations of this analysis that need to be addressed. First, the GM-SEUS dataset acknowledges omissions of within-array panel-rows, leaving those to be classified as ground cover. This may lead to overestimation of impervious surfaces. Second, given

that aerial imagery cannot see under the panels, we may also overestimate (Carvalho et al., 2025) or underestimate (Li et al., 2025) the extent of vegetation cover depending on management practices, plant mix, climate, and soil conditions. Finally, we have qualitatively observed ground cover class overlap, with sparse or dry grasses observed in NAIP being classified as barren, and impervious (e.g., parking lot) cover being classified as barren. The extent of error is not yet clear and requires further investigation.

3.4.4: Land use and management in a net-zero future

Net-zero energy generation in 2050 will require between 60,000 and 90,000 km^2 of the contiguous US land surface for solar, a 20- to 30-fold increase from the solar area reported here (Ardani et al., 2021; Heath et al., 2022; Jenkins et al., 2021; Larson et al., 2021). Despite broad concern over loss of agricultural land, it is clear that net-zero buildout in the US is and will be inextricably linked to agricultural land access and availability and that the two can co-exist in harmony when effectively sited, managed, and incentivized (Moore et al., 2022). These synergies can simultaneously include both a) siting on heavily depleted (marginal) croplands and managing with ground cover to regenerate natural resources, and b) siting within average or prime agricultural land and employing informed agrivoltaic production or cultivation that benefits or maintains land productivity and agricultural income. Both examples are viable forms of dual-use. However, to reduce the use of prime agricultural land, smaller and more distributed solar energy installations are better able to selectively identify and employ marginal lands. Given that ~46% of contiguous US land surface is actively cultivated (Winters-Michaud et al., 2024), and that up to 2.4% of that land may be needed for a net-zero future (Diffendorfer et al., 2024), it is crucial to understand current practices to better understand future development of solar installations across the country.

Although we do not directly interpret land ownership, our work is a modern complement to existing knowledge showing that solar energy is a commodity that individual, and often private landowners can and are actively taking advantage of (Hernandez, Hoffacker, et al., 2014). This also means that management is more often in the control of private individuals rather than utilities or federal, state, local, or other regulating authorities. Increasingly common bifacial module technologies benefit from highly reflective ground cover mediums (e.g., soils, gravels, concretes) compared with vegetation (Sun et al., 2018), which may reduce motivation to manage ground covers with dual-use practices. It is thus evident that extensive policy support and publicly

available resources are essential to make dual-use practices like ecovoltaics, agrisolar, and agrivoltaics, competitive with conventional (barren) solar practices for both individual landowners and larger entities (Carvalho, Lee, et al., 2024; Feuerbacher et al., 2021, 2022; Moore et al., 2022; Pascaris et al., 2023). Several tools, data products, and guidance insights have been created to aid in the application of such knowledge and retention of positive practices in siting (Ashraf et al., 2024; Hernandez et al., 2019; Sorensen et al., 2022) and effective ground cover design and management selection (Galzki & Mulla, 2024; Jamil et al., 2023; Kim Steinberger, 2021; Peterson et al., 2025; Warmann et al., 2024; Williams et al., 2025) for future solar installations.

Acknowledgements

This chapter was co-authored by Anthony D. Kendall, Annick Anctil, Rufus Isaacs, and Jeremy Rapp. Funding support was provided by the USDA National Institute of Food and Agriculture INFEWS grant number 2018-67003-27406 (accession No. 1013707). Additional funding came from the Michigan State University Climate Change Research Support Program. Any opinions, findings, and conclusions or recommendations expressed in this publication are those of the authors and do not necessarily reflect the views of the USDA or Michigan State University.

CHAPTER 4: WIND FARMS BOOST FARMER INCOME WITHOUT THREATENING AGRICULTURAL SECURITY ACROSS THE US CORN-BELT

Abstract

Renewable energy often requires the semi-permanent alteration of land from its prior use, creating potential tradeoffs. In the US, most wind farms have been installed in agricultural fields, yet the local and aggregate effects on agricultural lands remain unclear. This study examines the crop yield and economic impacts of 37 GW of wind turbine installations across the US Corn Belt. We introduce and quantify two metrics to assess each turbine: 1) the Agricultural Radius Of Effect (AgROE), which delineates the directly affected area, and 2) an agricultural land-use efficiency (*LUE*). Analyzing 17,557 turbines, we identified a total directly affected agricultural area of 65,000 ha and found that *LUE* has increased over threefold in the last two decades. Maize and soybean yield within the AgROE of each turbine showed statistically significant average yield reductions. However, the total impact on crop production was small (e.g., 78,000 tonnes of maize and soybeans in 2022), and land leases more than compensated for economic losses, increasing on-farm income by $63 million ($3,760 per average turbine) in 2022. Additionally, we observed a small preference for siting wind turbines on low-yielding cropland, offering marginal economic benefits. This study highlights the synergies of co-locating wind turbines with agriculture, demonstrating that wind power can enhance farm economic stability, thus supporting food security in a net-zero future.

4.1: Introduction

Renewable energy expansion is projected to directly transform 1 to 2%of the contiguous United States (CONUS) landscape by 2050, leading to indirect effects on 11% of land (Jenkins et al., 2021; Larson et al., 2021). Because renewable energy installations require transforming land (Lovering et al., 2022), it is imperative to consider the associated opportunity costs and trade-offs (Grodsky, 2021; Trainor et al., 2016). Given that most current solar and wind installations are co-located with and convert agricultural land (Harrison-Atlas et al., 2022; Kruitwagen et al., 2021; Maguire et al., 2024), these trade-offs involve food and economic security. Yet, despite decades of widespread deployment of wind turbines in agricultural lands, effects of those installations on agricultural production remain understudied.

Agricultural land use trade-offs of wind power are substantially less studied than those for solar PV, despite widespread global adoption of wind power. Co-locating renewable energy within agriculture can create opportunity costs related to food security, farm income, and food prices (Barrett, 2021) that depend on the total extent of land alteration. However, these can be offset either through financial compensation (e.g., land leases) to the land owner (Sutherland & Holstead, 2014), offset operational costs (Stid, Shukla, et al., 2025), or by possibly enhancing yields (Kaffine, 2019). Regarding the extent of alteration, available insights suggest that wind turbine direct footprints are ~10-times less intensive than solar (Lovering et al., 2022). This, in part, explains why farmer interviews indicate that wind is more desirable than solar, considering that cultivation can easily continue around the turbine (Moore et al., 2022). However, spatially defining a standardized footprint for wind power is difficult due to the lack of visual boundaries and discontinuous nature of wind farms (Harrison-Atlas et al., 2022). Some studies have broached this gap with wind power by manually digitizing visually-affected boundaries (Diffendorfer & Compton, 2014; Jones & Pejchar, 2013) or using machine learning (Dai et al., 2024). Others report average values for land use metrics rather than estimates for individual installations that can depend on region, level of modification (Dai et al., 2024), installation age (Harrison-Atlas et al., 2022; Rinne et al., 2018), land cover and topography (Diffendorfer & Compton, 2014; Qin et al., 2022), and system size (Saganeiti et al., 2020).

Siting renewable energy on consistently low-productivity (marginal) agricultural land is one potential solution to food, farmland, and economic security concerns (Khanna et al., 2021; Yang et al., 2020). Although definitions of marginality vary, several studies have shown the

potential for installing renewable energy on marginal lands (Adelaja & Hailu, 2008; Diffendorfer et al., 2019; Katkar et al., 2021; Milbrandt et al., 2014). Furthermore, farmers preferred the idea of converting non-prime farmland to renewable energy installations, given the cost-savings of forgoing low-return cultivation (Moore et al., 2022). However, demonstrated examples of preferential siting within marginal lands in practice are variable and scarce, and the agricultural effects of marginal placement have not been well studied.

Several studies have considered the possible regional effects of wind turbines on agriculture, and more broadly vegetation productivity. Diffendorfer et al. (2022) delineates two pathways through which wind turbines can impact vegetation that are supported by these studies; direct surface disturbance (Dai et al., 2024; Morris & Blekkenhorst, 2017) and wake effects that alter local microclimates and can thus go beyond direct surface disturbance (Aksoy et al., 2023; Cetin et al., 2022; T. Chen & Li, 2019; Diffendorfer et al., 2022; Kaffine, 2019; Li et al., 2018; Luo et al., 2021; Qin et al., 2022; Rajewski et al., 2013, 2014, 2016; D. Wu et al., 2023; W. Zhang et al., 2013). While the mechanisms for alteration of local microclimates are well documented (Baidya Roy & Traiteur, 2010; Keith et al., 2004; Zhou et al., 2012) and total direct surface disturbance due to new operational infrastructure is known to be small (Dai et al., 2024), outcomes for agricultural production in these studies vary or are absent leaving regional food security effects uncertain.

No studies have directly measured the local on-farm effects of existing wind turbines on agricultural yield and income. This gap in research may be due to the difficulty in identifying direct physical surface disturbances (Harrison-Atlas et al., 2022) or the low resolution of available yield data, which limits the refinement of studies reporting on local effects (Diffendorfer et al., 2022). The crop yield-focused studies from the Crop Wind Energy Experiment (CWEX) (Rajewski et al., 2013, 2014, 2016) provided the most spatially-refined assessment, but were not yet able to determine the effect of wind turbines on agricultural production (Rajewski et al., 2014). Many other studies define “local” as a multi-kilometer radius or directional distance from turbines, rather than isolating on-farm effects. Understanding these on-farm effects could provide insight into farmer decision-making, lease motivations, changes in farm production post-wind installation, and the anthropogenic factors influencing yield changes.

We provide the first comprehensive assessment of the local on-farm agricultural effects of wind turbine co-location on crop yield (maize and soybean) and farmer income through time. We

delineate the affected area of each turbine across the US Midwest using a new metric, the Agricultural Radius Of Effect (AgROE), a remotely-sensed measure of land disturbance surrounding turbines. Within and outside of the AgROE, we report on the direct operational footprint of wind turbines. We also identify and report on the total crop field area intersecting with wind turbine footprints, which we call the co-located field. To assess changes in crop yield within the AgROE, and within-field siting decisions for each turbine, we capitalize on a recently developed high-resolution dataset of maize and soybean yield maps (Deines et al., 2021; Lobell et al., 2015). This rich dataset captures within-field annual yield variations, both inside the AgROE and the co-located field, allowing the marginal placement of each turbine to be identified. We then quantify the field-level economic impact of estimated production losses relative to expected land lease income. Finally, we test three hypotheses (illustrated in Figure 22): (1) wind turbines create a disturbance within a co-located field that can extend beyond the operational infrastructure footprint, (2) this disturbance results in quantifiable yield reductions within the AgROE, and (3) wind turbines are preferentially sited in less-productive areas of a field to reduce negative impacts.

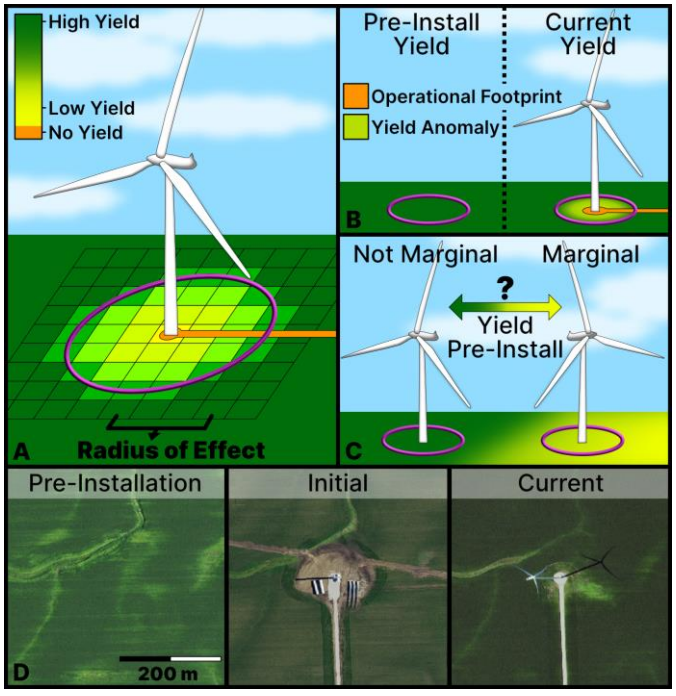

Figure 22. Illustrated hypotheses for within-field wind turbine effects on yield. (A) Radius of reduced agricultural productivity or yield termed the Agricultural Radius of Effect (AgROE), depicted as the magenta ring. (B) Resulting yield changes within AgROE and the co-located field post-installation of the wind turbine. (C) Marginal and non-marginal land placement or siting. (D) Example wind turbine site conditions prior to installation, during the year of installation (initial), and in the most recently available imagery. A and B depict two different regions responsible for a

Figure 22 (cont'd)

change in yield: operational footprint area (land removed from cultivation for infrastructure, including access roads and turbine operational footprint) in orange, and yield anomalies (land remaining in cultivation) in shades of yellow to light green. Imagery in D is from the National Agricultural Imagery Program (NAIP).

4.2: Methodology

4.2.1: Study area and data sources

Our study area encompasses twelve US states that are considered part of the US Midwest Corn Belt, and that contained Scalable satellite-based Crop Yield Mapper (SCYM) yield map data(Deines et al., 2021; Lobell et al., 2015). We used the United States Wind Turbine Database (USWTDB) v7.0 to supply the spatiotemporal information used in this study (B. D. Hoen et al., 2018; Rand et al., 2020). In addition to geospatial centroid coordinates, the USWTDB dataset includes information on wind turbine installation year, installed capacity, rotor diameter, and total turbine height. All remote sensing data processing was performed in Google Earth Engine (GEE), with post-processing and figure generation performed in R and Python.

We determined land cover co-location with wind turbines using USDA Cropland Data Layer (CDL) (Boryan et al., 2011; USDA NASS, 2024) within an estimated setback distance, or buffer around each turbine. We estimated setback distance (*Setback*, in meters) by:

$$Setback = Turbine\ Height * l \quad \textbf{Eq. 15}$$

where *Turbine Height* (m) is the total turbine height, defined as the hub height plus half of the rotor diameter (Hoen et al., 2018) and l (unitless) is 1.1, the median setback multiplier for road, transmission, rail, and property line features (Lopez et al., 2023). We assumed the primary land cover converted was the majority CDL land cover type during the year prior to installation within the setback buffer or field boundary (Xiarchos & Sandborn, 2017). Co-located farm field boundaries were modified from the USDA Crop Sequence Boundaries (CSB) (Abernethy et al., 2023), which were derived from CDL. Distance to existing road infrastructure was estimated from TIGER (U.S. Census Bureau, 2016).

We used Scalable satellite-based Crop Yield Mapper (SCYM) maps to estimate changes in maize and soybean yield across the US Corn Belt between 1999 and 2022 (Deines et al., 2021; Lobell et al., 2015, 2020). These 30 m resolution maps use Landsat-derived green chlorophyll vegetation index (GCVI), physiologically-based crop models, and ground-truthed validation to

estimate maize and soybean yields independently from Census reported yields (Lobell et al., 2015). We used SCYM maps to quantify the change in AgROE and field-level yields (Figure 22B) and to assess the relative land productivity of converted cropland (Figure 22C).

We also calculated GCVI derived from Landsat 5 TM, 7 ETM+, 8 OLI, and 9 OLI/TIRS Collection 2 (C. J. Crawford et al., 2023) collectively spanning 1984 to 2023 as a proxy for agricultural yield or productivity (Burke & Lobell, 2017; Gitelson et al., 2003). We used Landsat imagery exclusively for delineating AgROE (Figure 22A). *GCVI* is defined by:

$$GCVI = \frac{NIR}{Green} - 1 \qquad \textbf{Eq. 16}$$

We used annual state-level prices received for maize and soybean crops in 2022 from USDA NASS Monthly Agricultural Prices Report for the opportunity costs of wind turbines altering agricultural production (USDA, 2023). Wind turbine land lease rates were taken from Windustry (2009) ranging from 1,500 to 9,500 USD turbine^{-1} year^{-1} and an average of ~4,000 USD turbine^{-1} year^{-1}, with several other sources reporting or using similar rates (Brannstrom et al., 2015; Hitaj et al., 2018; Landmark Dividend, 2020; Sampson et al., 2020; Tegen et al., 2014; Weise, 2020; Winikoff & Parker, 2024). To adjust for inflation and estimate cash flow, we used the Producer Price Index (PPI) (U.S. Bureau of Labor Statistics, 2023).

4.2.2: The Agricultural Radius Of Effect (AgROE)

We define a new spatiotemporal metric to quantify the area directly affected by wind turbines, the Agricultural Radius Of Effect (AgROE). The workflow and logic for deriving AgROE is shown by Figure A50. The process is described below.

First, we defined a potential area of impact for each turbine. To allow for agricultural yield effects that may exist beyond the setback distance (i.e., turbine shadow impacting yield; change in farm management practices), we allow the total aerial extent of potential effect to be within a 300 m geodetic buffer around the centroid of a wind turbine installation, or ~28 ha at each site. Other studies have used this as a max aerial extent assuming that beyond this standard setback distance, boundary and mixed-land cover effects likely begin to emerge (Aydin et al., 2010; Harrison-Atlas et al., 2022; Maguire et al., 2024).

Next, we computed the change in spectral reflectance (disturbance) as a function of distance from the turbine centroid. In GEE, we calculated annual 90th-percentile Landsat *GCVI*

for each pixel two years prior to installation and two years post installation within the potentially affected aerial extent. Within each buffer, we normalize annual pre- and post-installation 90th-percentile *GCVI* rasters to the minimum and maximum local values to remove crop rotation and annual variation in agricultural practices. We then perform a difference-in-difference analysis (post-installation minus pre-installation) to remove prior-marginal land effects, thus emphasizing changes in productivity as a result of the turbine installation. The post-installation period was defined two different ways resulting in two different computed AgROE radii: (Initial) two-years directly post-installation and (Current) two-years of the most recently available imagery (2022 to 2023). The normalized *GCVI* was then averaged within a 30 m annulus at a range of radii (0 m to 300 m every 30 m) from the centroid of an agriculturally co-located turbine. We then fit a continuous smooth spline function to the discrete 30 m radial spectral disturbance values for each turbine. This was done using the *npreg* package in R (Helwig, 2024) and the Maximum Likelihood prediction method (Berry & Helwig, 2021), predicting disturbance values at each meter from the centroid of the turbine. To compare disturbance values across turbines, each spline value was then 0-1 normalized based on the minimum and maximum prediction within the 300 m range of distances. Thus, a value of 1 represents 100% recovery to background yields. To determine the threshold for recovery, we plotted the quartiles of all resulting splines, and selected an 85% recovery threshold qualitatively based on where the dataset median experienced diminishing growth and the eventual stationary phase, similar to carrying capacity estimates for a sigmoid growth curve (see Figure 25A). This 85% recovery value was then applied to each spline, resulting in the AgROE for each turbine. If the estimated affected radius was greater than the turbine's setback distance and the total observed spectral change was less than 1.5 times the interquartile range (IQR), we assumed that actual effect was minimal and set the AgROE radius to a minimum radius. The minimum radius, 12 m, is approximately the sum of the radius limit for transport (i.e., base width, 2.2 m from Dykes et al. (2018)) and an access road width around the turbine base (3-9 m from US BLM (2005)). Note, when AgROE is the minimum threshold, agricultural yield changes only occur due to change in operational footprint (see equation 5 and Figure A51).

In addition to AgROE, we estimated *LUE* (W m^{-2}) for each turbine by:

$$LUE = \frac{Capacity}{Area_{AgROE}} \quad \textbf{Eq. 17}$$

where *Capacity* is the installed capacity (watts or W) reported by USWTDB and $Area_{AgROE}$ (m^2)

is the resulting geodetic buffered area of the AgROE radius. As described above, we estimate the AgROE radius, AgROE area, and LUE directly after installation and in the most recently available imagery. We compare existing wind turbine AgROE to the AgROE for randomly generated locations within the crop-field boundary (see Figure A48 and AgROE Utility, Limitations, and Assumptions).

4.2.3: Co-located field selection and simplification

We selected and modified co-located field boundaries that intersected at least one wind turbine from Abernethy et al. (2023). Initial field boundaries (~10,000) were selected as those intersecting the larger of two buffered areas: the estimated setback distance of each turbine or the AgROE radius. We modified boundaries for fields smaller than 16 ha, the average area of Public Land Survey System (PLSS) quarter-quarter-section (QQsec), which is smaller than our potential impacted area. These small fields (~3,000) were merged with the nearest field exceeding the QQsec threshold, resulting in 5,963 total field boundaries. We dissolved the AgROE boundaries for all wind turbines from the intersecting fields for calculating the influence of wind turbines on field-level yield and production. We also generated wind turbine control points to evaluate the significance of AgROE and RLP. Turbine control point locations were randomly selected from co-located field boundaries, excluding land within the setback distance to the field edge and all existing AgROE affected areas. If a field was not included in Abernethy et al. (2023), but was classified as agricultural and contained a turbine, we used a PLSS QQsec bounding box to represent the co-located field area associated with each installation.

4.2.4: Local yield changes within AgROE and the operational footprint

We computed within-field yield changes as a result of wind turbine installation for maize and soybean co-located wind installations in the US Corn Belt. We separately considered two regions for within-field yield change: (1) the estimated direct operational footprint (2) the AgROE derived affected area outside the operational footprint. We estimated the operational footprint from the minimum AgROE (12 m around each turbine centroid) and a 9 m wide access road leading to the nearest road or existing turbine. We extracted SCYM yield estimates in GEE from AgROE and the co-located field for all available years (SCYM-limited) pre- and post-turbine installation. Each year contained values for maize and soybean yields to include crop rotation and AgROE overlap with adjacent fields.

We calculated the yield anomaly, the reduction in yield due to the installation of a wind turbine, for maize and soybeans ($Yield_{anomaly}$ in tonnes ha^{-1}) by:

$$Yield_{anomaly} = AvgYield_{AgROE} - AvgYield_{Field} * (1 + RLP) \quad \textbf{Eq. 18}$$

where $AvgYield_{boundary}$ is the average annual yield within the given boundary (AgROE or co-located field) and $AvgYield_{Field}$ is the average annual yield within the encompassing co-located field. Computing the yield anomaly relative to the co-located field average eliminates variability in climate, management, and improvements in crop genetics. Removing marginality (*RLP*) from $AvgYield_{boundary}$ removes Maize and soybean yields are known to have steadily increased over the last several decades due to improvements in seed density and yield per plant (Egli, 2023).

We estimated the total change in maize and soybean production (*ΔProduction*) within AgROE due to the yield anomaly and due to direct operational land footprint. Total *ΔProduction* after wind turbine installation (tonnes) by:

$$\Delta Production = Area_{post} * Yield_{anomaly} - Area_{opFoot} * AvgYield_{Field} \quad \textbf{Eq. 19}$$

where $Area_{opFoot}$ is the estimated new operational footprint area (access roads and turbine base) including the wind turbine base and an encircling access road (minimum AgROE threshold) and the estimated area of an access road extending to the nearest existing road or turbine (ha), $AvgYield_{Field}$ is the average annual crop-specific yield (tonnes ha^{-1}) within the co-located field for the predominant crop converted, and $Area_{Post}$ is the annual crop-specific aerial extent post-installation within AgROE (ha) but outside the operational area. The product of the terms on the left considers anomalous change in yield within cropland that remains cultivated within AgROE. The product of the terms on the right in equation 5 represents change in yield due to cropland taken out of production entirely for wind turbine operational infrastructure. We assumed that land taken out of production by the operational footprint, which is mostly outside AgROE, was of average field and yield conditions (*RLP* = 0). See Figure A51 for more information.

4.2.5: Quantifying the extent of marginal land placement

We used relative land productivity (*RLP*), defined in our earlier work on solar PV placement (Stid et al., 2022), as a metric of whether wind turbines are placed in low-productivity or high-productivity areas within a field. Here, we modified RLP (%) from Stid et al. (2022) to be based on SCYM yield estimates rather than spectral reflectance. We compute RLP (%) for each

turbine by:

$$RLP = \left(\frac{1}{n} \sum_{n\ years} \frac{AvgYield_{AgROE}^{1}}{AvgYield_{Field}^{1}} + \frac{AvgYield_{AgROE}^{2}}{AvgYield_{Field}^{2}} + \cdots + \frac{AvgYield_{AgROE}^{n}}{AvgYield_{Field}^{n}} - 1 \right) * 100 \qquad \textbf{Eq. 20}$$

where n is the number of years prior to the installation considered with available SCYM data (here n = 2 to 19 years depending on installation year), $AvgYield_{AgROE}$ is the average SCYM yield within the newly derived (AgROE) wind turbine direct area one year prior to installation, and $AvgYield_{Field}$ is the average SCYM yield within the co-located field boundary one year prior to installation. Thus defined, RLP ranges from -100% to Inf where negative values indicate low-productivity land use (marginal), zero indicates land use of average yield, and positive values indicate high-productivity land use (non-marginal). We report *RLP* for maize and soybeans, and the average for both crops. We also performed a sensitivity analysis where we set all *RLP* values to the 10th-percentile yielding land values in the co-located field, a counterfactual optimal placement in locally highly-marginal cropland.

For wind turbines placed in marginally productive land (RLP < 0), we calculated the saved crop production due to effective agricultural placement ($Yield_{placement}$ in tonnes) by:

$$Yield_{placement} = |\Delta Production| * -RLP \qquad \textbf{Eq. 21}$$

The resulting $Yield_{placement}$ is positive if *RLP* is negative (conservation of agricultural production) and negative if RLP is positive (loss of agricultural production).

4.2.6: Economic analysis

We calculated the economic consequences of the anomalous change in maize and soybean yield and a range of possible land lease agreements for each turbine. The total change in agricultural revenue due to wind turbine co-location and annual land lease returns ($Revenue_{ag}$ in 2020 USD) was calculated by:

$$Revenue_{ag} = \Delta Production * Price_{Crop} + Lease_{rate} \qquad \textbf{Eq. 22}$$

where $Price_{Crop}$ is the annual price received for maize and soybeans (USD tonne^{-1}) and $Lease_{rate}$ (USD year^{-1}) is the turbine^{-1} year^{-1} land lease. Note that this method leaves room for yield increases if such a relationship exists at the turbine- or field-level.

Similar to $Yield_{placement}$, we calculated the income saved due to effective agricultural

placement ($Revenue_{placement}$ in 2020 USD) by:

$$Revenue_{placement} = \left|Revenue_{ag}\right| * -RLP \quad \textbf{Eq. 23}$$

The resulting $Revenue_{placement}$ is positive if *RLP* is negative (conservation of agricultural revenue) and negative if *RLP* is positive (loss of agricultural revenue).

4.2.7: Statistical analysis

We used linear models to analyze trends in yield anomaly post-installation, and relationships between installed capacity and AgROE area, *RLP* and installed capacity, *RLP* and project number of turbines, and *RLP* and installation year. We used Kolmogorov-Smirnov to assess the normality of distributions in yield anomalies and *RLP*. Significance was determined by two-sided t-Test and using the confidence interval (95%) and Cohen's d effect size to determine the magnitude of change. For interpreting the distribution of *RLP*, we used Wilcoxon Signed-Rank (against median of zero) and Ranked-Sum (against control point distribution) to analyze significance against null hypothesis.

4.3: Results

4.3.1: Wind Power Co-location and Directly Affected Land Area

As of 2023, there were 27,297 turbines installed in the 12 states of the US Corn Belt (Figure 23) (USWTDB v6.1, Hoen et al. (2018)), and 97% were co-located with active agricultural land. Of those, we assessed 17,557 turbines (36.5 GW) that were installed prior to 2002 and co-located with maize and soybean cropland for the Agricultural Radius of Effect (AgROE) analysis. Within the setback buffer the year prior to installation, CDL land cover classification confidence was 92%. We also identified 5,963 crop fields covering 802,200 ha co-located with at least one wind turbine. The total extent of co-located fields and wind turbines is shown in Figure 23.

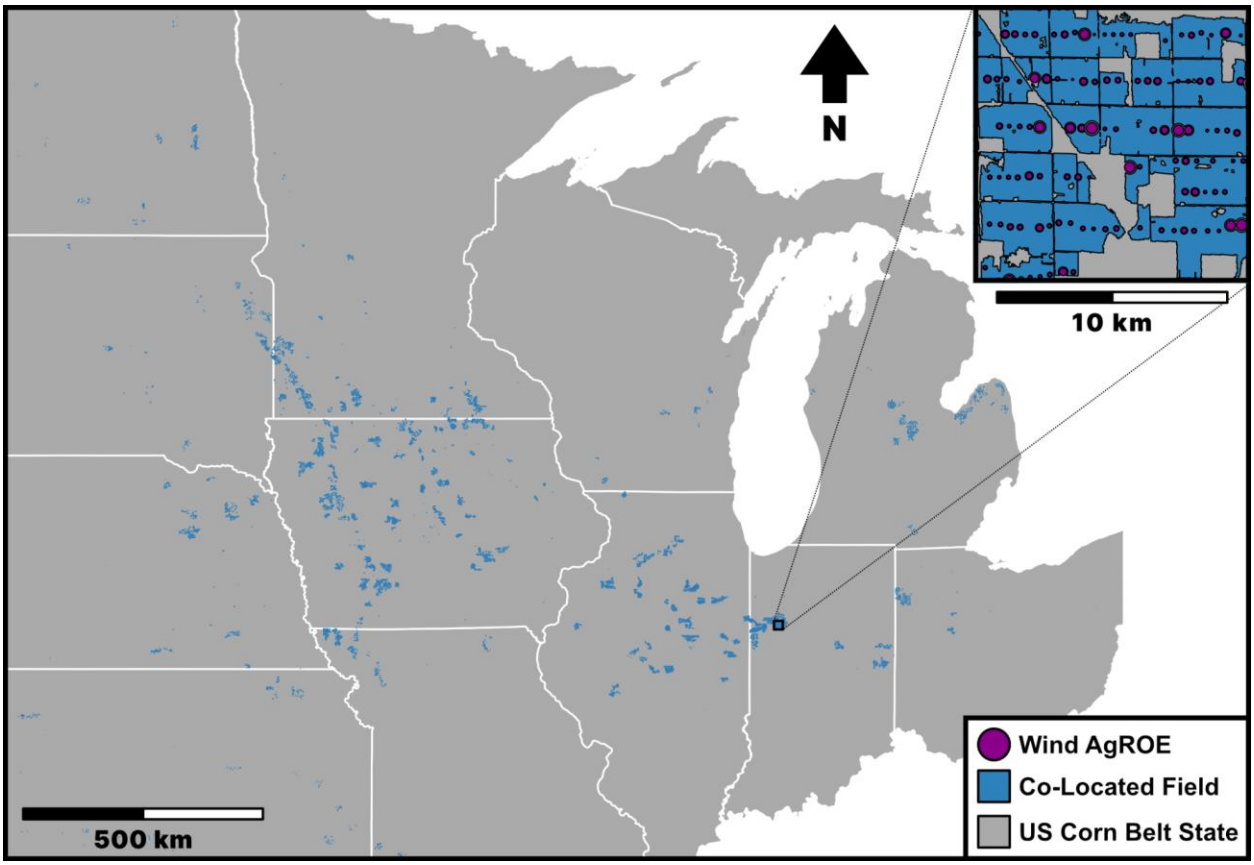

Figure 23. Land associated with co-located wind turbine installations. A map of the 12 US Corn Belt States containing yield and wind turbine data overlaid with newly derived Agricultural Radius Of Effect (AgROE) for each turbine and field boundaries co-located with wind turbines. Field boundaries are modified from (Abernethy et al., 2023).

The total area within co-located fields most affected by turbines, that within the AgROE, was 59,500 ha, with an additional 5,100 ha of direct operational footprint (infrastructure) area. We calculated AgROE directly after installation and in the most recently available imagery. The interdecile range (IDR) for wind turbine AgROE values in 2023 imagery ranged from 51 to 181 m, with a median of 77 m (see Figure 24). Notably, average AgROE area decreased by 0.03 ha relative to initial values after installation resulting in 494 ha of recovered agricultural land area (see Figure A47). There was no linear correlation between the directly affected agricultural area around wind turbines and installed capacity, rotor diameter, or total turbine height. On average, disturbance was significantly different from zero out to 150 m, and the counterfactual AgROE control points were not significantly different from zero at any distance (see Figure A48).

LUE, defined as the nameplate capacity of each turbine per unit of altered land area–here the AgROE area, is a widely-used metric to assess energy-land interactions (Cagle et al., 2023).

Here, IDR for LUE in 2023 ranged from 18 to 265 W m^{-2}. Like AgROE, *LUE* decreases for each turbine following installation. The resulting *LUE* in 2023 (102 W m^{-2}) was on average 16.7 W m^{-2} more efficient than directly after installation. Notably, median *LUE* (both initial and 2023) of turbines installed in a given year increased significantly through time (slope = 4.2 W m^{-2} yr^{-1}, p<0.001). For turbines installed in 1999, the average 2023 *LUE* is 41.33 W m^{-2}, while those installed in 2015 reached 155.4 W m^{-2}, with 147.5 W m^{-2} for the most recent installations (2021). We also found that the IQR and IDR of *LUE* nearly tripled over the same time period, indicating a wide range of installation practices.

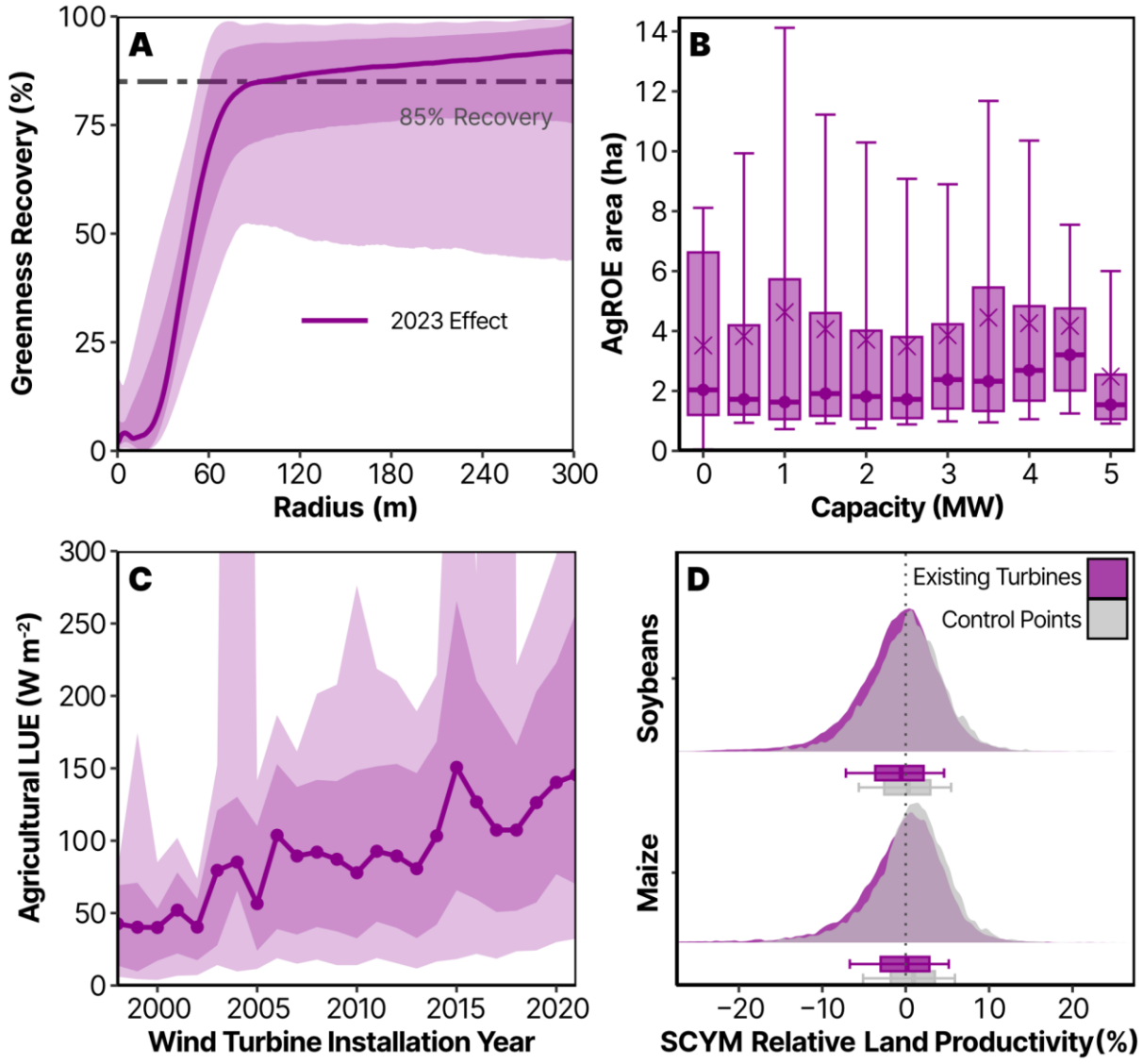

Figure 24. AgROE and resulting land metrics in most recent available imagery. (A) AgROE for 17,557 co-located wind turbines in the US Corn Belt. (B) Total AgROE area (hectares) as a

Figure 24 (cont'd)

function of installed capacity (MW) binned into 0.5 MW groups. Boxplots show the median and IQR, whiskers show the IDR, and the "x" shows the mean. (C) *LUE* of co-located turbines as a function of installation year. Note that 2023 AgROE represents "current disturbance" and is derived from the difference in difference of 2022 and 2023 GCVI and two-year pre-installation GCVI. Shaded regions in A and C show the IQR and IDR, with lines and points representing median values. (D) *RLP* of wind turbines in the US Corn Belt determined using SCYM annual yield maps for maize and soybeans and for control points in the respective co-located fields. The black dotted line (*RLP* = 0) indicates siting in land of average yield, negative values indicate siting in marginal (consistently low yielding) land, and positive values siting in high-yielding land. Boxplots represent median, IQR, and IDR. The representative conceptual depiction is found in Figure 22C.

4.3.2: Changes in Co-located Agricultural Production and Revenue

Wind installations reduce agricultural production by: 1) altering yields within the AgROE surrounding the turbine, and 2) displacing crops in the operational footprint (access roads and bases). Within the AgROE area, maize and soybean average yields were significantly reduced. Relative to pre-installation yields, initial construction reduced yields by 2.6 (maize) and 0.73 (soybeans) tonne ha^{-1}, which recovered somewhat in the following year to yield anomalies of -1.5 tonne ha^{-1} and -0.4 tonnes ha^{-1} (Figure 25A and 25C). In 2022, yield anomalies within AgROE averaged -12.8% and -12.1% of county average maize and soybean yields. Cumulatively across the Corn Belt in 2022, production of maize was reduced by 26,500 tonnes and soybeans by 7,800 tonnes (Figure 25B). Wind turbine operational footprints displaced an additional 34,700 tonnes of maize production and 8,900 tonnes of soybean production in 2022 (Figure 25B). US Corn Belt maize and soybean production was 368 million tonnes and 101 million tonnes respectively.

Across the US Corn Belt, changes in maize and soybean production in 2022 resulted in an estimated agricultural revenue loss of 20.6 million USD within AgROE (-1,240 USD $turbine^{-1}$ $year^{-1}$), shown in Figure 25D. However, when compensation from leases is included, total revenue increased 62.5 million USD (3,760 USD $turbine^{-1}$ $year^{-1}$, ranging from 4.3 million to 137.2 million USD, depending on assumptions). Given the average state-level prices received and remotely-sensed estimated production, agricultural revenue across the region for 2022 was 124 billion USD. Note that this analysis does not include savings from reduced farm operation and input expenses within the turbine operational footprint, nor does it include changes to expenses caused by altered within-field tractor paths.

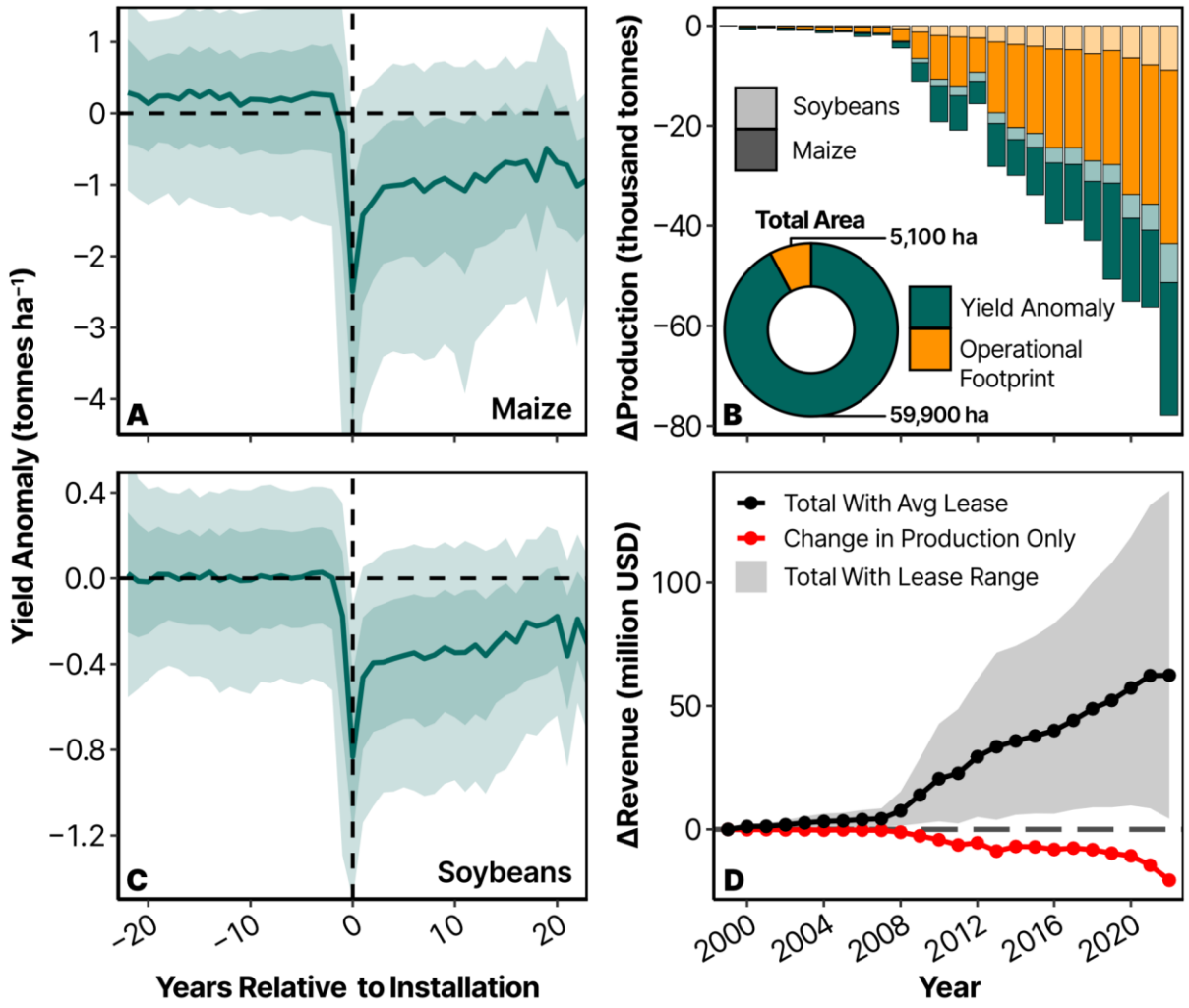

Figure 25. Annual change in on-farm agricultural production and revenue. Changes were consdiered within AgROE for 17,000 wind turbines in the US Corn Belt. Yield anomalies for maize (A) and soybeans (C) relative to the year of installation with a half year buffer. Plots A and C show the median (line) and IQR and IDR as shaded regions. The vertical shaded region in plots A and C represents a 2.6-year average commissioning timeline for the US from Gumber et al. (2024). (B) The total change in maize and soybean production for each year and all existing turbines in that year. Operational Footprint is change in yield due to the change in cultivated area that is now access roads and the wind turbine base. Yield Anomaly is the change in yield due to anomalous change in yield within cropland that is perceived to remain cultivated. (D) The range of land leases is 1,500 USD to 9,500 USD turbine^{-1} year^{-1} with an average of 5,000 USD turbine^{-1} year^{-1}.

4.3.3: The Effect of Placement on Agricultural Yield and Revenue Conservation

Wind turbines in the US Corn Belt have been installed with a small preference for marginal locations within the co-located field. For within-field maize and soybean placement, average pre-

installation yields relative to field averages (i.e., *RLP* values) at turbine locations were 0.78% and 0.86% less than those at control point locations for maize and soy (Figure 24D). Medians of the *RLP* distributions were significantly different from zero ($p<0.001$) and from that of control points ($p<0.001$). Total *RLP* considering all cropland within AgROE was less than zero for 8,375 turbines, indicating marginal placement. However, effect size from Cohen's were both small (<0.2) indicating little practical difference in productivity. There was no relationship between *RLP* and installed capacity, project number of turbines, or installation year.

While we have shown a very slight tendency for agriculturally marginal placement of wind turbines, the food security and economic incentives to do so are small. In 2022, crop tonnage conserved by marginal placement was 1,750 tonnes, or 0.21 tonnes turbine^{-1}. The economic benefit of effective placement within marginal agricultural lands was a total savings of 470,000 USD, or 55 USD turbine^{-1}. Under a counterfactual optimal siting scenario, where all 17,464 wind turbines were installed in agricultural land that was the 10th percentile yield within each co-located field, the reduction in production loss was 21,100 tonnes (1.3 tonnes turbine^{-1}), saving 5.5 million USD (330 USD turbine^{-1}).

4.4: Discussion and Conclusions

4.4.1: Agricultural Area Affected by Wind Turbines is Small and Diminishing with Time

While wind turbine capacities and sizes have increased, disturbed areas around them have remained small, and tended to recover with time. We have demonstrated that the newly-presented AgROE metric meaningfully describes the land area surrounding turbines within which agricultural yield is affected by their installation. The resulting *LUE* shows that the power-land relationship between wind farms and agriculture has improved by more than a factor of three over the last two decades. Additionally, we observed a slight recovery in yield (Figure 25A and 25C) and AgROE radius (Figure A47), suggesting revegetation and recovery plans are at least partly effective (Christol et al., 2021) and emphasizes the distinction between permanent and temporarily disturbed areas (Denholm et al., 2009; Dhar et al., 2020; Diffendorfer & Compton, 2014). We discuss AgROE limitations and validation in Appendix D Text A4.1.

Increases in *LUE* are being driven by ever larger and higher capacity wind turbines occupying essentially the same operational footprint and AgROE as their smaller predecessors. Although wind turbines have consistently increased in size (Christol et al., 2021; B. Hoen et al.,

2023; Wiser et al., 2023), more efficient turbine designs have resulted in more power per turbine (Veers et al., 2019, 2023). Additionally, innovative wind farm layouts combined with wake steering will increase power per turbine and further reduce land use concerns for the future landscape (Antonini & Caldeira, 2021; Harrison-Atlas et al., 2024). Even if a relationship between capacity and affected area existed as some previous studies have found (Denholm et al., 2009; Saganeiti et al., 2020), increased power per turbine, fewer turbines per farm, and observed recovery in the years following installation reduce concerns for food and farmland security.

The AgROE metric does not measure absolute land transformation or directly disturbed footprint and should not be interpreted as such. Instead, AgROE represents the turbine-specific distance within which 85% of the total radial change in spectral reflectance is observed. This concept assumes crops respond to changes in surface and subsurface conditions, microclimates, and agricultural management resulting in a yield cone of depression around turbines that manifests in crop productivity proxies. The magnitude of spectral disturbance varies across turbines, and the impacts at any given disturbance value vary. Crucially, larger AgROE areas do not necessarily correspond to greater losses in agricultural production because cultivation often continues adjacent to turbines (Christol et al., 2021; Harrison-Atlas et al., 2022; Moore et al., 2022). This is crucial, given that renewable energy land use is often associated with land transformation rather than land augmentation achieved with effective siting and management (Trainor et al., 2016). Following Cagle et al. (2023), we report this metric in terms of agricultural *LUE* making results comparable with a recent comprehensive study in the Western US (Dai et al., 2024).

The *LUE* results reported here (average IDR across years: 18 to 265 W m^{-2}) are consistent with studies that have reviewed and made similar estimates of wind turbine affected area (Dai et al., 2024; Denholm et al., 2009; Diffendorfer & Compton, 2014; Harrison-Atlas et al., 2022; Jones & Pejchar, 2013). Dai et al. (2024) provides the most comprehensive and up-to-date estimates in the western US, and found that *LUE* can range from 64 to 447 W m^{-2} depending on the level of landscape modification. Even on the low end of estimates, wind turbine *LUE* is generally greater than ground-mounted solar *LUE* (35 W m^{-2} from Hernandez et al. (2014)) where affected land more often corresponds with entirely forgone agricultural production (Stid, Shukla, et al., 2025).

The renewable energy terminology landscape is rapidly evolving and affecting the distribution of benefits, incentives, and grant awards (Hernandez et al., 2022). Land interaction metrics can vary spatially (direct vs. indirect), temporally (temporary vs. permanent), and across

system life-cycle phases (upstream, operational, and downstream) (Denholm et al., 2009; Fthenakis & Kim, 2009). Misrepresenting or omitting key concepts can lead to misinterpretation of results, especially when comparing studies (Hernandez et al., 2022). A recent review of ground-mounted solar-land interaction metrics identified land use efficiency (LUE, in W m^{-2}) as one possible standardized metric to compare energy footprints across energy technologies (Cagle et al., 2023). Importantly, LUE differs from power density which shares the same units (W m^{-2}) but reports on the spatial footprint of wind farms rather than individual wind turbines (Antonini & Caldeira, 2021; X. Feng et al., 2023; Harrison-Atlas et al., 2022; Miller & Keith, 2018; Van Zalk & Behrens, 2018).

4.4.2: Wind Power Minimally Reduce Local Agricultural Production

While agricultural yields within the AgROE-defined area around wind turbines were significantly reduced post-installation, the net effect of these production changes are insignificant relative to both field-level and regional production. More broadly, turbine-induced losses, due to both the AgROE and turbine operational footprints, amounted to just 0.02% of total 2022 Corn Belt production for each crop. The agricultural losses (61,200 tonnes for maize in 2022, 16,600 tonnes for soy) are negligible compared to interannual variability in Corn Belt yield (maize: ±26.7 million tonnes, soybean: ±9.1 million tonnes), themselves likely caused by changes in management and environmental conditions in the region (Deines et al., 2021). Yet, these turbines produce electricity on the order of ~6.5 million homes equivalent (~70 TWh, a simple estimation assuming a 22% capacity factor from Bolson et al. (2022)).

It is important to note that our estimates likely overestimate wind turbine impacts on production. We assumed a large access road width of 9 m, and that each turbine had its own access road to the nearest existing road or turbine rather than using existing in-field agricultural roads (Dai et al., 2024). Further, we assumed that all areas within the AgROE not occupied by new operational footprint continued to be cultivated and responded to yield anomalies equally, rather than having anomalies directionally focused down-wake (Diffendorfer et al., 2022) (Appendix D. Text A4.1). Moreover, the impact on food security may be even smaller than the 0.02% reduction in production estimated here, given that the Corn Belt is the primary contributor to the ~40% of U.S. maize and soybean production allocated to biofuels (USDA ERS, 2024; W. Wang & Khanna, 2023). Indeed, reclaiming land otherwise producing biofuels for renewable energy may reduce some of the severe negative environmental impacts created by The Renewable Fuel Standard (Lark

et al., 2022). Our previous work has shown that siting renewable energy in nutritionally indirect (e.g., feed and silage) or absent (e.g., biofuel, non-oil producing cotton, tobacco) croplands can be an effective pathway to help mitigate food security concerns for renewable energy land use while providing additional benefits (Stid, Shukla, et al., 2025).

We have shown that there are observable decreases in on-farm maize and soybean production at a highly-local scale. We isolated two pathways explaining the decrease: directly disturbed area for the operational footprint and radial yield anomalies. Although the radial anomalies may be due to increased crop water needs due to enhanced evapotranspiration (Li et al., 2018; W. Zhang et al., 2013), we believe initial site construction, foundation, and compaction (see Figure 22D) (Christol et al., 2021) and changes in agricultural management (e.g., increased equipment traffic causing additional soil compaction and change in irrigation or pesticide application in avoiding boom arm impact or aerial fly over) may also play a significant role (Hitaj et al., 2018). Importantly, this study does not address regional effects of wind turbines on agricultural production (see Appendix D Text A4.2). We did, however, estimate anomalous change in yield within the co-located field compared to county-level yields (modified equation 4) which showed yield anomalies an order of magnitude less than within AgROE. We discuss implications in Appendix D Text A4.2. If larger-scale regional effects do exist, they may play a more substantial role in regional agricultural security and should be further studied in combination with on-farm local effects. However, considering only the local effects quantified here, wind energy in the US Corn Belt is not posing a significant threat to agricultural security. Contextualizing these losses within the broader scope of agricultural security is important since impact overestimation can lead to viewing wind turbines as a threat to agriculture rather than an asset (Dai et al., 2024; Morris & Blekkenhorst, 2017).

4.4.3: Some Wind Turbines Are Sited in Marginal Croplands Providing Small Benefits

We provide the first empirical evidence showing that some wind turbines are sited in locally-marginal agricultural lands in the US. Although the benefits are small, land productivity should be taken into consideration when forming land lease contracts and crop damage payments. The slight preference results in marginal savings (55 USD turbine^{-1}) compared to the significant economic benefits of land leases (3,760 USD turbine^{-1} on average). The counterfactual highly-marginal placement scenario (locating turbines within 10th-percentile yield areas in the co-located field), reduced production losses and saved money (2.1 tonnes of maize and soybeans turbine^{-1}

and 500 USD turbine^{-1}) albeit still less than low-end lease rates (1,500 USD turbine–1). The presence of this small preference is intriguing given the limited flexibility in wind turbine placement due to siting and setback restrictions (Lopez et al., 2021) and potential power and revenue losses from uncoordinated placement within greater wind farms (Howland et al., 2019; Lundquist et al., 2018). A future wind energy landscape with fewer, larger turbines would reduce the per turbine benefits of such placement. We discuss future work on quantifying marginality of placement via *RLP* at more scales of assessment in Appendix D Text A4.2.

Co-prioritizing ecosystem conservation and wind farm generation may be more beneficial than focusing on marginal siting alone. The majority of future wind siting areas considered low-impact to wildlife are already agricultural in function (Fargione et al., 2012) and future buildout scenarios that enhance ecosystem protections double the share of agricultural co-location relative to other land uses (G. C. Wu et al., 2023). Additionally, most recent agricultural expansion has converted marginal land (Lark et al., 2020). By many accounts, there is more than enough low-impact land available to achieve net-zero electricity production and avoid negative consequences to wildlife and agricultural production in most regions across the US (Dunnett et al., 2022; X. Feng et al., 2023; Hise et al., 2022). However, without specific protections, significant high-ecological-value land could be lost to the footprint of new renewable energy projects (Hernandez, Hoffacker, Murphy-Mariscal, et al., 2015; Holland et al., 2019; G. C. Wu et al., 2023). Fortunately, several governmental and non-governmental initiatives are working to define and promote effective siting and management of renewable energy landscapes (Christol et al., 2021; Davis & Macknick, 2022; Hise et al., 2022; Hunter et al., 2022; TNC, 2024; USDA, 2024). Future legislation like the Protecting Future Farmland Act of 2023 (Protecting Future Farmland Act of 2023, 2023), which incentivizes marginal agricultural placement and conservation-focused management for solar PV arrays, should include wind power and might lead to a win-win for both agricultural and environmental goals.

4.4.4: Land Lease Revenue is 3x Greater than Lost Agricultural Production

While wind turbines were responsible for 0.02% losses in maize and soybean tonnage in the US Corn Belt in 2022, land lease revenue potentially increased agricultural net revenue across the region by up to 0.12% (from 124 billion USD). Appropriately priced land leases not only offset the costs of forgone agricultural revenue but provide additional financial security for farmers. Previous studies have demonstrated that installing wind turbines in farmland can diversify income,

reduce risks, and make operational succession more likely, helping to keep farmers and their families on their land and protecting future food security (Bolinger & Wiser, 2006; Copena & Simón, 2018; Ejdemo & Söderholm, 2015; Groth & Vogt, 2014; Mills, 2017; Sutherland & Holstead, 2014). Furthermore, recent media coverage has highlighted the financial benefits of wind energy compensation for farmers (Shamlian, 2024; Weise, 2020) and governmental initiatives have been launched to ensure these benefits reach the agricultural community (USDA, 2024). Our estimated positive income effect is also likely underestimated, as additional easements, tax incentives, option agreements, up-front payments, good-neighbor agreements, and crop damage payments were not included (Appendix D Text A4.4). Additionally, current land lease agreements may provide higher returns per turbine, or even per MW or MWh, than those documented in the 15-year-old report referenced in this study (Windustry, 2009). However, these benefits may also be unequally distributed, favoring larger, production-oriented farms over smaller operations needing enhanced financial security (Bessette & Mills, 2021). This disparity could be amplified as land for fewer, larger turbines may be leased from early adopters with more land and financially secure farms.

Our study contributes to the growing body of literature suggesting that wind turbine co-location on agricultural land can help farmers sustain cultivation in an uncertain future. The opportunity cost of small lost production may be offset by the increased security that farmers experience. For low-value commodity crops with small margins, this strategy is highly effective (2022 average price received–maize: 225 USD tonne^{-1}, soybeans: 400 USD tonne^{-1}). With such low margins, small production losses and improving LUE make wind power co-location an attractive strategy for achieving net-zero energy production while preserving food and farmland security.

Agriculture and wind energy are finding common ground, with farmers transitioning from just cultivating crops to diversified production including cultivating energy. Our study demonstrates that wind turbines in the US Corn Belt have observably reduced agricultural production. However, the magnitude of these reductions is small compared to overall maize and soybean production in the region–where most crop production does not directly contribute to human diets. Our economic analysis reveals that average land lease payments can more than compensate for lost agricultural revenue, enhancing farmers' financial stability. The detected slight preference for siting turbines on lower-yielding land suggests a strategic approach that reduces

crop losses, which may be even more effective for higher-value crops and when co-designed for other ecosystem services. Importantly, we show that wind turbine land use efficiency is improving, with new turbines having a substantially smaller land footprint per watt. This study shows that trade-offs of wind power and agricultural co-location can be monitored and are mutualistic to food and farm security in the current incentive landscape. Ensuring that benefits remain with those who contribute to our food security is essential, especially if their land is best suited for achieving net-zero and ecosystem conservation goals. Future research should explore the mechanisms driving these yield changes and extend the analysis to other regions and crops to refine sustainable co-location practices.

Acknowledgements

This chapter was co-authored by Anthony D. Kendall, Annick Anctil, and Jillian M. Deines. Funding support was provided by the USDA National Institute of Food and Agriculture INFEWS grant number 2018-67003-27406 (accession No. 1013707). Any opinions, findings, and conclusions or recommendations expressed in this publication are those of the authors and do not necessarily reflect the views of the USDA.

CHAPTER 5: CONCLUSIONS

Summary of conclusions

The consequences of the existing fossil fuel-driven energy landscape on climate change, air pollution, and energy insecurity, make clear the need to transition away from fossil fuel dependency. Renewable energy technologies like solar, wind, hydropower, and geothermal will be frontrunners in this transition. The recent IPCC AR6 Synthesis Report showed that together, solar and wind have twice the carbon emission reduction potential of other viable mitigation options (IPCC, 2023). At the same time, solar and wind energy might threaten or bolster food security (Cuppari et al., 2024; Curioni et al., 2025; Stid, Shukla, et al., 2025; N. Zhang et al., 2023) and biodiversity and conservation targets (Ashraf et al., 2024; Cameron et al., 2012; Condon et al., 2025; Dunnett et al., 2022; Grodsky et al., 2021; Grodsky & Hernandez, 2020; Hilker et al., 2024; Karban et al., 2024; Levin et al., 2023; Rehbein et al., 2020). Fortunately, existing frameworks, tools, and guidance lays out a path forward (Ashraf et al., 2024; Galzki & Mulla, 2024; Hernandez et al., 2019; Jamil et al., 2023; Kim Steinberger, 2021; Peterson et al., 2025; Sorensen et al., 2022; Warmann et al., 2024; Williams et al., 2025). One thing is clear though, more detailed and publicly available information on the existing energy landscape is critical to be able to implement these tools comprehensively and to understand their effectiveness.

This research offers current and comprehensive insight into the spatial footprint, design, management, and land use implications of solar and wind energy in the US. Notably, solar and wind energy have become agricultural commodities, with the majority of installations sited on historically arable lands. Though, my work also demonstrates that practices and impacts change across space and time, highlighting the need for continuous monitoring and updated assessments of the existing renewable energy landscape. Taken together, my findings underscore the scale and urgency of land-use planning for renewable energy.

The GM-SEUS dataset suggests that current solar land coverage in the contiguous US is ~3,000 km^2 through 2024. Net-zero energy generation in 2050 will require between 60,000 and 90,000 km^2 of the US land surface for solar, constituting a 20- to 30-fold increase in area (Ardani et al., 2021; Jenkins et al., 2021; Larson et al., 2021). Wind power may require thousands more square kilometers of direct land use, and between 500,000 and 1 million km^2 of indirectly impacted land area (Ardani et al., 2021; Denholm et al., 2022; Harrison-Atlas et al., 2022; Jenkins et al., 2021; Larson et al., 2021). This is a considerable amount of land (direct: ~1%, indirect: ~11%),

yet, other forms of existing or projected land use change provide helpful context for managing concern about solar and wind energy land use change.

Between 70,000 km^2 (~0.8%) and 130,000 km^2 (~1.4%) of the US landscape is currently disturbed, used, or set aside for fossil fuel procurement, use, and distribution (Bond et al., 2021; Denholm et al., 2022; Merrill, 2021). An additional 200,000 km^2 (~2.2%) are devoted to biofuels (Denholm et al., 2022; Merrill, 2021), land use that is currently doing more harm than good (Lark et al., 2022). Roughly 275,000 km^2 (~3%) is urbanized land area (Center for Sustainable Systems, 2021) and over 8,000 km^2 (~0.1%) hosts 16,000 golf courses, more than 2.5-times the land area of the existing solar landscape studied here (Denholm et al., 2022; Weinand et al., 2025). Diffendorfer et al. (2024) estimated a future conversion of 0.7% of US natural lands for net-zero solar energy, though, noting that these changes are an order of magnitude less than other expected pressures on natural lands over the same times period (Diffendorfer et al., 2024). These examples are not meant to diminish the importance of renewable energy land use conflicts, nor the beneficial outcomes of low-impact land use. Rather, these perspectives provide context for a broader discussion on how we use land in the US, and that considering synergies can offset some negative outcomes of land use conflicts.

The big picture (from the ground this time)

Renewable energies are a critical component of a sustainable global future. Land is both finite and valuable and is extensively required for this energy future. The outcomes of this new landscape depend on what land is used and how systems are designed and managed. Together, solar and wind energy have the potential to go beyond simply removing our dependence on fossil fuels by distributing new co-benefits to a broader community and environment. To understand, incentivize, and implement this potential, we have to have data on the dynamic nature of both theorized and existing practices and effects on ecosystem services. Here, we have used a collection of remote sensing datasets, federal products and resources, and new tools to address some key concerns about the sustainability of renewable energy land use. We have also provided new data for others to address deeper questions about the sustainability of these technologies.

Sustainability has two pillars: (1) meeting the needs of the present (2) without compromising the capacity for future generations to meet their own needs (UN, 1987). Throughout history, human society has unequivocally reshaped nearly all global systems in an attempt to meet the needs of its people, cultivating half of all terrestrial surfaces, deforesting a third of global

forested area, doubling the concentration of carbon dioxide in the atmosphere, and threatening the populations of thousands of other species (Ritchie, 2024). Yet, global occurrence and death from disease, famine, war, and child mortality have never been lower, education has never been more accessible, and many of the aforementioned consequences of anthropogenic needs are near or have already peaked in impact globally (both absolute and per capita) (Ritchie, 2024). For the first time in human history, people alive today have the opportunity to realize both pillars of sustainability. The technologies exist, the knowledge is robust, and the pathways towards sustainability are many. We just have to keep going.

REFERENCES

Abernethy, J., Beeson, P., Boryan, C., Hunt, K., & Sartore, L. (2023). Preseason crop type prediction using crop sequence boundaries. *Computers and Electronics in Agriculture*, *208*, 107768. https://doi.org/10.1016/j.compag.2023.107768

Achanta, R., & Susstrunk, S. (2017). Superpixels and Polygons Using Simple Non-iterative Clustering. *2017 IEEE Conference on Computer Vision and Pattern Recognition (CVPR)*, 4895–4904. https://doi.org/10.1109/CVPR.2017.520

Adeh, E. H., Good, S. P., Calaf, M., & Higgins, C. W. (2019). Solar PV Power Potential is Greatest Over Croplands. *Scientific Reports*, *9*(1), 11442. https://doi.org/10.1038/s41598-019-47803-3

Adeh, H.-E., Selker, J. S., & Higgins, C. W. (2018). Remarkable agrivoltaic influence on soil moisture, micrometeorology and water-use efficiency. *PLoS ONE*, *13*(11), e0203256. https://doi.org/10.1371/journal.pone.0203256

Adelaja, S., & Hailu, Y. G. (2008, July). *Renewable Energy Development and Implications to Agricultural Viability*. American Agricultural Economics Association Annual Meeting, Orlando, FL. https://doi.org/10.22004/ag.econ.6132

Aksoy, T., Cetin, M., Cabuk, S. N., Senyel Kurkcuoglu, M. A., Bilge Ozturk, G., & Cabuk, A. (2023). Impacts of wind turbines on vegetation and soil cover: A case study of Urla, Cesme, and Karaburun Peninsulas, Turkey. *Clean Technologies and Environmental Policy*, *25*(1), 51–68. https://doi.org/10.1007/s10098-022-02387-x

Al Garni, H. Z., Awasthi, A., & Wright, D. (2019). Optimal orientation angles for maximizing energy yield for solar PV in Saudi Arabia. *Renewable Energy*, *133*, 538–550. https://doi.org/10.1016/j.renene.2018.10.048

Amaducci, S., Yin, X., & Colauzzi, M. (2018). Agrivoltaic systems to optimise land use for electric energy production. *Applied Energy*, *220*, 545–561. https://doi.org/10.1016/j.apenergy.2018.03.081

Andrew, A. C., Higgins, C. W., Smallman, M. A., Graham, M., & Ates, S. (2021). Herbage Yield, Lamb Growth and Foraging Behavior in Agrivoltaic Production System. *Frontiers in Sustainable Food Systems*, *5*, 659175. https://doi.org/10.3389/fsufs.2021.659175

Antonini, E. G. A., & Caldeira, K. (2021). Spatial constraints in large-scale expansion of wind power plants. *Proceedings of the National Academy of Sciences*, *118*(27), e2103875118. https://doi.org/10.1073/pnas.2103875118

Aragon, N. U., Xie, Y., Bigelow, D., Lark, T. J., & Eagle, A. J. (2024). The Realistic Potential of Soil Carbon Sequestration in U.S. Croplands for Climate Mitigation. *Earth's Future*, *12*(6), e2023EF003866. https://doi.org/10.1029/2023EF003866

Ardani, K., Denholm, P., Mai, T., Margolis, R., O'Shaughnessy, E., Silverman, T. J., & Zuboy, J. (2021). *Solar Futures Study* (pp. 1–280). U.S. Department of Energy. https://www.energy.gov/sites/default/files/2021-09/Solar%20Futures%20Study.pdf

Arent, D., Pless, J., Mai, T., Wiser, R., Hand, M., Baldwin, S., Heath, G., Macknick, J., Bazilian, M., Schlosser, A., & Denholm, P. (2014). Implications of high renewable electricity penetration in the U.S. for water use, greenhouse gas emissions, land-use, and materials supply. *Applied Energy*, *123*, 368–377. https://doi.org/10.1016/j.apenergy.2013.12.022

Armstrong, A., Ostle, N. J., & Whitaker, J. (2016). Solar park microclimate and vegetation management effects on grassland carbon cycling. *Environmental Research Letters*, *11*(7), 074016. https://doi.org/10.1088/1748-9326/11/7/074016

Arnaudo, E., Blanco, G., Monti, A., Bianco, G., Monaco, C., Pasquali, P., & Dominici, F. (2023). A Comparative Evaluation of Deep Learning Techniques for Photovoltaic Panel Detection From Aerial Images. *IEEE Access*, *11*, 47579–47594. https://doi.org/10.1109/ACCESS.2023.3275435

Aschale, T. M., Sciuto, G., Peres, D. J., Gullotta, A., & Cancelliere, A. (2022). Evaluation of Reference Evapotranspiration Estimation Methods for the Assessment of Hydrological Impacts of Photovoltaic Power Plants in Mediterranean Climates. *Water*, *14*(14), 2268. https://doi.org/10.3390/w14142268

Ashraf, U., Morelli, T. L., Smith, A. B., & Hernandez, R. R. (2024). Aligning renewable energy expansion with climate-driven range shifts. *Nature Climate Change*, *14*(3), 242–246. https://doi.org/10.1038/s41558-024-01941-3

Aydin, N. Y., Kentel, E., & Duzgun, S. (2010). GIS-based environmental assessment of wind energy systems for spatial planning: A case study from Western Turkey. *Renewable and Sustainable Energy Reviews*, *14*(1), 364–373. https://doi.org/10.1016/j.rser.2009.07.023

Baiamonte, G., Gristina, L., & Palermo, S. (2023). Impact of solar panels on runoff generation process. *Hydrological Processes*, *37*(12), e15053. https://doi.org/10.1002/hyp.15053

Baidya Roy, S., & Traiteur, J. J. (2010). Impacts of wind farms on surface air temperatures. *Proceedings of the National Academy of Sciences*, *107*(42), 17899–17904. https://doi.org/10.1073/pnas.1000493107

Bakker, M., Post, V., Langevin, C. D., Hughes, J. D., White, J. T., Starn, J. J., & Fienen, M. N. (2016). Scripting MODFLOW Model DevelopmentUsing Python and FloPy. *Groundwater*, *54*(5), 733–739. https://doi.org/10.1111/gwat.12413

Barbose, G. L., Darghouth, N. R., O'Shaughnessy, E., & Forrester, S. (2024). *Tracking the Sun: Pricing and Design Trends for Distributed Photovoltaic Systems in the United States, 2024 Edition* [2024 Edition]. Lawrence Berkeley National Laboratory. https://emp.lbl.gov/publications/tracking-sun-pricing-and-design-3

Barnard, T., Agnaou, M., & Barbis, J. (2017). Two Dimensional Modeling to Simulate Stormwater Flows at Photovoltaic Solar Energy Sites. *Journal of Water Management Modeling*. https://doi.org/doi.org/10.14796/JWMM.C428

Barrett, C. B. (2021). Overcoming Global Food Security Challenges through Science and Solidarity. *American Journal of Agricultural Economics*, *103*(2), 422–447. https://doi.org/10.1111/ajae.12160

Barron-Gafford, G. A., Pavao-Zuckerman, M. A., Minor, R. L., Sutter, L. F., Barnett-Moreno, I., Blackett, D. T., Thompson, M., Dimond, K., Gerlak, A. K., Nabhan, G. P., & Macknick, J. E. (2019). Agrivoltaics provide mutual benefits across the food–energy–water nexus in drylands. *Nature Sustainability*, *2*(9), 848–855. https://doi.org/10.1038/s41893-019-0364-5

Berry, L. N., & Helwig, N. E. (2021). Cross-Validation, Information Theory, or Maximum Likelihood? A Comparison of Tuning Methods for Penalized Splines. *Stats*, *4*(3), 701–724. https://doi.org/10.3390/stats4030042

Berryhill, A. R. (2021). *Utility-Scale Solar in Virginia: An Analysis of Land Use and Development Trends*. Virginia Commonwealth University Virginia Commonwealth University. https://scholarscompass.vcu.edu/cgi/viewcontent.cgi?article=1043&context=murp_capstone

Bessette, D. L., Hoen, B., Rand, J., Hoesch, K., White, J., Mills, S. B., & Nilson, R. (2024). Good fences make good neighbors: Stakeholder perspectives on the local benefits and burdens of large-scale solar energy development in the United States. *Energy Research & Social Science*, *108*, 103375. https://doi.org/10.1016/j.erss.2023.103375

Bessette, D. L., & Mills, S. B. (2021). Farmers vs. lakers: Agriculture, amenity, and community in predicting opposition to United States wind energy development. *Energy Research & Social Science*, *72*, 101873. https://doi.org/10.1016/j.erss.2020.101873

Biggs, N. B., Shivaram, R., Lacarieri, E. A., Varkey, K., Hagan, D., Young, H., & Lambin, E. F. (2022). Landowner decisions regarding utility-scale solar energy on working lands: A qualitative case study in California. *Environmental Research Communications*, *4*(5), 055010. https://doi.org/10.1088/2515-7620/ac6fbf

Blaauw, B. R., & Isaacs, R. (2014). Flower plantings increase wild bee abundance and the pollination services provided to a pollination-dependent crop. *Journal of Applied Ecology*, *51*(4), 890–898. https://doi.org/10.1111/1365-2664.12257

Blaschke, T., Hay, G. J., Kelly, M., Lang, S., Hofmann, P., Addink, E., Queiroz Feitosa, R., Van Der Meer, F., Van Der Werff, H., Van Coillie, F., & Tiede, D. (2014). Geographic Object-Based Image Analysis – Towards a new paradigm. *ISPRS Journal of Photogrammetry and Remote Sensing*, *87*, 180–191. https://doi.org/10.1016/j.isprsjprs.2013.09.014

Blaydes, H., Gardner, E., Whyatt, J. D., Potts, S. G., & Armstrong, A. (2022). Solar park management and design to boost bumble bee populations. *Environmental Research Letters*, *17*(4), 044002. https://doi.org/10.1088/1748-9326/ac5840

Blaydes, H., Potts, S. G., Whyatt, J. D., & Armstrong, A. (2021). Opportunities to enhance pollinator biodiversity in solar parks. *Renewable and Sustainable Energy Reviews*, *145*, 111065. https://doi.org/10.1016/j.rser.2021.111065

Blaydes, H., Potts, S. G., Whyatt, J. D., & Armstrong, A. (2024). On-site floral resources and surrounding landscape characteristics impact pollinator biodiversity at solar parks. *Ecological Solutions and Evidence*, *5*(1), e12307. https://doi.org/10.1002/2688-8319.12307

Bolinger, M., & Wiser, R. (2006). A comparative analysis of business structures suitable for farmer-owned wind power projects in the United States. *Energy Policy*, *34*(14), 1750–1761. https://doi.org/10.1016/j.enpol.2005.01.003

Bolson, N., Prieto, P., & Patzek, T. (2022). Capacity factors for electrical power generation from renewable and nonrenewable sources. *Proceedings of the National Academy of Sciences*, *119*(52), e2205429119. https://doi.org/10.1073/pnas.2205429119

Bond, J. K., Hitaj, C., Smith, D., Hunt, K., Perez, A., & Ferreira, G. (2021). Economic Research Service Economic Research Report Number 290 Honey Bees on the Move: From Pollination to Honey Production and Back. *USDA Economic Research Service*, *290*. https://www.ers.usda.gov/publications/pub-details/?pubid=101475

Boryan, C., Yang, Z., Mueller, R., & Craig, M. (2011). Monitoring US agriculture: The US department of agriculture, national agricultural statistics service, cropland data layer program. *Geocarto International*, *26*(5), 341–358. https://doi.org/10.1080/10106049.2011.562309

Bradbury, K., Saboo, R., Johnson, T. L., Malof, J. M., Devarajan, A., Zhang, W., Collins, L. M., & Newell, R. G. (2016). Distributed solar photovoltaic array location and extent dataset for remote sensing object identification. *Scientific Data*. https://doi.org/10.1038/sdata.2016.106

Bradbury, K., Saboo, R., Malof, J. M., Johnson, T. L., Devarajan, A., Zhang, W., Collins, L., Newell, R. G., Streltsov, A., & Hu, W. (2020). *Distributed Solar Photovoltaic Array Location and Extent Data Set for Remote Sensing Object Identification* (Version 4) [Dataset]. figshare. https://doi.org/10.6084/m9.figshare.3385780.v4

Brannstrom, C., Tilton, M., Klein, A., & Jepson, W. (2015). Spatial Distribution of Estimated Wind-Power Royalties in West Texas. *Land*, *4*(4), 1182–1199. https://doi.org/10.3390/land4041182

Breiman, L. (2001). Random Forests. *Machine Learning*, *45*, 5–32. https://doi.org/10.1023/A:1010933404324

Breyer, C., Bogdanov, D., Aghahosseini, A., Gulagi, A., Child, M., Oyewo, A. S., Farfan, J., Sadovskaia, K., & Vainikka, P. (2018). Solar photovoltaics demand for the global energy transition in the power sector. *Progress in Photovoltaics: Research and Applications*, *26*(8), 505–523. https://doi.org/10.1002/pip.2950

Bright, J. M., Killinger, S., Lingfors, D., & Engerer, N. A. (2018). Improved satellite-derived PV power nowcasting using real-time power data from reference PV systems. *Solar Energy*, *168*, 118–139. https://doi.org/10.1016/j.solener.2017.10.091

Bunis, L., & Mootz, J. (2007). *Aerial Photography Field Office-National Agriculture Imagery Program (NAIP) Suggested Best Practices-Final Report* (CDRL A006). ITT Space Systems, LLC. https://www.fsa.usda.gov/Internet/FSA_File/naip_best_practice.pdf

Burger, J., & Gochfeld, M. (2012). A Conceptual Framework Evaluating Ecological Footprints and Monitoring Renewable Energy: Wind, Solar, Hydro, and Geothermal. *Energy and Power Engineering*, *04*(04), 303–314. https://doi.org/10.4236/epe.2012.44040

Burke, M., & Lobell, D. B. (2017). Satellite-based assessment of yield variation and its determinants in smallholder African systems. *Proceedings of the National Academy of Sciences of the United States of America*, *114*(9), 2189–2194. https://doi.org/10.1073/pnas.1616919114

Buster, G., Benton, B. N., Glaws, A., & King, R. N. (2024). High-resolution meteorology with climate change impacts from global climate model data using generative machine learning. *Nature Energy*, *9*(7), 894–906. https://doi.org/10.1038/s41560-024-01507-9

Byers, L., Friedrich, J., Hennig, R., Kressig, A., Li, X., Mccormick, C., & Valeri, L. M. (2021). *A Global Database of Power Plants* (pp. 1–18) [Technical Note]. World Resources Institute. https://files.wri.org/d8/s3fs-public/2021-07/global-power-plant-database-technical-note-v1.3.pdf?VersionId=KNA6zn0E2HgUcEsXhtZuvfAlIqWOjLib&_gl=1*t24zup*_gcl_au*https://files.wri.org/d8/s3fs-public/2021-07/global-power-plant-database-technical-note-v1.3.pdf.

Cagle, A. E., Shepherd, M., Grodsky, S. M., Armstrong, A., Jordaan, S. M., & Hernandez, R. R. (2023). Standardized metrics to quantify solar energy-land relationships: A global systematic review. *Frontiers in Sustainability*, *3*(1035705). https://doi.org/10.3389/frsus.2022.1035705

Calderone, N. W. (2012). Insect Pollinated Crops, Insect Pollinators and US Agriculture: Trend Analysis of Aggregate Data for the Period 1992–2009. *PLoS ONE*, *7*(5), e37235. https://doi.org/10.1371/journal.pone.0037235

Cameron, D. R., Cohen, B. S., & Morrison, S. A. (2012). An Approach to Enhance the Conservation-Compatibility of Solar Energy Development. *PLoS ONE*, *7*(6), e38437. https://doi.org/10.1371/journal.pone.0038437

Camilo, J., Wang, R., Collins, L. M., & Malof, J. M. (2018). Application of a semantic segmentation convolutional neural network for accurate automatic detection and mapping

of solar photovoltaic arrays in aerial imagery. *2017 IEEE Applied Imagery Pattern Recognition (AIPR) Workshop*. https://doi.org/10.48550/arXiv.1801.04018

Cardoso, A., Jurado-Rodríguez, D., López, A., Ramos, M. I., & Jurado, J. M. (2024). Automated detection and tracking of photovoltaic modules from 3D remote sensing data. *Applied Energy*, *367*, 123242. https://doi.org/10.1016/j.apenergy.2024.123242

Carr, N. B., Fancher, T., Freeman, A. T., & Manley, H. M. B. (2016). *Surface area of solar arrays in the conterminous United States* (Dataset USGS Data Release). ScienceBase-Catalog. http://dx.doi.org/10.5066/F79S1P57

Carvalho, F., Healing, S., & Armstrong, A. (2024). Enhancing soil carbon in solar farms through active land management: A systematic review of the available evidence. *Environmental Research: Ecology*, *3*(4), 042001. https://doi.org/10.1088/2752-664X/ad8ce4

Carvalho, F., Lee, H. K., Blaydes, H., Treasure, L., Harrison, L. J., Montag, H., Vucic, K., Scurlock, J., White, P. C. L., Sharp, S. P., Clarkson, T., & Armstrong, A. (2024). Integrated policymaking is needed to deliver climate and ecological benefits from solar farms. *Journal of Applied Ecology*, 1365-2664.14745. https://doi.org/10.1111/1365-2664.14745

Carvalho, F., Montag, H., Bentley, L., Šarlej, R., Broyd, R. C., Blaydes, H., Cattin, M., Burke, M., Wallwork, A., Ramanayaka, S., White, P. C. L., Sharp, S. P., Clarkson, T., & Armstrong, A. (2025). Plant and soil responses to ground-mounted solar panels in temperate agricultural systems. *Environmental Research Letters*, *20*(2), 024003. https://doi.org/10.1088/1748-9326/ada45b

Carvalho, F., Treasure, L., Robinson, S. J. B., Blaydes, H., Exley, G., Hayes, R., Howell, B., Keith, A., Montag, H., Parker, G., Sharp, S. P., Witten, C., & Armstrong, A. (2023). Towards a standardized protocol to assess natural capital and ecosystem services in solar parks. *Ecological Solutions and Evidence*, *4*(1), e12210. https://doi.org/10.1002/2688-8319.12210

Center for Sustainable Systems. (2021). *U.S. Cities Factsheet* (Pub. No. CSS09-06). Universtiy of Michigan. https://css.umich.edu/sites/default/files/2023-10/U.S.%20Cities_CSS09-06_0.pdf

Cetin, M., Aksoy, T., Bilge Ozturk, G., & Cabuk, A. (2022). Developing a Model for the Relationship Between Vegetation and Wind Power Using Remote Sensing and Geographic Information Systems Technology. *Water, Air, & Soil Pollution*, *233*(11), 450. https://doi.org/10.1007/s11270-022-05887-0

Chen, D., Peng, Q., Lu, J., Huang, P., Song, Y., & Peng, F. (2024). Classification and segmentation of five photovoltaic types based on instance segmentation for generating more refined photovoltaic data. *Applied Energy*, *376*, 124296. https://doi.org/10.1016/j.apenergy.2024.124296

Chen, J., Yang, K., Chen, S., Yang, C., Zhang, S., & He, L. (2019). Enhanced normalized difference index for impervious surface area estimation at the plateau basin scale. *Journal of Applied Remote Sensing*. https://doi.org/10.1117/1.jrs.13.016502

Chen, T., & Li, Q. (2019). *Wind Energy and Agricultural Production: Evidence from Farm-Level Data*. Agricultural & Applied Economics Association Annual Meeting, Atlanta, GA. https://doi.org/10.2139/ssrn.4854865

Chen, Y., Zhang, J., Dai, Q., Zeng, T., & Zhu, S. (2024). Investigation of terrestrial water saving from photovoltaic panels using energy-balance model. *Journal of Hydrology*, *645*, 132183. https://doi.org/10.1016/j.jhydrol.2024.132183

Chen, Y., Zhou, J., Ge, Y., & Dong, J. (2024). Uncovering the rapid expansion of photovoltaic power plants in China from 2010 to 2022 using satellite data and deep learning. *Remote Sensing of Environment, 305*, 114100. https://doi.org/10.1016/j.rse.2024.114100

Choi, C. S., Cagle, A. E., Macknick, J., Bloom, D. E., Caplan, J. S., & Ravi, S. (2020). Effects of Revegetation on Soil Physical and Chemical Properties in Solar Photovoltaic Infrastructure. *Frontiers in Environmental Science*, *8*, 140. https://doi.org/10.3389/fenvs.2020.00140

Choi, C. S., Macknick, J., Li, Y., Bloom, D., McCall, J., & Ravi, S. (2023). Environmental Co-Benefits of Maintaining Native Vegetation With Solar Photovoltaic Infrastructure. *Earth's Future*, *11*(6), e2023EF003542. https://doi.org/10.1029/2023EF003542

Choi, C. S., Macknick, J., McCall, J., Bertel, R., & Ravi, S. (2024). Multi-year analysis of physical interactions between solar PV arrays and underlying soil-plant complex in vegetated utility-scale systems. *Applied Energy*, *365*, 123227. https://doi.org/10.1016/j.apenergy.2024.123227

Choi, J.-K., & Fthenakis, V. (2014). Crystalline silicon photovoltaic recycling planning: Macro and micro perspectives. *Journal of Cleaner Production*, *66*, 443–449. https://doi.org/10.1016/j.jclepro.2013.11.022

Christol, C., Oteri, F., & Laurienti, M. (2021). *Land-Based Wind Energy Siting: A Foundational and Technical Resource* (NREL/TP-5000-78591, DOE/GO-102021-5608; p. NREL/TP-5000-78591, DOE/GO-102021-5608). https://doi.org/10.2172/1812706

Claire Coutinho. (2024, May 15). *Solar and protecting our Food Security and Best and Most Versatile (BMV) Land*. UK Parliament. https://questions-statements.parliament.uk/written-statements/detail/2024-05-15/hcws466

Clark, C. N., & Pacifici, F. (2023). A solar panel dataset of very high resolution satellite imagery to support the Sustainable Development Goals. *Scientific Data*, *10*(1), 636. https://doi.org/10.1038/s41597-023-02539-8

Cohen, J. (1988). Statistical power analysis for the behavioral sciences (2nd ed.). *Hillsdale, NJ: Lawrence Erlbaum*.

Cohen, W. B., Healey, S. P., Yang, Z., Zhu, Z., & Gorelick, N. (2020). Diversity of Algorithm and Spectral Band Inputs Improves Landsat Monitoring of Forest Disturbance. *Remote Sensing*, *12*(10), 1673. https://doi.org/10.3390/rs12101673

Comte, L., & Olden, J. D. (2017). Climatic vulnerability of the world's freshwater and marine fishes. *Nature Climate Change*, *7*(10), 718–722. https://doi.org/10.1038/nclimate3382

Condon, D., Scott, T. A., Smith, A. B., Morelli, T. L., Ashraf, U., Mojica, A., Chittanuru, H., Luu, R., Bear, R., & Hernandez, R. R. (2025). Practitioners' perceived risks to biodiversity from renewable energy expansion through 2050. *Humanities and Social Sciences Communications*, *12*(1), 263. https://doi.org/10.1057/s41599-025-04558-9

Cook, L. M., & McCuen, R. H. (2013). Hydrologic Response of Solar Farms. *Journal of Hydrologic Engineering*, *18*(5), 536–541. https://doi.org/10.1061/(asce)he.1943-5584.0000530

Copena, D., & Simón, X. (2018). Wind farms and payments to landowners: Opportunities for rural development for the case of Galicia. *Renewable and Sustainable Energy Reviews*, *95*, 38–47. https://doi.org/10.1016/j.rser.2018.06.043

Costa, M. V. C. V. D., Carvalho, O. L. F. D., Orlandi, A. G., Hirata, I., Albuquerque, A. O. D., Silva, F. V. E., Guimarães, R. F., Gomes, R. A. T., & Júnior, O. A. D. C. (2021). Remote Sensing for Monitoring Photovoltaic Solar Plants in Brazil Using Deep Semantic Segmentation. *Energies*, *14*(10), 2960. https://doi.org/10.3390/en14102960

Crago, C. L., & Chernyakhovskiy, I. (2017). Are policy incentives for solar power effective? Evidence from residential installations in the Northeast. *Journal of Environmental Economics and Management*, *81*, 132–151. https://doi.org/10.1016/j.jeem.2016.09.008

Crago, C. L., & Koegler, E. (2018). Drivers of growth in commercial-scale solar PV capacity. *Energy Policy*, *120*, 481–491. https://doi.org/10.1016/j.enpol.2018.05.047

Craig Kaiser. (2024a, February 2). *Earn Income from Wind Turbines on Your Land*. Landgate. https://www.landgate.com/news/earn-income-from-wind-turbines-on-your-land

Craig Kaiser. (2024b, February 6). *Getting Paid for a Wind Turbine Lease on Your Land*. Landgate. https://www.landgate.com/news/getting-paid-for-a-wind-turbine-lease-on-your-land#:~:text=Across%20the%20country%2C%20deal%20terms,to%2010%25%20in%20year%2020.

Crawford, C. J., Roy, D. P., Arab, S., Barnes, C., Vermote, E., Hulley, G., Gerace, A., Choate, M., Engebretson, C., Micijevic, E., Schmidt, G., Anderson, C., Anderson, M., Bouchard, M., Cook, B., Dittmeier, R., Howard, D., Jenkerson, C., Kim, M., … Zahn, S. (2023). The 50-year Landsat collection 2 archive. *Science of Remote Sensing*, *8*, 100103. https://doi.org/10.1016/j.srs.2023.100103

Crawford, J., Bessette, D., & Mills, S. B. (2022). Rallying the anti-crowd: Organized opposition, democratic deficit, and a potential social gap in large-scale solar energy. *Energy Research & Social Science*, *90*, 102597. https://doi.org/10.1016/j.erss.2022.102597

Crist, E. P., & Cicone, R. C. (1984). A Physically-Based Transformation of Thematic Mapper Data—The TM Tasseled Cap. *IEEE Transactions on Geoscience and Remote Sensing*, *GE-22*(3), 256–263. https://doi.org/10.1109/TGRS.1984.350619

Csikós, N., & Tóth, G. (2023). Concepts of agricultural marginal lands and their utilisation: A review. *Agricultural Systems*, *204*, 103560. https://doi.org/10.1016/j.agsy.2022.103560

Cunningham, M. A., & Seidman, J. (2024). Competition for Land: Equity and Renewable Energy in Farmlands. *Land*, *13*(7), 939. https://doi.org/10.3390/land13070939

Cuppari, R. I., Branscomb, A., Graham, M., Negash, F., Smith, A. K., Proctor, K., Rupp, D., Tilahun Ayalew, A., Getaneh Tilaye, G., Higgins, C. W., & Najm, M. A. (2024). Agrivoltaics: Synergies and trade-offs in achieving the sustainable development goals at the global and local scale. *Applied Energy*, *362*, 122970. https://doi.org/10.1016/j.apenergy.2024.122970

Curioni, M., Galli, N., Manzolini, G., & Rulli, M. C. (2025). Global Land-Water Competition and Synergy Between Solar Energy and Agriculture. *Earth's Future*, *13*(2), e2024EF005291. https://doi.org/10.1029/2024EF005291

Curtis, S., Etheridge, R., Malali, P., Peralta, A. L., & Filho, F. (2020). Planning for future solar farm development in North Carolina: A geographic food-energy-water approach. *Southeastern Geographer*, *60*(1), 48–64. https://doi.org/10.1353/sgo.2020.0004

Curtis, T., Heath, G., Walker, A., Desai, J., Settle, E., & Barbosa, C. (2021). *Best Practices at the End of the Photovoltaic System Performance Period* (Technical Report NREL/TP-5C00-78678). NREL. https://www.nrel.gov/docs/fy21osti/78678.pdf

Dahlke, H. E., LaHue, G. T., Mautner, M. R. L., Murphy, N. P., Patterson, N. K., Waterhouse, H., Yang, F., & Foglia, L. (2018). Managed Aquifer Recharge as a Tool to Enhance Sustainable Groundwater Management in California: Examples From Field and Modeling Studies. *Advances in Chemical Pollution, Environmental Management and Protection*, *3*, 215–275. https://doi.org/10.1016/bs.apmp.2018.07.003

Dai, T., Jose Valanarasu, J. M., Zhao, Y., Zheng, S., Sun, Y., Patel, V. M., & Jordaan, S. M. (2024). Land Resources for Wind Energy Development Requires Regionalized Characterizations. *Environmental Science & Technology*, *58*(11), 5014–5023. https://doi.org/10.1021/acs.est.3c07908

Davis, R., & Macknick, J. (2022). *ASTRO: Facilitating Advancements in Low-Impact Solar Research, Deployment, and Dissemination* (Technical Report NREL/TP-6A20-83442). NREL. https://doi.org/10.2172/1882388

De Boer, J., & Zuidema, C. (2015). Towards an integrated energy landscape. *Proceedings of the Institution of Civil Engineers: Urban Design and Planning*, *168*(5), 231–240. https://doi.org/10.1680/udap.14.00041

Deines, J. M., Patel, R., Liang, S.-Z., Dado, W., & Lobell, D. B. (2021). A million kernels of truth: Insights into scalable satellite maize yield mapping and yield gap analysis from an extensive ground dataset in the US Corn Belt. *Remote Sensing of Environment*, *253*, 112174. https://doi.org/10.1016/j.rse.2020.112174

Deline, C., Muller, M., Decegile, M., Jordan, D., Anderson, K., Simpson, L., Perry, K., & White, R. (2020). *PV Fleet Performance Data Initiative: March 2020 Methodology Report* (Technical Report NREL/TP-5K00-76687). https://www.nrel.gov/docs/fy20osti/76687.pdf

Deline, C., Perry, K., Deceglie, M., Muller, M., Sekulic, W., & Jordan, D. (2021). *Photovoltaic Data Acquisition (PVDAQ) Public Datasets* (doi:10.25984/1846021) [Dataset]. NREL. https://dx.doi.org/10.25984/1846021

Denholm, P., Brown, P., Cole, W., Mai, T., Sergi, B., Brown, M., Jadun, P., Ho, J., Mayernik, J., McMillan, C., & Sreenath, R. (2022). *Examining Supply-Side Options to Achieve 100% Clean Electricity by 2035* (NREL/TP-6A40-81644; p. NREL/TP-6A40-81644). NREL. https://doi.org/10.2172/1885591

Denholm, P., Hand, M., Jackson, M., & Ong, S. (2009). Land Use Requirements of Modern Wind Power Plants in the United States. *National Renewable Energy Laboratory*, *Technical*(August), 46.

Devitt, D. A., Young, M. H., & Pierre, J. P. (2020). Assessing the potential for greater solar development in West Texas, USA. *Energy Strategy Reviews*, *29*, 100490. https://doi.org/10.1016/j.esr.2020.100490

Dhar, A., Naeth, M. A., Jennings, P. D., & Gamal El-Din, M. (2020). Perspectives on environmental impacts and a land reclamation strategy for solar and wind energy systems. *Science of The Total Environment*, *718*, 134602. https://doi.org/10.1016/j.scitotenv.2019.134602

Diffendorfer, J. E., & Compton, R. W. (2014). Land Cover and Topography Affect the Land Transformation Caused by Wind Facilities. *PLoS ONE*, *9*(2), e88914. https://doi.org/10.1371/journal.pone.0088914

Diffendorfer, J. E., Dorning, M. A., Keen, J. R., Kramer, L. A., & Taylor, R. V. (2019). Geographic context affects the landscape change and fragmentation caused by wind energy facilities. *PeerJ*, *7*, e7129. https://doi.org/10.7717/peerj.7129

Diffendorfer, J. E., Sergi, B., Lopez, A., Williams, T., Gleason, M., Ancona, Z., & Cole, W. (2024). The interplay of future solar energy, land cover change, and their projected impacts on natural lands and croplands in the US. *Science of The Total Environment*, *947*, 173872. https://doi.org/10.1016/j.scitotenv.2024.173872

Diffendorfer, J. E., Vanderhoof, M. K., & Ancona, Z. H. (2022). Wind turbine wakes can impact down-wind vegetation greenness. *Environmental Research Letters*, *17*(10), 104025. https://doi.org/10.1088/1748-9326/ac8da9

Dilts, T. E., Black, S. H., Hoyle, S. M., Jepsen, S. J., May, E. A., & Forister, M. L. (2023). Agricultural margins could enhance landscape connectivity for pollinating insects across the Central Valley of California, U.S.A. *PLOS ONE*, *18*(2), e0267263. https://doi.org/10.1371/journal.pone.0267263

Dixon, D. J., Callow, J. N., Duncan, J. M. A., Setterfield, S. A., & Pauli, N. (2021). Satellite prediction of forest flowering phenology. *Remote Sensing of Environment*, *255*, 112197. https://doi.org/10.1016/j.rse.2020.112197

Dobos, A., Neises, T., & Wagner, M. (2014). Advances in CSP Simulation Technology in the System Advisor Model. *Energy Procedia*, *49*, 2482–2489. https://doi.org/10.1016/j.egypro.2014.03.263

Dunne, T., & Black, R. D. (1970). Partial Area Contributions to Storm Runoff in a Small New England Watershed. *Water Resources Research*, *6*(5), 1296–1311. https://doi.org/10.1029/WR006i005p01296

Dunnett, S. (2020). *Harmonised global datasets of wind and solar farm locations and power: Dataset* (Version v6) [Dataset]. figshare. https://doi.org/10.6084/m9.figshare.11310269.v6

Dunnett, S., Holland, R. A., Taylor, G., & Eigenbrod, F. (2022). Predicted wind and solar energy expansion has minimal overlap with multiple conservation priorities across global regions. *Proceedings of the National Academy of Sciences*, *119*(6), e2104764119. https://doi.org/10.1073/pnas.2104764119

Dunnett, S., Sorichetta, A., Taylor, G., & Eigenbrod, F. (2020). Harmonised global datasets of wind and solar farm locations and power. *Scientific Data*, *7*(1), 1–12. https://doi.org/10.1038/s41597-020-0469-8

Dykes, K., Damiani, R., Roberts, O., & Lantz, E. (2018, January 8). Analysis of Ideal Towers for Tall Wind Applications. *2018 Wind Energy Symposium*. 2018 Wind Energy Symposium, Kissimmee, Florida. https://doi.org/10.2514/6.2018-0999

Edalat, M. M. (2017). *Remote sensing of the environmental impacts of utility-scale solar energy plants* [University of Nevada, Las Vegas]. https://doi.org/10.34917/11156717

Edun, A. S., Perry, K., Harley, J. B., & Deline, C. (2021). Unsupervised azimuth estimation of solar arrays in low-resolution satellite imagery through semantic segmentation and Hough transform. *Applied Energy*, *298*, 117273. https://doi.org/10.1016/j.apenergy.2021.117273

EGLE. (2020). *Michigan Waterwells for WELLOGIC dataset* [Dataset]. https://gis-michigan.opendata.arcgis.com/search?collection=Dataset&q=Wellogic

Egli, D. B. (2023). Yield improvement and yield components: A comparison of corn and soybean. *Crop Science*, *63*(3), 1019–1029. https://doi.org/10.1002/csc2.20925

EIA. (2025). *Short-Term Energy Outlook* (Analysis & Projections). U.S. Energy Information Administration. https://www.eia.gov/outlooks/steo/report/BTL/2023/09-smallscalesolar/article.php#

Ejdemo, T., & Söderholm, P. (2015). Wind power, regional development and benefit-sharing: The case of Northern Sweden. *Renewable and Sustainable Energy Reviews*, *47*, 476–485. https://doi.org/10.1016/j.rser.2015.03.082

Elamri, Y., Cheviron, B., Lopez, J. M., Dejean, C., & Belaud, G. (2018). Water budget and crop modelling for agrivoltaic systems: Application to irrigated lettuces. *Agricultural Water Management*, *208*(April), 440–453. https://doi.org/10.1016/j.agwat.2018.07.001

Elamri, Y., Cheviron, B., Mange, A., Dejean, C., Liron, F., & Belaud, G. (2018). Rain concentration and sheltering effect of solar panels on cultivated plots. *Hydrology and Earth System Sciences*, *22*(2), 1285–1298. https://doi.org/10.5194/hess-22-1285-2018

Elmallah, S., Hoen, B., Fujita, K. S., Robson, D., & Brunner, E. (2023). Shedding light on large-scale solar impacts: An analysis of property values and proximity to photovoltaics across six U.S. states. *Energy Policy*, *175*, 113425. https://doi.org/10.1016/j.enpol.2023.113425

EPA. (2024). *Re-powering America's Land Initiative: Project Tracking Matrix* (EPA 540-R-24-002). EPA. https://www.epa.gov/system/files/documents/2024-12/re_on_cl_tracking_matrix_draft_2024_final_508_12.09.24.pdf

EPRI. (2021). *Pollinator-Friendly Solar Scorecards: Comprehensive Analysis of Scorecard Attributes* (3002022121). EPRI. https://www.epri.com/research/products/000000003002022121

ESA. (2024). *Copernicus Sentinel data* [Dataset]. Google Earth Engine Data Catalog. https://sentinels.copernicus.eu/documents/247904/690755/Sentinel_Data_Legal_Notice

European Commission. (2024). *Photovoltaic Geographical Information System (5.3)* (Version 5.3) [Dataset]. EU Science Hub. https://joint-research-centre.ec.europa.eu/photovoltaic-geographical-information-system-pvgis/pvgis-releases/pvgis-53_en

Evans, M. J., Mainali, K., & Soobitsky, R. (2021). *Chesapeake Solar Footprints* (Version 2023) [Dataset]. OSF.io. https://doi.org/10.17605/OSF.IO/VQ7MT

Evans, M. J., Mainali, K., Soobitsky, R., Mills, E., & Minnemeyer, S. (2023). Predicting patterns of solar energy buildout to identify opportunities for biodiversity conservation. *Biological Conservation*, *283*, 110074. https://doi.org/10.1016/j.biocon.2023.110074

Fargione, J., Kiesecker, J., Slaats, M. J., & Olimb, S. (2012). Wind and Wildlife in the Northern Great Plains: Identifying Low-Impact Areas for Wind Development. *PLoS ONE*, *7*(7), e41468. https://doi.org/10.1371/journal.pone.0041468

Farina, A., & Anctil, A. (2022). Material consumption and environmental impact of wind turbines in the USA and globally. *Resources, Conservation and Recycling*, *176*, 105938. https://doi.org/10.1016/j.resconrec.2021.105938

Feng, Q., Niu, B., Ren, Y., Su, S., Wang, J., Shi, H., Yang, J., & Han, M. (2024). A 10-m national-scale map of ground-mounted photovoltaic power stations in China of 2020. *Scientific Data*, *11*(1), 198. https://doi.org/10.1038/s41597-024-02994-x

Feng, X., Li, S., Kalies, E. L., Markus, C., Harrell, P., & Patiño-Echeverri, D. (2023). Low impact siting for wind power facilities in the Southeast United States. *Wind Energy*, *26*(12), 1254–1275. https://doi.org/10.1002/we.2868

Feuerbacher, A., Herrmann, T., Neuenfeldt, S., Laub, M., & Gocht, A. (2022). Estimating the economics and adoption potential of agrivoltaics in Germany using a farm-level bottom-up approach. *Renewable and Sustainable Energy Reviews*, *168*, 112784. https://doi.org/10.1016/j.rser.2022.112784

Feuerbacher, A., Laub, M., Högy, P., Lippert, C., Pataczek, L., Schindele, S., Wieck, C., & Zikeli, S. (2021). An analytical framework to estimate the economics and adoption potential of dual land-use systems: The case of agrivoltaics. *Agricultural Systems*, *192*, 103193. https://doi.org/10.1016/j.agsy.2021.103193

Frank, S., Lessa Derci Augustynczik, A., Havlík, P., Boere, E., Ermolieva, T., Fricko, O., Di Fulvio, F., Gusti, M., Krisztin, T., Lauri, P., Palazzo, A., & Wögerer, M. (2024). Enhanced agricultural carbon sinks provide benefits for farmers and the climate. *Nature Food*, *5*(9), 742–753. https://doi.org/10.1038/s43016-024-01039-1

Fresh Energy. (2025). *Pollinator-Friendly Solar Scorecards*. Fresh Energy. https://fresh-energy.org/beeslovesolar/pollinator-friendly-solar-scorecards

Fthenakis, V., & Kim, H. C. (2009). Land use and electricity generation: A life-cycle analysis. *Renewable and Sustainable Energy Reviews*, *13*(6–7), 1465–1474. https://doi.org/10.1016/j.rser.2008.09.017

FTWRC. (2017). *Gull and Augusta Creeks Watershed Management Plan: The Four Township Watershed Area*. Four-Township Water Resources Council. https://kalamazooriver.org/wp-content/uploads/2022/11/FTWA_WMP_text_FINAL_8.7.17.pdf

Fujita, K. S., Ancona, Z. H., Kramer, L. A., Garrity, C. P., Diffendorfer, J. E., & Hoen, B. (2024). *United States Large-Scale Solar Photovoltaic Database* (Version 2.0) [U.S. Geological Survey and Lawrence Berkeley National Laboratory data release]. ScienceBase-Catalog. https://doi.org/10.5066/P9IA3TUS

Fujita, K. S., Ancona, Z. H., Kramer, L. A., Straka, M., Gautreau, T. E., Robson, D., Garrity, C., Hoen, B., & Diffendorfer, J. E. (2023). Georectified polygon database of ground-mounted large-scale solar photovoltaic sites in the United States. *Scientific Data*, *10*(1), 760. https://doi.org/10.1038/s41597-023-02644-8

Gallant, A. L., Euliss, N. H., & Browning, Z. (2014). Mapping Large-Area Landscape Suitability for Honey Bees to Assess the Influence of Land-Use Change on Sustainability of National Pollination Services. *PLoS ONE*, *9*(6), e99268. https://doi.org/10.1371/journal.pone.0099268

Galzki, J., & Mulla, D. (2024). Stormwater runoff calculator for evaluation of low impact development practices at ground-mounted solar photovoltaic farms. *Discover Water*, *4*(1), 35. https://doi.org/10.1007/s43832-024-00093-x

Gao, B. (1996). NDWI—A normalized difference water index for remote sensing of vegetation liquid water from space. *Remote Sensing of Environment*, *58*(3), 257–266. https://doi.org/10.1016/S0034-4257(96)00067-3

García, M. J. L., & Caselles, V. (1991). Mapping burns and natural reforestation using thematic Mapper data. *Geocarto International*, *6*(1), 31–37. https://doi.org/10.1080/10106049109354290

Ge, F., Wang, G., He, G., Zhou, D., Yin, R., & Tong, L. (2022). A Hierarchical Information Extraction Method for Large-Scale Centralized Photovoltaic Power Plants Based on Multi-Source Remote Sensing Images. *Remote Sensing*, *14*(17), 4211. https://doi.org/10.3390/rs14174211

GEM. (2024). *Global Solar Power Tracker, Global Energy Monitor, June 2024 release* (Dataset Global Energy Monitor). Global Energy Monitor. https://doi.org/Creative Commons CC BY 4.0 International License

Gilman, P., DiOrio, N. A., Freeman, J. M., Janzou, S., Dobos, A., & Ryberg, D. (2018). *SAM Photovoltaic Model Technical Reference Update* (Technical Report NREL/TP--6A20-67399). NREL. https://doi.org/10.2172/1429291

Gitelson, A. A., Gritz, Y., & Merzlyak, M. N. (2003). Relationships between leaf chlorophyll content and spectral reflectance and algorithms for non-destructive chlorophyll assessment in higher plant leaves. *Journal of Plant Physiology*, *160*(3), 271–282. https://doi.org/10.1078/0176-1617-00887

Global Energy Observatory, Google, KTH Royal Institute of Technology in Stockholm, Enipedia, & World Resources Institute. (2021). *Global Power Plant Database version 1.3.0* (Dataset WRI; Version 1.3.0). WRI. https://datasets.wri.org/datasets/global-power-plant-database

Goldstein, J. (1999). Emergence as a Construct: History and Issues. *Emergence*, *1*(1), 49–72. https://doi.org/10.1207/s15327000em0101_4

Gomez-Casanovas, N., Mwebaze, P., Khanna, M., Branham, B., Time, A., DeLucia, E. H., Bernacchi, C. J., Knapp, A. K., Hoque, M. J., Du, X., Blanc-Betes, E., Barron-Gafford, G. A., Peng, B., Guan, K., Macknick, J., Miao, R., & Miljkovic, N. (2023). Knowns, uncertainties, and challenges in agrivoltaics to sustainably intensify energy and food production. *Cell Reports Physical Science*, *4*(8), 101518. https://doi.org/10.1016/j.xcrp.2023.101518

Gómez-Catasús, J., Morales, M. B., Giralt, D., Del Portillo, D. G., Manzano-Rubio, R., Solé-Bujalance, L., Sardà-Palomera, F., Traba, J., & Bota, G. (2024). Solar photovoltaic energy development and biodiversity conservation: Current knowledge and research gaps. *Conservation Letters*, *17*(4), e13025. https://doi.org/10.1111/conl.13025

Gonzales, D., Hempel De Ibarra, N., & Anderson, K. (2022). Remote Sensing of Floral Resources for Pollinators – New Horizons From Satellites to Drones. *Frontiers in Ecology and Evolution*, *10*, 869751. https://doi.org/10.3389/fevo.2022.869751

Google Maps. (2024). *[Contiguous United States]* [Dataset]. Google Earth Engine Data Catalog. https://code.earthengine.google.com/

Gordon, J. M., & Wenger, H. J. (1991). Central-station solar photovoltaic systems: Field layout, tracker, and array geometry sensitivity studies. *Solar Energy*, *46*(4), 211–217. https://doi.org/10.1016/0038-092X(91)90065-5

GPI. (2023). *Best Practices: Photovoltaic Stormwater Management Research and Testing (PV-SMaRT)*. Great Plains Institute. https://betterenergy.org/wp-content/uploads/2023/01/PV-SMaRT-Best-Practice.pdf

Graham, M., Ates, S., Melathopoulos, A. P., Moldenke, A. R., DeBano, S. J., Best, L. R., & Higgins, C. W. (2021). Partial shading by solar panels delays bloom, increases floral abundance during the late-season for pollinators in a dryland, agrivoltaic ecosystem. *Scientific Reports*, *11*(1), 1–13. https://doi.org/10.1038/s41598-021-86756-4

Grippo, M., Hayse, J. W., & O'Connor, B. L. (2015). Solar Energy Development and Aquatic Ecosystems in the Southwestern United States: Potential Impacts, Mitigation, and Research Needs. *Environmental Management*, *55*(1), 244–256. https://doi.org/10.1007/s00267-014-0384-x

Grodsky, S. M. (2021). Matching renewable energy and conservation targets for a sustainable future. *One Earth*, *4*(7), 924–926. https://doi.org/10.1016/j.oneear.2021.07.001

Grodsky, S. M., Behr, M. J., Gendler, A., Drake, D., Dieterle, B. D., Rudd, R. J., & Walrath, N. L. (2011). Investigating the causes of death for wind turbine-associated bat fatalities. *Journal of Mammalogy*, *92*(5), 917–925. https://doi.org/10.1644/10-MAMM-A-404.1

Grodsky, S. M., Campbell, J. W., & Hernandez, R. R. (2021). Solar energy development impacts flower-visiting beetles and flies in the Mojave Desert. *Biological Conservation*, *263*, 109336. https://doi.org/10.1016/j.biocon.2021.109336

Grodsky, S. M., & Hernandez, R. R. (2020). Reduced ecosystem services of desert plants from ground-mounted solar energy development. *Nature Sustainability*, *3*(12), 1036–1043. https://doi.org/10.1038/s41893-020-0574-x

Groth, T. M., & Vogt, C. A. (2014). Rural wind farm development: Social, environmental and economic features important to local residents. *Renewable Energy*, *63*, 1–8. https://doi.org/10.1016/j.renene.2013.08.035

Gullotta, A., Aschale, T. M., Peres, D. J., Sciuto, G., & Cancelliere, A. (2023). Modelling Stormwater Runoff Changes Induced by Ground-Mounted Photovoltaic Solar Parks: A Conceptualization in EPA-SWMM. *Water Resources Management*, *37*(11), 4507–4520. https://doi.org/10.1007/s11269-023-03572-3

Guo, W., Wenz, L., & Auffhammer, M. (2024). The visual effect of wind turbines on property values is small and diminishing in space and time. *Proceedings of the National Academy of Sciences of the United States of America*, *121*(13), e2309372121. https://doi.org/10.1073/pnas.2309372121

Haegel, N. M., Atwater, H., Barnes, T., Breyer, C., Burrell, A., Chiang, Y.-M., De Wolf, S., Dimmler, B., Feldman, D., Glunz, S., Goldschmidt, J. C., Hochschild, D., Inzunza, R., Kaizuka, I., Kroposki, B., Kurtz, S., Leu, S., Margolis, R., Matsubara, K., … Bett, A. W. (2019). Terawatt-scale photovoltaics: Transform global energy. *Science*, *364*(6443), 836–838. https://doi.org/10.1126/science.aaw1845

Hall, P. K., Morgan, W., & Richardson, J. (2022). *Land Use Conflicts Between Wind and Solar Renewable Energy and Agriculture Uses* (104; Law Faculty Scholarship). West Virginia Universiy College of Law. https://researchrepository.wvu.edu/cgi/viewcontent.cgi?article=1104&context=law_faculty

Hamlin, Q. F., Martin, S. L., Kendall, A. D., & Hyndman, D. W. (2022). Examining Relationships Between Groundwater Nitrate Concentrations in Drinking Water and Landscape Characteristics to Understand Health Risks. *GeoHealth*, *6*(5), e2021GH000524. https://doi.org/10.1029/2021GH000524

Hanna, F., Nain, P., & Anctil, A. (2024). Material availability assessment using system dynamics: The case of tellurium. *Progress in Photovoltaics: Research and Applications*, *32*(4), 253–266. https://doi.org/10.1002/pip.3760

Hao, S., & Michaud, G. (2024). Assessing property value impacts near utility-scale solar in the Midwestern United States. *Solar Compass*, *12*, 100090. https://doi.org/10.1016/j.solcom.2024.100090

Haralick, R. M., Shanmugam, K., & Dinstein, I. (1973). Textural Features for Image Classification. *IEEE Transactions on Systems, Man, and Cybernetics*, *SMC-3*(6), 610–621. https://doi.org/10.1109/TSMC.1973.4309314

Haralick, R. M., & Shanmugam, K. S. (1974). Combined spectral and spatial processing of ERTS imagery data. *Remote Sensing of Environment*, *3*(1), 3–13. https://doi.org/10.1016/0034-4257(74)90033-9

Harris, C. R., Millman, K. J., Van Der Walt, S. J., Gommers, R., Virtanen, P., Cournapeau, D., Wieser, E., Taylor, J., Berg, S., Smith, N. J., Kern, R., Picus, M., Hoyer, S., Van Kerkwijk, M. H., Brett, M., Haldane, A., Del Río, J. F., Wiebe, M., Peterson, P., … Oliphant, T. E. (2020). Array programming with NumPy. *Nature*, *585*(7825), 357–362. https://doi.org/10.1038/s41586-020-2649-2

Harrison-Atlas, D., Glaws, A., King, R. N., & Lantz, E. (2024). Artificial intelligence-aided wind plant optimization for nationwide evaluation of land use and economic benefits of wake steering. *Nature Energy*, *9*(6), 735–749. https://doi.org/10.1038/s41560-024-01516-8

Harrison-Atlas, D., Lopez, A., & Lantz, E. (2022). Dynamic land use implications of rapidly expanding and evolving wind power deployment. *Environmental Research Letters*, *17*(4), 044064. https://doi.org/10.1088/1748-9326/ac5f2c

He, X., Feng, K., Li, X., Craft, A. B., Wada, Y., Burek, P., Wood, E. F., & Sheffield, J. (2019). Solar and wind energy enhances drought resilience and groundwater sustainability. *Nature Communications*, *10*(4893), 1–8. https://doi.org/10.1038/s41467-019-12810-5

Heath, G., Ravikumar, D., Ovaitt, S., Walston, L., Curtis, T., Millstein, D., Mirletz, H., Hartmann, H., & McCall, J. (2022). *Environmental and Circular Economy Implications of Solar Energy in a Decarbonized U.S. Grid* (NREL/TP-6A20-80818, 1844985, MainId:78596; p. NREL/TP-6A20-80818, 1844985, MainId:78596). https://doi.org/10.2172/1844985

Helwig, N. E. (2024). *Nonparametric Regressionvia Smoothing Splines (npreg)* (Version 1.1.0) [R]. https://doi.org/doi:10.4135/9781526421036885885

Heris, M. P., Foks, N. L., Bagstad, K. J., Troy, A., & Ancona, Z. H. (2020). A rasterized building footprint dataset for the United States. *Scientific Data*, *7*(1), 207. https://doi.org/10.1038/s41597-020-0542-3

Hernandez, R. R., Armstrong, A., Burney, J., Ryan, G., Moore-O'Leary, K., Diédhiou, I., Grodsky, S. M., Saul-Gershenz, L., Davis, R., Macknick, J., Mulvaney, D., Heath, G. A., Easter, S. B., Hoffacker, M. K., Allen, M. F., & Kammen, D. M. (2019). Techno–ecological synergies of solar energy for global sustainability. *Nature Sustainability*, *2*(7), 560–568. https://doi.org/10.1038/s41893-019-0309-z

Hernandez, R. R., Cagle, A. E., Grodsky, S. M., Exley, G., & Jordaan, S. M. (2022). Comments on: Land use for United States power generation: A critical review of existing metrics with suggestions for going forward (Renewable and Sustainable Energy Reviews 2021; 143: 110911). *Renewable and Sustainable Energy Reviews*, *166*, 112526. https://doi.org/10.1016/j.rser.2022.112526

Hernandez, R. R., Easter, S. B., Murphy-Mariscal, M. L., Maestre, F. T., Tavassoli, M., Allen, E. B., Barrows, C. W., Belnap, J., Ochoa-Hueso, R., Ravi, S., & Allen, M. F. (2014). Environmental impacts of utility-scale solar energy. *Renewable and Sustainable Energy Reviews*, *29*, 766–779. https://doi.org/10.1016/j.rser.2013.08.041

Hernandez, R. R., Hoffacker, M. K., & Field, C. B. (2014). Land-use efficiency of big solar. *Environmental Science and Technology*, *48*(2), 1315–1323. https://doi.org/10.1021/es4043726

Hernandez, R. R., Hoffacker, M. K., & Field, C. B. (2015). Efficient use of land to meet sustainable energy needs. *Nature Climate Change*, *5*(4), 353–358. https://doi.org/10.1038/nclimate2556

Hernandez, R. R., Hoffacker, M. K., Murphy-Mariscal, M. L., Wu, G. C., & Allen, M. F. (2015). Solar energy development impacts on land cover change and protected areas. *Proceedings of the National Academy of Sciences*, *112*(44), 13579–13584. https://doi.org/10.1073/pnas.1517656112

Hernandez, R. R., Jordaan, S. M., Kaldunski, B., & Kumar, N. (2020). Aligning Climate Change and Sustainable Development Goals With an Innovation Systems Roadmap for Renewable Power. *Frontiers in Sustainability*, *1*, 583090. https://doi.org/10.3389/frsus.2020.583090

Hilker, J. M., Busse, M., Müller, K., & Zscheischler, J. (2024). Photovoltaics in agricultural landscapes: "Industrial land use" or a "real compromise" between renewable energy and biodiversity? Perspectives of German nature conservation associations. *Energy, Sustainability and Society*, *14*(1), 6. https://doi.org/10.1186/s13705-023-00431-2

Hise, C., Obermeyer, B., Ahlering, M., Wilkinson, J., & Fargione, J. (2022). Site Wind Right: Identifying Low-Impact Wind Development Areas in the Central United States. *Land*, *11*(4), 462. https://doi.org/10.3390/land11040462

Hitaj, C., Webber, J., & Erickson, K. (2018). *Ownership of Oil and Gas Rights: Implications for U.S. Farm Income and Wealth* (EIB-193; Economic Information Bulletin). USDA ERS. https://ers.usda.gov/sites/default/files/_laserfiche/publications/89325/EIB-193.pdf?v=26392

Hoen, B., Brown, J. P., Jackson, T., Thayer, M. A., Wiser, R., & Cappers, P. (2015). Spatial Hedonic Analysis of the Effects of US Wind Energy Facilities on Surrounding Property Values. *The Journal of Real Estate Finance and Economics*, *51*(1), 22–51. https://doi.org/10.1007/s11146-014-9477-9

Hoen, B. D., Diffendorfer, J. E., Rand, J. T., Kramer, L. A., Garrity, C. P., & Hunt, H. E. (2018). *United States Wind Turbine Database v5.3 (January 13, 2023)* (Version 6.1) [Dataset]. ScienceBase-Catalog. https://doi.org/10.5066/F7TX3DN0

Hoen, B., Darlow, R., Haac, R., Rand, J., & Kaliski, K. (2023). Effects of land-based wind turbine upsizing on community sound levels and power and energy density. *Applied Energy*, *338*, 120856. https://doi.org/10.1016/j.apenergy.2023.120856

Hoesch, K. W., Mills, S. B., Rand, J., Nilson, R., Bessette, D. L., White, J., & Hoen, B. (2025). What to expect when you're expecting engagement: Delivering procedural justice in large-scale solar energy deployment. *Energy Research & Social Science*, *120*, 103893. https://doi.org/10.1016/j.erss.2024.103893

Hoffacker, M. K., Allen, M. F., & Hernandez, R. R. (2017). Land-Sparing Opportunities for Solar Energy Development in Agricultural Landscapes: A Case Study of the Great Central Valley, CA, United States. *Environmental Science & Technology*, *51*(24), 14472–14482. https://doi.org/10.1021/acs.est.7b05110

Holland, R. A., Scott, K., Agnolucci, P., Rapti, C., Eigenbrod, F., & Taylor, G. (2019). The influence of the global electric power system on terrestrial biodiversity. *Proceedings of the*

National Academy of Sciences, *116*(51), 26078–26084. https://doi.org/10.1073/pnas.1909269116

Holmgren, W. F., Hansen, C. W., & Mikofski, M. A. (2018). pvlib python: A python package for modeling solar energy systems. *Journal of Open Source Software*, *3*(29), 884. https://doi.org/10.21105/joss.00884

Hou, X., Wang, B., Hu, W., Yin, L., & Wu, H. (2019). SolarNet: A Deep Learning Framework to Map Solar Power Plants In China From Satellite Imagery. *ICLR 2020*, *6*. https://doi.org/10.48550/arXiv.1912.03685

Howland, M. F., Lele, S. K., & Dabiri, J. O. (2019). Wind farm power optimization through wake steering. *Proceedings of the National Academy of Sciences*, *116*(29), 14495–14500. https://doi.org/10.1073/pnas.1903680116

Hu, W., Bradbury, K., Malof, J. M., Li, B., Huang, B., Streltsov, A., Sydny Fujita, K., & Hoen, B. (2022). What you get is not always what you see—Pitfalls in solar array assessment using overhead imagery. *Applied Energy*, *327*, 120143. https://doi.org/10.1016/j.apenergy.2022.120143

Huete, A., Didan, K., Miura, T., Rodriguez, E. P., Gao, X., & Ferreira, L. G. (2002). Overview of the radiometric and biophysical performance of the MODIS vegetation indices. *Remote Sensing of Environment*, *83*(1–2), 195–213. https://doi.org/10.1016/S0034-4257(02)00096-2

Hughes, J. D., Langevin, C. D., Paulinski, S. R., Larsen, J. D., & Brakenhoff, D. (2023). FloPy Workflows for Creating Structured andUnstructured MODFLOW Models. *Groundwater*, *62*(1), 124–139. https://doi.org/10.1111/gwat.13327

Hunt, K. A., Abernethy, J., Beeson, P. C., Bowman, M., Wallander, S., & Williams, R. (2024). Crop sequence boundaries using USDA National Agricultural Statistics Service historic cropland data layers. *Statistical Journal of the IAOS: Journal of the International Association for Official Statistics*, *40*(2), 237–246. https://doi.org/10.3233/SJI-230078

Hunter, M., Sorensen, A., Nogeire-McRae, T., Beck, S., Shutts, S., & Murphy, R. (2022). *Farms Under Threat 2040: Choosing an Abundant Future*. American Farmland Trust. https://farmlandinfo.org/wp-content/uploads/sites/2/2022/08/AFT_FUT_Abundant-Future-7_29_22-WEB.pdf

IEA. (2024). *Strategies for Affordable and Fair Clean Energy Transitions*. International Energy Agency. https://iea.blob.core.windows.net/assets/86f2ba8c-f44b-494a-95cc-e75863cebf95/StrategiesforAffordableandFairCleanEnergyTransitions.pdf

IEA SHC. (2023). *New Conversion Factor for Concentrating Collector Statistics* (Task 64). IEA. https://www.iea-shc.org/Data/Sites/1/publications/2023-07-Task64-New-Conversion-Factor.pdf

IESO. (2025). *IESO Long-Term 2 Energy Supply (Window1) Request for Proposals*. Independent Electricity System Operator. https://www.ieso.ca/Sector-Participants/Resource-Acquisition-and-Contracts/Long-Term-2-RFP

Imamoglu, N., Kimura, M., Miyamoto, H., Fujita, A., & Nakamura, R. (2017). Solar Power Plant Detection on Multi-Spectral Satellite Imagery using Weakly-Supervised CNN with Feedback Features and m-PCNN Fusion. *Britich Machine Vision Conference*. https://doi.org/10.5244/C.31.183

IPCC. (2023). Synthesis Report of the IPCC Sixth Assessment Report (AR6). *Summary for Policymakers*, *March*, 1–36.

IRENA. (2024). *Renewable power generation costs in 2023*. International Renewable Energy Agency. https://www.irena.org/-/media/Files/IRENA/Agency/Publication/2024/Sep/IRENA_Renewable_power_generation_costs_in_2023.pdf

Jacobson, M. Z., Delucchi, M. A., Cameron, M. A., & Frew, B. A. (2017). The United States can keep the grid stable at low cost with 100% clean, renewable energy in all sectors despite inaccurate claims. *Proceedings of the National Academy of Sciences*, *114*(26), E5021–E5023. https://doi.org/10.1073/pnas.1708069114

Jahanfar, A., Drake, J., Gharabaghi, B., & Sleep, B. (2020). An experimental and modeling study of evapotranspiration from integrated green roof photovoltaic systems. *Ecological Engineering*, *152*, 105767. https://doi.org/10.1016/j.ecoleng.2020.105767

Jamil, U., Bonnington, A., & Pearce, J. M. (2023). The Agrivoltaic Potential of Canada. *Sustainability*, *15*(4), 3228. https://doi.org/10.3390/su15043228

Jenkins, J. D., Mayfield, E. N., Larson, E. D., Pacala, S. W., & Greig, C. (2021). Mission net-zero America: The nation-building path to a prosperous, net-zero emissions economy. *Joule*, *5*(11), 2755–2761. https://doi.org/10.1016/j.joule.2021.10.016

Jensen, A. R., Anderson, K. S., Holmgren, W. F., Mikofski, M. A., Hansen, C. W., Boeman, L. J., & Loonen, R. (2023). pvlib iotools—Open-source Python functions for seamless access to solar irradiance data. *Solar Energy*, *266*, 112092. https://doi.org/10.1016/j.solener.2023.112092

Ji, L., Wu, Y., Sun, L., Zhao, X., Wang, X., Xie, Y., Guo, J., & Huang, G. (2022). Solar photovoltaics can help China fulfill a net-zero electricity system by 2050 even facing climate change risks. *Resources, Conservation and Recycling*, *186*, 106596. https://doi.org/10.1016/j.resconrec.2022.106596

Jiang, C., Guan, K., Khanna, M., Chen, L., & Peng, J. (2021). Assessing Marginal Land Availability Based on Land Use Change Information in the Contiguous United States. *Environmental Science & Technology*, *55*(15), 10794–10804. https://doi.org/10.1021/acs.est.1c02236

Jiang, C., Guan, K., Khanna, M., Chen, L., & Peng, J. (2022). *Data for Assessing Marginal Land Availability Based on Land Use Change Information in the Contiguous United States* (Version 1) [Dataset]. Illinois Data Bank. https://doi.org/10.13012/B2IDB-6395937_V1

Jiang, H., Yao, L., Lu, N., Qin, J., Liu, T., Liu, Y., & Zhou, C. (2021). Multi-resolution dataset for photovoltaic panel segmentation from satellite and aerial imagery. *Earth System Science Data*, *13*(11), 5389–5401. https://doi.org/10.5194/essd-13-5389-2021

Jiang, H., Yao, L., Lu, N., Qin, J., Liu, T., Liu, Y., & Zhou, C. (2022). Geospatial assessment of rooftop solar photovoltaic potential using multi-source remote sensing data. *Energy and AI*, *10*, 100185. https://doi.org/10.1016/j.egyai.2022.100185

Johnson, R. (2010). *Honey Bee Colony Collapse Disorder* (7–5700). Congressional Research Service. https://nationalaglawcenter.org/wp-content/uploads/assets/crs/RL33938.pdf

Jones, N. F., & Pejchar, L. (2013). Comparing the Ecological Impacts of Wind and Oil & Gas Development: A Landscape Scale Assessment. *PLoS ONE*, *8*(11), e81391. https://doi.org/10.1371/journal.pone.0081391

Joshi, S., Mittal, S., Holloway, P., Shukla, P. R., Ó Gallachóir, B., & Glynn, J. (2021). High resolution global spatiotemporal assessment of rooftop solar photovoltaics potential for renewable electricity generation. *Nature Communications*, *12*(1), 5738. https://doi.org/10.1038/s41467-021-25720-2

Kaffine, D. T. (2019). Microclimate effects of wind farms on local crop yields. *Journal of Environmental Economics and Management*, *96*, 159–173. https://doi.org/10.1016/j.jeem.2019.06.001

Kannenberg, S. A., Sturchio, M. A., Venturas, M. D., & Knapp, A. K. (2023). Grassland carbon-water cycling is minimally impacted by a photovoltaic array. *Communications Earth & Environment*, *4*(1), 238. https://doi.org/10.1038/s43247-023-00904-4

Karban, C. C., Lovich, J. E., Grodsky, S. M., & Munson, S. M. (2024). Predicting the effects of solar energy development on plants and wildlife in the Desert Southwest, United States. *Renewable and Sustainable Energy Reviews*, *205*, 114823. https://doi.org/10.1016/j.rser.2024.114823

Karban, C. C., Munson, S. M., Kobelt, L. A., & Lovich, J. E. (2025). Short-term ecological effects of solar energy development depend on plant community, soil type and disturbance intensity. *Journal of Applied Ecology*, 1365-2664.14882. https://doi.org/10.1111/1365-2664.14882

Kasmi, G., Saint-Drenan, Y.-M., Trebosc, D., Jolivet, R., Leloux, J., Sarr, B., & Dubus, L. (2023). A crowdsourced dataset of aerial images with annotated solar photovoltaic arrays and installation metadata. *Scientific Data*, *10*(1), 59. https://doi.org/10.1038/s41597-023-01951-4

Katkar, V. V., Sward, J. A., Worsley, A., & Zhang, K. M. (2021). Strategic land use analysis for solar energy development in New York State. *Renewable Energy*, *173*, 861–875. https://doi.org/10.1016/j.renene.2021.03.128

Kaufman, L., & Rousseeuw, P. J. (1990). *Finding Groups in Data: An Introduction to Cluster Analysis*. John Wiley & Sons, Inc. https://doi.org/10.1002/9780470316801

Kausika, B. B., Nijmeijer, D., Reimerink, I., Brouwer, P., & Liem, V. (2021). GeoAI for detection of solar photovoltaic installations in the Netherlands. *Energy and AI*, *6*, 100111. https://doi.org/10.1016/j.egyai.2021.100111

Kauth, R. J., & Thomas, G. S. (1976). *The Tasselled Cap—A Graphic Description of the Spectral-Temporal Development of Agricultural Crops as Seen by LANDSAT*. *Paper 159*. http://docs.lib.purdue.edu/lars_symp/159

Keith, D. W., DeCarolis, J. F., Denkenberger, D. C., Lenschow, D. H., Malyshev, S. L., Pacala, S., & Rasch, P. J. (2004). The influence of large-scale wind power on global climate. *Proceedings of the National Academy of Sciences*, *101*(46), 16115–16120. https://doi.org/10.1073/pnas.0406930101

Kennedy, R., Yang, Z., Gorelick, N., Braaten, J., Cavalcante, L., Cohen, W., & Healey, S. (2018). Implementation of the LandTrendr Algorithm on Google Earth Engine. *Remote Sensing*, *10*(5), 691. https://doi.org/10.3390/rs10050691

Khanna, M., Chen, L., Basso, B., Cai, X., Field, J. L., Guan, K., Jiang, C., Lark, T. J., Richard, T. L., Spawn-Lee, S. A., Yang, P., & Zipp, K. Y. (2021). Redefining marginal land for bioenergy crop production. *GCB Bioenergy*, *13*(10), 1590–1609. https://doi.org/10.1111/gcbb.12877

Kim Steinberger. (2021). *Native Plant Installation and Maintenance for Solar Sites*. The Nature Concervancy. https://www.nature.org/content/dam/tnc/nature/en/documents/Native-Plant-Management-at-Solar-Sites.pdf

Klise, G. T., Tidwell, V. C., Reno, M. D., Moreland, B. D., Katie, M., & Macknick, J. (2013). *Water Use and Supply Concerns for Utility-Scale Solar Projects in the Southwestern United States* (Technical Report July; pp. 1–61). NREL. www.osti.gov/servlets/purl/1090206

Knapp, A. K., & Sturchio, M. A. (2024). Ecovoltaics in an increasingly water-limited world: An ecological perspective. *One Earth*, *7*(10), 1705–1712. https://doi.org/10.1016/j.oneear.2024.09.003

Koh, I., Lonsdorf, E. V., Williams, N. M., Brittain, C., Isaacs, R., Gibbs, J., & Ricketts, T. H. (2016). Modeling the status, trends, and impacts of wild bee abundance in the United States. *Proceedings of the National Academy of Sciences*, *113*(1), 140–145. https://doi.org/10.1073/pnas.1517685113

Krasner, N. Z., Fox, J., Armstrong, A., Ave, K., Carvalho, F., Li, Y., Walston, L. J., Ricketts, M. P., Jordaan, S. M., Abou Najm, M., Hartmann, H. M., Lybrand, R., & Hernandez, R. R. (2025). Impacts of photovoltaic solar energy on soil carbon: A global systematic review and framework. *Renewable and Sustainable Energy Reviews*, *208*, 115032. https://doi.org/10.1016/j.rser.2024.115032

Kriegler, F. J., Malila, W. A., Nalepka, R. F., & Richardson, W. (1969). Preprocessing transformations and their effect on multispectral recognition. *The Proceedings of the Sixth International Symposium on Remote Sensing of Environment*, 97–131. https://cir.nii.ac.jp/crid/1572261549021269760

Kruitwagen, L., Story, K. T., Friedrich, J., Byers, L., Skillman, S., & Hepburn, C. (2021). A global inventory of photovoltaic solar energy generating units. *Nature*, *598*(7882), 604–610. https://doi.org/10.1038/s41586-021-03957-7

Lambert, Q., Bischoff, A., Cueff, S., Cluchier, A., & Gros, R. (2021). Effects of solar park construction and solar panels on soil quality, microclimate, CO_2 effluxes, and vegetation under a Mediterranean climate. *Land Degradation & Development*, *32*(18), 5190–5202. https://doi.org/10.1002/ldr.4101

Landmark Dividend. (2020). *Wind Turbine Lease Rates – How Valuable is Your Wind Farm Lease?* Landmark Dividend. https://www.landmarkdividend.com/wind-turbine-lease-rates-2/#:~:text=A%20geologist%20will%20likely%20be,greatly%20from%20location%20to%20location.

Langevin, C. D., Hughes, J. D., Banta, E. R., Niswonger, R. G., Panday, Sorab, & Provotst, A. M. (2017). Documentation for the MODFLOW 6 Groundwater Flow Model. *United States Geological Survey*, *6*(A55), 197. https://doi.org/10.3133/tm6A55

Lark, T. J., Hendricks, N. P., Smith, A., Pates, N., Spawn-Lee, S. A., Bougie, M., Booth, E. G., Kucharik, C. J., & Gibbs, H. K. (2022). Environmental outcomes of the US Renewable Fuel Standard. *Proceedings of the National Academy of Sciences*, *119*(9), e2101084119. https://doi.org/10.1073/pnas.2101084119

Lark, T. J., Mueller, R. M., Johnson, D. M., & Gibbs, H. K. (2017). Measuring land-use and land-cover change using the U.S. department of agriculture's cropland data layer: Cautions and recommendations. *International Journal of Applied Earth Observation and Geoinformation*, *62*, 224–235. https://doi.org/10.1016/j.jag.2017.06.007

Lark, T. J., Schelly, I. H., & Gibbs, H. K. (2021). Accuracy, Bias, and Improvements in Mapping Crops and Cropland across the United States Using the USDA Cropland Data Layer. *Remote Sensing*, *13*(5), 968. https://doi.org/10.3390/rs13050968

Lark, T. J., Spawn, S. A., Bougie, M., & Gibbs, H. K. (2020). Cropland expansion in the United States produces marginal yields at high costs to wildlife. *Nature Communications*, *11*(1), 4295. https://doi.org/10.1038/s41467-020-18045-z

Larson, E., Greig, J., Mayfield, E., Pascale, A., Zhang, C., Drossman, J., Williams, R., Pacala, S., Soclolw, R., Baik, E., Birdsey, R., Duke, R., Jones, R., Haley, B., Leslie, E., Paustian, K., & Swan, A. (2021). *Net-Zero America: Potential Pathways, Infrasturcutre, and Impacts*. Princeton University. https://www.dropbox.com/s/ptp92f65lgds5n2/Princeton NZA FINAL REPORT {\%}2829Oct2021{\%}29.pdf?dl=0

Laws, N. D., Epps, B. P., Peterson, S. O., Laser, M. S., & Wanjiru, G. K. (2017). On the utility death spiral and the impact of utility rate structures on the adoption of residential solar photovoltaics and energy storage. *Applied Energy*, *185*, 627–641. https://doi.org/10.1016/j.apenergy.2016.10.123

Leskova, O. V., Frakes, R. A., & Markwith, S. H. (2022). Impacting habitat connectivity of the endangered Florida panther for the transition to utility-scale solar energy. *Journal of Applied Ecology*, *59*(3), 822–834. https://doi.org/10.1111/1365-2664.14098

Levandowsky, M., & Winter, D. (1971). Distance between Sets. *Nature*, *234*, 34–35. https://doi.org/10.1038/234034a0

Levin, M. O., Kalies, E. L., Forester, E., Jackson, E. L. A., Levin, A. H., Markus, C., McKenzie, P. F., Meek, J. B., & Hernandez, R. R. (2023). Solar Energy-driven Land-cover Change Could Alter Landscapes Critical to Animal Movement in the Continental United States. *Environmental Science & Technology*, *57*(31), 11499–11509. https://doi.org/10.1021/acs.est.3c00578

Li, Y., Armstrong, A., Simmons, C., Krasner, N. Z., & Hernandez, R. R. (2025). Ecological impacts of single-axis photovoltaic solar energy with periodic mowing on microclimate and vegetation. *Frontiers in Sustainability*, *6*, 1497256. https://doi.org/10.3389/frsus.2025.1497256

Li, Y., Kalnay, E., Motesharrei, S., Rivas, J., Kucharski, F., Kirk-Davidoff, D., Bach, E., & Zeng, N. (2018). Climate model shows large-scale wind and solar farms in the Sahara increase rain and vegetation. *Science*, *361*(6406), 1019–1022. https://doi.org/10.1126/science.aar5629

Liu, H., Wu, C., Yu, Y., Zhao, W., Liu, J., Yu, H., Zhuang, Y., & Yetemen, O. (2023). Effect of Solar Farms on Soil Erosion in Hilly Environments: A Modeling Study From the Perspective of Hydrological Connectivity. *Water Resources Research*, *59*(12), e2023WR035067. https://doi.org/10.1029/2023WR035067

Liu, J., Wang, J., & Li, L. (2024). Vectorized solar photovoltaic installation dataset across China in 2015 and 2020. *Scientific Data*, *11*(1), 1446. https://doi.org/10.1038/s41597-024-04356-z

Lobell, D. B., Deines, J. M., & Tommaso, S. D. (2020). Changes in the drought sensitivity of US maize yields. *Nature Food*, *1*(11), 729–735. https://doi.org/10.1038/s43016-020-00165-w

Lobell, D. B., Thau, D., Seifert, C., Engle, E., & Little, B. (2015). A scalable satellite-based crop yield mapper. *Remote Sensing of Environment*, *164*, 324–333. https://doi.org/10.1016/j.rse.2015.04.021

Lopez, A., Cole, W., Sergi, B., Levine, A., Carey, J., Mangan, C., Mai, T., Williams, T., Pinchuk, P., & Gu, J. (2023). Impact of siting ordinances on land availability for wind and solar development. *Nature Energy*, *8*(9), 1034–1043. https://doi.org/10.1038/s41560-023-01319-3

Lopez, A., Mai, T., Lantz, E., Harrison-Atlas, D., Williams, T., & Maclaurin, G. (2021). Land use and turbine technology influences on wind potential in the United States. *Energy*, *223*, 120044. https://doi.org/10.1016/j.energy.2021.120044

Lovering, J., Swain, M., Blomqvist, L., & Hernandez, R. R. (2022). Land-use intensity of electricity production and tomorrow's energy landscape. *PLoS ONE*, *17*(7 July). https://doi.org/10.1371/journal.pone.0270155

Lundquist, J. K., DuVivier, K. K., Kaffine, D., & Tomaszewski, J. M. (2018). Costs and consequences of wind turbine wake effects arising from uncoordinated wind energy development. *Nature Energy*, *4*(1), 26–34. https://doi.org/10.1038/s41560-018-0281-2

Luo, L., Zhuang, Y., Duan, Q., Dong, L., Yu, Y., Liu, Y., Chen, K., & Gao, X. (2021). Local climatic and environmental effects of an onshore wind farm in North China. *Agricultural and Forest Meteorology*, *308–309*, 108607. https://doi.org/10.1016/j.agrformet.2021.108607

Macknick, J., & Cohen, S. (2015). *Water Impacts of High Solar PV Electricity Penetration* (NREL/TP-6A20--63011, 1225894; p. NREL/TP-6A20--63011, 1225894). https://doi.org/10.2172/1225894

Macknick, J., Lee, C., Mosey, G., & Melius, J. (2013). *Solar Development on Contaminated and Disturbed Lands* (NREL/TP--6A20-58485; p. NREL/TP--6A20-58485). NREL. https://doi.org/10.2172/1260337

Maechler, M., Rousseeuw, P., Struyf, A., Hubert, M., Hornik, K., Studer, M., Roudier, P., Gonzalez, J., Kozlowski, K., Schubert, E., & Murphy, K. (2024). *Cluster: "Finding Groups in Data": Cluster Analysis Extended Rousseeuw et al.* (Version 2.1.8) [R]. https://CRAN.R-project.org/package=cluster

Maguire, K., Tanner, Winikoff, & Williams, R. (2024). *Utility-Scale Solar and Wind Development in Rural Areas: Land Cover Change (2009–20)* (ERR-330). USDA ERS. https://ers.usda.gov/sites/default/files/_laserfiche/publications/109209/ERR-330.pdf?v=70086

Malof, J. M., Bradbury, K., Collins, L. M., & Newell, R. G. (2016). Automatic detection of solar photovoltaic arrays in high resolution aerial imagery. *Applied Energy*. https://doi.org/10.1016/j.apenergy.2016.08.191

Mamun, M. A. A., Dargusch, P., Wadley, D., Zulkarnain, N. A., & Aziz, A. A. (2022). A review of research on agrivoltaic systems. *Renewable and Sustainable Energy Reviews*, *161*, 112351. https://doi.org/10.1016/j.rser.2022.112351

Markwith, S. (2025). Solar parking lot capacity: An abundant dual-use alternative to meet demand for the renewable energy transition. *Environmental Research: Infrastructure and Sustainability*, *5*(1), 015004. https://doi.org/10.1088/2634-4505/adaa9a

Marrou, H., Dufour, L., & Wery, J. (2013). How does a shelter of solar panels influence water flows in a soil–crop system? *European Journal of Agronomy*, *50*, 38–51. https://doi.org/10.1016/j.eja.2013.05.004

Marrou, H., Guilioni, L., Dufour, L., Dupraz, C., & Wery, J. (2013). Microclimate under agrivoltaic systems: Is crop growth rate affected in the partial shade of solar panels? *Agricultural and Forest Meteorology*, *177*, 117–132. https://doi.org/10.1016/j.agrformet.2013.04.012

Martín-Chivelet, N. (2016). Photovoltaic potential and land-use estimation methodology. *Energy*. https://doi.org/10.1016/j.energy.2015.10.108

Maxwell, A. E., Strager, M. P., Warner, T. A., Ramezan, C. A., Morgan, A. N., & Pauley, C. E. (2019). Large-Area, High Spatial Resolution Land Cover Mapping Using Random Forests, GEOBIA, and NAIP Orthophotography: Findings and Recommendations. *Remote Sensing*, *11*(12), 1409. https://doi.org/10.3390/rs11121409

Maxwell, A. E., Warner, T. A., Vanderbilt, B. C., & Ramezan, C. A. (2017). Land Cover Classification and Feature Extraction from National Agriculture Imagery Program (NAIP) Orthoimagery: A Review. *Photogrammetric Engineering & Remote Sensing*, *83*(11), 737–747. https://doi.org/10.14358/PERS.83.10.737

Mayer, K., Rausch, B., Arlt, M.-L., Gust, G., Wang, Z., Neumann, D., & Rajagopal, R. (2022). 3D-PV-Locator: Large-scale detection of rooftop-mounted photovoltaic systems in 3D. *Applied Energy*, *310*, 118469. https://doi.org/10.1016/j.apenergy.2021.118469

McCall, J., Beatty, B., Janski, J., Doubleday, K., Martin, J., Hartmann, H., Walston, L. J., & Macknick, J. (2024). Little prairie under the panel: Testing native pollinator habitat seed mix establishment at three utility-scale solar sites in Minnesota. *Environmental Research Communications*, *6*(7), 075012. https://doi.org/10.1088/2515-7620/ad5b3c

McCall, J., Daw, J., Day, M., Galzki, J., Hanson, A., Mulla, D., & Ross, B. (2023). *PV Stormwater Management Research and Testing (PV-SMaRT) (Final Technical Report)* (Technical Report NREL/TP--6A20-87555). NREL. https://doi.org/10.2172/2203518

McCall, J., Macdonald, J., Burton, R., & Macknick, J. (2023). Vegetation Management Cost and Maintenance Implications of Different Ground Covers at Utility-Scale Solar Sites. *Sustainability*, *15*(7), 5895. https://doi.org/10.3390/su15075895

McDonnell, J. J., Evaristo, J., Bladon, K. D., Buttle, J., Creed, I. F., Dymond, S. F., Grant, G., Iroume, A., Jackson, C. R., Jones, J. A., Maness, T., McGuire, K. J., Scott, D. F., Segura, C., Sidle, R. C., & Tague, C. (2018). Water sustainability and watershed storage. *Nature Sustainability*, *1*(8), 378–379. https://doi.org/10.1038/s41893-018-0099-8

McEowen, R. A. (2011). *Wind Energy Production: Legal Issues and Related Liability Concerns for Landowners*. Iowa State University CLAT. https://www.calt.iastate.edu/system/files/CALT%20Legal%20Brief%20-%20Wind%20Energy%20Production.pdf

McFeeters, S. K. (1996). The use of the Normalized Difference Water Index (NDWI) in the delineation of open water features. *International Journal of Remote Sensing*, *17*(7), 1425–1432. https://doi.org/10.1080/01431169608948714

McKuin, B., Zumkehr, A., Ta, J., Bales, R., Viers, J. H., Pathak, T., & Campbell, J. E. (2021). Energy and water co-benefits from covering canals with solar panels. *Nature Sustainability*, *4*(7), 609–617. https://doi.org/10.1038/s41893-021-00693-8

Meneses, D. M., Zheng, L., & Guo, Q. (2023). Stormwater-Retaining Ground Surface Depressions of Solar Photovoltaic Farms. *Journal of Sustainable Water in the Built Environment*, *10*(1). https://doi.org/10.1061/JSWBAY.SWENG-525

Mengi, E., Samara, O. A., & Zohdi, T. I. (2023). Crop-driven optimization of agrivoltaics using a digital-replica framework. *Smart Agricultural Technology*, *4*, 100168. https://doi.org/10.1016/j.atech.2022.100168

Merrifield, A. L., Brunner, L., Lorenz, R., Medhaug, I., & Knutti, R. (2020). An investigation of weighting schemes suitable for incorporating large ensembles into multi-model ensembles. *Earth System Dynamics*, *11*(3), 807–834. https://doi.org/10.5194/esd-11-807-2020

Merrill, D. (2021, April 29). The U.S. Will Need a Lot of Land for a Zero-Carbon Economy. *Bloomberg*. https://www.bloomberg.com/graphics/2021-energy-land-use-economy/?leadSource=uverify%20wall&embedded-checkout=true

Mier-Valderrama, L., Leal, J., Perotto-Baldivieso, H. L., Hedquist, B., Menendez, H. M., Anoruo, A., & Turner, B. L. (2024). Evaluating soil erosion and runoff dynamics in a humid subtropic, low stream order, southern plains watershed from cultivation and solar farm development. *International Soil and Water Conservation Research*, *12*(2), 432–445. https://doi.org/10.1016/j.iswcr.2023.09.004

Milbrandt, A. R., Heimiller, D. M., Perry, A. D., & Field, C. B. (2014). Renewable energy potential on marginal lands in the United States. *Renewable and Sustainable Energy Reviews*, *29*, 473–481. https://doi.org/10.1016/j.rser.2013.08.079

Miller, L. M., & Keith, D. W. (2018). Climatic Impacts of Wind Power. *Joule*. https://doi.org/10.1016/j.joule.2018.09.009

Mills, S. (2017). *Handbook of Sustainability and Social Science Research: Wind Energy and Rural Community Sustainability* (pp. 215–225). Springer. https://link.springer.com/chapter/10.1007/978-3-319-67122-2_12

Molotoks, A., Stehfest, E., Doelman, J., Albanito, F., Fitton, N., Dawson, T. P., & Smith, P. (2018). Global projections of future cropland expansion to 2050 and direct impacts on biodiversity and carbon storage. *Global Change Biology*, *24*(12), 5895–5908. https://doi.org/10.1111/gcb.14459

Moore, S., Graff, H., Ouellet, C., Leslie, S., & Olweean, D. (2022). Can we have clean energy and grow our crops too? Solar siting on agricultural land in the United States. *Energy Research & Social Science, 91*, 102731. https://doi.org/10.1016/j.erss.2022.102731

Moore-O'Leary, K. A., Hernandez, R. R., Johnston, D. S., Abella, S. R., Tanner, K. E., Swanson, A. C., Kreitler, J., & Lovich, J. E. (2017). Sustainability of utility-scale solar energy – critical ecological concepts. *Frontiers in Ecology and the Environment*, *15*(7), 385–394. https://doi.org/10.1002/fee.1517

Morris, D. W., & Blekkenhorst, N. (2017). Wind Energy versus Sustainable Agriculture: An Ontario Perspective. *Journal of Rural and Community Development*, *12*(1). https://journals.brandonu.ca/jrcd/article/view/1337/307

Mulla, D., Galzki, J., Hanson, A., & Simunek, J. (2024). Measuring and modeling soil moisture and runoff at solar farms using a disconnected impervious surface approach. *Vadose Zone Journal*, *23*(4), e20335. https://doi.org/10.1002/vzj2.20335

Nair, A. A., Rohith, A. N., Cibin, R., & McPhillips, L. E. (2024). A Framework to Model the Hydrology of Solar Farms Using EPA SWMM. *Environmental Modeling & Assessment*, *29*(1), 91–100. https://doi.org/10.1007/s10666-023-09922-0

Narvarte, L., & Lorenzo, E. (2008). Tracking and ground cover ratio. *Progress in Photovoltaics: Research and Applications*, *16*(8), 703–714. https://doi.org/10.1002/pip.847

Neesham-McTiernan, T. H., Randle-Boggis, R. J., Buckley, A. R., & Hartley, S. E. (2025). The spatial potential for agrivoltaics to address energy-agriculture land use conflicts in Great Britain. *Applied Energy*, *385*, 125527. https://doi.org/10.1016/j.apenergy.2025.125527

Nilson, R. S., & Stedman, R. C. (2022). Are big and small solar separate things?: The importance of scale in public support for solar energy development in upstate New York. *Energy Research & Social Science*, *86*, 102449. https://doi.org/10.1016/j.erss.2021.102449

NREL. (2020). *Low-Impact Solar Development Strategies Guidebook*. https://openei.org/wiki/InSPIRE/Guidebook

NREL. (2025). Agrivoltaics Map [Dataset]. In *InSPIRE*. OpenEI. https://openei.org/wiki/InSPIRE/Agrivoltaics_Map

NYSERDA. (2025). *Smart Solar Siting Scorecard* (RESRFP23-1 Appendix 2). NYSERDA. https://portal.nyserda.ny.gov/servlet/servlet.FileDownload?file=00P8z000003ZJJwEAO

Ong, S., Campbell, C., Denholm, P., Margolis, R., & Heath, G. (2013). *Land-Use Requirements for Solar Power Plants in the United States* (Technical Report NREL/TP-6A20-56290, 1086349; p. NREL/TP-6A20-56290, 1086349). NREL. https://doi.org/10.2172/1086349

OpenStreeMap Wiki. (2024). *OpenStreetMap Using Aerial Imagery* [Dataset]. OpenStreetMap Wiki. https://wiki.openstreetmap.org/wiki/Using_aerial_imagery

OpenStreetMap Contributors. (2024). *OpenStreetMap Elements* [Dataset]. OpenStreetMap Wiki. https://doi.org/OpenStreetMap Wiki

Ortiz, A., Negandhi, D., Mysorekar, S. R., Nagaraju, S. K., Kiesecker, J., Robinson, C., Bhatia, P., Khurana, A., Wang, J., Oviedo, F., & Ferres, J. L. (2022). An Artificial Intelligence Dataset for Solar Energy Locations in India. *Scientific Data*, *9*(1), 497. https://doi.org/10.1038/s41597-022-01499-9

O'Shaughnessy, E. (2022). Rooftop solar incentives remain effective for low- and moderate-income adoption. *Energy Policy*, *163*, 112881. https://doi.org/10.1016/j.enpol.2022.112881

Otto, C. R. V., Roth, C. L., Carlson, B. L., & Smart, M. D. (2016). Land-use change reduces habitat suitability for supporting managed honey bee colonies in the Northern Great Plains. *Proceedings of the National Academy of Sciences*, *113*(37), 10430–10435. https://doi.org/10.1073/pnas.1603481113

Oulefki, A., Himeur, Y., Trongtirakul, T., Amara, K., Agaian, S., Benbelkacem, S., Guerroudji, M. A., Zemmouri, M., Ferhat, S., Zenati, N., Atalla, S., & Mansoor, W. (2024). Detection and analysis of deteriorated areas in solar PV modules using unsupervised sensing algorithms and 3D augmented reality. *Heliyon*, *10*(6), e27973. https://doi.org/10.1016/j.heliyon.2024.e27973

PA 233 of 2023, House Bill No. 5120, Michigan Legislature 102nd Legislature, Regular Session of 2023, MCL 460.1013 (2024). Approved by the Governor on November 28, 2023; Filed with the Secretary of State on November 29, 2023 https://www.legislature.mi.gov/documents/2023-2024/publicact/htm/2023-PA-0233.htm

Palmer, J. F. (2022). Deconstructing viewshed analysis makes it possible to construct a useful visual impact map for wind projects. *Landscape and Urban Planning*.

Parkinson, S., & Hunt, J. (2020). Economic Potential for Rainfed Agrivoltaics in Groundwater-Stressed Regions. *Environmental Science & Technology Letters*, *7*(7), 525–531. https://doi.org/10.1021/acs.estlett.0c00349

Pascaris, A. S., Gerlak, A. K., & Barron-Gafford, G. A. (2023). From niche-innovation to mainstream markets: Drivers and challenges of industry adoption of agrivoltaics in the U.S. *Energy Policy*, *181*, 113694. https://doi.org/10.1016/j.enpol.2023.113694

Pascaris, A. S., Schelly, C., Burnham, L., & Pearce, J. M. (2021). Integrating solar energy with agriculture: Industry perspectives on the market, community, and socio-political dimensions of agrivoltaics. *Energy Research and Social Science*, *75*, 102023. https://doi.org/10.1016/j.erss.2021.102023

Pascaris, A. S., Schelly, C., & Pearce, J. M. (2020). A First Investigation of Agriculture Sector Perspectives on the Opportunities and Barriers for Agrivoltaics. *Agronomy*, *10*(12), 1885. https://doi.org/10.3390/agronomy10121885

Pascaris, A. S., Schelly, C., Rouleau, M., & Pearce, J. M. (2022). Do agrivoltaics improve public support for solar? A survey on perceptions, preferences, and priorities. *Green Technology, Resilience, and Sustainability*, *2*(8), 1–17. https://doi.org/10.1007/s44173-022-00007-x

Pathak, M., Slade, R., Pichs-Madruga, R., Diana Ürge-Vorsatz, Shukla, P. R., & Skea, J. (2023). *Technical Summary—Climate Change 2022: Mitigation of Climate Change. Contribution of Working Group III to the Sixth Assessment Report of the Intergovernmental Panel on Climate Change*. Intergovernmental Panel On Climate Change. https://doi.org/10.1017/9781009157926.002

Pengra, B. W., Stehman, S. V., Horton, J. A., Dockter, D. J., Schroeder, T. A., Yang, Z., Cohen, W. B., Healey, S. P., & Loveland, T. R. (2020). Quality control and assessment of interpreter consistency of annual land cover reference data in an operational national monitoring program. *Remote Sensing of Environment*, *238*, 111261. https://doi.org/10.1016/j.rse.2019.111261

Perry, K., & Campos, C. (2023). Panel Segmentation: A Python Package for Automated Solar Array Metadata Extraction Using Satellite Imagery. *IEEE Journal of Photovoltaics*, *13*(2), 208–212. https://doi.org/10.1109/JPHOTOV.2022.3230565

Perry, K., Nguyen, Q., & White, R. (2024). *Quantifying Error in Photovoltaic Installation Metadata*. *NREL/CP-5K00-90318*. https://www.nrel.gov/docs/fy24osti/90318.pdf

Peterson, S., Lent, C., Little, C., Richmond-Mueller, A., Bernsten, C., Barron-Gafford, G. A., Rouini, N., Neesham-McTiernan, T. H., Swanson, T., Lepley, K., McCall, J., Martin, J., Pascaris, A., Macknick, J., Beatty, B., Walston, L. J., Hartmann, H., Fox, L., Ricketts, M., … Kolbeck-Urlacher, H. (2025). *Best Practices in Agrisolar*. Agrisolar Clearinghouse. https://www.agrisolarclearinghouse.org/wp-content/uploads/2025/02/Best-Practices-in-Agrisolar.pdf

Phillpott, M., O'Connor, J., Ferreria, A., Santos, M., Kruitwagen, L., & Guzzardi, M. (2024a). *Solar Asset Mapper: A continuously-updated global inventory of solar energy facilities built with satellite data and machine learning*. https://blog.transitionzero.org/hubfs/Data%20Products/TZ-SAM/tz-sam-scientific-methodology-Q12024.pdf

Phillpott, M., O'Connor, J., Ferreria, A., Santos, M., Kruitwagen, L., & Guzzardi, M. (2024b). *Solar Asset Mapper: A continuously-updated global inventory of solar energy facilities*

built with satellite data and machine learning: Dataset (Version Q3 2024) [Dataset]. Zenodo. https://doi.org/10.5281/zenodo.11368203

Pisinaras, V., Wei, Y., Bärring, L., & Gemitzi, A. (2014). Conceptualizing and assessing the effects of installation and operation of photovoltaic power plants on major hydrologic budget constituents. *Science of The Total Environment*, *493*, 239–250. https://doi.org/10.1016/j.scitotenv.2014.05.132

Pitt, D., Berryhill, A. R., & Ciminelli, J. M. (2024). *Re-Evaluating The Land Use Impacts of Utility-Scale Solar Energy Development in Virginia*. Virginia Commonwealth University Virginia Commonwealth Univers. https://scholarscompass.vcu.edu/wilder_pubs/58

Plakman, V., Rosier, J., & Van Vliet, J. (2022). Solar park detection from publicly available satellite imagery. *GIScience & Remote Sensing*, *59*(1), 462–481. https://doi.org/10.1080/15481603.2022.2036056

Polsby, D. D., & Popper, R. (1991). The Third Criterion: Compactness as a Procedural Safeguard Against Partisan Gerrymandering. *Yale Law and Policy Review*, *9*(2), 301–353. http://dx.doi.org/10.2139/ssrn.2936284

Potts, S. G., Biesmeijer, J. C., Kremen, C., Neumann, P., Schweiger, O., & Kunin, W. E. (2010). Global pollinator declines: Trends, impacts and drivers. *Trends in Ecology & Evolution*, *25*(6), 345–353. https://doi.org/10.1016/j.tree.2010.01.007

Preziuso, D., Dimond, K., Ko, Y., Iii, W. D. G., Planinac, K., Rempel, A., Yu, Y., Ribe, R., Gonzalez, M., Sperenza, P., Meier, B., & Buson, I. L. (2023). *Southwest and Pacific Northwest Workshops* (PNNL-34218). Pacific Northwest National Laboratory. https://www.osti.gov/servlets/purl/2395951

Price, I., Sanchez-Gonzalez, A., Alet, F., Andersson, T. R., El-Kadi, A., Masters, D., Ewalds, T., Stott, J., Mohamed, S., Battaglia, P., Lam, R., & Willson, M. (2025). Probabilistic weather forecasting with machine learning. *Nature*, *637*(8044), 84–90. https://doi.org/10.1038/s41586-024-08252-9

Prilliman, M., Smith, S. E., Stanislawski, B. J., Keith, J. M. F., Silverman, T. J., Calaf, M., & Cal, R. B. (2022). Technoeconomic Analysis of Changing PV Array Convective Cooling Through Changing Array Spacing. *IEEE Journal of Photovoltaics*, *12*(6), 1586–1592. https://doi.org/10.1109/JPHOTOV.2022.3201464

Protecting Future Farmland Act of 2023, 2931, US Senate 1st, S.2931 (2023). https://www.congress.gov/118/bills/s2931/BILLS-118s2931is.pdf

Qin, Y., Li, Y., Xu, R., Hou, C., Armstrong, A., Bach, E., Wang, Y., & Fu, B. (2022). Impacts of 319 wind farms on surface temperature and vegetation in the United States. *Environmental Research Letters*, *17*(2), 024026. https://doi.org/10.1088/1748-9326/ac49ba

Qiu, B., Zhang, K., Tang, Z., Chen, C., & Wang, Z. (2017). Developing soil indices based on brightness, darkness, and greenness to improve land surface mapping accuracy. *GIScience & Remote Sensing*, *54*(5), 759–777. https://doi.org/10.1080/15481603.2017.1328758

Quinlan, G. M., Milbrath, M. O., Otto, C. R. V., & Isaacs, R. (2021). Honey bee (Apis mellifera) colonies benefit from grassland/pasture while bumble bee (Bombus impatiens) colonies in the same landscapes benefit from non-corn/soybean cropland. *PLoS ONE*, *16*(9 September), e0257701. https://doi.org/10.1371/journal.pone.0257701

Rajewski, D. A., Takle, E. S., Lundquist, J. K., Oncley, S., Prueger, J. H., Horst, T. W., Rhodes, M. E., Pfeiffer, R., Hatfield, J. L., Spoth, K. K., & Doorenbos, R. K. (2013). Crop Wind Energy Experiment (CWEX): Observations of Surface-Layer, Boundary Layer, and Mesoscale Interactions with a Wind Farm. *Bulletin of the American Meteorological Society*, *94*(5), 655–672. https://doi.org/10.1175/BAMS-D-11-00240.1

Rajewski, D. A., Takle, E. S., Lundquist, J. K., Prueger, J. H., Pfeiffer, R. L., Hatfield, J. L., Spoth, K. K., & Doorenbos, R. K. (2014). Changes in fluxes of heat, H2O, and CO2 caused by a large wind farm. *Agricultural and Forest Meteorology*, *194*, 175–187. https://doi.org/10.1016/j.agrformet.2014.03.023

Rajewski, D. A., Takle, E. S., Prueger, J. H., & Doorenbos, R. K. (2016). Toward understanding the physical link between turbines and microclimate impacts from in situ measurements in a large wind farm. *Journal of Geophysical Research: Atmospheres*, *121*(22). https://doi.org/10.1002/2016JD025297

Rand, J. T., Kramer, L. A., Garrity, C. P., Hoen, B. D., Diffendorfer, J. E., Hunt, H. E., & Spears, M. (2020). A continuously updated, geospatially rectified database of utility-scale wind turbines in the United States. *Scientific Data*, *7*(1), 15. https://doi.org/10.1038/s41597-020-0353-6

Ravi, S., Macknick, J., Lobell, D., Field, C., Ganesan, K., Jain, R., Elchinger, M., & Stoltenberg, B. (2016). Colocation opportunities for large solar infrastructures and agriculture in drylands. *Applied Energy*, *165*, 383–392. https://doi.org/10.1016/j.apenergy.2015.12.078

Ravishankar, R., AlMahmoud, E., Habib, A., & De Weck, O. L. (2022). Capacity Estimation of Solar Farms Using Deep Learning on High-Resolution Satellite Imagery. *Remote Sensing*, *15*(1), 210. https://doi.org/10.3390/rs15010210

Rehbein, J. A., Watson, J. E. M., Lane, J. L., Sonter, L. J., Venter, O., Atkinson, S. C., & Allan, J. R. (2020). Renewable energy development threatens many globally important biodiversity areas. *Global Change Biology*, *26*(5), 3040–3051. https://doi.org/10.1111/gcb.15067

Reitz, M., Sanford, W. E., Senay, G. B., & Cazenas, J. (2017). Annual Estimates of Recharge, Quick-Flow Runoff, and Evapotranspiration for the Contiguous U.S. Using Empirical Regression Equations. *JAWRA Journal of the American Water Resources Association*, *53*(4), 961–983. https://doi.org/10.1111/1752-1688.12546

RGI Consortium. (2023). *Randolph Glacier Inventory—A Dataset of Global Glacier Outlines (NSIDC-0770, Version 7)* (Version Version 7) [Dataset]. National Snow and Ice Data Center. https://doi.org/10.5067/F6JMOVY5NAVZ

Rinne, E., Holttinen, H., Kiviluoma, J., & Rissanen, S. (2018). Effects of turbine technology and land use on wind power resource potential. *Nature Energy*, *3*(6), 494–500. https://doi.org/10.1038/s41560-018-0137-9

Ritchie, H. (2022). *How does the land use of different electricity sources compare?* OurWorldinData. https://ourworldindata.org/land-use-per-energy-source

Ritchie, H. (2024). *Not the end of the world*. Little Brown Spark.

Rößner, J.-V. (2022). Rainwater Management in Agrivoltaci Systems—Research & Development Potential. *8th World Conference on Photovoltaic Energy Conversion*. https://www.agrisolarclearinghouse.org/wp-content/uploads/2022/10/Roessner_4AO84.pdf

Rouse, J. W. Jr., Haas, R. H., Schell, J. A., & Deering, D. W. (1974). *Monitoring vegetation systems in the Great Plains with ERTS*. *PAPER-A20*. https://doi.org/19740022614

ROWHWG. (2023). *Pollinator Scorecard—2023 Edition* (Version 2.2). Rights-of-Way as Habitat Working Group. https://rightofway.erc.uic.edu/wp-content/uploads/Pollinator-Scorecard-Users-Guide-V2.2.pdf

Roy, R., & Pearce, J. M. (2024). Is small or big solar better for the environment? Comparative life cycle assessment of solar photovoltaic rooftop vs. ground-mounted systems. *The International Journal of Life Cycle Assessment*, *29*(3), 516–536. https://doi.org/10.1007/s11367-023-02254-x

Ruhala, S. S., Zarnetske, J. P., Long, D. T., Lee-Cullin, J. A., Plont, S., & Wiewiora, E. R. (2018). Exploring dissolved organic carbon cycling at the stream–groundwater interface across a third-order, lowland stream network. *Biogeochemistry*, *137*(1–2), 105–126. https://doi.org/10.1007/s10533-017-0404-z

Saganeiti, L., Pilogallo, A., Faruolo, G., Scorza, F., & Murgante, B. (2020). Territorial Fragmentation and Renewable Energy Source Plants: Which Relationship? *Sustainability*, *12*(5), 1828. https://doi.org/10.3390/su12051828

Sampson, G. S., Perry, E. D., & Taylor, M. R. (2020). The On-Farm and Near-Farm Effects of Wind Turbines on Agricultural Land Values. *Journal of Agricultural and Resource Economics*, *45*(3), 410–427. https://www.jstor.org/stable/10.2307/27154076

Samu, R., Calais, M., Shafiullah, G. M., Moghbel, M., Shoeb, M. A., Nouri, B., & Blum, N. (2021). Applications for solar irradiance nowcasting in the control of microgrids: A review. *Renewable and Sustainable Energy Reviews*, *147*, 111187. https://doi.org/10.1016/j.rser.2021.111187

Seel, J., Kemp, J. M., Cheyette, A., Millstein, D., Gorman, W., Seongeun Jeon, Dana Robson, Rachman Setiawan, & Mark Bolinger. (2024). *Utility-Scale Solar, 2024 Edition* (LBNL; Version 2024 Edition) [Dataset]. OEDI. https://dx.doi.org/10.25984/2460457

SEIA & Wood Mackenzie. (2024). *Solar Market Insight Report Q4 2024* (Q4 2024). SEIA. https://seia.org/research-resources/solar-market-insight-report-q4-2024/

Semeraro, T., Scarano, A., Curci, L. M., Leggieri, A., Lenucci, M., Basset, A., Santino, A., Piro, G., & De Caroli, M. (2024). Shading effects in agrivoltaic systems can make the difference in boosting food security in climate change. *Applied Energy*, *358*, 122565. https://doi.org/10.1016/j.apenergy.2023.122565

Şevik, S., & Aktaş, A. (2022). Performance enhancing and improvement studies in a 600 kW solar photovoltaic (PV) power plant; manual and natural cleaning, rainwater harvesting and the snow load removal on the PV arrays. *Renewable Energy*, *181*, 490–503. https://doi.org/10.1016/j.renene.2021.09.064

Shamlian, J. (2024, June 5). An Iowa farmer had $350,000 in debt. Wind turbines are helping her get out. *CBS News*. https://www.cbsnews.com/news/iowa-farmer-debt-wind-turbines/

Shao, C., Shuai, Y., Wu, H., Deng, X., Zhang, X., & Xu, A. (2023). Development of a Spectral Index for the Detection of Yellow-Flowering Vegetation. *Remote Sensing*, *15*(7), 1725. https://doi.org/10.3390/rs15071725

Sharma, A., Tiwari, K. N., & Bhadoria, P. B. S. (2011). Effect of land use land cover change on soil erosion potential in an agricultural watershed. *Environmental Monitoring and Assessment*, *173*(1–4), 789–801. https://doi.org/10.1007/s10661-010-1423-6

Sharma, S., & Waldman, J. (2021). Potential Solar Replacement of Hydroelectricity to Reopen Rivers: Maine as a Case Example. *Fisheries*, *46*(8), 383–390. https://doi.org/10.1002/fsh.10619

Shepley, M. G. (2024). Vertical hydraulic conductivity and layered heterogeneity: From measurements to models. *Hydrogeology Journal*, *32*(4), 1017–1042. https://doi.org/10.1007/s10040-024-02773-3

Shobe, C. M. (2022). How impervious are solar arrays? On the need for geomorphic assessment of energy transition technologies. *Earth Surface Processes and Landforms*, *47*(14), 3219–3223. https://doi.org/10.1002/esp.5489

Shoemaker, J. A. (2007). *Negotiating Wind Energy Property Agreements*. Farmers' Legal Action Group. http://www.flaginc.org/wp-content/uploads/2013/03/WindPropertyAgrmnts20071.pdf

Singha, K., & Navarre-Sitchler, A. (2022). The Importance of Groundwater in Critical Zone Science. *Groundwater*, *60*(1), 27–34. https://doi.org/10.1111/gwat.13143

Sivapalan, M., Takeuchi, K., Franks, S. W., Gupta, V. K., Karambiri, H., Lakshmi, V., Liang, X., McDONNELL, J. J., Mendiondo, E. M., O'Connell, P. E., Oki, T., Pomeroy, J. W., Schertzer, D., Uhlenbrook, S., & Zehe, E. (2003). IAHS Decade on Predictions in Ungauged Basins (PUB), 2003–2012: Shaping an exciting future for the hydrological sciences. *Hydrological Sciences Journal*, *48*(6), 857–880. https://doi.org/10.1623/hysj.48.6.857.51421

Sklash, M. G., & Farvolden, R. N. (1979). The Role of Groundwater in Storm Runoff. *Journal of Hydrology*, *43*, 45–65. https://doi.org/10.1016/0022-1694(79)90164-1

Smith, B., Sekar, A., Mirletz, H., Heath, G., & Margolis, R. (2024). *An Updated Life Cycle Assessment of Utility-Scale Solar Photovoltaic Systems Installed in the United States* (NREL/TP--7A40-87372; p. NREL/TP--7A40-87372). https://doi.org/10.2172/2331420

So, B., Nezin, C., Kaimal, V., Keene, S., Collins, L., Bradbury, K., & Malof, J. M. (2017). Estimating the electricity generation capacity of solar photovoltaic arrays using only color aerial imagery. *International Geoscience and Remote Sensing Symposium (IGARSS)*. https://doi.org/10.1109/IGARSS.2017.8127279

Soler, D. R., & Garrity, C. P. (2018). *Quaternary sediment thickness and bedrock topography of the glaciated United States east of the Rocky Mountains* [Dataset]. USGS Publications Warehouse. https://doi.org/10.3133/sim3392

Sorensen, A., Nogeire, T., & Hunter, M. (2022). *Potential Placement of Utility-Scale Solar Installations on Agricultural Lands in the U.S. to 2040*. American Farmland Trust. https://www.farmlandinfo.org/wp-content/uploads/sites/2/2023/03/AFT_FUT2040-solar-white-paper.pdf

Stid, J. T., Kendall, A. D., Anctil, A., Rapp, J., & Hyndman, D. W. (2023). The United States Renewable Energy Landscape: Siting, Management, and Potential Impacts. *2023 IEEE 50th Photovoltaic Specialists Conference (PVSC)*, 1–1. https://doi.org/10.1109/PVSC48320.2023.10359813

Stid, J. T., Kendall, A. D., Rapp, J., & Bingaman, J. C. (2025). *GM-SEUS Initial Release* (Version v1.0) [Software]. Zenodo. https://doi.org/10.5281/zenodo.14829530

Stid, J. T., Shukla, S., Anctil, A., Kendall, A. D., Rapp, J., & Hyndman, D. W. (2022). Solar array placement, electricity generation, and cropland displacement across California's Central Valley. *Science of The Total Environment*, *835*, 155240. https://doi.org/10.1016/j.scitotenv.2022.155240

Stid, J. T., Shukla, S., Anctil, A., Kendall, A. D., Rapp, J., & Hyndman, D. W. (2023). *Spatiotemporally Characterized Ground-Mounted Solar PV Arrays Within California's Central Valley* (Version 1) [Dataset]. figshare. https://doi.org/10.6084/m9.figshare.23629326.v1

Stid, J. T., Shukla, S., Kendall, A. D., Anctil, A., Rapp, J., & Anex, R. (2025). Food-energy-water and economic outcomes of agrisolar co-location in irrigated regions. *Nature Sustainability*, *accepted*. https://doi.org/10.21203/rs.3.rs-3475091/v1

Stowell, D., Kelly, J., Tanner, D., Taylor, J., Jones, E., Geddes, J., & Chalstrey, E. (2020). A harmonised, high-coverage, open dataset of solar photovoltaic installations in the UK. *Scientific Data*, *7*(1), 394. https://doi.org/10.1038/s41597-020-00739-0

Stowell, D., Kelly, J., Tanner, D., Taylor, J., Jones, E., Geddes, J., Chalstrey, E., Williams, G., & Clough, J. (2020). *Solar panels and solar farms in the UK - geographic open data (UKPVGeo)* (Version 1.0) [Dataset]. Zenodo. https://doi.org/10.5281/zenodo.4059881

Sturchio, M. A., Kannenberg, S. A., & Knapp, A. K. (2024). Agrivoltaic arrays can maintain semi-arid grassland productivity and extend the seasonality of forage quality. *Applied Energy*, *356*, 122418. https://doi.org/10.1016/j.apenergy.2023.122418

Sturchio, M. A., Kannenberg, S. A., Pinkowitz, T. A., & Knapp, A. K. (2024). Solar arrays create novel environments that uniquely alter plant responses. *Plants, People, Planet*, *6*(6), 1522–1533. https://doi.org/10.1002/ppp3.10554

Sturchio, M. A., & Knapp, A. K. (2023). Ecovoltaic principles for a more sustainable, ecologically informed solar energy future. *Nature Ecology & Evolution*, *7*(11), 1746–1749. https://doi.org/10.1038/s41559-023-02174-x

Sturchio, M. A., Macknick, J. E., Barron-Gafford, G. A., Chen, A., Alderfer, C., Condon, K., Hajek, O. L., Miller, B., Pauletto, B., Siggers, J. A., Slette, I. J., & Knapp, A. K. (2022). Grassland productivity responds unexpectedly to dynamic light and soil water environments induced by photovoltaic arrays. *Ecosphere*, *13*(12), 1–14. https://doi.org/10.1002/ecs2.4334

Sulik, J. J., & Long, D. S. (2015). Spectral indices for yellow canola flowers. *International Journal of Remote Sensing*, *36*(10), 2751–2765. https://doi.org/10.1080/01431161.2015.1047994

Sulik, J. J., & Long, D. S. (2020). Automated detection of phenological transitions for yellow flowering plants such as Brassica oilseeds. *Agrosystems, Geosciences & Environment*, *3*(1), e20125. https://doi.org/10.1002/agg2.20125

Sun, X., Khan, M. R., Deline, C., & Alam, M. A. (2018). Optimization and performance of bifacial solar modules: A global perspective. *Applied Energy*, *212*, 1601–1610. https://doi.org/10.1016/j.apenergy.2017.12.041

Supe, H., Avtar, R., Singh, D., Gupta, A., Yunus, A. P., Dou, J., A. Ravankar, A., Mohan, G., Chapagain, S. K., Sharma, V., Singh, C. K., Tutubalina, O., & Kharrazi, A. (2020). Google Earth Engine for the Detection of Soiling on Photovoltaic Solar Panels in Arid Environments. *Remote Sensing*, *12*(9), 1466. https://doi.org/10.3390/rs12091466

Sutherland, L.-A., & Holstead, K. L. (2014). Future-proofing the farm: On-farm wind turbine development in farm business decision-making. *Land Use Policy*, *36*, 102–112. https://doi.org/10.1016/j.landusepol.2013.07.004

Tanner, K. E., Moore-O'Leary, K. A., Parker, I. M., Pavlik, B. M., & Hernandez, R. R. (2020). Simulated solar panels create altered microhabitats in desert landforms. *Ecosphere*, *11*(4). https://doi.org/10.1002/ecs2.3089

Tao, S., Rogan, J., Ye, S., & Geron, N. (2023). Mapping photovoltaic power stations and assessing their environmental impacts from multi-sensor datasets in Massachusetts, United States. *Remote Sensing Applications: Society and Environment*, *30*, 100937. https://doi.org/10.1016/j.rsase.2023.100937

Tegen, S., Keyser, D., Flores-Espino, F., & Hauser, R. (2014). *Economic Impacts from Indiana's First 1,000 Megawatts of Wind Power* (NREL/TP-5000-60914; p. NREL/TP-5000-60914). https://doi.org/10.2172/1150178

Terry, G. (2020). *State Pollinator-Friendly Solar Initiatives*. Clean Energy States Alliance. https://www.cesa.org/wp-content/uploads/State-Pollinator-Friendly-Solar-Initiatives.pdf

Thonig, R., Gilmanova, A., & Lilliestam, J. (2023). *CSP.guru 2023-07-01* (Version 2023-07-01) [Dataset]. Zenodo. https://doi.org/10.5281/zenodo.1318151

TNC. (2024). *Site Renewables Right*. The Nature Concervancy. https://www.nature.org/en-us/what-we-do/our-priorities/tackle-climate-change/climate-change-stories/site-wind-right/

Tonita, E. M., Russell, A. C. J., Valdivia, C. E., & Hinzer, K. (2023). Optimal ground coverage ratios for tracked, fixed-tilt, and vertical photovoltaic systems for latitudes up to 75°N. *Solar Energy*, *258*, 8–15. https://doi.org/10.1016/j.solener.2023.04.038

Trainor, A. M., McDonald, R. I., & Fargione, J. (2016). Energy Sprawl Is the Largest Driver of Land Use Change in United States. *PLOS ONE*, *11*(9), e0162269. https://doi.org/10.1371/journal.pone.0162269

Troch, P. A., Carrillo, G. A., Heidbüchel, I., Rajagopal, S., Switanek, M., Volkmann, T. H. M., & Yaeger, M. (2009). Dealing with Landscape Heterogeneity in Watershed Hydrology: A Review of Recent Progress toward New Hydrological Theory. *Geography Compass*, *3*(1), 375–392. https://doi.org/10.1111/j.1749-8198.2008.00186.x

UK Government. (2024, November 18). *Renewable Energy Planning Database: Quarterly extract*. GOV.UK. https://www.gov.uk/government/publications/renewable-energy-planning-database-monthly-extract

UN. (1987). *Report of the World Commission on Environment and Development: Our Common Future*. United Nations. http://www.un-documents.net/our-common-future.pdf

US BLM. (2005). *Wind Energy Development on BLM-Administered Lands in the Western United States* (FES-05-11). Department of the Interior Bureau of Land Management. https://windeis.anl.gov/documents/fpeis/maintext/Vol1/Vol1Complete.pdf

U.S. Bureau of Labor Statistics. (2023). *Producer Price Index (PPI) Databases* [Dataset]. https://www.bls.gov/data/

U.S. Census Bureau. (2016). *TIGER Roads* (Version 2016 release) [Dataset]. Census.gov. https://www.census.gov/geographies/mapping-files/time-series/geo/tiger-line-file.html

US DOE. (2022). *Land-Based Wind Energy: Economic Development Guide* (WindExchange). Office of Energy Efficiency and Renewable Energy. https://windexchange.energy.gov/economic-development-guide.pdf

US DOE. (2024). *National Transmission Planning Study. Executive Summary*. US DOE Grid Deployment Office. https://www.energy.gov/gdo/national-transmission-planning-study

US EPA. (2015). *Stormwater Discharges from Construction Activities [Overviews and Factsheets]*. Environmental Protection Agency. https://epa.gov/npdes/stormwater-discharges-construction-activities

USDA. (2023). *Agricultural Prices*. National Agricultural Statistics Service. https://usda.library.cornell.edu/concern/publications/c821gj76b?locale=en

USDA. (2024, February 26). *Department of Agriculture, Department of Energy Launch Initiative to Help Farmers Reduce Costs with Underutilized Renewable Technologies as part of President Biden's Investing in America Agenda*. USDA. https://www.usda.gov/about-usda/news/press-releases/2024/02/26/department-agriculture-department-energy-launch-initiative-help-farmers-reduce-costs-underutilized

USDA ERS. (2024). *U.S. Bioenergy Statistics* [Dataset]. USDA Data Product. https://www.ers.usda.gov/data-products/us-bioenergy-statistics

USDA FPAC-BC-GEO. (2023). *National Agriculture Imagery Program (NAIP) Imagery* (NAIP; Version 2023) [Dataset]. Google Earth Engine Data Catalog. https://naip-usdaonline.hub.arcgis.com/

USDA NASS. (2024). *Cropland Data Layer* [Dataset]. USDA. https://croplandcros.scinet.usda.gov/

USDA NASS. (2025). *Cropland Data Layers—FAQs*. USDA NASS Research and Science. https://www.nass.usda.gov/Research_and_Science/Cropland/sarsfaqs2.php#common.18

USDA NRCS. (2024). *Conservation Guidance for Utility-Scale Solar Projects*. https://intranet.usda.gov/sites/default/files/media/documents/NRCS_ConservationGuidance_USSP_121024.pdf

USGS. (2020). *NHDPlus High Resolution (NHDPlus HR)—A Hydrography Framework for the Nation* [Dataset]. USGS Publications Warehouse. https://doi.org/10.3133/fs20203033

USGS. (2023). *1/3rd arc-second Digital Elevation Models (DEMs)—USGS National Map 3DEP Downloadable Data Collection* [National Geospatial Technical Operations Center]. Science Data Catalog (SDC). http://www.usa.gov/publicdomain/label/1.0/

USGS. (2024). *Annual National Land Cover Database (NLCD) Collection 1 Products* (Version 1) [Dataset]. ScienceBase-Catalog. https://doi.org/10.5066/P94UXNTS

Valle, B., Simonneau, T., Sourd, F., Pechier, P., Hamard, P., Frisson, T., Ryckewaert, M., & Christophe, A. (2017). Increasing the total productivity of a land by combining mobile photovoltaic panels and food crops. *Applied Energy*, *206*, 1495–1507. https://doi.org/10.1016/j.apenergy.2017.09.113

Van Zalk, J., & Behrens, P. (2018). The spatial extent of renewable and non-renewable power generation: A review and meta-analysis of power densities and their application in the U.S. *Energy Policy*, *123*, 83–91. https://doi.org/10.1016/j.enpol.2018.08.023

Veers, P., Bottasso, C. L., Manuel, L., Naughton, J., Pao, L., Paquette, J., Robertson, A., Robinson, M., Ananthan, S., Barlas, T., Bianchini, A., Bredmose, H., Horcas, S. G., Keller, J., Madsen, H. A., Manwell, J., Moriarty, P., Nolet, S., & Rinker, J. (2023). Grand challenges in the design, manufacture, and operation of future wind turbine systems. *Wind Energy Science*, *8*(7), 1071–1131. https://doi.org/10.5194/wes-8-1071-2023

Veers, P., Dykes, K., Lantz, E., Barth, S., Bottasso, C. L., Carlson, O., Clifton, A., Green, J., Green, P., Holttinen, H., Laird, D., Lehtomäki, V., Lundquist, J. K., Manwell, J., Marquis, M., Meneveau, C., Moriarty, P., Munduate, X., Muskulus, M., … Wiser, R. (2019). Grand challenges in the science of wind energy. *Science*, *366*(6464), eaau2027. https://doi.org/10.1126/science.aau2027

Victoria, M., Haegel, N., Peters, I. M., Sinton, R., Jäger-Waldau, A., Del Cañizo, C., Breyer, C., Stocks, M., Blakers, A., Kaizuka, I., Komoto, K., & Smets, A. (2021). Solar photovoltaics is ready to power a sustainable future. *Joule*, *5*(5), 1041–1056. https://doi.org/10.1016/j.joule.2021.03.005

VIDA, Google, & Microsoft. (2023). *Global Google-Microsoft Open Buildings* (Version 2.0) [Dataset]. awesome-gee-community-catalog. https://source.coop/repositories/vida/google-microsoft-open-buildings/description

Waechter, K., O'Shaughnessy, E., Kannan, S., & Burton, R. (2024). *Technical Potential and Meaningful Benefits of Community Solar in the United States* (NREL/TP--6A20-87524). NREL. https://doi.org/10.2172/2308823

Wagner, M. J., & Wendelin, T. (2018). SolarPILOT: A power tower solar field layout and characterization tool. *Solar Energy*, *171*, 185–196. https://doi.org/10.1016/j.solener.2018.06.063

Wagner, M. J., & Zhu, G. (2011). *Generic CSP Performance Model for NREL's System Advisor Model: Preprint*. SolarPACES 2011, Granada, Spain. https://doi.org/NREL/CP-5500-52473

Walston, L. J., Barley, T., Bhandari, I., Campbell, B., McCall, J., Hartmann, H. M., & Dolezal, A. G. (2022). Opportunities for agrivoltaic systems to achieve synergistic food-energy-environmental needs and address sustainability goals. *Frontiers in Sustainable Food Systems*, *6*, 932018. https://doi.org/10.3389/fsufs.2022.932018

Walston, L. J., Hartmann, H. M., Fox, L., Macknick, J., McCall, J., Janski, J., & Jenkins, L. (2024). If you build it, will they come? Insect community responses to habitat establishment at solar energy facilities in Minnesota, USA. *Environmental Research Letters*, *19*(1), 014053. https://doi.org/10.1088/1748-9326/ad0f72

Walston, L. J., Li, Y., Hartmann, H. M., Macknick, J., Hanson, A., Nootenboom, C., Lonsdorf, E., & Hellmann, J. (2021). Modeling the ecosystem services of native vegetation management practices at solar energy facilities in the Midwestern United States. *Ecosystem Services*, *47*, 101227. https://doi.org/10.1016/j.ecoser.2020.101227

Walston, L. J., Mishra, S. K., Hartmann, H. M., Hlohowskyj, I., McCall, J., & Macknick, J. (2018). Examining the Potential for Agricultural Benefits from Pollinator Habitat at Solar Facilities in the United States. *Environmental Science and Technology*, *52*(13), 7566–7576. https://doi.org/10.1021/acs.est.8b00020

Wang, F., & Gao, J. (2023). How a photovoltaic panel impacts rainfall-runoff and soil erosion processes on slopes at the plot scale. *Journal of Hydrology*, *620*, 129522. https://doi.org/10.1016/j.jhydrol.2023.129522

Wang, J., Chen, X., Jiang, W., Hua, L., Liu, J., & Sui, H. (2023). PVNet: A novel semantic segmentation model for extracting high-quality photovoltaic panels in large-scale systems from high-resolution remote sensing imagery. *International Journal of Applied Earth Observation and Geoinformation*, *119*, 103309. https://doi.org/10.1016/j.jag.2023.103309

Wang, J., Chen, X., Shi, T., Hu, L., Shi, W., Du, Z., Zhang, X., Zhang, H., Zeng, Y., Hua, L., & Sui, H. (2024). Mapping national-scale photovoltaic power stations using a novel enhanced photovoltaic index and evaluating carbon reduction benefits. *Energy Conversion and Management*, *318*, 118894. https://doi.org/10.1016/j.enconman.2024.118894

Wang, W., & Khanna, M. (2023). Land use effects of biofuel production in the US. *Environmental Research Communications*, *5*(5), 055007. https://doi.org/10.1088/2515-7620/acd1d7

Ward, A. S., Wondzell, S. M., Schmadel, N. M., & Herzog, S. P. (2020). Climate Change Causes River Network Contraction and Disconnection in the H.J. Andrews Experimental Forest, Oregon, USA. *Frontiers in Water*, *2*, 7. https://doi.org/10.3389/frwa.2020.00007

Warmann, E., Jenerette, G. D., & Barron-Gafford, G. A. (2024). Agrivoltaic system design tools for managing trade-offs between energy production, crop productivity and water

consumption. *Environmental Research Letters*, *19*(3), 034046. https://doi.org/10.1088/1748-9326/ad2ab8

Weidner, C., Zarnetske, J. P., Shogren, A., Martin, S. L., & Grose, A. (2022). Subcatchment Spatiotemporal Solute Trends in a Wetland-Dominated Catchment in Michigan, USA. *H22G-06*. AGU Fall Meeting 2022, Chicago, IL. https://doi.org/2022AGUFM.H22G..06W

Weinand, J. M., Pelser, T., Kleinebrahm, M., & Stolten, D. (2025). Countries across the world use more land for golf courses than wind or solar energy. *Environmental Research Communications*, *7*(2), 021012. https://doi.org/10.1088/2515-7620/adb7bd

Weise, E. (2020, February 20). Wind energy gives American farmers a new crop to sell in tough times. *USA Today*. https://www.usatoday.com/story/news/nation/2020/02/16/wind-energy-can-help-american-farmers-earn-money-avoid-bankruptcy/4695670002/

Weselek, A., Ehmann, A., Zikeli, S., Lewandowski, I., Schindele, S., & Högy, P. (2019). Agrophotovoltaic systems: Applications, challenges, and opportunities. A review. *Agronomy for Sustainable Development*, *39*(4), 35. https://doi.org/10.1007/s13593-019-0581-3

Weyman, D. R. (1970). THROUGHFLOW ON HILLSLOPES AND ITS RELATION TO THE STREAM HYDROGRAPH. *International Association of Scientific Hydrology. Bulletin*, *15*(3), 25–33. https://doi.org/10.1080/02626667009493969

Whalen, C. E. (2019). Effects of wind turbine noise on the surrounding soundscape in the context of greater-prairie chicken courtship vocalizations. *Applied Acoustics*.

Wilcoxon, F. (1945). Individual comparisons by ranking methods. *Biometrics Bulletin*, *1*(6), 80–83.

Williams, H. J., Hashad, K., Wang, H., & Zhang, K. M. (2023). The potential for agrivoltaics to enhance solar farm cooling. *Applied Energy*, *332*(June 2022), 120478. https://doi.org/10.1016/j.apenergy.2022.120478

Williams, H. J., Wang, Y., Yuan, B., Wang, H., & Zhang, K. M. (2025). Rethinking agrivoltaic incentive programs: A science-based approach to encourage practical design solutions. *Applied Energy*, *377*, 124272. https://doi.org/10.1016/j.apenergy.2024.124272

Windustry. (2009). *Wind Energy Easements and Leases: Compensation Packages*. Windustry's Wind Easement Work Group. https://web.archive.org/web/20150905203918/https://d3n8a8pro7vhmx.cloudfront.net/windustry/legacy_url/944/Compensation-2009-07-06.pdf?1421782808

Winikoff, J. B., & Parker, D. P. (2024). Farm size, spatial externalities, and wind energy development. *American Journal of Agricultural Economics*, *106*(4), 1518–1543. https://doi.org/10.1111/ajae.12438

Winters-Michaud, C., Haro, A., Callahan, S., & Bigelow, D. P. (2024). *Major Uses of Land in the United States, 2017* (Economic Information Bulletin Number 275). USDA ERS. https://search.nal.usda.gov/discovery/delivery/01NAL_INST:MAIN/12458024340007426

Wiser, R., Bolinger, M., Hoen, B., Millstein, D., Rand, J., Barbose, G., Darghouth, N., Gorman, W., Jeong, S., O'Shaughnessy, E., & Paulos, B. (2023). *Land-Based Wind Market Report: 2023 Edition*. US DOE. https://emp.lbl.gov/sites/default/files/emp-files/2023_lbwmr_final.pdf

Wolfe, P. (2012). *The Wiki-Solar Database* [Dataset]. Wiki-Solar. https://wiki-solar.org/data/

Wu, C., Liu, H., Yu, Y., Zhao, W., Liu, J., Yu, H., & Yetemen, O. (2022). Ecohydrological effects of photovoltaic solar farms on soil microclimates and moisture regimes in arid Northwest China: A modeling study. *Science of the Total Environment*, *802*, 149946. https://doi.org/10.1016/j.scitotenv.2021.149946

Wu, D., Grodsky, S. M., Xu, W., Liu, N., Almeida, R. M., Zhou, L., Miller, L. M., Roy, S. B., Xia, G., Agrawal, A. A., Houlton, B. Z., Flecker, A. S., & Xu, X. (2023). Observed impacts of large wind farms on grassland carbon cycling. *Science Bulletin*, *68*(23), 2889–2892. https://doi.org/10.1016/j.scib.2023.10.016

Wu, G. C., Jones, R. A., Leslie, E., Williams, J. H., Pascale, A., Brand, E., Parker, S. S., Cohen, B. S., Fargione, J. E., Souder, J., Batres, M., Gleason, M. G., Schindel, M. H., & Stanley, C. K. (2023). Minimizing habitat conflicts in meeting net-zero energy targets in the western United States. *Proceedings of the National Academy of Sciences*, *120*(4), e2204098120. https://doi.org/10.1073/pnas.2204098120

Wu, G. C., Leslie, E., Sawyerr, O., Cameron, D. R., Brand, E., Cohen, B., Allen, D., Ochoa, M., & Olson, A. (2020). Low-impact land use pathways to deep decarbonization of electricity. *Environmental Research Letters*, *15*(7), 074044. https://doi.org/10.1088/1748-9326/ab87d1

Xia, Z., Li, Y., Guo, S., Chen, R., Zhang, W., Zhang, P., & Du, P. (2023). Mapping global water-surface photovoltaics with satellite images. *Renewable and Sustainable Energy Reviews*, *187*, 113760. https://doi.org/10.1016/j.rser.2023.113760

Xiarchos, I. M., & Sandborn, A. (2017). *Wind Energy Land Distribution In The United States of America* (Office of Energy Policy and New Uses Office of the Chief Economist). USDA. https://www.usda.gov/sites/default/files/documents/FINAL-Wind_Energy_Land_Distribution_in_the_United_States_of_America_7282017.pdf

Xu, K., Chan, G., & Kannan, S. (2024). *Sharing the Sun Community Solar Project Data* (Dataset NREL; Version 2024). NREL Data Catalog. https://doi.org/10.7799/2438583

Yang, Y., Hobbie, S. E., Hernandez, R. R., Fargione, J., Grodsky, S. M., Tilman, D., Zhu, Y.-G., Luo, Y., Smith, T. M., Jungers, J. M., Yang, M., & Chen, W.-Q. (2020). Restoring

Abandoned Farmland to Mitigate Climate Change on a Full Earth. *One Earth*, *3*(2), 176–186. https://doi.org/10.1016/j.oneear.2020.07.019

Yavari Bajehbaj, R., Cibin, R., Duncan, J. M., & McPhillips, L. E. (2024). Quantifying soil moisture and evapotranspiration heterogeneity within a solar farm: Implications for stormwater management. *Journal of Hydrology*, *638*, 131474. https://doi.org/10.1016/j.jhydrol.2024.131474

Yavari, R., Zaliwciw, D., Cibin, R., & McPhillips, L. (2022). Minimizing environmental impacts of solar farms: A review of current science on landscape hydrology and guidance on stormwater management. *Environmental Research: Infrastructure and Sustainability*, *2*(3), 032002. https://doi.org/10.1088/2634-4505/ac76dd

Yu, J., Wang, Z., Majumdar, A., & Rajagopal, R. (2018). DeepSolar: A Machine Learning Framework to Efficiently Construct a Solar Deployment Database in the United States. *Joule*, *2*(12), 2606–2617. https://doi.org/10.1016/j.joule.2018.11.021

Yuan, L., Nain, P., Kothari, M., & Anctil, A. (2024). Material intensity and carbon footprint of crystalline silicon module assembly over time. *Solar Energy*, *269*, 112336. https://doi.org/10.1016/j.solener.2024.112336

Zaunbrecher, B. S. (2018). The social and ecological footprint of renewable power generation plants. Balancing social requirements and ecological impacts in an integrated approach. *Social Science*.

Zell, W. O., & Sanford, W. E. (2020). Calibrated Simulation of the Long-Term Average Surficial Groundwater System and Derived Spatial Distributions of its Characteristics for the Contiguous United States. *Water Resources Research*, *56*(8), e2019WR026724. https://doi.org/10.1029/2019WR026724

Zhang, N., Duan, H., Shan, Y., Miller, T. R., Yang, J., & Bai, X. (2023). Booming solar energy is encroaching on cropland. *Nature Geoscience*, *16*(11), 932–934. https://doi.org/10.1038/s41561-023-01304-1

Zhang, W., Markfort, C. D., & Porté-Agel, F. (2013). Experimental study of the impact of large-scale wind farms on land–atmosphere exchanges. *Environmental Research Letters*, *8*(1), 015002. https://doi.org/10.1088/1748-9326/8/1/015002

Zhang, X., Xu, M., Wang, S., Huang, Y., & Xie, Z. (2022). Mapping photovoltaic power plants in China using Landsat, random forest, and Google Earth Engine. *Earth System Science Data*, *14*(8), 3743–3755. https://doi.org/10.5194/essd-14-3743-2022

Zhou, L., Tian, Y., Baidya Roy, S., Thorncroft, C., Bosart, L. F., & Hu, Y. (2012). Impacts of wind farms on land surface temperature. *Nature Climate Change*, *2*(7), 539–543. https://doi.org/10.1038/nclimate1505

Zhuang, L., Zhang, Z., & Wang, L. (2020). The automatic segmentation of residential solar panels based on satellite images: A cross learning driven U-Net method. *Applied Soft Computing*, *92*, 106283. https://doi.org/10.1016/j.asoc.2020.106283

APPENDIX A: SUPPLEMENTARY INFORMATION FOR CHAPTER 1

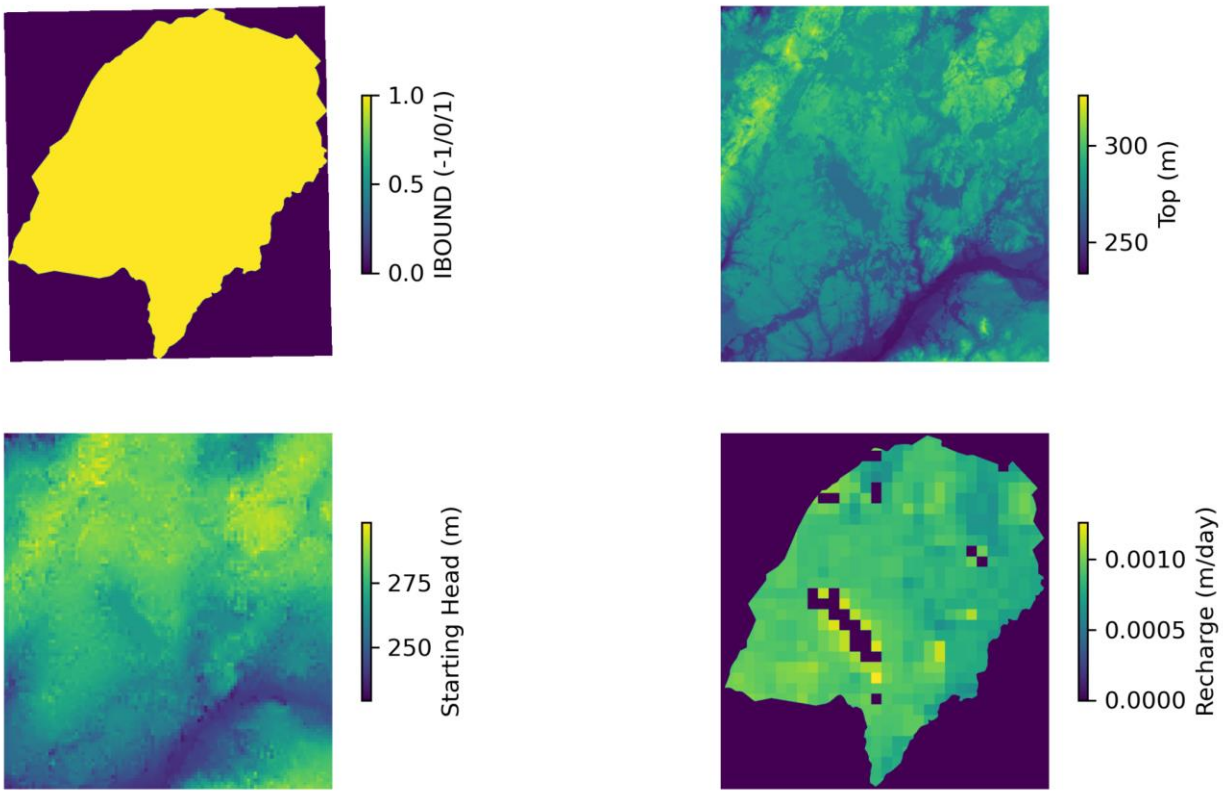

Figure A26. Single-layer steady-state MODFLOW simulation inputs. Inputs include model active region (IBOUND, upper left), digital elevation model (model top, upper right), starting heads (lower left), and recharge (lower right).

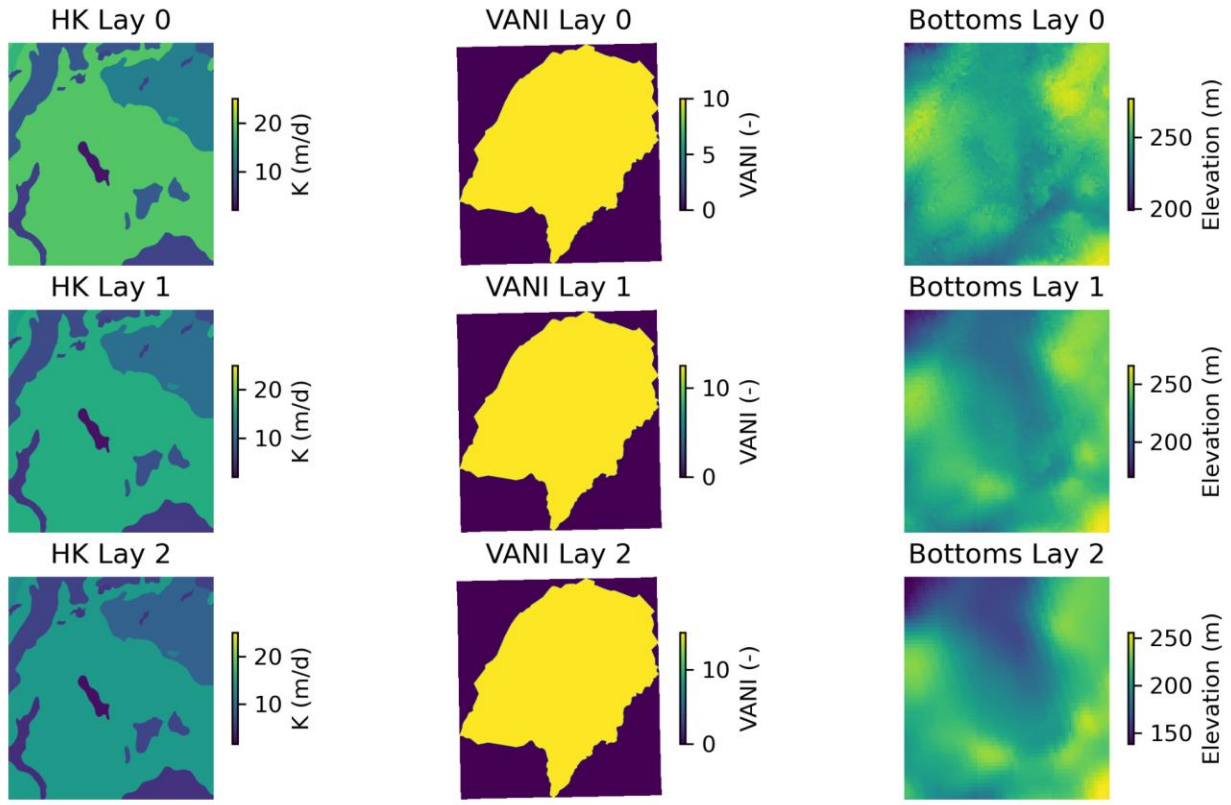

Figure A27. Multi-layer steady-state MODFLOW simulation inputs. Layers are labeled from model top (Layer 0) to bottom (Layer 2). Inputs include aquifer hydraulic conductivity (HK, left), vertical anisotropy (VANI, middle), and layer bottom elevation (right).

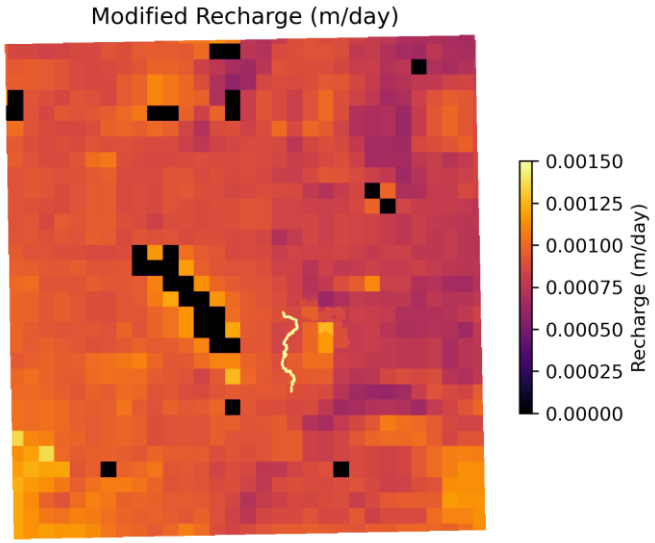

Figure A28. Modified recharge layer for the high-impact solar simulation scenario. Note that this layer is unchanged from the values in Figure A26 except where the increase in runoff and recharge from Figure 2 were applied to model cells in the middle to lower right region.

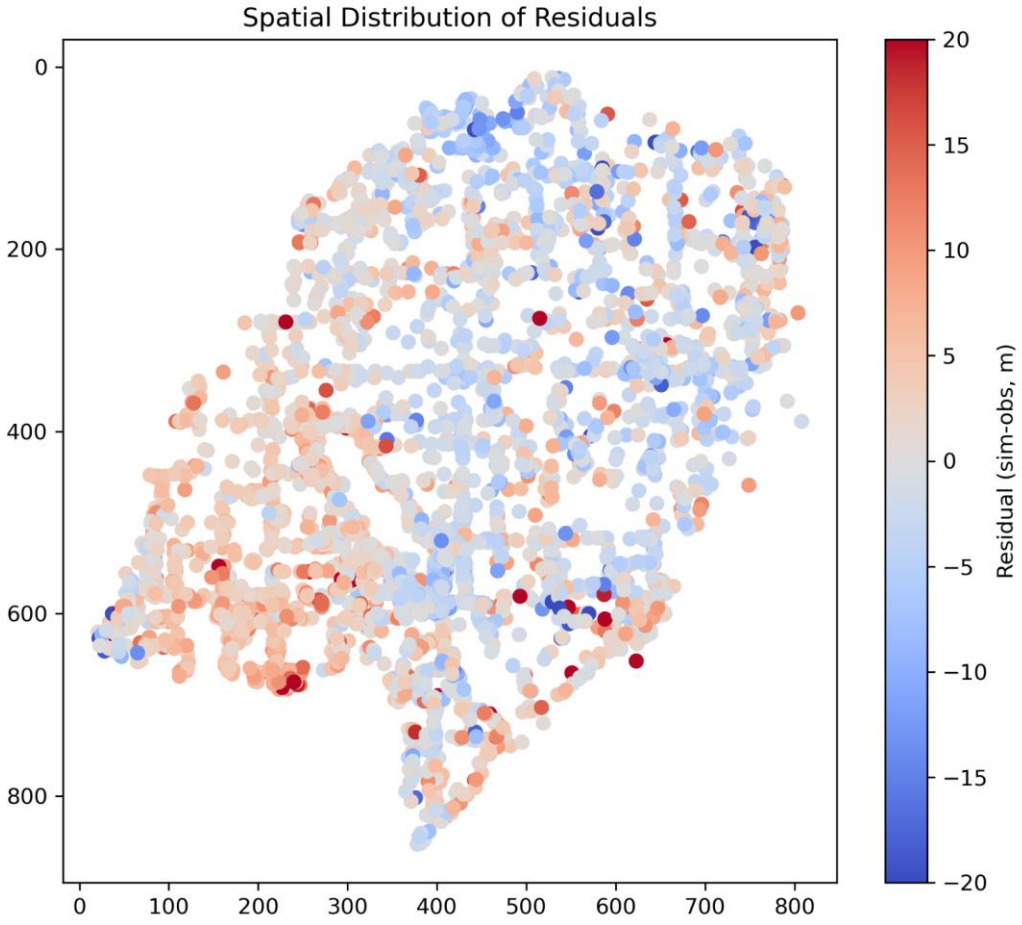

Figure A29. Spatial simulated head residuals. Difference in simulated heads and observed heads at 4,970 observation wells in the region in the top model layer (Layer 0).

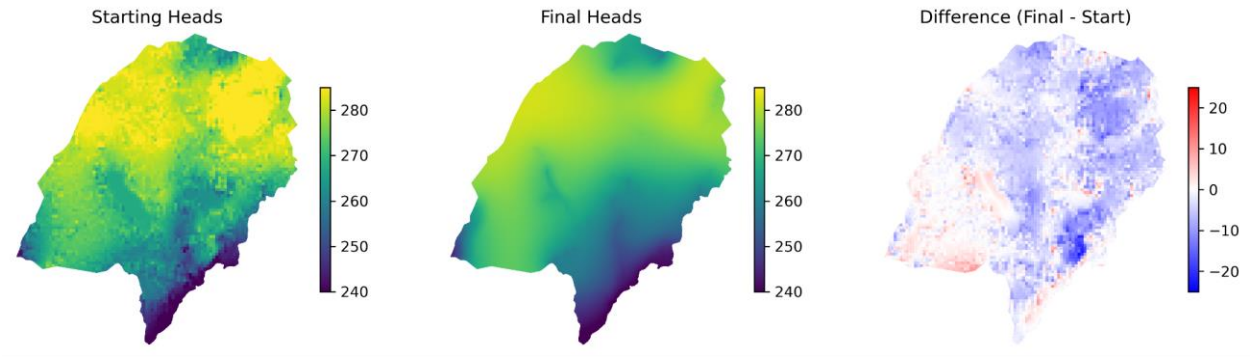

Figure A30. Difference in starting and final model hydraulic heads (meters). Note that final heads (middle) are the simulated heads in the top model layer (Layer 0).

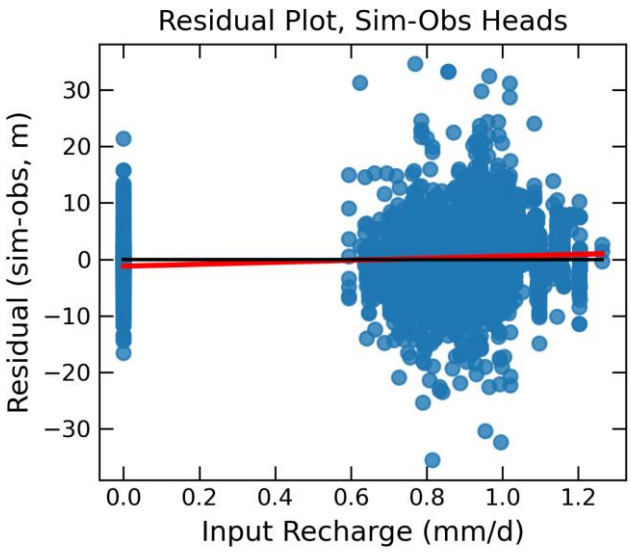

Figure A31. Simulated head residuals compared to 2013 recharge. The red line is the line of best fit.

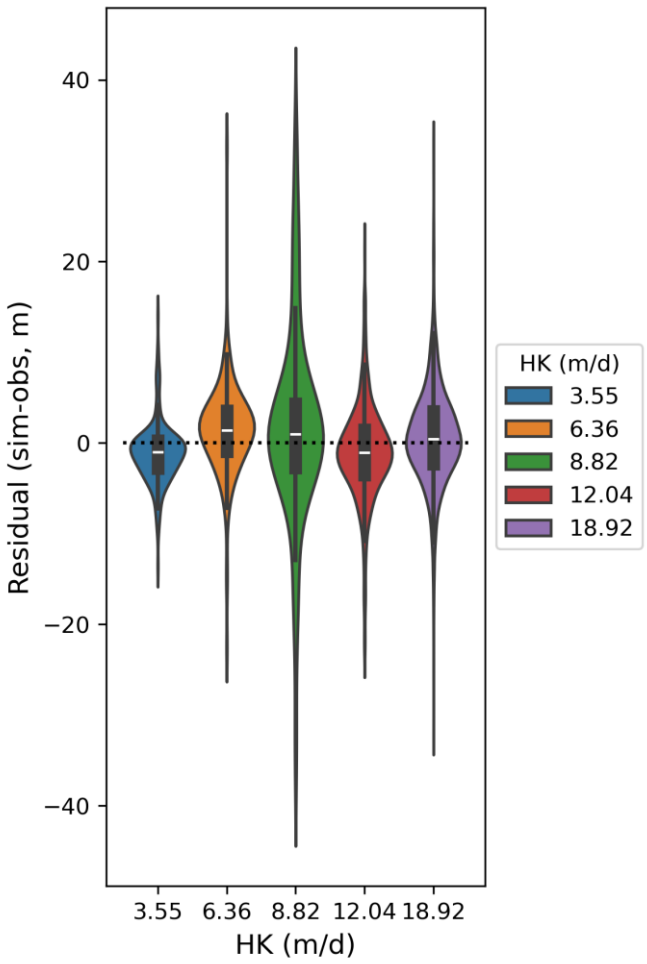

Figure A32. Simulated head residuals compared to aquifer hydraulic conductivity. Note that hydraulic conductivity (HK) is grouped into five quantiles.

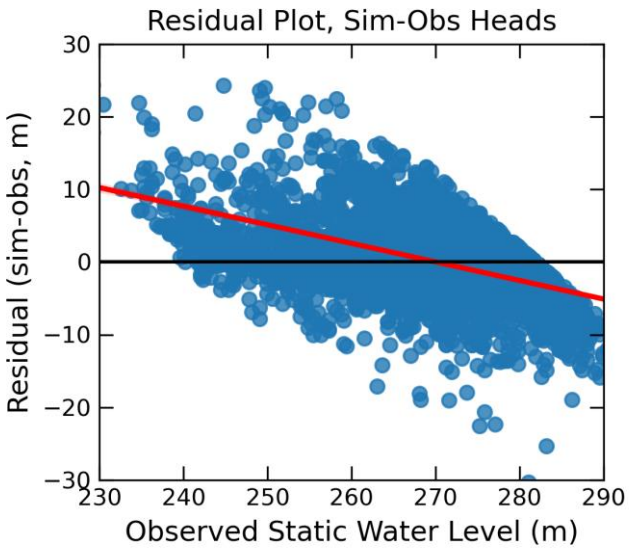

Figure A33. Simulated head residuals compared to observed heads. The red line is the line of best fit.

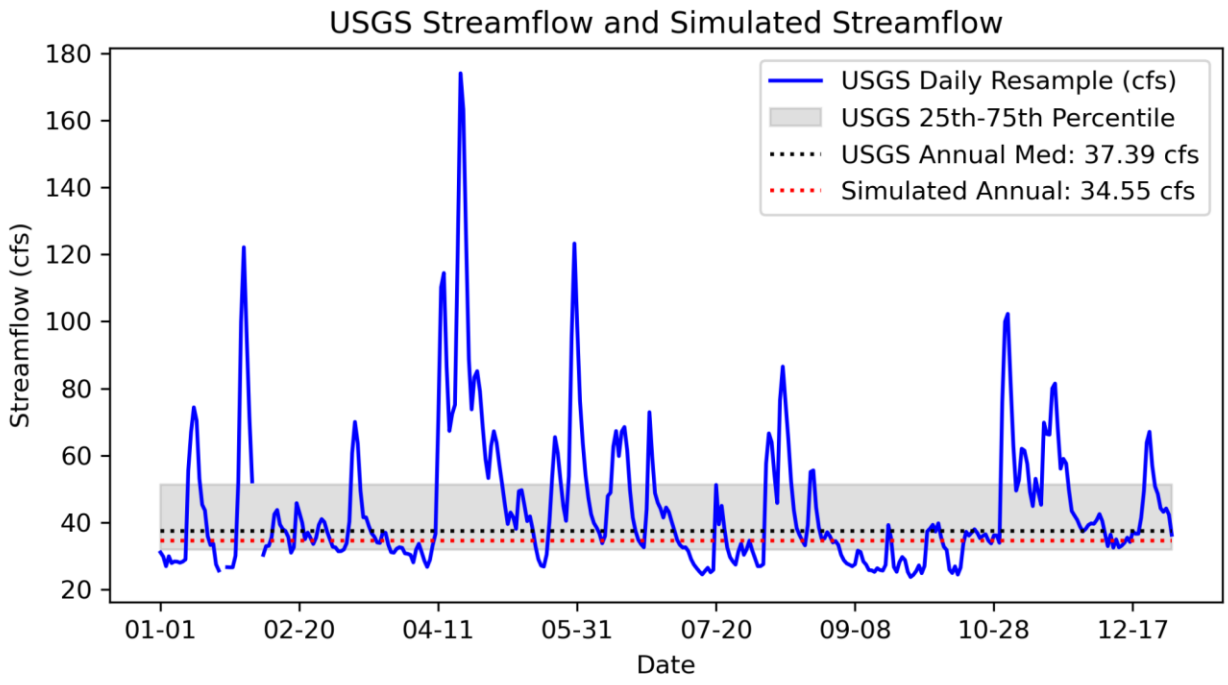

Figure A34. Observed and modeled annual streamflow. USGS hourly streamflow estimates (observations) from the national gauging network for Augusta Creek Near Augusta, MI (USGS 04105700), resampled to daily estimates (solid blue) and to an annual median value (dotted black) for the year 2013. Simulated cumulative streamflow estimates from within the watershed boundary at the stream outlet (dotted red).

APPENDIX B: SUPPLEMENTARY INFORMATION FOR CHAPTER 2

Text A2.1: GM-SEUS data repository description

Text A2.1.1: GM-SEUS open repository file descriptions

- **GMSEUS_Arrays_Final:** Final array dataset containing boundaries from existing datasets and enhanced by buffer-dissolve-erode technique with GM-SEUS panel-rows containing all array-level attributes (EPSG:102003), geopackage, shapefile, csv
- **GMSEUS_Panels_Final:** Final panel-row dataset containing boundaries from existing datasets and newly delineated GM-SEUS panel-rows containing all panel-row-level attributes (EPSG:102003), geopackage, shapefile, csv
- **GMSEUS_NAIP_Arrays:** All array boundaries created by buffer-dissolve-erode method of newly delineated (NAIP) GM-SEUS panel-rows (EPSG:102003), geopackage, shapefile, csv
- **GMSEUS_NAIP_Panels:** Newly delineated panel-rows from NAIP imagery with low-quality panel-rows removed (EPSG:102003), geopackage, shapefile, csv
- **GMSEUS_NAIP_PanelsNoQAQC:** All newly delineated panel-rows from NAIP imagery without any quality control (EPSG:102003), geopackage, shapefile, csv
- **NAIPtrainRF:** Training dataset of 12,000 NAIP training points (2,000 class^{-1}) containing class values, spectral index values, the year of NAIP imagery accessed, and point coordinates (EPSG:4326), comma separated values
- **LabeledImages:** Directory containing image and mask subdirectories with ~17,500 input and target images for deep learning pattern recognition applications, GeoTIFF

Text A2.1.2: GM-SEUS attribute fields for arrays

- **arrayID:** unique numeric ID of each solar array in GM-SEUS, unitless
- **Source:** original array boundary source from existing datasets or manual digitization, unitless
- **nativeID:** numeric ID of each solar array in from source spatial dataset if an indexing system existed, unitless
- **latitude:** latitude of the array boundary centroid (EPSG:4269), decimal degrees
- **longitude:** longitude of the array boundary centroid (EPSG:4269), decimal degrees
- **newBound:** binary, whether the array boundary was derived from the existing data sources (0) or from a buffer-dissolve-erode of panel-rows following our definition of an array boundary (1), unitless
- **totArea:** total land footprint of panel-rows and the space between them, m^2
- **totRowArea:** If numRow is greater than 0, sum of rowArea within an array. Otherwise, estimated based on totArea and GCR1 estimation where no panel-rows were detected, m^2

- **numRow:** number of panel-rows within an array, m^2
- **instYr:** installation year from existing sources, with gaps filled in by instYrLT, year
- **instYrLT:** LandTrendr-derived installation year independent of any data source other than Landsat spectral trajectory, year
- **capMW:** installed peak capacity from existing sources, with gaps filled in by capMWest, MW_{DC} or MW_{th}
- **capMWest:** estimated installed peak capacity derived from capacity to panel-row area relationships described in Eq. 10-13 independent of any data source, MW_{DC} or MW_{th}
- **modType**: reported panel-row (module) technology at the array level (c-si, thin-film, csp). If unreported, assumed to be c-si, unitless
- **effInit:** initial panel-rows efficiency from existing sources with gaps filled in by based on efficiency estimation from modType and instYr taken from the annual Tracking the Sun report, %
- **GCR1:** 0-1, the ratio of totRowArea to the total area of panel-rows and the space between them. For arrays with complete panel delineation and arrays where newBound is 1, this is equivalent to totArea. This is also called packing factor. If numRow is greater than 0, GCR1 is an actual GCR_1 for the array. Otherwise, GCR is estimated by linear regression of latitude and longitude by mount and module type, unitless
- **GCR2:** 0-1, the ratio of the average width of the panel-row short edge (rowWidth) to the horizontal ground distance between identical panel-rows points, defined as the sum of widthAvg and rowSpace. If numRow is greater than 0, GCR2 is an actual GCR_2 for the array. Otherwise, GCR2 is estimated by linear regression of latitude and longitude by mount and module type, unitless
- **mount:** mount technology derived from the azimuth and geometry of each panel-row within the array or from existing sources, with preference given to newly derived mount technology. Either 'fixed_axis', 'single_axis', 'dual_axis', or 'mixed_' with a lower-case letter denoting the mixed mounts (e.g., mixed_fs), unitless
- **tilt:** panel-row tilt for fixed-axis arrays (including arrays with mixed-mounting) from existing sources and filled in by tiltEst, degrees above horizontal
- **tiltEst:** estimated panel-row tilt for fixed-axis arrays (including arrays with mixed-mounting) estimated using *pvlib*, degrees above horizontal
- **avgAzimuth:** median estimated azimuth of panel-rows within array bounds or reported azimuth from existing sources, with preference given to newly estimated azimuth. For single-axis tracking arrays this is the cardinal direction of the long-edge. For all other mount types, this is the cardinal direction of the panel-row face, degrees from north
- **avgLength:** median length of the long edge of panel-rows within an array, meters
- **avgWidth:** median length of the short edge of panel-rows within an array, meters
- **avgSpace:** median spacing between the solar array rows, in meters, between edges of the panel-row projected onto the ground, meters
- **STATEFP:** unique geographic identifier for the U.S. Census Bureau state entity, unitless

- **COUNTYFP:** unique geographic identifier for the U.S. Census Bureau county entity, unitless
- **geometry:** best new or available geometry matching the array definition which contains panel-rows and the space between them, derived from existing sources (newBound = 0) or from a buffer-dissolve-erode of newly delineated panel-rows (newBound = 1), meters
- **version:** GM-SEUS version in which the array geometry and attributes are derived. Each subsequent version will re-derive new geometries and the best delineation from each version will be selected, unitless

Text A2.1.3: GM-SEUS attribute fields for panel-rows

- **panelID:** unique numeric ID of the panel-row in GM-SEUS, unitless
- **arrayID:** unique numeric ID of each solar array in GM-SEUS that the panel-row is associated with, unitless
- **Source:** panel-row boundary source from existing datasets or GM-SEUS, unitless
- **rowArea:** top-down or apparent panel-row area directly from the output of image classification, m^2
- **rowWidth:** length of the short-edge of the panel-row, meters
- **rowLength:** length of the long-edge of the panel-row, meters
- **rowAzimuth:** azimuth of the panel-row, with 0 at North, degrees
- **rowMount:** mount technology (fixed-axis, single-axis, or dual-axis) of the panel-row, unitless
- **rowSpace:** the inter-row spacing between the panel-row and the nearest panel-row in the azimuthal direction (fixed- and single-axis) or any direction (dual-axis), meters
- **geometry:** top-down or perceived geometry, meters
- **version:** GM-SEUS version in which the panel-row geometry and attributes are derived. Each subsequent version will re-derive new geometries and the best delineation from each version will be selected, unitless

Text A2.2: Limitations of input polygon and point array dataset metadata

Aside from manual digitization of point data to polygon data, GM-SEUS does not search for new arrays that are not contained within existing reference polygon datasets (Main Text Table 1). Thus, GM-SEUS completeness is currently limited by coverage of existing datasets. As mentioned, the coverage and metadata completeness and quality of input dataset varies depending on the scope and age of the dataset. The following are limitations of metadata attributes of input dataset.

The TransitionZero Solar Asset Mapper (TZ-SAM) (Phillpott et al., 2024b, 2024a) contains metadata on installation year, installed capacity, and ground cover ratio (GCR). TZ-SAM installation year is based on Copernicus Sentinel-2 imagery (S2) change detection, which is limited to installations after 2017. TZ-SAM also reports installation year as a range of potential dates based on the timing of imagery where change was detected. We select the median date within this range (only if the start of the range is 2018 or later) as the TZ-SAM provided installation year. TZ-SAM installation year is also not complete. TZ-SAM GCR estimates are derived from an OpenStreetMap (OSM) validation dataset, are used to estimate installed capacity, and are provided at the country-level rather than the array level.

The Chesapeake Watershed solar dataset (CWSD) (Evans et al., 2021, 2023) contains metadata on installation year. As with TZ-SAM, CWSD installation year is based on S2 change detection, which is limited to installations after 2017.

OpenStreetMap (OSM) (OpenStreetMap Contributors, 2024) contains metadata on installation year and installed capacity. OSM installation years are based on the 'start_date' attribute which contains crowd sourced uncertainty in definition. The same issue exists with installed capacity reporting in OSM.

SolarPACES CSP.guru (Thonig et al., 2023) contains metadata on installation year and installed capacity. The SolarPACES CSP.guru dataset also contains technology information (e.g., Parabolic Trough, Power Tower), from which we made assumptions about mount technologies.

The World Resources Institute's Global Power Plant Database v1.3.0 (GPPDB) (Byers et al., 2021; Global Energy Observatory et al., 2021) contains metadata on installation year and installed capacity. GPPDB installation years were inferred from a commissioning year attribute, which may not be the same as the year of completed installation.

Text A2.3: Use case product: labeled imagery for semantic segmentation

To display utility in the granularity of GM-SEUS arrays and panel-rows, we provide solar-labeled images as an auxiliary data product intended for training deep learning models for pattern recognition (e.g., semantic segmentation). Deep learning convolutional neural networks (DCNN) require abundant and well-labeled training data and are used in a number of existing solar identification and characterization efforts (Arnaudo et al., 2023; Camilo et al., 2018; D. Chen et al., 2024; Y. Chen, Zhou, et al., 2024; Costa et al., 2021; Edun et al., 2021; Evans et al., 2023; Ge et al., 2022; Hou et al., 2019; Hu et al., 2022; Imamoglu et al., 2017; H. Jiang et al., 2021, 2022;

Kasmi et al., 2023; Kausika et al., 2021; Kruitwagen et al., 2021; Malof et al., 2016; Mayer et al., 2022; Ortiz et al., 2022; Perry et al., 2024; Perry & Campos, 2023; Phillpott et al., 2024b; Ravishankar et al., 2022; J. Wang et al., 2023; Yu et al., 2018; Zhuang et al., 2020).

Labeled imagery was created for solar energy arrays within GM-SEUS that contained NAIP generated panel-rows (CCVPV or GM-SEUS Source) and at least 10 identified panel-rows. To reduce panel-row omission error, imagery was only selected in sub-array regions where panel-rows were present. Images (inputs) are 4-band (R, G, B, and NIR) rasters masks (targets) are binary single band rasters (0: non-solar, 1: solar), where solar labels are GM-SEUS panel-row vectors rasterized at local NAIP resolution and projection. Images and masks are provided at 256x256 pixel dimensions. We allowed arrays to contain random point centered image windows equal to 50% of the panel-row containing array area divided by tiled area. This resulted in ~17,500 images and masks within 4,452 arrays. We intend on updating this dataset with higher density sampling to include 200,000+ training images in following GM-SEUS versions. Example images and masks for fixed-, single-, and dual-axis mounted installations are shown in Appendix Figure A36.

All files are stored at GeoTIFF files, with native NAIP imagery projections (UTM Zone for source imagery location, spatial reference information is included in both images and masks if reprojection is needed). Images and masks retain the same file naming logic for easy application. Importantly, file nomenclature includes the respective arrayID from the GM-SEUS, meaning images can be selected for metadata-specific applications (e.g., avgAzimuth, mount). File nomenclature is (for example): “id3044_tile0.tif", where '3044' is the arrayID from GM-SEUS and 'tile0' is the tile number for that array.

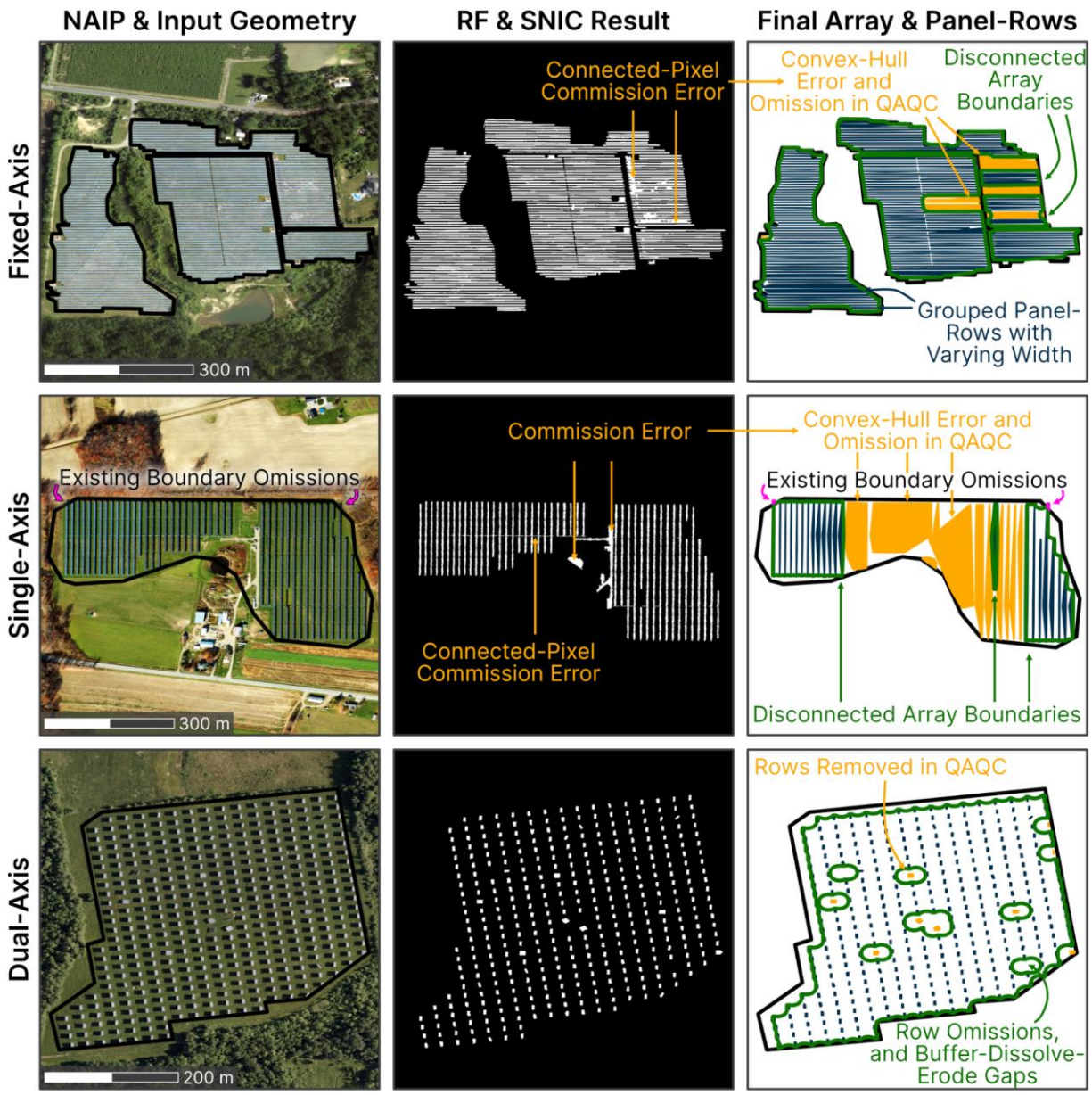

Figure A35. Panel-row and array boundary delineation errors and limitations. The left column contains NAIP aerial imagery and input geometries originating from the Source dataset of greatest spatial quality for that array.

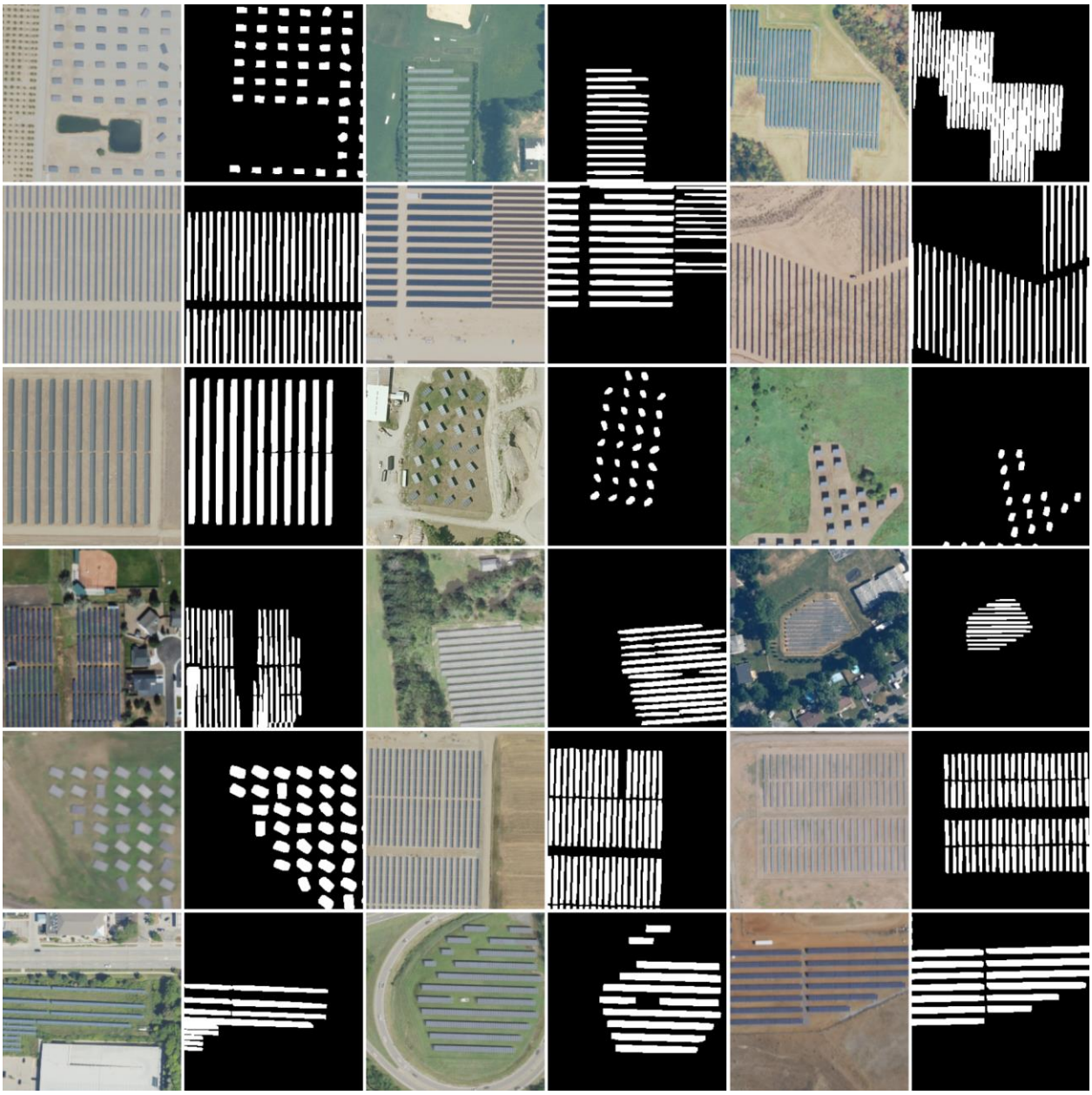

Figure A36. Deep learning and pattern recognition use case image product examples. Three columns of six examples containing inputs or images (left) and targets or masks (right) for fixed-, single-, and dual-axis mounted arrays contained within GM-SEUS. Note, this data was not used to create GM-SEUS, but is provided as a value added product within the data repository. Image products were created from NAIP imagery and GM-SEUS panel-rows.

APPENDIX C: SUPPLEMENTARY INFORMATION FOR CHAPTER 3

Text A3.1: Methods: Future work in classifying ground cover management through time

To classify high-temporal resolution changes in ground cover practices, we used Level-2A surface reflectance (SR) Copernicus Sentinel-2 imagery (10 m, 5 day revisit cycle) from the European Space Agency (ESA) (ESA, 2024). Sentinel-2 SR mean *NDVI* within the array bounds was extracted for images with low cloud coverage across all years of available imagery. *NDVI* values were then resampled to a 15 day mean composite to remove gaps in data due to cloud coverage. We assessed changes in annual intensity of vegetation by calculating the area under the curve (AUC) for each year of data using *numpy* polyfit regression and integrate using *numpy* trapezoidal integration (Harris et al., 2020). To emphasize year to year changes rather than *NDVI* magnitude, we normalize AUC to the minimum and maximum values across years.

Text A3.2: Methods: Future work in differentiating blooming and non-blooming vegetation

Several studies have successfully observed bloom occurrence, duration, or magnitude using aerial and satellite remote sensing across a variety of bloom types (J. Chen et al., 2019; Dixon et al., 2021; Gonzales et al., 2022; Shao et al., 2023; Sulik & Long, 2015, 2020). Chen et al. (2019) developed the enhanced bloom index (*EBI*) to track bloom information for almond orchards and found that Sentinel-2-derived EBI was highly correlated with EBI from higher resolution imagery. Dixon et al. (2021) applied temporal changes in *EBI* and a greenness index to track forest flowering dynamics in *Corymbia calophylla* trees. Sentinel-2 *EBI* is calculated by:

$$EBI = \frac{R + G + B}{\frac{G}{B} * (R - B + \varepsilon)} \quad \textbf{Eq. 24}$$

where ε is set to the maximum reflectance value (1).

Dixon et al. (2021) showed that blooming periods were marked by a temporally related increase in *EBI* and decrease in greenness. We used this relationship to examine periods of decreased *NDVI* greenness (valleys) and increased EBI bloom signatures (peaks). If the *NDVI* valley and *EBI* peak were within 30-days of each other (two resampled time steps), we classified the array as managed with pollinator-friendly habitat with floral resources for that year. Otherwise, the array year was given a classification of grasses. Given that *EBI* is heavily influenced by snow, we only considered changes in *EBI* and *NDVI* between April 10th (day of year: 100) and October

27th (day of year: 300) within each year. To validate this approach, we intend to compare the pollinator habitat classification for NREL InSPIRE arrays known to be managed with pollinator habitat, and those managed with grazing or other forms of agrivoltaics (NREL, 2025).

Proportion of vegetation coverage will be tested against the existence of an active pollinator scorecard across the state compared to no active scorecard (EPRI, 2021). We will use Wilcoxon Rank-Sum test to test for significance and Cohen's d to evaluate effect size.

Text A3.3: On pollinator habitat dual-use

Anthropogenically caused pollinator decline has raised concerns regarding global food security and related ecosystem services (Otto et al., 2016; Potts et al., 2010). In the United States pollinator dependent agriculture accounts for about 23% of agricultural production (Johnson, 2010) and about $70 billion (2009 USD) as of 2009 (Calderone, 2012). Habitat fragmentation, transition to biofuel crops, synthetic fertilizers exposure, and parasitic infection (largely agricultural and land use change side-effects) are thought to be some of the largest contributing anthropogenic factors to both native wild pollinator and managed honey bee (*Apis mellifera*) decline (Gallant et al., 2014).

Pollinator habitats are one of the most feasible and broadly deployed dual-use practices in the US (NREL, 2025). Unlike other forms of dual-use (e.g., crop production agrivoltaics), pollinator habitats do not traditionally require additional site design or management considerations beyond seed mix selection, vegetation establishment, and seasonal management (McCall, Macdonald, et al., 2023). Beyond the general benefits of vegetation ground cover, pollinator habitats also exhibit some of the only well-documented co-benefits that extend beyond the fenced in area, with evidence for boosted pollinator abundance, richness, diversity and forage quality, and enhanced pollination services extending to adjacent cropland and potentially, adjacent farmland income (Blaydes et al., 2021, 2022; Graham et al., 2021; Walston et al., 2018, 2024). Benefits of informed forage habitat can also extend to both native and managed pollinators (Blaauw & Isaacs, 2014; Graham et al., 2021; Walston et al., 2021) with grassland and pasture also having been shown to be beneficial for pollinator health (Quinlan et al., 2021). Interestingly, improved landscape connectivity can be achieved by reverting agricultural margins, a potential siting decision for future solar arrays, to pollinator-friendly habitat, even in some of the most dense agricultural landscapes in the world (Dilts et al., 2023). Together, this means that pollinator-friendly ground cover management would not benefit both local agriculture and the pollinators.

Though, surrounding landscapes are a significant driver of pollinator diversity at solar sites as well, which places less control in the hands of a farmland owner or landscape manager (Blaydes et al., 2024).

Text A3.4: Future work in assessing the effectiveness of pollinator scorecards

Currently, 18 US states actively maintain or are preparing a solar pollinator scorecard (EPRI, 2021; NYSERDA, 2025), along with several state-neutral or independently developed scorecards (Fresh Energy, 2025; ROWHWG, 2023). In agreement or requirements by states regulating agencies, these scorecards permit landowners of facilities that achieve a sufficient score to be eligible for income or tax incentives, and in some cases certain assessment exemptions (Terry, 2020).

However, many scorecards are also based on practices with unverified benefits, and only five require seasonal to 5-year inspections ensuring continued compliance. The remaining scorecards either recommend or do not mention regular monitoring of management practice upkeep (EPRI, 2021; Fresh Energy, 2025; NYSERDA, 2025; Terry, 2020). Additionally, seven of these state scorecards are currently state mandated, while the rest remain optional (Fresh Energy, 2025). This necessitates a standardized approach for evaluating the outcomes of scorecard values, and regular monitoring of the retention of practices and outcomes (Carvalho et al., 2023).

Effective scorecard evaluation and monitoring will require a combination of on-the-ground assessments and broader spatial and temporal data assimilation. Field surveys should assess forage quality, plant density, and pollinator abundance, while large-scale data acquisition can track long-term trends in habitat quality. One potential resource for this effort is the native pollinator abundance map (Koh et al., 2016), which would provide a spatial account of a key metric in habitat mix, design, and establishment.

In a preliminary analysis (see Appendix C Text A.3.3 and A3.4), we classified temporal ground cover management practices for 3,760 solar energy installations (411 km^2 and 26.1 GW_{DC}) that were determined to contain low-coverage or highly vegetated ground covers. Within vegetated arrays, we also attempted to go further by differentiating vegetated ground covers into two classes: blooming and non-blooming vegetation. However, we do not yet have preliminary data for blooming vegetation classification.

First, regarding general ground cover mixes, 532 km^2 of 584 km^2 of array area with low- or high-vegetation cover contained at least 10% barren cover, potentially providing ground nesting

habitat, crucial for some wild bee species (Blaydes et al., 2021, 2022). Regarding AUC, Figure A42-A44 shows the polynomial (degree=3) fit for each year of available Sentinel-2 data. Note that we limited time series data to full years post-installation year. In Figure A42-A43, these curves peak in the mid-summer, and generally peak higher (with more AUC) in later years. Figure A44 shows an earlier season peak (mid-April), and more variability between years. Figure A45-A46 show state-aggregated and normalized AUC trends for Michigan and California. Qualitatively, Michigan (Figure A46) tends to have increasing normalized AUC with greater years since installation, potentially indicating increasing occurrence of vegetation establishment and greater vegetation coverage. Conversely, California (Figure A46) seems to have little to no temporal relationship, either indicating a) early and effectively complete vegetation establishment or b) little to not progress in vegetation establishment. These relationships have not yet been statically validated. Additionally, crucial in future work, will be including a local control (non-solar vegetation) to perform a difference in difference analysis and remove year to year variation from the spectral signature.

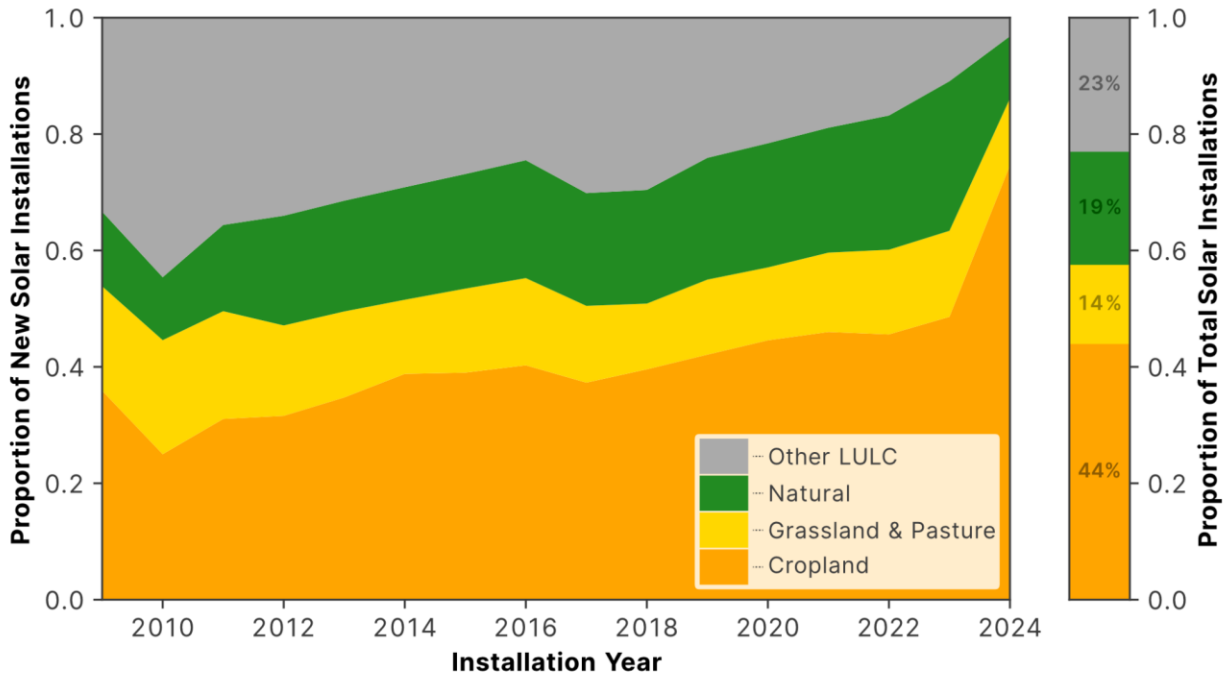

Figure A37. US solar energy prior land use proportion by installation through time. Compare to Main text Figure 18 (by area).

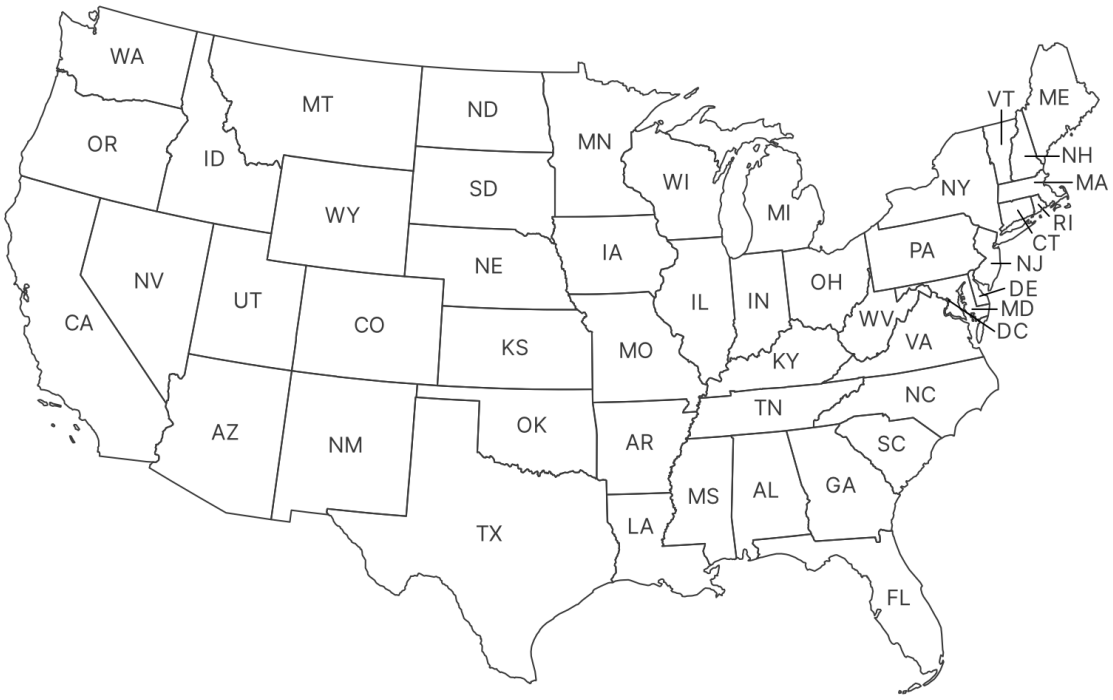

Figure A38. United States state name shorthand with geographical context. Compare with Main text Figure 17 and 19.

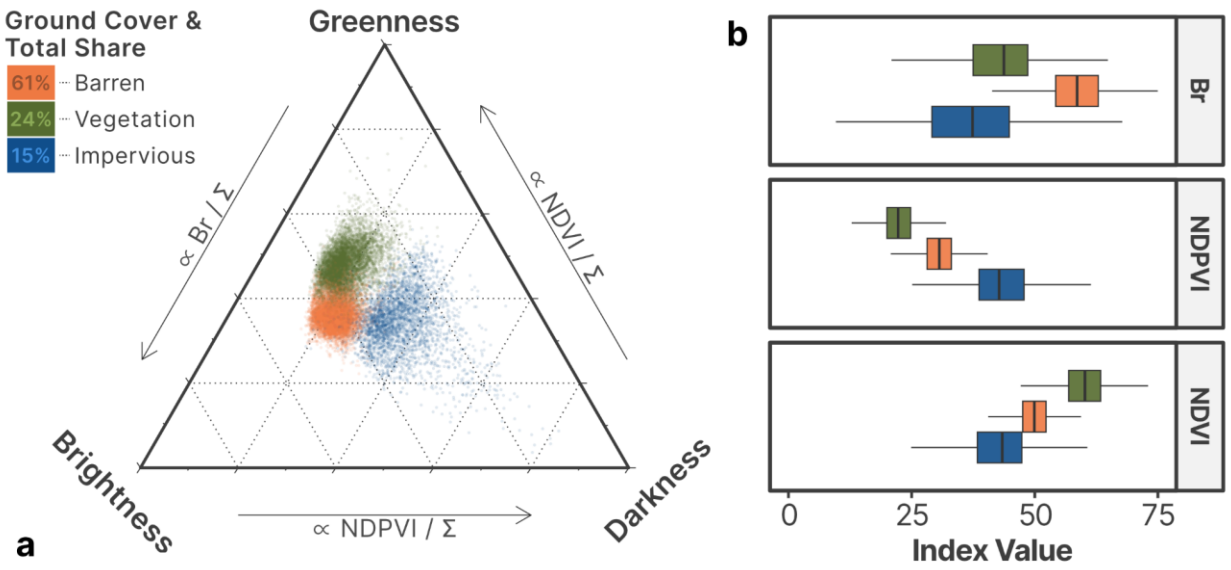

Figure A39. Global logical clustering of solar ground covers using the B-D-G model. Index values shown here are mean values across a given local, within-array cluster. We also used max and min local cluster values for global clustering. The ternary diagram (a) does not represent actual index values, where "$\propto$ NDVI / Σ", for example, indicates proportional NDVI value to the sum of the values for all three indices (Br, NDVI, NDPVI) for ternary plotting purposes only. Boxplots represent actual index values normalized from 0 to 100.

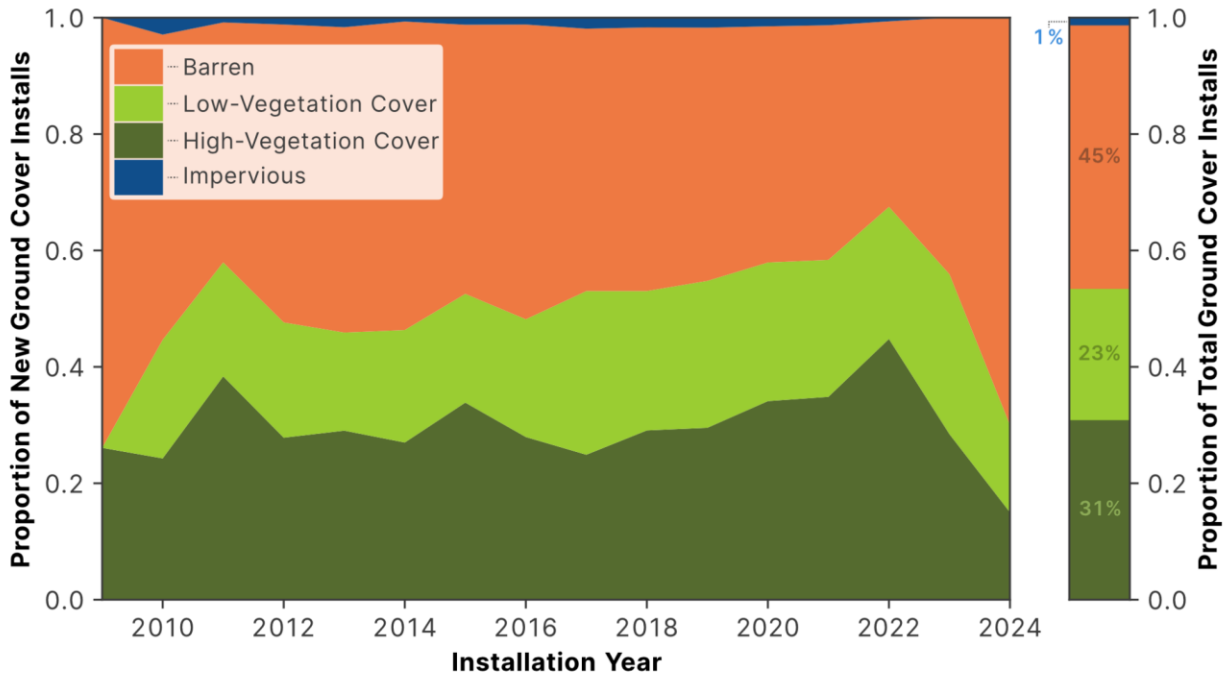

Figure A40. US solar energy ground cover proportion by installation through time. Compare to Main text Figure 20 (by area).

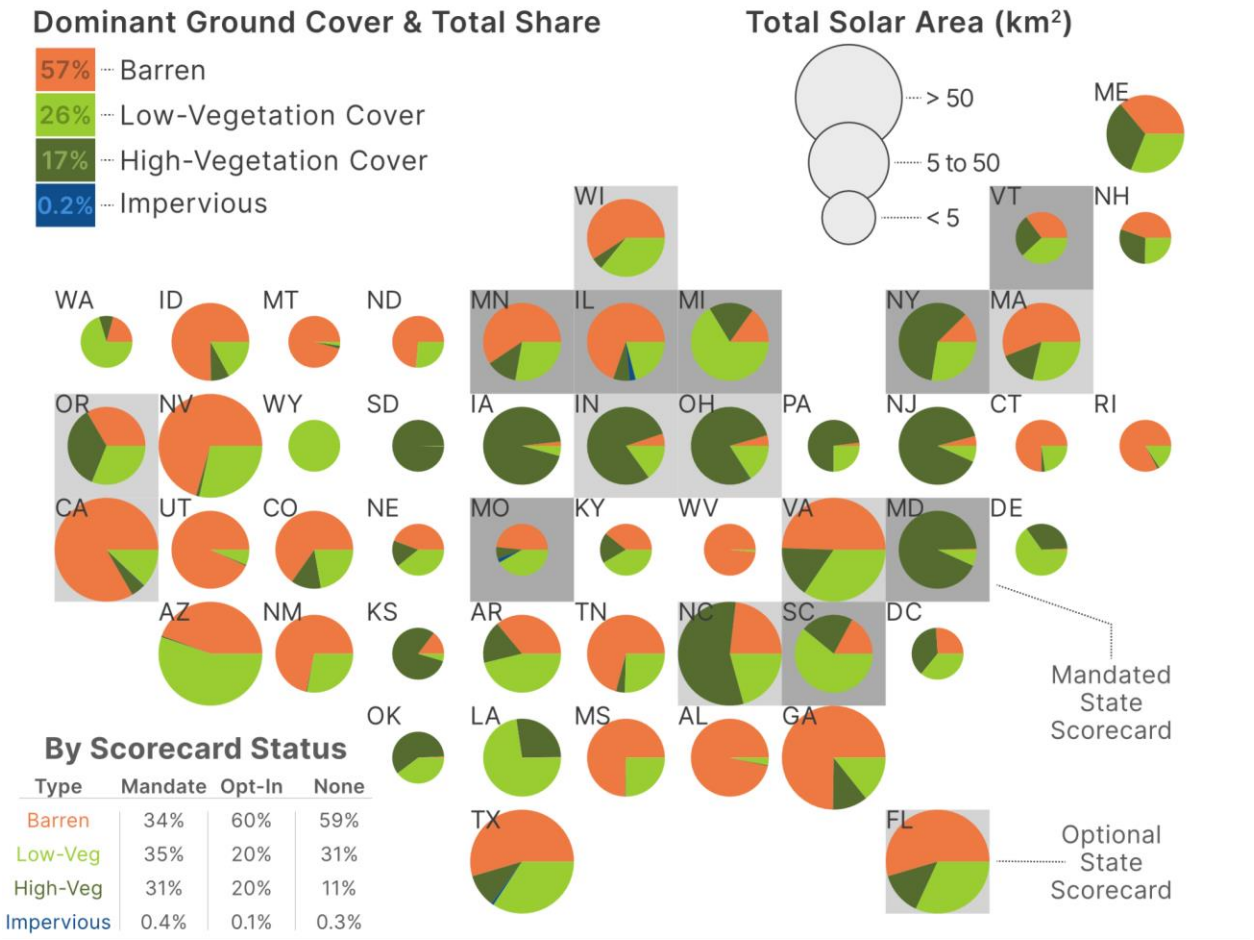

Figure A41. Ground cover practice proportional area by state and scorecard status. Dominant ground cover classification delineated by state total proportion, with pie chart size representative of the total solar area within the state. Additionally, Fresh Energy and ROWHWG both provide independent state-level or regional pollinator scorecards with full US coverage (Fresh Energy, 2025; ROWHWG, 2023). Scorecard status was derived from existing resources (Fresh Energy, 2025).

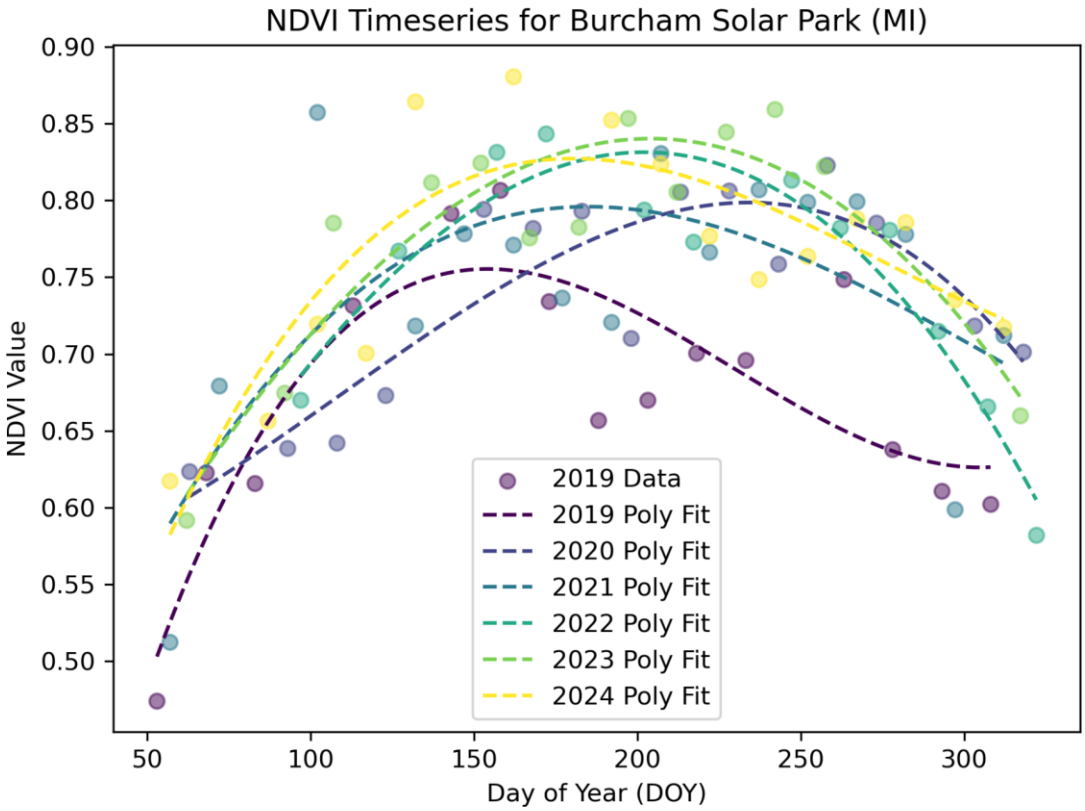

Figure A42. Resampled NDVI timeseries for Burcham Solar Park in Michigan. Timeseries is limited to non-winter months and fitted with polynomial trendlines across years. Note that this array is known to be managed with pollinator habitat from existing work at Michigan State University and was installed in 2018.

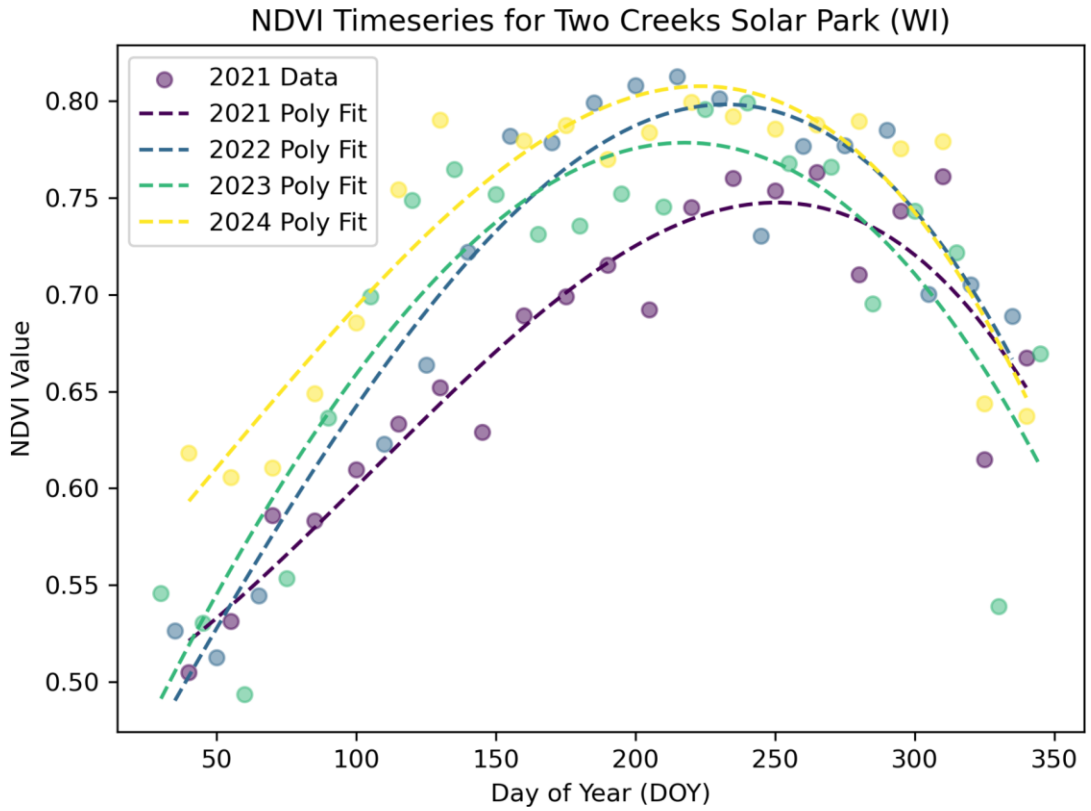

Figure A43. Resampled NDVI timeseries for Two Creeks Solar Park in Wisconsin. Timeseries is limited to non-winter months and fitted with polynomial trendlines across years. Note that this array is known to be managed with pollinator habitat from the InSPIRE Agrivoltaic Map (NREL, 2025) and was installed in 2020.

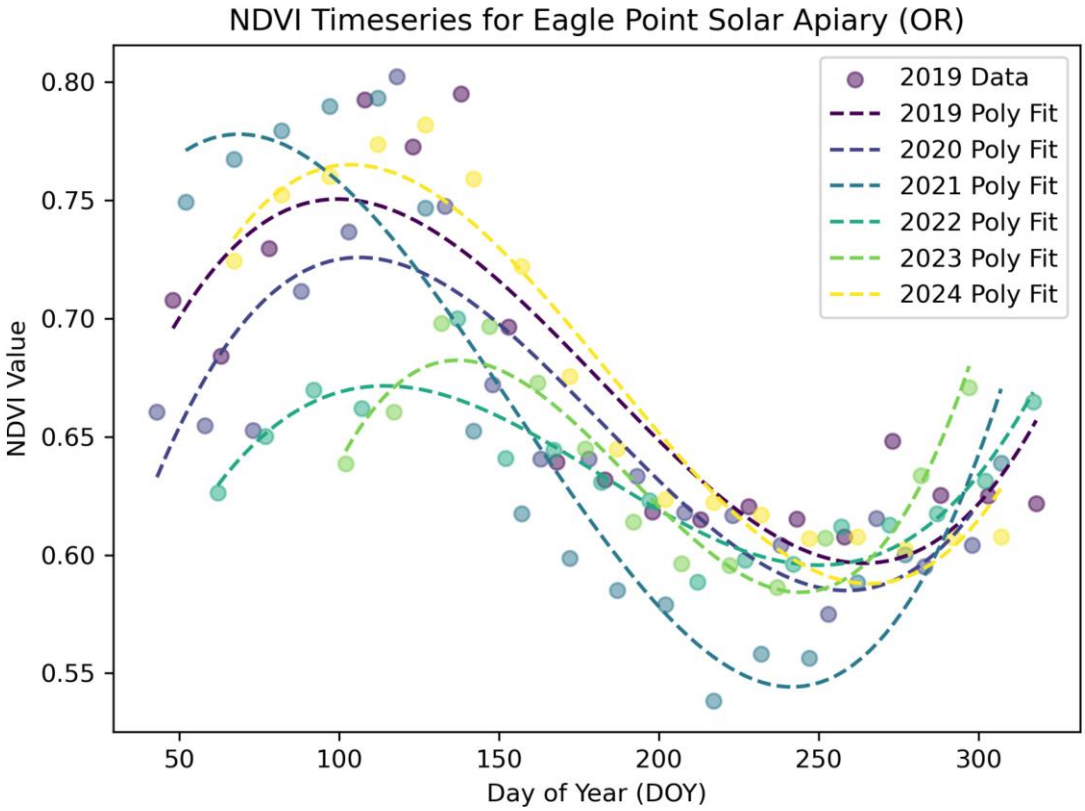

Figure A44. Resampled NDVI timeseries for Eagle Point Solar Apiary in Oregon. Timeseries is limited to non-winter months and fitted with polynomial trendlines across years. Note that this array is known to be managed with pollinator habitat from the InSPIRE Agrivoltaic Map (NREL, 2025) and (Graham et al., 2021) and was installed in 2018.

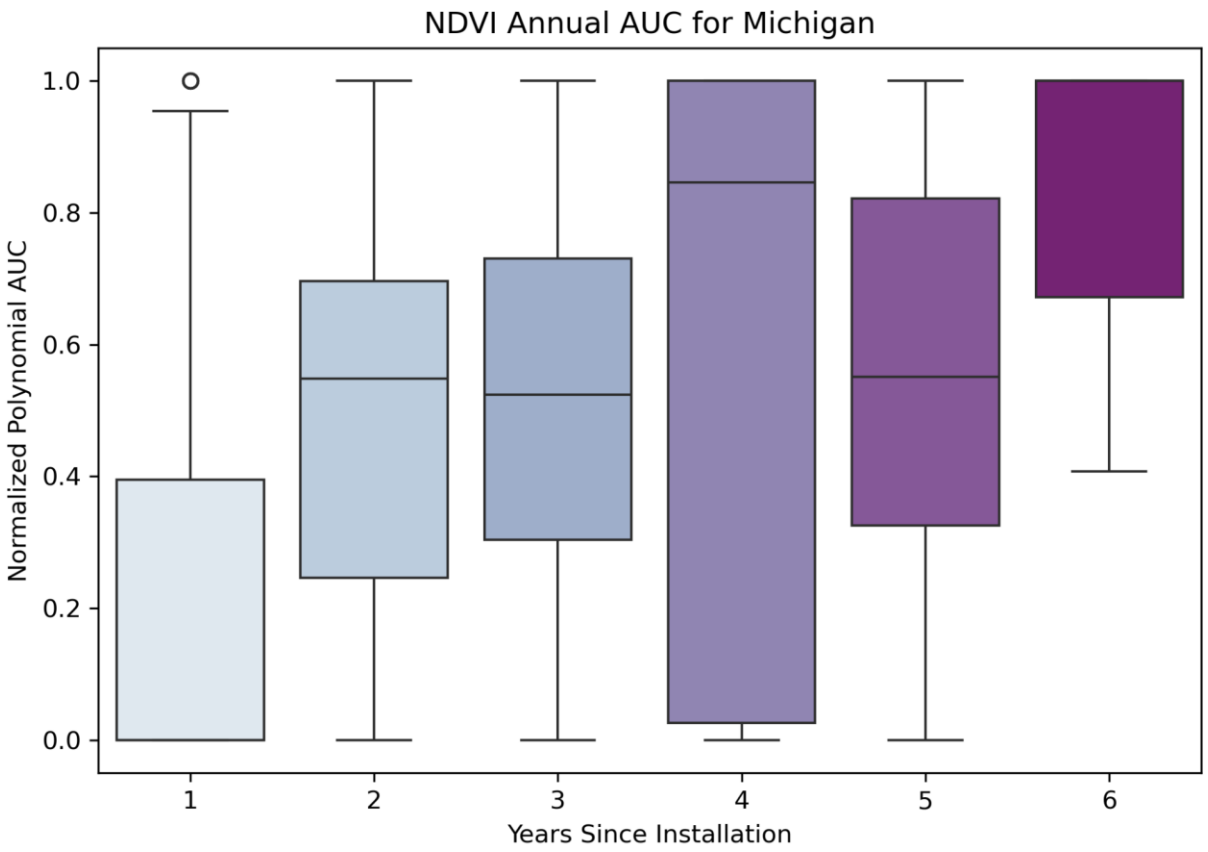

Figure A45. Annual NDVI AUC for 37 arrays in Michigan managed with vegetation.

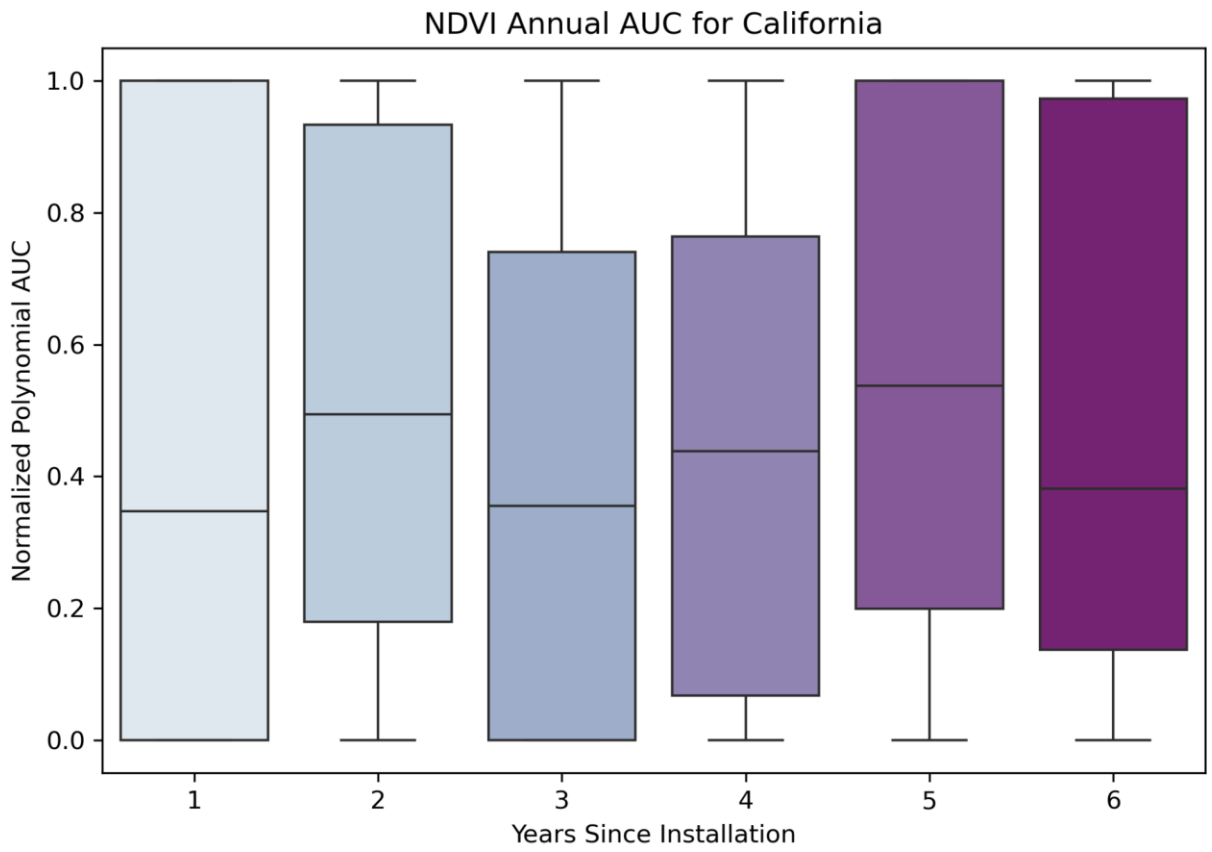

Figure A46. Annual NDVI AUC for 55 arrays in California managed with vegetation.

APPENDIX D: SUPPLEMENTARY INFORMATION FOR CHAPTER 4

Text A4.1: AgROE Utility, Limitations, and Assumptions

Conceptually, the AgROE concept is similar to the cone of depression created by irrigation pumping of groundwater, in that yields are generally radially reduced rather than entirely absent. Methodologically, AgROE applies a minMax function to the source value (*GCVI*) resulting in a 0 to 1 raster value within the setback boundary regardless of crop type and multi-annual yield trends (Figure A50). Therefore, AgROE is independent of crop type and CDL limitations and includes yield changes and productivity of crop rotations (maize and soybeans).

However, the newly derived AgROE power-land metric requires additional validation. While Landsat provides the desired temporal resolution for a pre- and post-installation analysis, higher spatial resolution imagery, such as National Agriculture Imagery Program (NAIP) imagery (Dai et al., 2024) could refine the "current" radius of effect. However, low-temporal resolution imagery such as NAIP would limit the ability to remove marginal land use effects. Additionally, we chose to cut-off the logarithmic-like growth in the AgROE cumulative disturbance (Main Text, Figure 3A) at 85%, leaving ~15% of detected yield effects within the co-located field. Consequently, the total yield effect within the co-located field was an order of magnitude less than the AgROE effect. This total change is observable in average yield (Figure A49E-A49G), which is not biased towards CDL-derived crop area or land cover change and total estimated yield (Figure A49F-A49H), which has not been de-trended but includes spatiotemporal change in SCYM yield maps created by CDL masking. Note that field-level changes in yield (Figure A49) were smaller compared to adjacent changes in yield (Figure 25) and we are unable to determine the effect of larger scale changes in cropping practice. Dependence on CDL is always an issue given known limitations in accuracy of the widely used product (Lark et al., 2017).

SCYM maps are limited spatially, temporally, and CDL accuracy (which qualitatively classifies wind infrastructure in some cases). It is also unclear how wind turbine reflectance (in GCVI) is represented in SCYM yield methods. Using Landsat-derived GCVI directly to delineate AgROE addresses these concerns and provides support for future work outside of the US Corn Belt and with different crops. The most commonly referenced work on wind turbine affected areas is (Denholm et al., 2009) that reports 0.3 ha MW^{-1} of permanently converted area (if all AgROE) would result in AgROE radii between 30 m and 70 m for a 1 and 5 MW turbine respectively.

Several observations also suggest that the radial AgROE relationship is not an artifact of the methods. Firstly, the AgROE relationship does not exist for randomly selected control points within the co-located field that are outside existing AgROE radii. Secondly, the median negative yield effect within AgROE exists in average yield (spatially independent from CDL) and actual yield (spatially dependent on CDL). Thirdly, the lack of relationship between capacity or rotor diameter with AgROE radius suggests that AgROE is more than just the result of a change in spectral-GCVI signatures from the physical turbine.

To provide a conservative estimate of forgone agricultural production within the operational footprint–within and outside AgROE–we have assumed that all wind turbines coincide with a new large access road. However, it is likely that many turbines employ existing road networks (Diffendorfer et al., 2019). We have also not accounted for directional effects such as downwind wake (Diffendorfer et al., 2022) or reported on and the county-level effects of wind turbines (Kaffine, 2019). We intend to address these limitations in a follow-on study. We also acknowledge that the effects of co-located wind turbines go beyond agricultural, with examples including ecological and social footprint (Burger & Gochfeld, 2012; Zaunbrecher, 2018), viewshed (Guo et al., 2024; Palmer, 2022), soundscape (Whalen, 2019), all requiring attention.

Text A4.1: Scale of Assessment

Most recent agricultural expansion has converted marginal land (Lark et al., 2020), suggesting that the definition of marginal may have a multi-scale effect temporally and spatially (Csikós & Tóth, 2023). We report marginality at the within-field scale, only one of many scales that should be considered. At such a local scale, marginality is likely driven by factors such as topography, soil composition, or cultural farming practices (e.g., irrigation and pesticide application). At larger scales, drivers of marginality likely differ. Understanding the effects of agricultural placement and management across scales is essential (Csikós & Tóth, 2023) and can help achieve win-win scenarios for energy and agricultural production, and carbon sequestration (Diffendorfer et al., 2022).

Text A4.1: Co-located Fields: Yields and Limitations

We observed a statistically significant, though low magnitude reduction in within-field maize and soybean yields within co-located fields These changes can be found in Figure A49E-A49H. Those these are significant; these changes had a low effect size (<0.2) indicating little or

no practical change. Additionally, we did not assume that field-scale yield changes were the result of wind installation but are more likely to be caused by changes in larger scale cropping practice.

A limitation of the crop sequence boundary dataset (Abernethy et al., 2023; Hunt et al., 2024) is that this product is a stagnant crop field boundary dataset derived from CDL. Beyond limitations of CDL, field boundaries can change for a variety of reasons including transition of ownership, regional crop type shifts, changes siting (RLP metric) and yield anomalies across years when the field boundaries may have been changing. Note though, this is also the case for other existing field boundary datasets, and CSB is the most recently available and likely the most accurate to existing field boundaries (Abernethy et al., 2023; Hunt et al., 2024).

Text A4.1: Economic Analysis Assumptions and Limitations

We assumed that all affected land was under a land lease legal agreement with a farmer landowner rather than purchased by developers. We do not consider additional easements or tax incentives for leased or neighboring farms (Shoemaker, 2007), option agreements to landowner farms during project planning (US DOE, 2022), crop damage payments (McEowen, 2011), good-neighbor agreements, and up-front payments (Windustry, 2009). We also assumed all wind turbines were under leasing agreements between utilities or third parties and the farmer landowners rather than purchased and installed by farmers themselves. We do not include field-level yield changes in this economic analysis.

We also assumed that there was no change in property values. (Guo et al., 2024) found that while home values decreased within 8 km of a wind turbine, the effect diminished substantially over time and at greater distances. Regarding agriculturally co-located wind turbines, lower adjacent home density would lead to reduced negative property value impact, and has been shown to not produce significant positive or negative effects for on-farm and near-farm parcels (B. Hoen et al., 2015; Sampson et al., 2020). Thus, we feel that our assumption of no change in on-farm property value is justified.

An additional limitation of the economic analysis is the limited knowledge on the spatial or temporal layout of lease agreements that are often private agreements determined on a case-by-case basis (Brannstrom et al., 2015). We used a turbine^{-1} year^{-1} leasing structure, although existing structures are also based on a turbine^{-1}, acre^{-1}, MW^{-1}, or royalty return structures (Craig Kaiser, 2024a, 2024b).

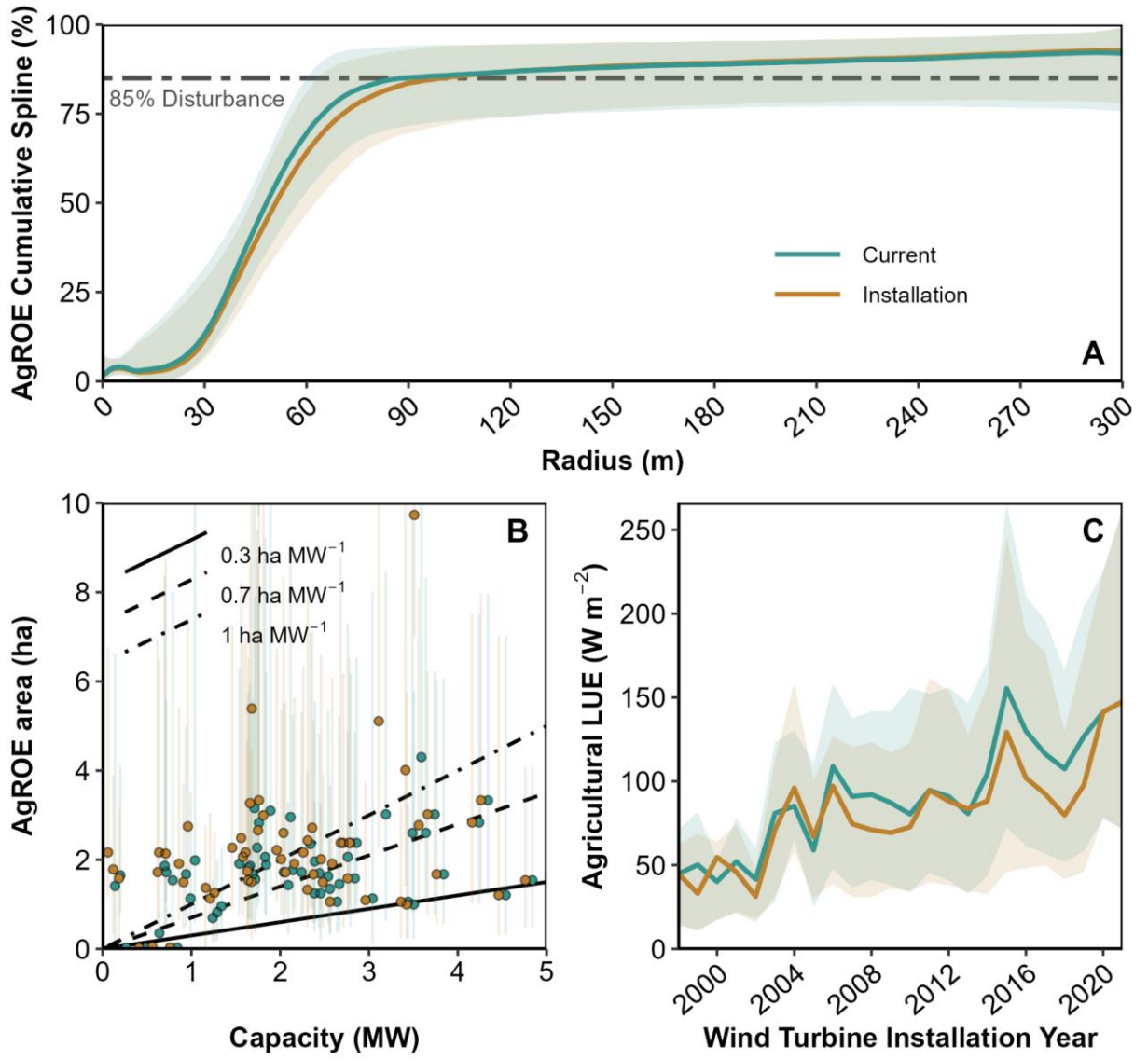

Figure A47. AgROE and resulting land use at most recent available imagery. (A) AgROE for 17,557 co-located wind turbines in the US Corn Belt. AgROE is the normalized (0 to 1) spline estimation of radial effect within the 300 m of potentially altered yield. The AgROE spline was estimated for each turbine with these quantiles showing the distribution of installation-unique splines. (B) Total estimated affected area (hectares) as a function of installed capacity (MW) grouped by wind farm. Sloped lines are the estimated area by capacity assuming direct permanent (0.3 ha MW^{-1}) and permanent plus temporary area disturbed (total: 1.0 ha MW^{-1}) from Denholm et al. (2009). The smoothed line and loess regression with a 95% confidence interval. (C) Power-land interaction (land use efficiency) of co-located turbines as a function of installation year. Shaded regions in A and C show the IQR and IDR, with lines and points representing median values.

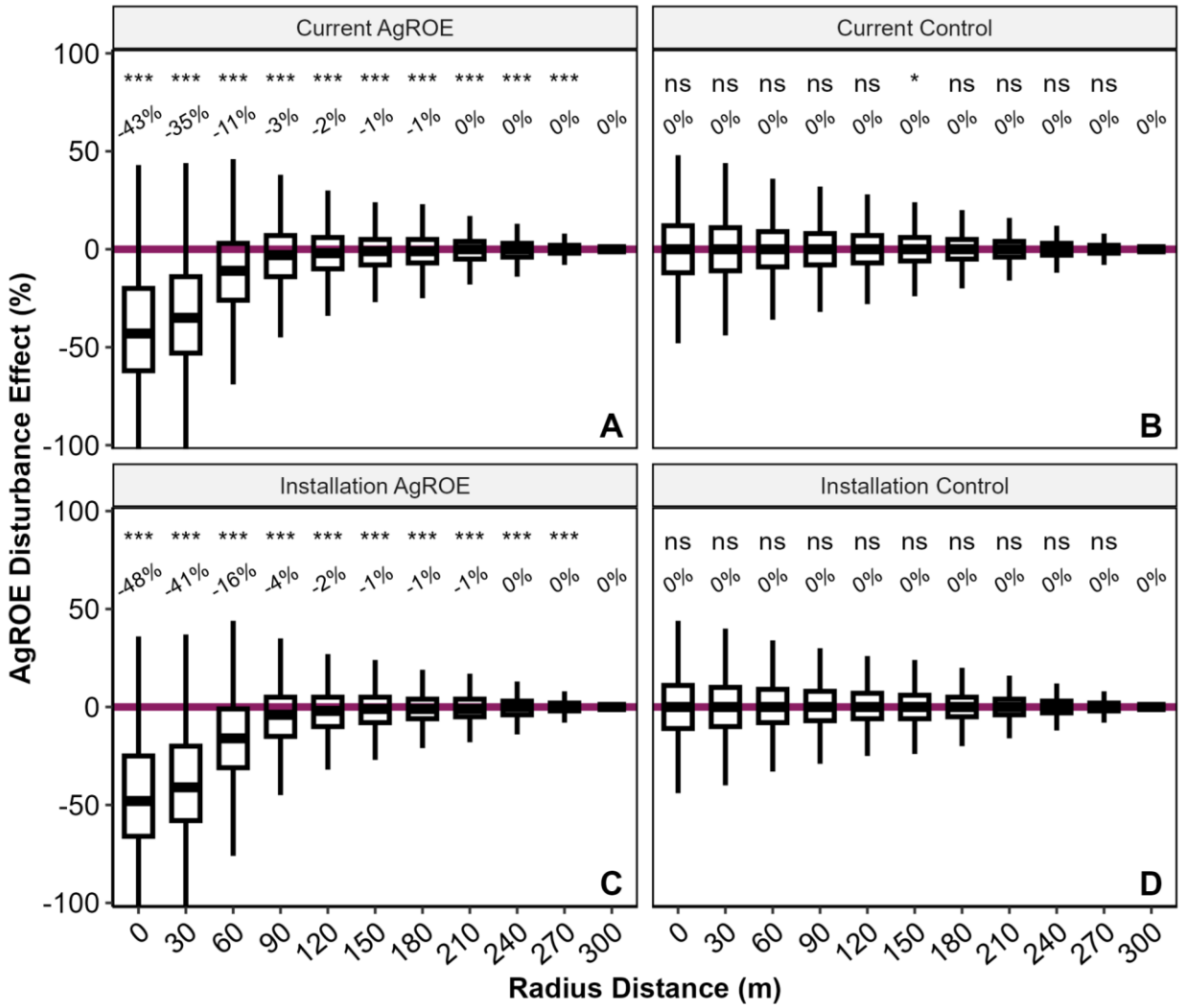

Figure A48. Non-normalized AgROE for all wind turbines and control points. The AgROE for agricultural co-located wind turbines in the US derived using Landsat *GCVI* after installation (A) and in most recent available imagery (C). AgROE for randomly generated control points within the same crop field as each respective wind turbine derived using Landsat *GCVI* after installation (B) and in most recent available imagery (D). Boxplots represent the quartiles with the middle line and the reported value (%) representing median AgROE for each radii. Values are not normalized by minimum to maximum total effect as they are in Figure 24. The purple dashed line represents the average local *GCVI*, with AgROE above and below the dashed line representing degraded yield and enhanced yield respectively relative to the average. One-sided t-test p-values are denoted with "***" for $p < 0.001$, "**" for $p < 0.01$, and "*ns*" for non-significant results.

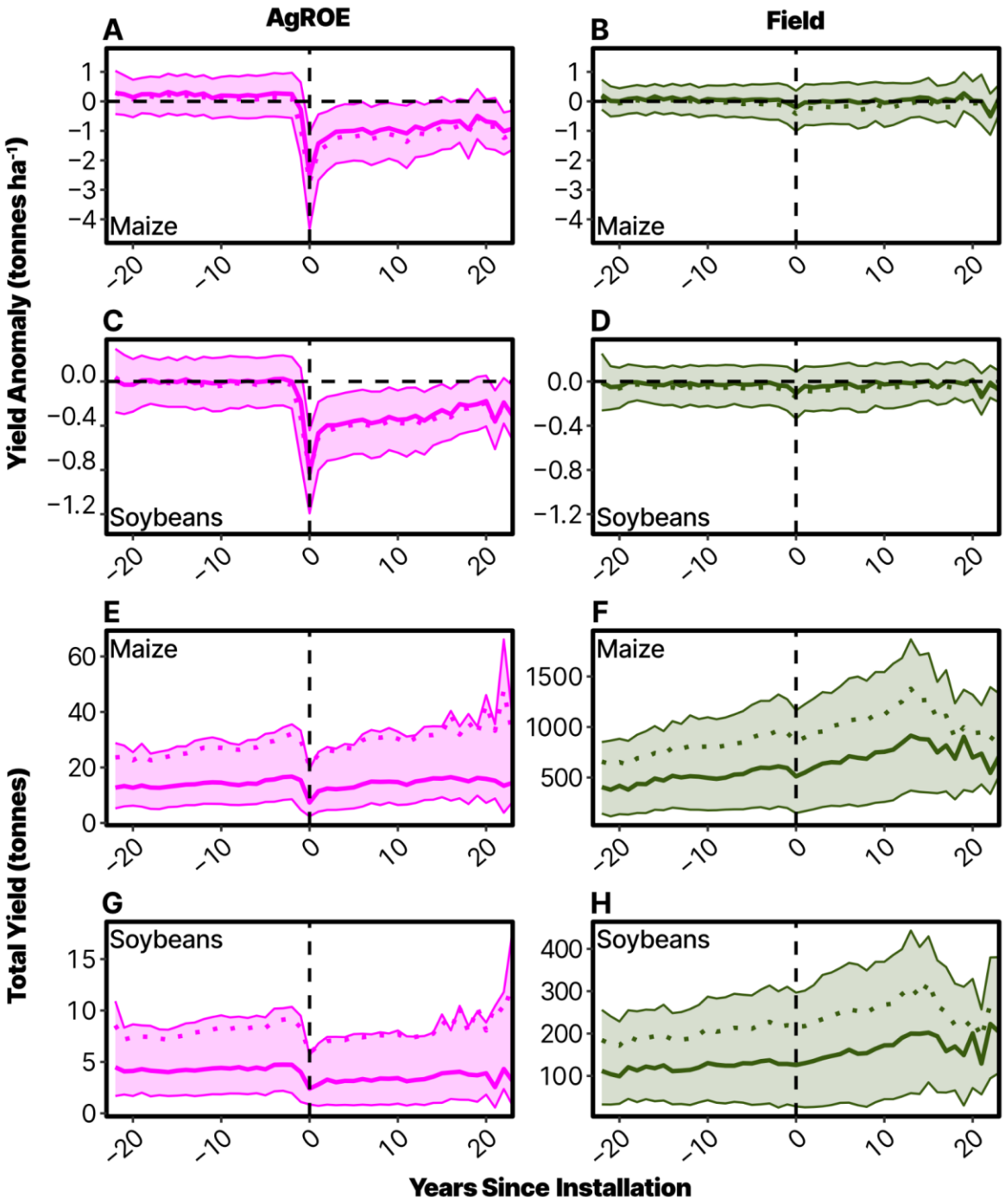

Figure A49. Co-located field yield anomalies and total yield with wind installation. Average yield anomaly plots within the newly derived AgROE area (A and C) and within the co-located field (B and D), and total yield plots within the newly derived AgROE area (E and G) and within the co-located field (F and H). Total yield is not corrected for county-level yields (detrended) and represents actual estimated total yield within the respective boundary. Solid and dotted lines show the median and mean yield anomalies respectively and shaded regions display the IQR range. The vertical dashed line represents the installation year and the horizontal dashed line (A to D) represents yields comparable to county averages (null anomaly).

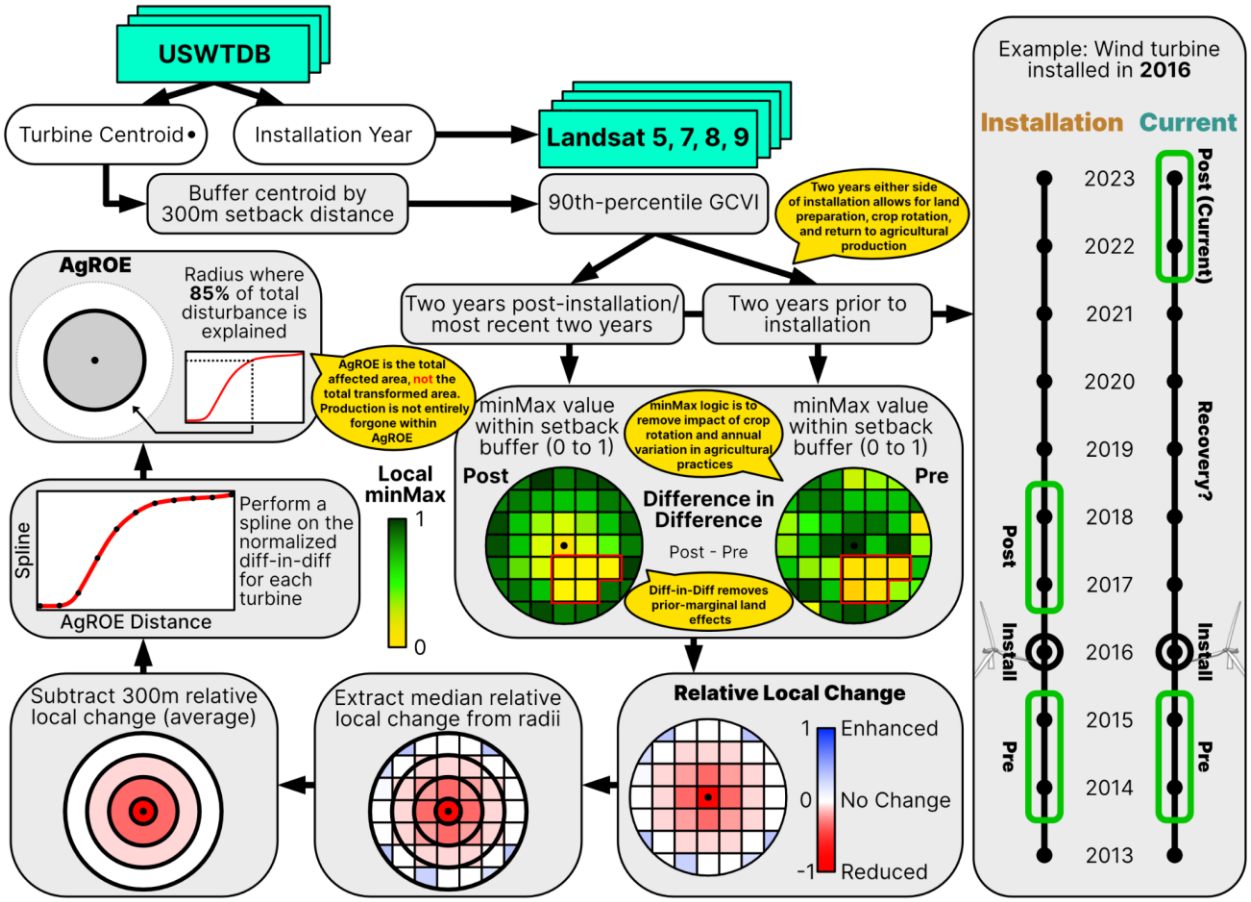

Figure A50. Workflow overview for estimating agricultural footprint using AgROE. Teal boxes indicate input datasets, white ovals indicate direct dataset attributes, gray boxes indicate newly calculated values or operations, and yellow dialog boxes provide context and reasoning for some more complex operations.

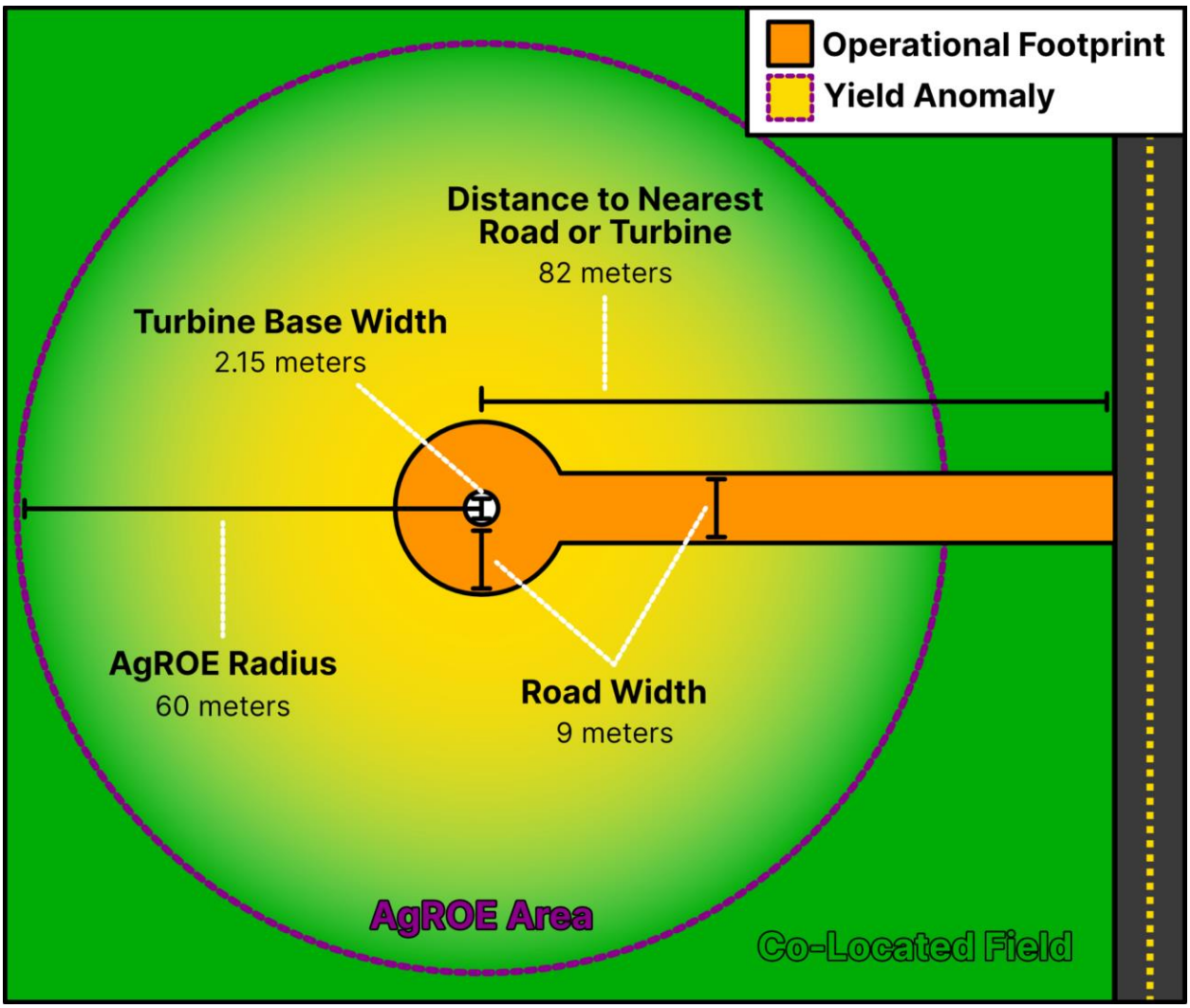

Figure A51. Conceptual example operational footprint and yield anomaly extent. The example is for a turbine with an AgROE of 60 m.